Departamento de Ingeniería Mecánica y Fabricación

Escuela Técnica Superior de Ingenieros Industriales

Tesis Doctoral

ANALYSIS OF THE KEY PARAMETERS IN PEDESTRIAN SAFETY ASSESSMENT FOR THE EUROPEAN VEHICLE FLEET USING MULTIBODY AND FINITE ELEMENT MATHEMATICAL MODELS.

Autor

Luis J. Guerra Casanova

Ingeniero Industrial Mecánico

Director

Luis Martínez Sáez

Doctor Ingeniero Industrial

2011

A todos los que quiero, y en especial, a todos los que me quieren.

AGRADECIMIENTOS

Quiero aprovechar estas primeras líneas para dar las gracias a todos los que habéis hecho posible que esta tesis sea hoy una realidad, ya que por momentos, ciertamente largos, mis condiciones de contorno invitaban a pensar que este trabajo nunca iba a tener el final feliz que ahora ya se vislumbra.

Es complicado describir en palabras mis sensaciones viendo esta tesis terminada; una tesis a la que he dedicado prácticamente tres años a tiempo completo para realizar los trabajos técnicos que aquí se describen, ligado al proyecto europeo APROSYS y a mi estancia en el INSIA y otros tres, sacando huecos en mi día a día como padre de familia y de mis viajes nacionales e internacionales con CDTI que me han permitido desde la distancia ir recopilando, escribiendo y editando este documento que resume todos esos años de trabajo en apenas 300 hojas.

Creo que podría resumir dicha sensación como si de un material compuesto se tratara, con una matriz de orgullo, por haber concluido esta tesis aun estando fuera del ámbito universitario, a la que se añade una gran cantidad de nano-partículas de agradecimiento, tanto a todos los que me han ayudado o sencillamente animado en este camino durante las diferentes etapas de este proceso, tanto en el INSIA como en CDTI, como a mi familia, que siempre ha tenido unas palabras de aliento en los momentos que más lo he necesitado.

Sin embargo, al mirar hacia atrás en el camino creo identificar el hecho singular definitivo que ha sido el verdadero "facilitador" para que esta tesis llegara a buen puerto: El levantarme todos los días a las 6 de la mañana para poder desayunar con mi mujer y lo bello durmiente que es nuestro hijo Sergio que se quedaba dormidito hasta que yo le despertaba a las 8, lo que me ha permitido dedicar una hora diaria a esta tesis durante los últimos 18 meses.

Además de este hecho puntual que me ha permitido tener el tiempo necesario para moldear formalmente esta tesis (gracias Bea, gracias Sergio), creo que he tenido el privilegio de poder formar parte de la familia investigadora del INSIA, institución que me ha tratado con mucho cariño, en la que he crecido como investigador y como persona, y en la que he tenido la gran suerte de tener a Luis Martínez como director de tesis. Le doy infinitas gracias por haber confiado en mí y permitirme desarrollar esta tesis en el entorno del proyecto APROSYS, proyecto europeo del VI Programa Marco de altísimo nivel científico-técnico.

Finalmente es este cúmulo de agradecimientos, no puedo dejar de destacar a Antonio García y Gustavo Ferichola, compañeros y amigos de fuegos y fatigas en el INSIA. Chicos, creo que una parte de esta tesis os pertenece y ha sido un placer trabajar y sobre todo compartir todo este tiempo con vosotros…seguiremos haciéndolo aunque sea entorno a otros fuegos…

TABLE OF CONTENT

LIST OF FIGURES.

LIST OF TABLES.

RESUMEN

Esta tesis investiga cuales son los parámetros más críticos que condicionan los resultados que obtienen en los ensayos de protección de peatones la flota Europea de vehículos, según la reglamentación europea de protección de peatones de 2003 (Directiva CE 2003/102) y el posterior Reglamento de 2009 (Reglamento CE 2009/78).

En primer lugar se ha analizado el contexto de la protección de peatones en Europa, viendo la historia de las diferentes propuestas de procedimientos de ensayo así como los cambios (y las razones de los mismos) que han sufrido a lo largo del proceso de definición de la normativa Europea. Con la información disponible de más de 400 de estos ensayos se han desarrollado corredores de rigidez para los frontales de los diferentes segmentos de la flota de vehículos europea, siendo este uno de los resultados más relevantes de esta tesis.

Posteriormente, esta tesis ha realizado un estudio accidentológico en detalle de los escenarios de atropello de peatones, identificando sus características más relevantes, los grupos de población con mayor riesgo y los tipos de lesiones más importantes que aparecen (en frecuencia y severidad), que han sentado las bases para analizar con modelos matemáticos hasta qué punto los métodos de ensayo propuestos realmente tienen estos factores en cuenta. Estos análisis no habrían sido posibles sin el desarrollo de las nuevas herramientas que se presentan en esta tesis, que permiten construir instantáneamente el modelo matemático de cualquier vehículo y cualquier peatón adulto para analizar su iteración. Así, esta tesis ha desarrollado una metodología rápida para desarrollar modelos matemáticos de vehículos a demanda, de cualquier marca y modelo y con las características geométricas y de rigidez deseados que permitan representarlo matemáticamente y del mismo modo, ha investigado cómo evoluciona el comportamiento del cuerpo humano durante el envejecimiento y ha implementado una funcionalidad de escalado en edad al modelo de peatón en multicuerpo de MADYMO (ya escalable en tamaño) para permitir modelar ad hoc cualquier peatón adulto (en género y edad).

Finalmente, esta tesis también ha realizado, utilizando modelos de elementos finitos del cuerpo humano, diferentes estudios sobre la biomecánica de las lesiones más frecuentes de este tipo de accidentes, (en piernas y cabeza) con el objetivo de mejorar los procedimientos de ensayo para que predigan mejor el tipo de lesiones que se quieren evitar. Con el marco temporal y las condiciones de contorno de esta tesis se han centrado los esfuerzos en reforzar algunos aspectos críticos pero puntuales sobre cómo mejorar el ensayo de cabeza y, sobretodo, en proponer soluciones viables y con un valor añadido real al ensayo de pierna contra parachoques, sin cambiar la esencia del mismo pero proponiendo un nuevo impactador mejorado que incorpore una masa extra que representa a la parte superior del cuerpo y sea válido para toda la flota europea de vehículos independiente de la geometría de su frontal.

INTRODUCCIÓN

La seguridad de peatones se ha convertido en un campo importante de investigación desde principios de los años 80 cuando se desarrollaron los primeros modelos matemáticos de peatón (Lestrelin 1980, Wismans, 1982) y se creó en el seno del EEVC (European Enhanced Safety Vehicle Committee), un primer grupo de trabajo en este tema, el WG7. Gracias al trabajo intensivo de este grupo de alto nivel y el efecto arrastre que sus trabajos tuvieron en el resto de la comunidad investigadora del mundo de la automoción, se consiguió tener la base científica y masa crítica necesarias para empezar a pensar en una posible directiva relativa a seguridad para peatones no sólo en Europa sino en otras regiones importantes como Estados Unidos, Japón o Australia.

El primer borrador de esta reglamentación para Europa se lanzó por el EEVC WG10 (continuación del EEVC WG7) en 1995 usando como base la evidencia accidentológica relativa a atropellos de peatón y usando modelos matemáticos multicuerpo para fijar las condiciones de impacto más adecuadas de los ensayos que se definieron. En 2002, el EEVC WG17 revisó el trabajo del EEVC WG10 modificando ligeramente los ensayos propuestos presentando a la Comisión Europea su propuesta definitiva de reglamentación para protección de peatones en Europa.

Hay que tener en cuenta que los ensayos definidos por el WG10 y posteriormente retocados por el WG17 y a petición expresa de la Comisión, deberían ser adecuados para usarse en una reglamentación que exigiera a los fabricantes incorporar en sus vehículos medidas para la protección de peatones por lo que era muy importante que estos ensayos y sus impactadores fueran simples, precisos, robustos y con una alto

grado de repetibilidad. Para conseguirlo se necesitaba una gran simplificación tanto en las condiciones del ensayo como en los impactadores que lograra un compromiso entre las condiciones propuestas y las infinitas posibilidades que se planteaban en los accidentes reales de atropello.

Como resultado final, el EEVC recomendó una matriz de ensayos con cuatro impactadores diferentes en cada vehículo: un simulador de pierna, un simulador de la parte superior de la pierna, un simulador de cabeza niño y un simulador de cabeza adulto, con condiciones de ensayo fijas en tres de los cuatro ensayos (pierna y cabezas) y una dependiente de la geometría del vehículo para el simulador de la parte superior de la pierna.

Estos cuatro ensayos se incluyeron en 1997 en el programa EuroNCAP, el programa oficial de consumidores que compara la seguridad de los vehículos en Europa. Este hecho y los resultados que se obtuvieron fueron clave para concienciar a la sociedad de lo necesario que era aumentar los estándares de la flota europea de vehículos en términos de protección de peatones y dieron un impulso definitivo para que se considerase en serio la adopción de una directiva de peatones en Europa. Además, el incluir la protección de peatones en las puntuaciones que obtenían los vehículos ensayados en términos de estrellas tuvo dos consecuencias colaterales:

- Mostró la robustez de los ensayos propuestos por el EEVC y su alta repetibilidad en entornos de reglamentación.
- Demostró que era técnicamente factible encontrar soluciones técnicas para que los vehículos fueran “pedestrian-friendly”.

Los procedimientos de ensayo con los límites propuestos, con el respaldo de los resultados de los ensayos de EuroNCAP se discutieron en profundidad entre la comunidad científica y los fabricantes y finalmente la Comisión Europea decidió implementarlos en 2003 como una directiva relativa a protección a peatones (Directiva 102/2003 EU). Esta directiva mantenía la parte fundamental de la propuesta del EEVC pero con ciertas divergencias ya que requería el cumplimento de los límites propuestos en dos fases con una primera fase con límites menos exigentes, y una segunda fase con los límites, en principio, propuestos por el EEVC WG17 pero que tras varios estudios de viabilidad han derivado en el Reglamento CE 2009/78, con ciertos matices.

A lo largo de este proceso, existen multitud de artículos que han investigado en profundidad las características de los atropellos de peatones, en términos de mecanismos de lesión o de cinemática en el accidente como también la lógica de los procedimientos de ensayos, del porqué usar sub-impactadores o desarrollando impactadores que sean más biofieles. Todas estas publicaciones han identificado puntos críticos para la revisión de estos procedimientos y de hecho, parte de ellos se han tenido en cuenta en este proceso de mejora y negociación que han sufrido estos procedimiento

de ensayo y sus impactadores desde la primera propuesta del EEVC WG10 en 1995 hasta el reglamento actual 2009/78 de 2009.

Aún así, todavía hay varios puntos de futura mejora que no se han abordado debido a la falta de evidencia científica que los avale y la mayoría de ellos están recopilados en el análisis de "los siguientes pasos para los procedimientos de ensayo de protección de peatones", que Lawrence (2005) hizo como parte final del trabajo del EEVC WG17. De este compendio, se obtienen tres recomendaciones:

- Recomendación 1: Garantizar que las condiciones de impacto definidas para los procedimientos de ensayo dan cobertura a los rangos de accidentes que se pretenden reproducir o al menos al caso más desfavorable de dicho rango. Además, los criterios de lesión propuestos no sólo debe evitar lesiones mortales sino también, en la medida de lo posibles, lesiones que dejen secuelas de movilidad o calidad de vida a largo plazo, manteniéndolos a un nivel de riesgo de lesión cuyo cumplimiento por parte del fabricante tenga un coste asumible.
- Recomendación 2: Avanzar en el desarrollo de modelos matemáticos más robustos tanto del cuerpo humano como de los vehículos que lo atropellan para permitir que en el futuro estos modelos se puedan incluir en la directiva, por ejemplo, para definir el escenario más desfavorable en cada vehículo que determine las condiciones de impacto del sub-impactador en cada caso.
- Recomendación 3: Formular mejoras en los métodos y herramientas de ensayos actuales para que sean más realistas y biofieles, especialmente en aquellos en los que existan evidencias de beneficios potenciales, como en el caso de añadir la masa de la parte superior del cuerpo al impactador de pierna

Con estas tres recomendaciones en el horizonte, es el humilde objetivo de esta tesis aporta evidencias científicas en cada una de ellas definiéndose para ello los siguientes cuatro objetivos:

- **Objetivo 1: Análisis de la vinculación de los métodos de ensayo para peatones con los datos accidentológicos actuales.** Para poder garantizar que el proceso de pasar de las infinitas posibilidades de los escenarios reales a unas condiciones de impacto fijas para cada ensayo sigue siendo el apropiado se necesita necesariamente vincularlo a la flota de vehículos actuales y las tendencias que aparecen relativa a accidentes con peatones. Es el primer objetivo de esta tesis abordar este proceso analizando datos accidentológicos actuales españoles de protección de peatones, no sólo identificando los puntos más críticos de esta simplificación sino analizando los pormenores de cada uno de ellos para poder estar en disposición de formular mejoras a futuro tanto en los procedimientos como en las herramientas de ensayo de protección de peatones, como se sugiere en la recomendación 3.

- **Objetivo 2: Desarrollo de mejores herramientas matemáticas para analizar la protección de los peatones ante atropello.** Directamente vinculada a la recomendación 2 y, como una necesidad derivada para poder investigar más en detalle los puntos críticos identificados previamente, esta tesis va a desarrollar un conjunto de nuevas herramientas para analizar con mayor eficiencia no solo en tiempo sino también en términos de coste-beneficio, los detalles de los escenarios reales de atropello de peatones. Estas herramientas son un modelo matemático de peatón en multibody que se pueda escalar en tamaño y en edad, una metodología para construir modelos matemáticos de vehículos y unos corredores que definen la rigidez de la parte frontal de la flota de vehículos Europeos en su interacción con los peatones. Aunque estas herramientas se han desarrollado como medio para alcanzar los objetivos de esta tesis son en sí mismos resultados muy relevantes ya que pueden ser utilizados por la comunidad científica en un sinfín de estudios y análisis para protección de peatones.
- **Objetivo 3: Medir la relevancia de los parámetros más críticos identificados de cara a su consideración en los ensayos de protección de peatones.** En línea con la recomendación 3, esta tesis analiza cómo influyen en la protección de los peatones los tres parámetros críticos identificados en el estudio accidentológico, que son, a nivel de cuerpo entero, cómo la edad del peatón influye a su cinemática en el atropello, que se ha analizado utilizando modelos multibody y a nivel de lesiones y utilizando modelos de elementos finitos, qué influencia tiene la aceleración angular en la aparición de lesiones no mortales en la cabeza y cómo es de importante la aportación de la masa de la parte superior del cuerpo en la aparición de lesiones en las piernas en un atropello, lesiones que suelen tener secuelas a largo plazo. Los modelos matemáticos desarrollados como parte del objetivo 2 se han utilizado extensivamente en estos análisis para modelar adecuadamente la realidad y poder valorar objetivamente la relevancia de cada uno de los parámetros estudiados.
- **Objetivo 4: Proponer mejoras técnica y económicamente factibles a los procedimientos de ensayo de peatones.** El último objetivo de esta tesis es el de proponer mejoras que sean factibles de implementar relativas a cómo los procedimientos de ensayo incorporan los aspectos críticos que se han analizado. Considerando las condiciones de contorno de esta tesis con un nuevo Reglamento de peatones publicado en 2009 tras muchos años de discusiones, las recomendaciones que se dan en este trabajo se limitarán a aquellas que tengan un coste-beneficio muy positivo, sean técnicamente factibles y no alteren sensiblemente ni la base del ensayo ni la de los impactadores. Con esas condiciones, los esfuerzos se han centrado en la que a priori tiene mayor

potencial que es la de incluir un lastre al impactor de pierna para simular el efecto de la parte superior del cuerpo, como ya se comentaba en la recomendación 3.

Para conseguir estos cuatro objetivos, esta tesis se ha dividido en tres secciones que cubre los diferentes aspectos descritos anteriormente.

La sección I presenta el marco y el fundamento de esta investigación, cubriendo tanto el análisis de la evidencia accidentológica de este tipo de accidentes como una descripción del proceso de desarrollo de los ensayos de peatones diseñados como respuesta a estas tendencias. La sección comienza dando una visión general pero detallada de cómo los procedimientos de ensayo de peatones se gestaron y cómo han sido retocados desde la recomendación inicial del EEVC WG10 hasta el reglamento actual 2009/78. En este proceso se observa que aunque las condiciones de ensayo no han sufrido casi ningún cambio, los límites de cumplimiento han sido una continua fuente de discusión.

Vinculado a estos ensayos, y aprovechando la gran cantidad de ensayos de este tipo realizadas por EuroNCAP como parte de este proceso y habiendo tenido acceso a parte de dichos ensayos, esta sección I presenta uno de los primeras herramientas que se mencionaban en el objetivo 2 que puede considerarse como una de las aportaciones más importantes de esta tesis a la comunidad científica: “el primer estudio a gran escala para definir unos corredores de rigidez para protección de peatones de la flota de vehículos europeos”. Este estudio es el primero de este tipo realizado a nivel Europeo con un objetivo tan ambicioso y ha utilizado los datos en bruto de estos ensayos de EuroNCAP para obtener corredores de rigidez de las diferentes partes de los vehículos de acuerdo a la puntuación obtenida en los ensayos de EuroNCAP.

Aunque el objetivo de estos ensayos es evaluar la protección ante peatones que ofrecen los diferentes vehículos, se han ideado un procesado de estos datos por el que se obtiene información del comportamiento de la estructura del vehículo y por lo tanto se pueden derivar sus propiedades para usarse como características de contacto en las simulaciones de impacto con modelos de peatón. Este enfoque abre un amplio abanico de posibles estudios de protección de peatones utilizando rigideces realistas en los vehículos y con un coste de validación de los modelos de vehículo muy reducido si se conocen sus puntuaciones de EuroNCAP. Esto es especialmente interesante en la reconstrucción de accidentes de peatón y convierte a estos corredores una herramienta esencial para estas tareas que podría ser integrada fácilmente en software de reconstrucción de accidentes.

Finalmente, en la última parte de la sección I se aborda el estudio accidentológico, parte fundamental del objetivo 1 de la tesis. Como los métodos de ensayo son un compromiso de los peores escenarios posibles, es fundamental garantizar que siguen siendo representativos de los escenarios que buscaban reproducir. Esta tesis ha abordado este aspecto analizando una base de datos española de estudios de peatones en profundidad

prestando especial atención no sólo a las diferentes variables relativas al accidente en sí sino también a los patrones de lesiones que aparecen tanto en caso de fallecidos como de los heridos.

Este análisis identifica los aspectos críticos de la simplificación de la realidad en un conjunto de condiciones de impacto fijas para cada ensayo, como se citaba en la recomendación 1, que es en los que esta tesis pretende aportar evidencias cuantificables de su relevancia.

Esta simplificación se ha analizado primero en base a la simulación de escenarios reales con tecnologías multicuerpo (Sección II) con especial énfasis en la edad del peatón ya que en el estudio accidentológico se mostraba como el colectivo de personas mayores era un grupo crítico para este tipo de accidentes, y posteriormente enfocado en la medida de las lesiones que aparecen, utilizando modelos de elementos finitos (Sección III) ya que la variedad de lesiones que aparecen en la vida real se cubren con un número muy reducido de criterios en los ensayos.

Aunque la naturaleza de los estudios realizados para la edad en la Sección II y para las lesiones en cabeza y piernas de la Sección III han sido muy diferentes en todos los casos, las preguntas que se intentaban contestar eran las mismas: ¿Cómo de relevante es este parámetro para medir la protección del peatón? (Objetivo 3) ¿Cómo de factible es introducir su efecto en los ensayos de peatones? (Objetivo 4).

En la Sección II se aborda el análisis de escenarios reales seleccionando cuatro atropellos no mortales con peatones adultos de todas las edades y que resultaron en lesiones en piernas, en cabeza o en ambas. La naturaleza de este análisis, incluyendo la edad como parámetro, ha sido novedad en el estado del arte de la reconstrucción de accidentes y ha requerido el desarrollo de nuevas herramientas matemáticas para construir adecuadamente estos modelos, en concreto un modelo de peatón escalable en tamaño y en edad y unos modelos matemáticos de vehículos, de la misma marca y modelo que los de los accidentes reproducidos, con unas características detalladas de geometría y rigidez.

El potencial de estas herramientas por sí mismas han hecho que no sólo hayan sido fundamentales para llevar a cabo este análisis sino que se los pueden considerar como uno de los resultados más tangibles de esta tesis, como se reconocen en el objetivo 2.

En el caso de los modelos matemáticos de vehículos, se han construido ex profeso para esta tesis ya que no existían comercialmente. Para ello, la Sección II desarrolla y presenta una metodología muy robusta y económica que no solo garantiza un gran detalle de la geometría de los modelos de vehículos sino también una distribución de rigideces de cara a protección de peatones muy pormenorizada.

En el caso del modelo de peatón, se ha realizado una mejora al modelo de peatón en multibody disponible en MADYMO, y que se puede escalar en tamaño. En esta tesis a este modelo ampliamente validado y utilizado habitualmente en reconstrucción de accidentes, se le ha dotado con la capacidad de ser también escalado en edad, multiplicando así sus posibilidades de uso.

Para esto, se ha desarrollado en la Sección II un estudio extensivo sobre cómo la edad influye en las propiedades de los diferentes tejidos del cuerpo humano, mostrándose en general que la edad tiene un efecto debilitador en todos los tejidos reduciendo sus límites de fractura o rotura hasta un 20% en algunos casos. Este efecto de la edad se ha analizado estadísticamente, y en los casos en que ha resultado relevante se ha incluido en el software AgedMAT, software desarrollado en esta tesis que permite el "envejecimiento" directo de los diferentes tejidos humanos a nivel de modelo de material. Las salidas de este software junto con las funciones de transferencia por cuestiones geométricas necesarias han hecho posible implementar la edad como factor de influencia en el modelo de MADYMO de peatón, escalando a demanda dicho peatón para reproducir los cuatro escenarios reales seleccionados con el peatón más adecuado en términos de género, tamaño y edad.

Con el desarrollo de estos modelos se han simulado los cuatro accidentes en MADYMO encontrándose cinemáticas que reproducían fielmente las evidencias recogidas en los accidentes. Los detalles de cada una de ellas (la evidencia del accidente, las lesiones del peatón, los puntos de contacto en el vehículo) así como las cinemáticas obtenidas se presentan en la Sección II.

Se ha realizado además un estudio paramétrico para entender si este efecto debilitador causado por la edad es relevante para obtener cinemáticas realistas en la reconstrucción de accidentes viendo si el hecho de incluir o no límites de fractura dependientes de la edad condiciona los resultados de las simulaciones. Estos estudios han respondido a la pregunta propuesta en el objetivo 3 sobre la relevancia de la edad en estos temas concluyéndose que existe una relación importante entre las fracturas en las piernas y la posterior localización del impacto de la cabeza con el vehículo, que podría ser muy relevante si en un futuro se incluye más directamente el uso de modelos matemáticos en la directiva/reglamento.

La última parte de la Sección II considera si es factible considerar la edad como una variable extra en los ensayos de protección de peatones. Dado que la inclusión de la edad como parámetro incluiría hasta cierto punto rebajar los límites de lesión, habría que considerar que este aspecto ha sido muy discutido durante el desarrollo de los ensayos para dar una respuesta adecuada a la pregunta del objetivo 4 sobre posibles mejoras en los procedimientos de ensayos actuales. Esta posible reducción en los límites de los ensayos tendría que estar basada en el desarrollo de unas curvas de lesión específicas para personas de la tercera edad ampliamente aceptadas por la comunidad científica y

los fabricantes. Dada la magnitud de tal desarrollo, éste no se ha abordado en esta tesis pero ofrece la posibilidad de seguir investigando en un futuro en dicha dirección para obtener dichas curvas de lesión.

En término de las medidas de las lesiones, aunque se pueden concluir algunas tendencias de lo observado en las simulaciones de la Sección II, las salidas utilizadas para predecirlas están en la frontera de fiabilidad de los modelos multibody de MADYMO, por la simplificación del mismo en la definición de algunas zonas, como la cabeza o la rodilla, zonas de lesiones frecuentes en estos escenarios o por la no consideración en detalle de todos los mecanismos de lesión posibles que aparecen en las mismas.

La Sección III evita estas limitaciones al trabajar con modelos matemáticos de elementos finitos, dotando de un punto de vista normativo a los análisis que se realizan para poder responder adecuadamente a los objetivos 3 y 4 de esta tesis.

En el caso de las lesiones en cabeza, la Sección III recoge dos colaboraciones realizadas con ULP (Universidad Louis Pasteur) y con TNO que analizan en detalle dos de los accidentes reales presentados en la Sección II. En ambos casos, se reproduce con modelos de elementos finitos de cabeza el momento del impacto de la cabeza con el vehículo analizándose un número de parámetros internos de los modelos que predicen las lesiones en cabeza en todos los posibles mecanismos de lesión de la misma. Estos estudios han demostrado que las salidas de los modelos de elementos finitos muestran gran correlación con las lesiones observadas en los accidentes reales y han puesto de manifiesto la importancia de mecanismos de lesión no basados en aceleración lineal en la producción de lesiones no mortales en la cabeza.

Esto significa que los criterios de lesión solo basados en la aceleración lineal no son suficientes, ni en muchos casos son los mejores, para predecir todos los tipos de lesión de cabeza que aparecen en los escenarios de peatones, especialmente cuando hay claras evidencias accidentológicas de que en estos casos suelen haber una gran rotación de la cabeza durante el impacto.

En este sentido, estos estudios han permitido obtener una serie de conclusiones para responder al objetivo 3 de la tesis e identificar futuras líneas de mejora de cara al objetivo 4, que pasarían necesariamente por cambiar las bases de los ensayos de cabeza, no solo cambiando significativamente las condiciones de los ensayos sino también el diseño de los impactadores. Por la envergadura de estos cambios, estas tareas se han dejado fuera del alcance de la tesis y como conclusión de lo aquí presentado se proponen únicamente algunas recomendaciones de los detalles que se deben investigar más a detalle en el futuro.

En el segundo caso, como las condiciones de impacto en las piernas de los peatones están más acotadas, se ha planteado el estudio analizando y comparando las lesiones que ocurren en las piernas cuando al peatón le atropellan vehículos de los diferentes

segmentos de la flota europea con las que se predicen con el ensayo de pierna propuesto originariamente por el EEVC.

Para eso, se han construido matemáticamente dos tipos de escenarios:

- Un conjunto de simulaciones donde modelos matemáticos de vehículos de los diferentes segmentos de la flota europea atropellan a un peatón modelado con elementos finitos, THUMS 50%, modelo de elementos finitos del cuerpo humano desarrollado por Toyota que incorpora criterio de fallo en huesos y ligamentos y por tanto puede predecir la fractura de huesos y la ruptura de los ligamentos en escenarios de atropello.
- Un conjunto de simulaciones con los mismos modelos matemáticos de vehículos ensayados en las condiciones propuestas por el EEVC usando el modelo matemático del impactador de pierna del EEVC.

Los modelos de vehículo se han elegido en base a un estudio en profundidad de la flota europea de vehículos, que ha clasificado los segmentos teniendo en cuenta sus parámetros geométricos relevantes de cara a la protección de las piernas de los peatones. En estas condiciones, se han reagrupados los segmentos en sólo tres que tienen características geométricas y estructurales suficientemente diferentes como para ser analizados por separado: Los vehículos compactos/sedan, los monovolúmenes y los todoterrenos.

Se ha elegido un modelo real de cada segmento (Audi A3, Ford S-Max, Hyundai Santa Fe) y utilizando la metodología ya presentada en esta tesis se han construido sus modelos matemáticos correspondientes. Como en este caso, los modelos de vehículo van a interactuar con modelos de elementos finitos, la geometría de los mismos se ha definido con superficies facetadas en vez de con elipsoides, como se hizo en los usados en la Sección II.

Una vez construidos estos modelos, se han simulado ambas matrices de simulaciones para comparar en cada segmento los resultados de las simulaciones realizadas con el modelo de elementos finitos del cuerpo humano, THUMS y con el impactador de pierna de la Directiva de peatones. Este análisis se ha realizado desde una perspectiva reguladora importante ya que la base de ese análisis ha sido detectar si las lesiones encontradas con el THUMS se predecían o no con el impactador, dejando posibles diferencias en términos cinemáticos en un segundo nivel.

Los resultados de esta comparación han contribuido significativamente al objetivo 3 de la tesis destacando la necesidad de considerar en el procedimiento de ensayo con impactador de pierna el efecto de la masa de la parte superior del cuerpo para valorar adecuadamente las lesiones que aparecen en las piernas, y este efecto es de mayor importancia a medida que el punto de impacto entre el vehículo y el peatón se eleva.

En la última parte de la Sección III se ha investigado la esencia de este problema y se ha propuesto un impactador mejorado que incorpore una masa extra que representa a la parte superior del cuerpo. Esta propuesta es una mejora técnicamente factible a la Directiva actual y no afecta a las bases del ensayo como se sugería en el objetivo 4 de la tesis. Esta propuesta ha analizado la naturaleza de este ensayo y se ha construido en base a un proceso de optimización que fuera técnicamente viable y no sólo mediante un enfoque meramente matemático. Así esta propuesta ha seguido un proceso en tres fases:

1. Definir las condiciones mínimas para que el impactador con la masa extra esté siempre en las condiciones de ensayo válidas para todos los vehículos europeos.
2. Identificar las limitaciones técnicas para garantizar que la base del ensayo no se modifica y aún así poder añadir la masa extra al impactador que represente la parte superior del cuerpo
3. Explorar las diferentes alternativas para alcanzar el mejor compromiso analizando como este procedimiento mejorado funciona con todos los segmentos de la flota europea.

Esta metodología ha concluido añadir al impactador rígidamente en su parte superior una masa de 5,3 kg. Con este impactador y las condiciones de ensayo del Reglamento 2009/78, (que eleva ligeramente el punto de impacto del impactador respecto al usado en la Directiva 2003/102) se observa que se mejora significativamente la predicción de lesiones con este procedimiento respecto al original, y esto es válido para todos los segmentos de la flota europea.

Para concluir la tesis, se presenta un último capítulo de resultados que recopila las conclusiones principales de la tesis y describe individualmente cada uno de sus resultados más significativos. En este capítulo se presentan los resultados uno a uno identificando cómo contribuye al estado del arte actual en seguridad de peatones y referenciando las publicaciones más relevantes que ha generado esta tesis en cada uno de ellos, con especial énfasis en aquellos de congresos, conferencias o revistas con revisión detallada por parte de expertos.

Como parte de esta tesis se ha desarrollado bajo el marco del proyecto Europeo APROSYS (Advanved Protection Systems, FP6-TIP3-CT-2004-506503) este capítulo final también vincula los resultados de esta tesis a los obtenidos en el proyecto para recomendar futuras líneas de desarrollo. En algunos casos, estas líneas futuras se proponen como tales dado que no se han abordado en esta tesis ni tampoco en el proyecto APROSYS y en otros, porque vale la pena analizar más en detalle algunas de las conclusiones aquí presentadas y en el proyecto APROSYS no estaba contemplado.

ABSTRACT

This thesis aims to investigate the critical parameters for pedestrian safety assessment of the current European fleet within the boundary conditions of the European Directives for pedestrian protection, first adopted in 2003 (EC Directive 2003/102) and later refined in 2009 (EU Regulation 78/2009).

It has first looked into the context on pedestrian safety regulation in Europe, analysing in detail the history of the different test procedures and the changes (and their reasons) they have suffered along the way. An innovative insight has been considered with the test data available on these tests, using it not only to rate the vehicles but also to gain knowledge into their stiffness characteristics, leading to one of the most relevant result of the thesis developing wide test-based stiffness corridors of the European fleet.

The in-depth accidentology analysis developed has identified for the pedestrian scenarios their key characteristics, the target population groups most involved and the most relevant type of injuries (in frequency and severity), making emphasis on the real interaction evidence between the two actual actors of this type of accidents: the impacting vehicle and the pedestrian concerned. In order to mathematically model them and simulate its interaction (in multibody environments), and considering that any vehicle make and model can be involved in a pedestrian accident influencing definitively the pedestrian outcome, a cost-efficient methodology has been developed within the thesis to construct any vehicle mathematical model with the needed detailed geometry and the stiffness characteristics required. Similarly, as any individual can be a pedestrian, this thesis has investigated in detail the important difference of mechanical properties that can be found within this age range and has implemented age scaling functionalities in the widely validated MADYMO pedestrian multibody model (already scalable in size) to allow the mathematical modelling of all possible pedestrians situations. How relevant is the change in the outcome of the accident due to the age as well as how feasible is to take this age effect into account in the test procedures are some of the most important conclusions of this thesis.

Finally, the focus is put on analysing the biomechanical nature of the most frequent injuries found in pedestrian scenarios, (head and leg injuries) using FE human body models but maintaining a testing procedural perspective. This approach has analysed how to improve the current test procedures to correlate better the injuries they prevent with the test procedures themselves, assuming that they are designed, as in any Directive, as the best simplifications of reality that could predict it. With the timeframe and the boundary conditions of the thesis in mind, the thesis has focused on just reinforcing some key issues with respect to the headform test procedures and proposing real added-value solutions to the lower legform test procedure, without changing its core basis but proposing a new impactor with an upper body mass valid for all the EU fleet segments, independent from its front part geometry.

EXECUTIVE SUMMARY

Pedestrian safety has been a leading issue on research from the early 80s when the first pedestrian models were developed (Lestrelin 1980, Wismans, 1982) and a first working group on this issue was set in the framework of the European Enhanced Safety Vehicle Committee (EEVC WG7) Thanks to the intensive research performed in this group, together with the pulling effect this work had on the rest of the worldwide automotive community, the necessary scientific basis and critical mass were developed to begin thinking on a possible regulation for pedestrian safety within Europe but also on other regions as US, Japan or Australia.

The draft of this regulation for Europe was first released under EEVC WG10 (continuation of the EEVC WG7) in 1995 using as basis accidentology evidence on pedestrian accident and mathematical multibody (MB) modelling to define the suitable impact conditions for the different test configurations, while in 2002, EEVC WG17 re-launched the work of EEVC W10, slightly amending the proposed testing procedures.

It should be noted that the tests methods developed by WG10 and later refined by WG17 were, at the request of the European Commission, developed to be suitable for use in a regulation to require manufacturers to make vehicles with pedestrian protection, and therefore, it was important that the test methods and tools were simple, accurate, repeatable and robust. To achieve this, an exercise of simplification and compromise in reproducing the accident conditions in both the test method(s) and tool(s) was necessary, since in real life each pedestrian accident is unique in some way so that there are an almost infinite number of real accident situations.

As a result, this work recommended four type of sub-system tests in each vehicle, namely legform test, upper legform test, child headform test and adult headform test, along

different parts of the vehicle front end, with testing conditions fixed for three of them (legform and the two headform) and for the upper legform based on the vehicle geometry.

These four tests were including from 1997 in the EuroNCAP programme, the official consumer test programme for vehicle safety in Europe, rising awareness of the necessity of higher standards of pedestrian safety in the European vehicles fleet and giving a decisive impulse to encourage the adoption of pedestrian testing regulation in Europe.

Moreover, including pedestrian rating in EuroNCAP had two positive collateral effects:

- It gave evidence of the robustness of the proposed EEVC pedestrian test procedures.
- It demonstrated the technical feasibility of finding solutions to ensure that vehicles could be pedestrian friendly.

The proposed pedestrian test procedures and limits, with the vast support of the EuroNCAP testing results, were intensively discussed with all the involved stakeholders and the scientific community and finally the European Commission decided in 2003 to implement a pedestrian test Directive, mainly based on the recommended test procedures proposed by the EEVC.

The final implementation of this European Directive 102/2003 diverged in some issues with the final proposed EEVC WG17 procedures but maintained its core content. However, taking into account the stringent requirements of EEVC proposal, these were decided to be required in two phases, the first in 2003, with Directive 102/2003 EC on pedestrian safety, allowing softer requirements and afterwards, in 2009 with Regulation 2009/78 with more stringent ones, close to the original proposed by the EEVC, but with some remarks.

Along this long way, many papers worldwide have been investigating further the pedestrian accident scenarios, in terms of the injury mechanisms involved and the whole body response, as well as the pedestrian test procedures themselves, in terms of the rationale of using sub-system tests instead of whole pedestrian dummy or developing new more biofidelic impactors. All this literature has already identified key points to re-visit the pedestrian procedures according to the situation today of the European fleet and part of them has been taken into account in the fine-tuning process from the first proposal of EEVC WG10 in 1995 to the current Regulation 2009/78 EC from 2009.

However, there are still some open issues for improvement not addressed due to lack of enough research based evidence and most of them have been compiled, in a comprehensive way, in the objective analysis on the “next steps for pedestrian test methods” that Lawrence (2005) did as part of the latest works of the EEVC WG17.

1. *Testing with physical pedestrian dummies might initially appear to be the most obvious test tool for assessing a car’s pedestrian protection, but there are a*

number of good reasons why this would be an impractical method when the wide range of variables that occur in real life accidents are taken into account. However, dummies will continue to be very useful for research and for testing the performance of deployable protection measures such as pop-up bonnets.

2. *For pedestrian protection, sub-systems test methods offer many advantages over dummies. However, great care should be taken to ensure that the simplifications in the test methods and tools are appropriate. One of the disadvantages of sub-system test methods is that the impact conditions for each impactor have to be specified in the test method. These impact conditions can be obtained from the results of real or simulated pedestrian impacts using appropriate vehicles. Therefore if the test methods are intended to be used to approve pedestrian safe cars, then the cars used to derive the sub-system test impact conditions must also be pedestrian friendly.*
3. *It is recommended that future research be concentrated on improving the current test tools and methods to make them more biofidelic and realistic, and on developing new test methods and test tools for other parts of the vehicle and other areas of the pedestrian's body. Considerable effort has been expended by the EEVC experts in developing the current test methods and tools. Therefore in future it may be better to capitalise on this existing knowledge by refining and improving these methods and tools rather than developing alternatives from scratch; i.e. the possibility of using a cut-down pedestrian dummy or a legform impactor combined with an upper body mass for assessing the bumper and bonnet leading edge in one test or for testing vehicles with high bumpers has been discussed. It is thought that this method offers some advantages, provided that it is found to be feasible to propel such a large impactor.*
4. *To provide protection to the selected proportion of pedestrian accidents requires impact conditions that represent the selected range of accident scenarios or the worst case within that range as well as appropriate protection criteria, although care should be taken when using injury trends from current cars to set priorities for protection to reduce specific injury types, because such targeted protection could result in transferring injuries to another part of the body.*
5. *The potential savings from pedestrian protection measures increase disproportionately with test speeds in excess of those currently being considered; however, the crush depth required to provide protection also increases disproportionately with speed. It is recommended that impact conditions for a range of speeds are provided in any new test methods, so that the final decision can be made by the appropriate authorities. However, the speed ultimately selected must remain within what is feasible to provide in terms of vehicle crush depth.*

6. *It is recommended that protection measures be kept at an injury risk of about 20 percent, because reducing them further would give little benefit at high cost. Preventing life threatening injuries is the first priority but priority should also be given to preventing injuries that are detrimental to quality of life, such as injuries likely to result in diminished mobility or mental impairment.*

7. *Mathematical simulation of the human and the car have a lot to offer in developing pedestrian test methods and cars. In fact, they have been used to specify impact conditions for the EEVC sub-system tests. In the future, a more direct inclusion of mathematical models in regulations is thought to be valuable. It is the view of WG17 that the current standards of simulation and data for validating the models are not yet suitable for virtual approval methods to replace physical testing.*

From this set of conclusions from WG17, there are 3 clear recommendations:

- Recommendation 1: Guarantee that the impact conditions set for the test procedures do still provide protection to the selected range of accident scenarios or the worst case within that range. Moreover the protection criteria suggested for them should not only prevent life threatening injuries but also injuries that are detrimental to quality of life, diminished mobility or mental impairment and be kept at an injury risk level relevant to be cost effective.
- Recommendation 2: Progress in a robust mathematical modelling of the human and the car would pave the way for a more direct inclusion of mathematical models in regulations; i.e. to define the worst case scenarios to specify impact conditions for the sub-system tests in each vehicle.
- Recommendation 3: Formulate improvements in the current test tools and methods to make them more biofidelic and realistic, especially those where there are some evidence of potential benefits, as in the case of the upper body mass.

With these three recommendations in mind, it is the humble aim of this thesis to provide research based evidence in those directions defining the following four objectives.

- **Objective 1: Analyse the accidentology evidence of pedestrian safety measures.** Reducing the uncountable possibilities of real world scenarios into specific impact conditions from recommendation 1 needs a mandatory link with the reality of pedestrian protection improvements and the evolution of the vehicle fleet. It is the first objective of this thesis to assess how the current test methods are still relevant to current accidentology trends not only highlighting its critical issues but also investigating them further to be in a position to formulate improvements in the current test tools with research based evidence, as suggested in recommendation 3.

- **Objective 2: Develop improved mathematical tools for pedestrian safety.** Directly targeted to recommendation 2, and as a need for the in-depth study of some of the critical issues identified previously, this thesis would provide new tools to analyse in detail pedestrian real world scenarios with high time and cost efficiency, namely, a scalable pedestrian MB model in size and age, a robust methodology to build vehicle mathematical models and a wide test based stiffness corridors representing the European fleet. These tools have been developed to reach the main objective of the thesis but are already very interesting results on their own, as they open wide possibilities for pedestrian safety analyses and studies to the research community.
- **Objective 3: Assess critical parameters relevance to pedestrian protection.** In line with recommendation 3, three critical parameters are analysed to show its potential to make the current test more biofidelic and realistic; one covering the whole body behaviour, in terms of how the pedestrian age influences the overall pedestrian kinematics, using MB models, and other two, using FE models, looking specifically to injury outcomes, the first on the importance of rotational acceleration for not fatal head injuries and the second on the influence of the upper body mass in the occurrence of leg injuries, typical injuries leading to long term mobility loss of injured pedestrians. The improved mathematical tools commented previously are extensively used in these assessments to model accurately real life and reach a clear understanding of the actual relevance of these parameters.
- **Objective 4: Propose feasible improvement to current test procedures.** The last objective of this thesis is to propose feasible improvements in the way the current test procedures deal with the three critical parameters identified. Considering the boundary conditions of the thesis in which the new Regulation for pedestrian safety was released in 2009, recommendations will be limited to those that demonstrate to be cost effective, technically feasible and not alter significantly the basis of the tests nor the impactors. As such, efforts have been focus on the legform test including an upper body mass, as already suggested in recommendation 3.

To achieve these four objectives, the thesis has been divided in three sections that cover the different aspects proposed above.

The Section I aims to present the framework and basis for this research, covering both the accidentology evidence in pedestrian accidents and the pedestrian test methods developed in order to countermeasure it. The section starts giving an overall but detailed vision on how the test methods were defined and how they have been tuned from the EEVC WG10 recommendation to the final European Regulation 2009/78. This process

has highlighted that the test conditions themselves have been maintained almost unaltered while the performance limits have been a continuous source of disagreement.

Linked to these methods, and taking advantage of the huge set of pedestrian test performed in EuroNCAP during this “learn by doing” process and the possibility to access part of this data, this section I also present one of the fist tools mentioned in Objective 2, which can also be considered one of most important contribution of this thesis to the research community: “the first large scale study defining the stiffness characteristics of the European fleet frontal part relevant for pedestrian protection”. This study is the first one of this kind approached at European level with such ambitious objectives and has used these EuroNCAP raw data as input to determine stiffness corridors in the different vehicle parts according to the pedestrian EuroNCAP rating system.

Although the formal objective of these tests were focused on evaluating the pedestrian friendliness of the different vehicles, having accessed the raw data channels it has been possible to process these data to obtain information regarding the behaviour of the vehicle structure and therefore use it as contact characteristics into pedestrian simulation models. This approach has opened a very wide range of studies on pedestrian safety using very realistic stiffness values and limits the cost of validating the vehicle models if their EuroNCAP ratings are known. This is especially interesting in reconstructing real world pedestrian accidents and has converted these corridors into a key tool for such tasks that can be easily integrated in accident reconstruction software.

Finally, in the last part of this Section I the accidentology basis of these methods is analysed in detail to address Objective 1. As the test methods are a compromise of worst cases scenarios, a regular link to real life is mandatory to ensure they are still representative of the original scenarios they were based on. This link to real life has been done through analysing a relevant Spanish pedestrian in-depth database, paying attention to the different variables regarding the impact conditions but also to the different injury patterns observed in fatal pedestrian and non-fatal pedestrian. The findings of this real life close look have identified the critical topics where this thesis aims to provide further research evidence recalling EEVC WG17 (2005) recommendation 1 on how real life is simplified into a relevant set of impact conditions of the different pedestrian tests.

The basics of these simplifications are analysed first in terms of real world scenarios using multibody technologies, (Section II) especially focused on the age of the pedestrian since elder pedestrians have been shown to be a critical population in these accidents, and afterwards, in terms of injury assessment using FE technologies (Section III), as the variety of possible injury outcomes that can occur in real life is covered with just a limited number of estimators in the pedestrian test methods.

Although the nature of the assessments performed for age in Section II and both head and leg injuries in Section III have been relatively different, in all cases the same

questions have been raised: How relevant is the parameter in term of assessing the pedestrian protection (Objective 3) and how feasible is introducing this effect in the pedestrian testing procedure (Objective 4).

In Section II, the analysis of real world is undertaken selecting four real non fatal scenarios that included pedestrians from the whole age range and resulted either in head injuries, leg injuries or both. The nature of this analysis, including age as a parameter, has stepped forward the current state of the art in accident reconstructions and has requested the development of new tools to build mathematically these real world scenarios, namely a scalable pedestrian in size and age as well as vehicle models, of the same make and model of the real world, with detailed geometry and stiffness characteristics.

The potential of these tools on their own has promoted them from being just a mere step needed in the process to become some of the most important tangible results of this thesis, as collected in Objective 2.

In the case of the vehicle models, as they were not commercially available as such they have been constructed ad hoc. For that a robust and cost effective methodology that ensures adequate geometrical characteristics and stiffness distribution of the vehicle models has been developed and presented in Section II.

In the case of the pedestrian model, an upgrade of the MADYMO pedestrian human model, a widely validated multibody model for accident reconstructions with the capability of being scalable in size, has been done in this thesis to allow it to be also scalable in age.

For that, an extensive study has been conducted in this Section II on how age influences the different human body tissue properties showing that, in general terms, age has a weakening effect on human tissue and therefore diminishes fracture/rupture limits up to 20% in some cases. This age effect has been analysed statistically and where relevant, has been programmed into AgedMAT; a software package developed within the thesis that allows a direct aging on different properties of the human body tissues at material levels. The outputs of this software together with appropriate geometrical transference functions have made possible to implement age characteristics in the multibody legs of the MADYMO pedestrian human model scaling on request the pedestrian model to reconstruct the four simulations with a suitable pedestrian gender, age and height.

With these models in place, the four simulations have been conducted in MADYMO using multibody techniques finding plausible pedestrian kinematics that matched accurately the evidences on the scene. The details of the four simulations (the data available from the scene, vehicle contact point and pedestrian injuries) as well as the pedestrian kinematics have been reported in Section II.

Parametric studies have been undertaken to analyse how this weakening due to age is a relevant topic to obtain realistic kinematics of the accident reconstructions and how

including or not these age fracture limits in the pedestrian models makes a difference in the outcome of the simulations. These studies have answered the question on the relevance of age proposed in Objective 3 showing a strong coupling between the fracture in the legs and the latter head impact location that can be of special relevance in the long term if a more direct inclusion of mathematical models in regulations is achieved.

Considerations regarding the feasibility to take into account age as an extra variable of the test procedures are the basis of the last part of this Section II. As this inclusion of age as parameter would imply to decrease the injury threshold at some extent, the answer to Objective 4 on feasible improvements of the current test procedures should take into account the continuous source of disagreement around the leg injury thresholds seen in the past and assume that this needed decrease would only be possible based on the development of a widely accepted elder-specific injury risk functions which, due to its magnitude, has not been feasible to be addressed within this thesis but that opens wide possibilities to continue this research on that direction.

In terms of injury assessment, although some trends can be depicted from the simulations in Section II, the measurements used to predict these injuries are not adequate enough for that purpose as they are on the inherent edge of reliability for MADYMO multibody models. This edge is defined by the simplifications done in the biomechanical modelling of some areas of the pedestrian, especially on the head and the knee regions where relevant injuries occur and not all injury mechanisms are considered in detail.

The Section III has overcome these limitations working with FE human models adding a testing procedural perspective to the injury assessment analysis as requested to address Objective 3 and 4.

In the case of head injuries, separate collaborations with ULP (Louis Pasteur University) and TNO analyse further two of the real world scenarios presented in Section II. These two separate studies reproduce with FE head models the impact window of the simulations when the head impacts with the vehicle and analyse a number of internal parameters in the head to predict the injuries.

They have demonstrated that FE tools show high correlations with the real life outcomes of the accidents and have assessed the relevance of non lineal acceleration based injury mechanisms in the non fatal pedestrian head injuries. Consequently, it has been highlighted that lineal acceleration based injury criteria is not the only nor the best estimator for all types of head injuries occurring in pedestrian scenarios (especially non fatal), particularly when there are clear accidentology evidences that high rotations are likely to occur in these cases.

In this sense, this study has allowed to obtain a number of conclusions addressing Objective 3 and identified some paths of improvements for Objective 4. These paths of improvement would necessarily involve changing the basis of the head test procedure

itself, including significant changes not only to the test conditions but also modifications to the impactor. Due to the magnitude of such tasks, they cannot be undertaken in the scope of this thesis and just some guidelines on where to focus have been proposed to be looked in detail in the future.

In the second case, as the leg impact conditions are rather more fixed in most pedestrian cases, the study is focused on which and how leg injuries occur with full body pedestrian along the different segments of the EU fleet and compares them with the injury outcome obtained with the proposed EEVC legform impactor test.

For that, two types of simulation scenarios have been constructed mathematically:

- A set of full body pedestrian scenarios where the mathematical models of representative vehicles of the EU fleet segments are impacting a THUMS 50%ile FE model, an FE human model developed by Toyota that is implemented with failure criteria for the bones and the ligaments to allow the assessment of bone fracture and ligament rupture in pedestrian accidents.
- A set of pedestrian legform test scenarios, according EEVC impact conditions, where the same representative vehicles models have been impacted by the EEVC legform impactor FE model.

The representative vehicle models have been selected based on an in-depth analysis of the UE fleet segments according to its relevance to pedestrian leg protection. Under these conditions, three segments have been identified with clear geometrical and stiffness characteristics differences that are worth to be analysed separately: Family cars, Multi Purpose Vehicle and SUVs.

A real representative vehicle in each segment (Audi A3, Ford S-Max and Hyundai Santa Fe) has been chosen and the same methodology developed and used previously within this thesis has been followed to develop its mathematical model ensuring detailed geometry and stiffness distribution. As in this case, the vehicle models are interacting with FE models, the geometry has been described using facet surfaces instead of the ellipsoids used in the vehicles from Section II.

With these models in place, two sets of simulations have been performed in order to compare in each segment, the outcomes of the simulation with THUMS FE human pedestrian model and the EEVC pedestrian legform FE model. A strong procedural perspective has been the basis of this analysis as its main focus has been in detecting if the result on pedestrian friendliness with the THUMS and the one obtained with the impactor matched or not, leaving kinematics difference and resemblances in a second level for comparison.

The results of this comparison have significantly contributed to the Objective 3 of the thesis, highlighting the need to consider in the legform test procedure the influence of the

upper part of the body for correctly assess the leg injuries, and this is of increasing importance as the height of the impact point with the pedestrian increases.

In this case, the essence of the problem has been investigated in the last part of Section III and an improved legform impactor with an extra upper body mass is proposed. This proposal is a technically feasible improvement in the test procedure without affecting to its core content as suggested in Objective 4. The nature of the legform pedestrian test itself has been taken into account when proposing an improved method with an extra upper body mass to guarantee its technical feasibility, disregarding mere mathematical approaches and addressing the problem from a three-stepped feasible optimization point of view.

1. Define the minimum conditions where the impactor with the upper body mass is always on acceptable working conditions for all EU vehicles.
2. Identify the technical limitations currently in place to ensure that the basics of this test are not altered significantly and still an upper body mass could be added.
3. Explore the different alternatives to reach the best compromise solution analysing how this upgraded test procedure would perform along the whole EU fleet.

This methodology has led to propose a mass increase in the current impactor of 5.3 kg attached rigidly to its upper part. With this impactor and the conditions of current EC Regulation 2009/78 amending slightly EEVC impact conditions, the injury outcomes as well as the leg kinematics from the real world scenarios are closely reproduced, and this is valid for all the EU segments.

Following these three main sections of the thesis, a final summary completes this work. It compiles the main conclusions of the thesis and describes individually the main results obtained. In this chapter, each result is presented one by one identifying how they contribute to the state of the art in pedestrian safety, making especial focus in the publications in peer review congresses, conferences or journals derived from them.

As part of this thesis has been performed within the framework of the European project, APROSYS (FP6-TIP3-CT-2004-506503) this final chapter also links the results of this thesis with those achieved in this project to provide coherent future paths of work. In some cases, these future paths are proposed here because they have been kept out of the scope of this thesis and nor have been addressed within APROSYS projects and in some others, because it is worth to analyse further some of the conclusions herein evidenced and APROSYS project did neither had time nor budget to do it.

SECTION I: PEDESTRIAN PROTECTION IN EUROPE.

I

This Section I aims to present the framework and basis for the research undertaken in this thesis covering both the accidentology evidence in pedestrian accidents and the pedestrian test methods developed in order to countermeasure it. This section I starts giving in Chapter 1 an overall but detailed vision on how the test methods were defined and how they have been tuned from the EEVC WG10 recommendation to the final European Regulation 2009/78. This process has highlighted that the test conditions themselves have been maintained almost unaltered while the performance limits have been a continuous source of disagreement.

Linked to these methods, and taking advantage of the huge set of pedestrian test performed in EuroNCAP during this “learn by doing” process and the possibility to access part of this data, the chapter 2 presents the first important contribution of this thesis to the research community: “the first large scale study defining the stiffness characteristics of the European fleet frontal part relevant for pedestrian protection”. This study is the first one of this kind approached at European level with such ambitious objectives and has used these EuroNCAP raw data as input to determine stiffness corridors in the different vehicle parts according to the pedestrian EuroNCAP rating system.

Finally, and giving coherence to this process, in chapter 3, focus is put back on real world in order to understand the current pedestrian protection situation needs and how they are tackled in the pedestrian test methods. The findings of this real life close look have identified the critical topics where this thesis aims to provide further research evidence recalling EEVC WG17 (2005) recommendation 1 on how real life is simplified into a relevant set of impact conditions of the different pedestrian tests.

1 PEDESTRIAN SUB-SYSTEM TESTS EVOLUTION

In most European countries, unprotected road users like pedestrians account for a significant proportion of the road accident casualties. This was recognized by the European Experimental Vehicles Committee and several studies in this field (EEVC 1982, 1984, 1985). Based on this research various recommendations for the front structure design of passenger cars were developed along with test methods and regulations to assess pedestrian protection.

In the spring of 1987 one of these proposals was discussed by the EEVC concluding that the basis of the proposal was promising however additional research was needed to fill up some gaps. The European Experimental Vehicles Committee was asked to coordinate this research and at the end of 1987 EEVC Working Group 10 was set up with the following mandate:

'To determine test methods and acceptance levels for assessing the protection afforded to pedestrians by the fronts of cars in an accident. The test methods should be based on sub-system tests, essentially to the bumper, bonnet leading edge and bonnet top surface. The bumper test should include the air dam; the bonnet leading edge test should include the headlight surround and the leading edge of the wings; the test to the bonnet top should include the scuttle, the lower edge of the windscreen frame and the top of the wings. Test methods should be considered that evaluate the performance of each part of the vehicle structure with respect to both child and adult pedestrians, at car to pedestrian impact speeds of 40 km/h. The different impact characteristics associated with changes in the general shape of the car front should be allowed for by variations in the test conditions (e.g. impact mass and velocity, direction of impact)'

EEVC WG10 started its activities in January 1988. Both governments (mostly represented by research institutes) and automobile industry were represented in the working group. A programme was set-up intended to develop the required test methods as described by the mandate.

The studies necessary to develop test methods were summarised in a first report of EEVC WG10 (1989). These development studies included full scale dummy tests, cadaver tests, accident reconstructions, analysis of accident data and computer simulations. Furthermore the developed test proposals had to be tested against representative cars of current designs to determine the feasibility of the proposals. The compatibility with existing regulations, other safety features and basic operational requirements for cars was assessed under a contract to the European Commission and under the auspices of EEVC. The contract was completed in June 1991 and included an Annex called "Frontal surfaces in the event of impact with a vulnerable road user - proposal for test methods" and was part of the second EEVC WG10 report, presented to the 13th ESV Conference in 1991.

The third and final report of EEVC WG10 was written in 1994 and focused especially on the changes and improvements with respect to the previous version of the proposed test methods described in reports from 1991, giving general background information and explaining the choices finally recommended. After that report, the Working Group 10 was dissolved.

The recommendation of EEVC WG10 defined four sub-system tests to assess pedestrian protection afforded by passenger cars:

- A legform to bumper test, performed in three locations of the vehicle bumper at 40 km/h with a legform impactor (13.4 kg) able to measure tibia acceleration and knee bending and shear. The proposed limit for tibia acceleration was 150g and those for knee bending and shear were 15º and 6 mm respectively.
- An upper legform to bonnet leading edge test in three locations of the bonnet leading edge with an upper legform impactor at impact conditions (mass up to 17 kg, velocity up to 40 km/h) depending on the vehicle geometry, able to measure femur force and bending. The acceptance limits were a total force in the femur of 4 kN and a bending moment of 220Nm.
- A child headform (2.5 kg) to bonnet top test at 40 km/h in nine locations of the front part of the bonnet, measuring head lineal acceleration to compute the Head Injury Criteria (HIC). The acceptance level for the nine tests was HIC below 1000.
- An adult headform (4.8 kg) to bonnet top test at 40 km/h in nine locations of the front part of the bonnet, measuring head lineal acceleration to compute the Head Injury Criteria (HIC). The acceptance limits for the nine tests was HIC below 1000.

$$\text{HIC} = \left[\frac{1}{t_2 - t_1} \int_{t_1}^{t_2} a \, dt \right]^{2.5} (t_2 - t_1)$$

Formula 1-1: Head injury criterion definition.

In May 1997 the former members of EEVC WG10, on request of the EEVC Steering Committee, met again to discuss technical progress and new developments with respect to the EEVC pedestrian protection test methods. Based on these discussions the Steering Committee decided in June 1997 to set-up a new EEVC working group -WG 17 Pedestrian Safety to review of the EEVC WG10 test methods (final report 1994) and propose possible adjustments taking into account new and existing data in the field of accident statistics, biomechanics and test results. Between October 1997 and November 1998 more than 100 documents were presented, analysed and discussed in six WG17 meetings, including inputs from several organisations, including ACEA, JARI and JAMA.

More recent accident statistics were analysed, showing among other findings a decrease in the proportion of injuries caused by the bonnet leading edge of modern streamlined passenger cars and that the windscreen and A-pillars of these cars are important injury areas, not covered by the EEVC test methods.

Biomechanical tests were analysed and additional accident reconstructions were performed, deriving injury risk functions, especially for leg and pelvis injuries. This resulted in an increase of the acceptance levels for the upper legform to bonnet leading edge test.

In parallel to this process, in 1997 the recommended EEVC WG10 procedures on pedestrian safety were also included in the test matrix that EuroNCAP programme performed in order to rate vehicle safety features of the European fleet. This inclusion in a consumer programme was the perfect platform to extensively prove the proposed test methods but also to get a first overview of how far were the current car design to a pedestrian-friendly vehicle. The first results on the vehicle performance were not very positive regarding pedestrian protection but boost research on pedestrian friendly solutions in passenger cars, rising to the top research issues pedestrian protection.

In both forums the pedestrian sub-system tests have been extensively evaluated and improved and EEVC WG17 has included in its report many improvements in these sub-systems. The final recommendation of EEVC WG17 (2002) included the following tests:

- A legform to bumper test, performed in three locations of the bumper, with an improved legform impactor (13.4 kg) at 40 km/h, able to measure tibia acceleration and knee bending and shear. The acceptance levels of this test were those from EEVC WG10; that is tibia acceleration less than 150g, knee bending less than 15º and knee shear less than 6mm. As this test is representative for a complete

dummy test if the bumper impact occurs at or below the knee joint, an alternative horizontal upper legform test (9.5 kg) is proposed with an impact speed of 40 km/h, when the lower bumper height is more than 500 mm above the ground. In this case, 5.0kN and 300Nm are the maximum acceptance levels for femur force and bending respectively.

- An upper legform to bonnet leading edge test (three impact locations) with an upper legform impactor at updated impact conditions (mass, velocity and angle) depending on the vehicle geometry, able to measure femur force and bending. The impact energy curves were updated, based on the results of computer simulation studies, indicating lower impact energy for streamlined vehicles, readjusting also the velocity look-up curves in order to prevent the mass being less than the practical lower limit of 9.5 kg. Due to these updates, the acceptance limits were increased to 5.0 kN of maximum force and 300Nm for maximum bending.
- A child headform, build with a new material to improve durability and avoid vibrations, (2.5 kg) to bonnet test at 40 km/h and impact angle of 50º (with respect the ground reference level) in nine locations of the front part of the bonnet (refined definition to avoid overlapping with the upper legform impact area) measuring head lineal acceleration to compute the Head Injury Criteria (HIC) and acceptance levels of HIC below 1000.
- An adult headform (4.8 kg), build with a new material to improve durability and avoid vibrations, to bonnet top test at 40 km/h and impact angle of 65º (with respect the ground reference level) in nine locations of the rear part of the bonnet (refined definition to avoid windscreen impacts), measuring head lineal acceleration to compute the Head Injury Criteria (HIC) and acceptance levels of HIC below 1000.

These final recommendations were adopted in EuroNCAP from January 2001 and were the basis for the COM to define the EC Directive on pedestrian protection, 2003/102/EC; however, as EEVC WG17 requirements were very stringent, a two stages Directive was proposed. Both stages utilised the same test procedures developed by the EEVC, but the injury limits for Stage 1 were less stringent than those from EEVC WG17, to be applied in Stage 2.

Despite the fact that the technical requirements for 2003/102/EC were only finalised after many years of discussion and negotiation, and numerous cost/benefit and feasibility studies, many vehicle manufacturers were still of the opinion that compliance with the Stage 2 limits (in fact EEVC WG17 requirements) was not feasible. For this reason, 2003/102/EC included a review clause on the feasibility of the Stage 2 limits, with the review to be undertaken using data gathered during testing to the Stage 1 requirements.

The Stage 1 of the Directive 2003/102/EC came into force in 2004, applying all vehicles with category M1, of a maximum mass not exceeding 2,5 tonnes, and N1 derived from M1, of a maximum mass not exceeding 2,5 tonnes.

The requested requirements were:

- Mandatory lower legform to bumper test. The test procedure is identical to the one defined by EEVC WG17 but the acceptance level are relaxed, allowing tibia acceleration up to 200g, knee bending angle up to 21º and a knee shear up to 6 mm. If the lower bumper height is above 500 mm, the upper legform to bumper test is performed instead at an impact speed of 40 km/h with a maximum femur force of 7.5 kN and bending moment not exceeding 510 Nm.
- Mandatory headform to bonnet test. The test procedure proposed by the EEVC WG17 is used reducing the impact energy by using an intermediate child/small adult headform of 3.5 kg impacting the bonnet top at 35 km/h in free flight. The acceptance level is set to HIC less than 1000 in 2/3 of the bonnet areas impacted and less than 2000 in the rest 1/3.
- Monitoring adult headform to bonnet and windscreen test. The adult headform test procedure suggested by the EEVC WG17 is extended to the windscreen area, reducing the speed to 35 km/h maintaining the 4.8 kg headform but for monitory purpose only. The acceptance level is set to HIC less than 1000.
- Monitoring upper legform to bonnet leading edge test performed at speed up to 40 km/h. The same procedure proposed by EEVC WG17 is adopted with monitory purpose only with acceptance levels of a maximum of 5.0 kN of femur force and a maximum of 300 Nm of femur bending.

The review on the feasibility of the Stage 2 limits was concluded in 2007 and, as a result, a number of relaxations to the Stage 2 limits were proposed. To offset these relaxations and to ensure that the reductions in pedestrian fatalities and injuries predicted for the original Stage 2 limits were still achieved, the European Commission proposed as an alternative make mandatory the fitment of Brake Assist systems, as the capacity of assisting the driver in achieving the maximum achievable deceleration in a braking situation has shown to have significant benefits in terms of pedestrian protection.

Moreover, to also contribute to this objective, the scope of the directive was extended to cover vehicles of categories M1 and N1 with Gross Vehicle Weight (GMW) above 2500 kg. These two types of vehicles are only exempted to meet Phase 1 and Phase 2 requirements if the driver's R point is either forward of the front axle or longitudinally rearwards of the front axle transverse centre line by a maximum of 1100 mm.

The Commission proposed that these revised pedestrian protection requirements should be published in a new EC Regulation which would repeal and replace the existing EC

Directive on pedestrian protection (2003/102/EC) and the related EC Directive on frontal protection systems (2005/66/EC). This new regulation, (2009/78/EC) that introduced revised Stage 2 limits and mandated the fitment of brake assist systems was published on 4th February 2009 and is also formulated in two steps approach to be consistent with the directive it replaced. Phase 1 of this 2009/78/EC is identical to 2003/102/EC and the updates are done in the phase 2 requirements. This 2009/78/EC regulation proposed the following test in the phase 2 along with requirements for the mandatory fitment of Brake Assist systems:

- Lower legform to bumper test performed with the EEVC legform impactor (13,4kg) at 40 km/h in three locations of the bumper and measuring tibia acceleration and knee bending and shear. The acceptance level for these tests were a tibia acceleration less than 170 g, a knee bending less than 19º and a knee shear less than 6 mm. In addition, the manufacturer may nominate bumper test widths of up to 264 mm in total where the acceleration measured at the upper end of the tibia shall not exceed 250 g.
- If the lower bumper height is above 500 mm, the upper legform to bumper test is performed instead at an impact speed of 40 km/h with a maximum femur force of 7.5 kN and bending moment not exceeding 510 Nm.
- Mandatory child/small adult headform to bonnet test. The test procedure proposed in the Stage 1 is maintained with a child/small adult headform of 3.5 kg impacting the bonnet at 35 km/h.
- Mandatory adult to bonnet test. The monitoring test proposed in Stage 1 is again restricted to the bonnet area, performing the test at an impact speed of 35 km/h using a 4.5 kg test impactor instead that a 4.8 kg headform.
- For both type of tests, the HIC recorded shall not exceed 1000 over one half of the child headform test area and, in addition, shall not exceed 1000 over 2/3 of the combined child and adult headform test areas. The HIC for the remaining areas shall not exceed 1700 for both headforms.
- Monitoring upper legform to bonnet leading edge test, performed at impact speed up to 40 km/h. The proposed EEVC WG17 procedure is adopted with acceptance levels equal to those to Stage 1, maximum of 5.0 kN of femur force and a maximum of 300 Nm of femur bending.

Taking into account the process as a whole and considering the time frame in which this thesis has been developed, it has been used as basis the EEVC WG17 recommended test procedures. This option has been supported on the fact that these were the tests used in EuroNCAP for rating and classifying vehicles according their pedestrian

friendliness but also because the different modification of the Directive have been based on the requirements to be set to approve the test rather than on the test procedure itself.

2 STIFFNESS CORRIDORS FOR THE EUROPEAN FLEET

As previously commented, EuroNCAP adopted in 1997 the pedestrian test procedures proposed by the EEVC to rate the friendliness of the different cars to pedestrians. Since then, EuroNCAP, own a huge database with over 3,000 pedestrian tests, typically covering at least 18 pedestrian potential impacting areas in each car, in four different test configurations (adult and child headform, legform and upper legform). (EuroNCAP, 2004).

Although these tests were designed to assess the likelihood of different injuries in the case of a pedestrian accident, considering the raw data channels, it is feasible to define procedures to process these data and derive information regarding the behaviour of the vehicle structure in those tests that can be used as contact characteristics into pedestrian simulation models.

Based on the 425 tests that EuroNCAP has made available for this, this thesis has defined procedures to derive the vehicle stiffness out of these pedestrian tests, has applied them extensively to these 425 test and has built a set of stiffness corridors for the different vehicle front parts areas.

In a first phase, the kinematics of the different test configurations has been analysed. This analysis has led to identify a set of assumptions to define a unique methodology to obtain the force-deflection characteristics for each of the three test configurations (headform tests, legform tests and upper legform tests).

Secondly, these methodologies have been applied widely to the whole set of tests (425), differentiating the adult headform tests impacting on the bonnet from the ones impacting on the windscreen base. The responses have been grouped for each test configuration (legform tests, upper legform tests, child headform tests, adult headform tests on the bonnet and adult headform tests on the windscreen base) in five vehicle groups (super mini cars (SMC), small family cars (SFC), large family cars (LFC), multi purpose vehicles (MPV) and sport utility vehicles (SUV)). An analysis on these 25 groups showed the existence of different stiffness trends in the same test configurations not linked to the vehicle groups; therefore if the corridors were based on them and take these trends together into account, it would have resulted in too broad and unhelpful corridors.

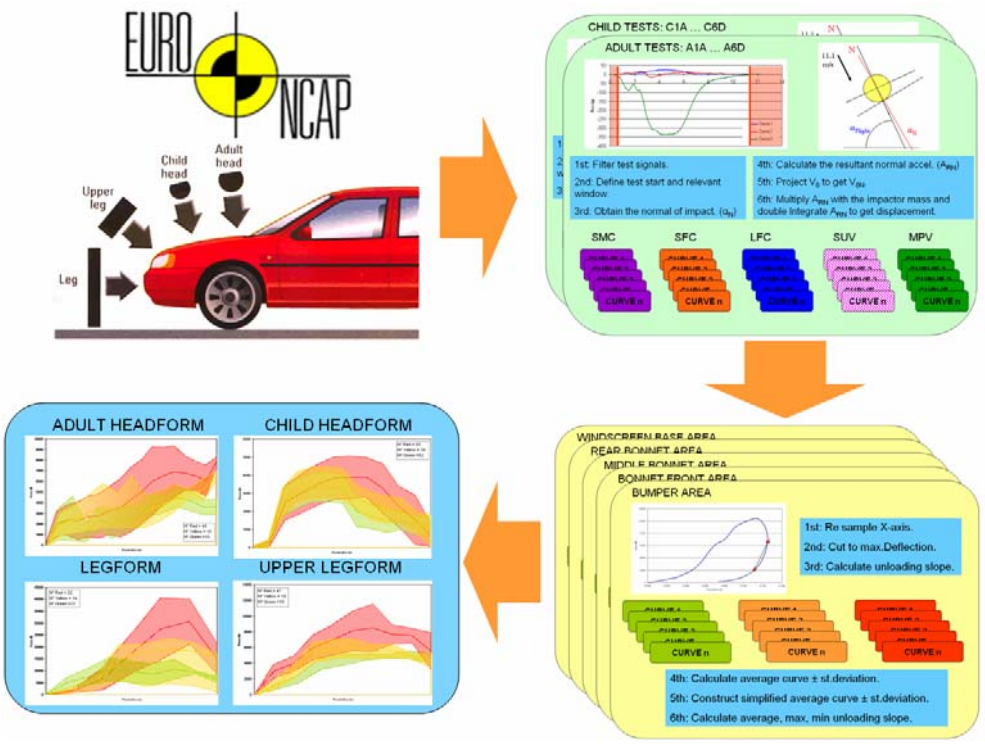

Figure 2-1: Methodology followed to develop stiffness corridors.

The EuroNCAP rating variable (red, yellow, green) was included to explain these differences and, in effect, it has turned out to match accurately the trends observed. Consequently, each test was rated individually, following EuroNCAP rating protocols, and a re-grouping was performed to the whole set of tests into red, yellow and green groups in each test configuration.

As a next step, average parameters have been calculated for each of the 15 groups (red, yellow and red groups in each of the 5 test configurations defined). To fulfil these calculations, two issues have been needed to be solved: how to deal with the difference in maximum deflection of the curves from the same group and how to work with different sample rates in deflection of the different curves of the same group to calculate averages.

Once solved, average curves, standard deviation and average unloading slopes were obtained for each of the 15 groups.

Subsequently, the corridors for these 15 groups have been derived. From the different techniques commonly used to derive corridors, collected in Hynd 2005, the average ±1 standard deviation at each point in deflection is the method used as it describes accurately the local behaviour of the curves. Moreover, in order to ease handling and dissemination of the corridors, simplified straight lines corridors have been generated for each group and they are presented in table format.

2.1 Methodology.

Considering the kinematics of the different impactors along with the instrumentation used in each of the test configurations, the most suitable methods have been chosen that obtain the force-deflection characteristics, for each of the three test configurations (headform tests, legform tests and upper legform tests) in the most realistic and univocally possible way.

2.1.1 T_0 calculation.

In most cases, no trigger signal has been available for the analysis; therefore a t_0 has needed to be set. This t_0 has been defined as the time when the corresponding acceleration or force in the impactor exceeded a certain limit, as described in Table 2-1.

Test	T_0 definition	Average time delay
Headforms	Time where Fore-aft acceleration > 2g	0.3 ms
Legform	Time where Tibia acceleration > 2g	0.4 ms
Upper legform	Time where Sum of forces > 100 N	0.5 ms

Table 2-1: T_0 definition for the different test configurations and time delay to reach it.

In order to ensure that the non-zero value of the acceleration or force in t_0 does not have an influence in the force-deflection curve calculation, an error analysis has been performed for the different test configurations.

The average time delay for the different channels to exceed their limits with respect its zero value has been calculated and summarized in Table 2-1.

Supposing a linear behaviour of the acceleration within this delay, an error in the change of velocity and in terms of deflection can be calculated as shown in the Table 2-2.

In the case of headform and legform tests, the velocity is fixed to 11.1m/s in the protocol. However, in the case of the upper legform tests, the parameters are dependent on the geometry of the vehicle.

This test configuration is performed at energy levels between 200 J and 700 J with a practical lower limit in the impactor mass (M_{UL}) of 9.5 kg, which limits the maximum speed in this configuration to 12.13 m/s. In this configuration, the worst case is considered to calculate the error.

Test	Parameter	Error
Headform	ΔV error	$\Delta v = \frac{1}{2} \cdot (2g) \cdot (0.0003\ s) = 0.00294\, m/s$
	Deflection error	$d = (11.1 m/s) \cdot (0.0003\ s) = 0.00333 m$
Legform	ΔV error	$\Delta v = \frac{1}{2} \cdot (2g) \cdot (0.0004\ s) = 0.00392\, m/s$
	Deflection error	$d = (11.1 m/s) \cdot (0.0004\ s) = 0.00444 m$
Upper legform	ΔV error	$\Delta v = \frac{1}{2} \cdot (\frac{100}{M_{LC}\ \min}) \cdot (0.0005\ s) = 0.00359\, m/s$
	Deflection error	$d = (12.13\ m/s) \cdot (0.0005\ s) = 0.00605 m$

Table 2-2: Summary of error parameters calculated.

These change of velocity errors are rather below the impact velocity tolerance of the test (± 0.2 m/s). Furthermore, these errors are within the range the accuracy for the speed measurement devices and no extra error is added in these calculations.

Regarding deflection, the error obtained in the calculation process is of 3, 4 and 6 mm for the headforms, legform and upper legform respectively, which represent 3-4% with respect to the maximum deflection values found in the different test configurations.

It can be concluded from these velocity and deflection errors that the t_0 definition is suitable as its influence in the force-deflection curve is acceptable.

2.1.2 Methodology applied for headform tests.

The pedestrian headform tests consist of a set of free flight impacts at 11.1 m/s (± 0.2) of a headform into the bonnet and windscreen area of the vehicle between wrap around distances (WAD) 1000 and 2100 mm.

The pedestrian adult headform is a 4.8kg ± 0.1 rigid sphere of 165mm ± 1 diameter fitted with a vinyl skin. It impacts on the vehicle area determined by WADs between 1500 and 2100 mm, with an impact angle of 65º (± 2º) to the ground.

The pedestrian child headform is a smaller rigid sphere, 2.5 kg ± 0.05 kg and 130 mm ± 0.1 diameter also fitted with a vinyl skin. It impacts on a vehicle area determined by WADs between 1000 and 1500 mm, with an impact angle of 50º (± 2º) to the ground.

These two headforms are equipped with a tri-axial accelerometer in the centre of the sphere and the HIC is used as the rating criterion. Further details on the headforms and the procedure are given in (EEVC WG17 2002, EuroNCAP 2001, 2004).

The next table summarizes the test parameters measured in the test and calculated in the post-process to derive the force deflection functions from the headform tests.

Parameter	Value	How to obtain
Headform mass (M_H)	A (4.8 kg);C (2.5 kg)	From the protocol.
Impact angle (α_I)	Measured.	From the test report.
Impact speed (V_0)	Measured.	From the test report.
Fore/aft acceleration (A_{FH})	Channel output.	From the test data output.
Vertical acceleration (A_{VH})	Channel output.	From the test data output.
Lateral acceleration (A_{LH})	Channel output.	From the test data output.
Normal angle at the Impact point (α_N)	*Calculated.*	*Derived from the data output.*
Normal Force at the impact (F_N)	*Calculated*	*Derived from the data output.*
Normal velocity at the impact (V_N)	*Calculated*	*Derived from the data output.*
Normal deflection (D_N)	*Calculated*	*Derived from the data output.*

Table 2-3: Tests parameters for headform tests.

Considering that the characteristic functions in multibody and facet surfaces pedestrian simulations in MADYMO need to be defined in terms of normal force vs. normal penetration (TNO, 2005), the normal at the impact point is a key parameter to get the stiffness. Moreover, its importance is higher as the headform angles of impact with the car are not always perpendicular.

The headform protocol requires that the free flight headform direction prior to impact is to be contained in a vertical plane parallel to the midline of the car. However, in the rebound phase of the tests, the headform may be ejected from this plane due to many factors, for example the structure deformation, the surface curvature. Moreover, as the impact is not performed perpendicular to the car surface, tangent forces will also appear that may induce rotation in the headform. These two effects are not considered to be relevant in the important window analysed in the tests and, therefore rotations around both axis are neglected.

In the first moment of impact, the acceleration channels signs and values are such that the resultant acceleration coincides with the normal direction of impact. In this moment, the three angles of the acceleration components with respect to the headform reference coordinate system define the orientation of the normal at the impact point in the headform reference coordinate system.

If rotations are neglected during the relevant time window of the tests, it can be assumed that:

- These three angles will be constant during the relevant test window.
- As the headform centre of gravity (c.o.g) is contained in a vertical plane parallel to the midline of the car, the lateral acceleration contribution to the normal will be always equal to zero.
- The normal resultant acceleration will be the result of projecting, with their signs, the fore/aft and the vertical components of the acceleration.

2.1.2.1 Orientation of the normal direction at the impact point.

To calculate the normal direction at the impact point, the first step is to calculate the angle ($\alpha_H(t)$) of the resultant acceleration with respect to the headform coordinate system.

This angle is the result of calculating the inverse tangent of A_{VH} and A_{FH}, transformed to degrees, for each time step in the (t_0, t_0+1 ms) interval. (For this, ATAN2 [A_{VH}, A_{FH}] Excel function is preferred to ATAN [A_{FH}/A_{VH}] because the former allows A_{VH} to be null).

This value ($\alpha_H(t)$) represents the evolution in the first moments of the impact of the angle between the A_{VH} positive direction and the normal direction at the impact point, which determines the orientation of the normal direction of the impact with respect to the headform reference coordinate system.

If this function results in a negative angle, this angle is measured in clockwise-direction and if it is positive, it is measured reversely.

The average of the ($\alpha_H(t)$) angle in this 1ms interval (t_0, t_0+1ms) is selected and defined as the normal angle at the impact point (α_H) with respect the headform reference coordinate system.

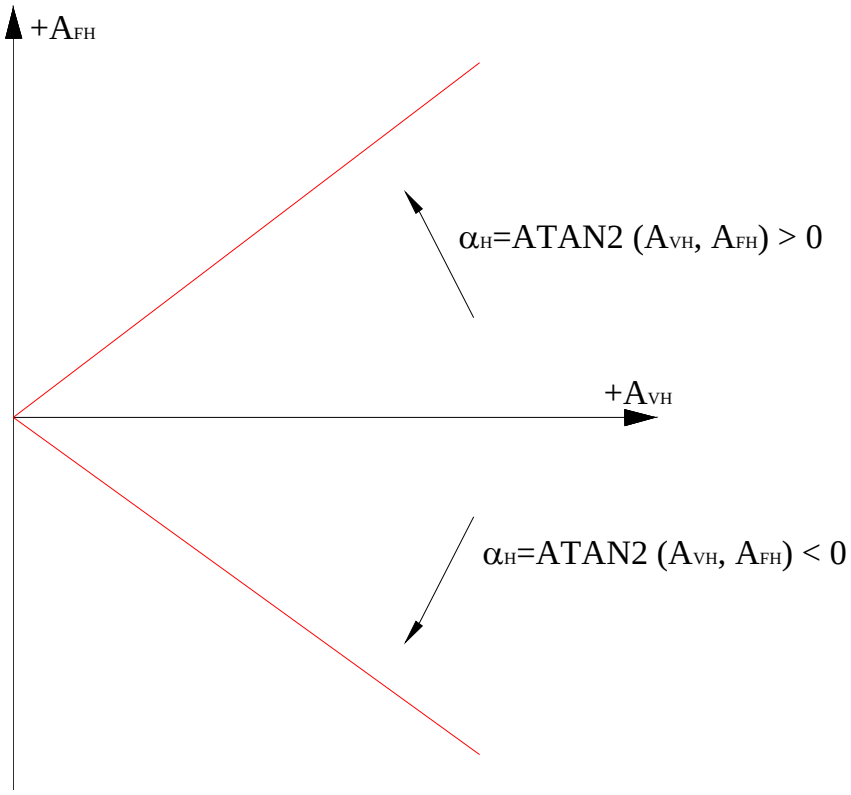

Figure 2-2: ATAN2 sign criteria for the headforms.

To compare this angle with the one measured in the real car, a conversion to the laboratory coordinate system needs to be performed. To ease this conversion, α_H is expressed with respect to the fore-aft headform direction by a 90º rotation, which lead to the α_N angle, that added to the impact angle (α_I) results in the normal direction angle at the impact point with respect to the ground level (α_{NG}). (See Figure 2-4).

This methodology has been verified geometrically in a number of tests through the measurement in the lab of the normal to the impact point in several adult and child headform test locations and compared to the data obtained analytically. Two cases on a BMW Series 1 are shown below as an example: An adult headform test impacting on the windscreen and a child headform test impacting on the bonnet.

In the case of the adult headform test, the obtained normal angle at the impact point (α_N) with respect the fore-aft direction, following the above calculations, has resulted to be -7º, which means that the normal angle at the impact point with respect the ground level (α_{NG}), considering an impact angle of 65º, turns out to be 58º.

In the child case, as the impact occurs in the bonnet, the calculated normal angle at the impact point (α_N) with respect the fore-aft directions is 27º, which lead to a α_{NG} of 77º with an impact angle for the child headform of 50º.

On the other hand, the measures obtained in the laboratory for a BMW series 1 in the same impact locations has led to normal angle at the impact point of 57º for the adult case and 79º for the child case.

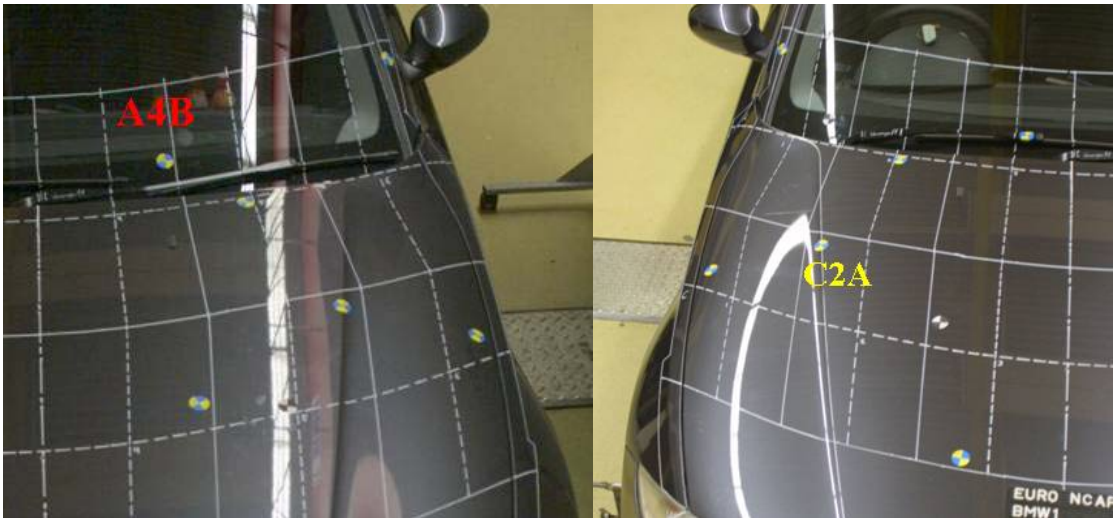

Figure 2-3: Impact point location of the adult headform and child headform tests examples.

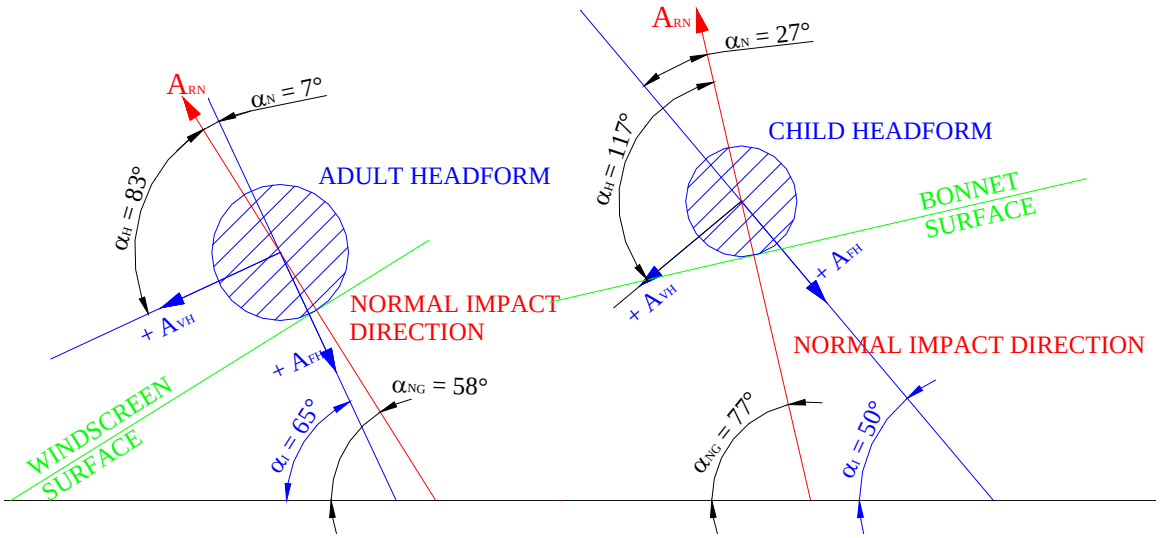

Figure 2-4: Summary of angles calculated for both tests.

These results show that the method proposed to calculate the normal at the impact point (α_N) has an error within the tolerance interval that EuroNCAP permits for the impact angles in these tests protocols, therefore it is considered to be valid for the purpose of this methodology.

Case	Calculated α_{NG}	Measured α_{NG}	Difference	Impact angle tolerance
Adult case example	58º	57º	1º	± 2º
Child case example	77º	79º	2º	± 2º

Table 2-4: Summary of angles calculated and measured compared to the tolerances in the EuroNCAP headform protocols.

2.1.2.2 Headform tests stiffness calculation.

With the assumption given regarding the lack of rotation, the next figure shows the steps followed to derive the stiffness.

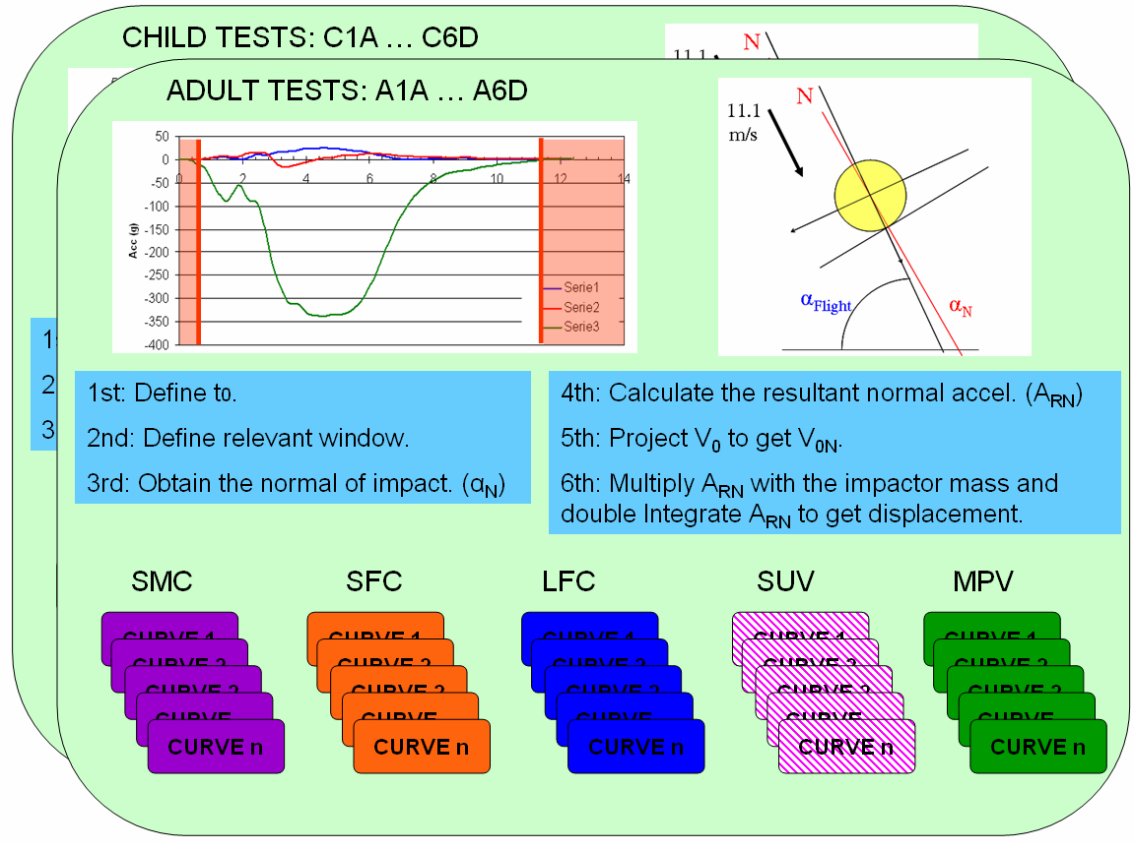

Figure 2-5: Headform tests stiffness calculation.

- The test t_0 is determined when the fore-aft acceleration (A_{FH}) exceeds 2g.
- In the (t_0, t_0 + 1 ms) interval, the normal angle at the impact point with respect the fore-aft direction (α_N) is obtained as it has been described earlier.

- The vertical and the fore-aft acceleration signals are projected with respect the normal of impact obtaining the resultant normal acceleration (A_{RN}) as the addition of both projections.
- Multiply the A_{RN} with the impactor mass, M_H to obtain the normal force in the impact F_N.
- Project the impact velocity (V_0) to the normal of impact to get the initial normal velocity (V_{0N}) at t_0.
- Double integrate the A_{RN} to get deflection D_N using the V_{0N} as the initial velocity, making the zero of the displacement at t_0.

2.1.3 Methodology applied in legform tests.

The pedestrian legform tests involve a set of, at least three tests, of a legform impacting horizontally in free flight with the bumper area of the car. The bottom of the legform impactor shall be at Ground Reference Level at the time of first contact with the bumper (tolerance ± 10 mm) and the impact velocity of the legform at this instant shall be 11.1 ± 0.2 m/s.

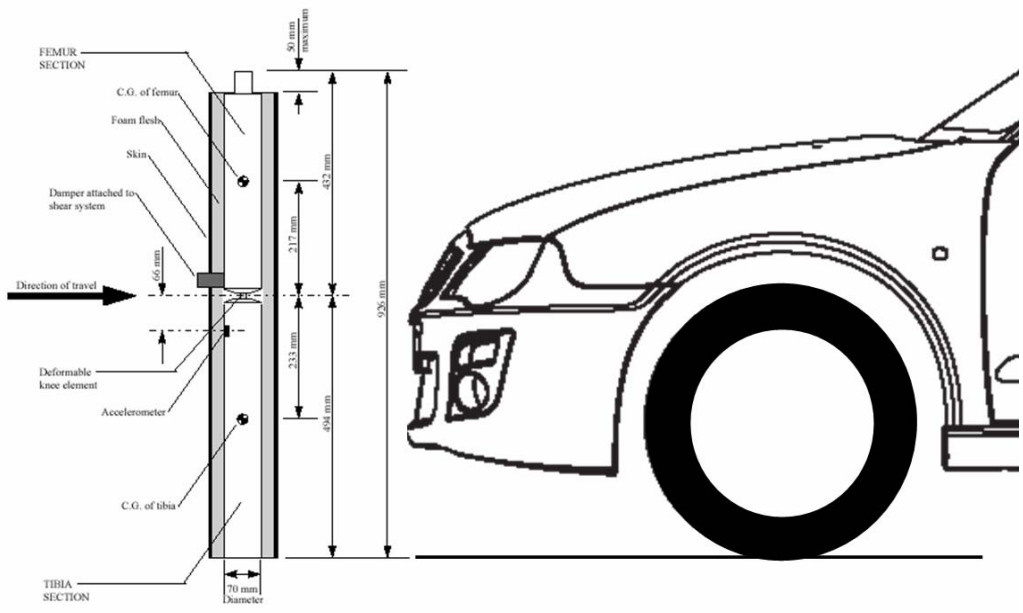

Figure 2-6: Legform test configuration.

This test is only performed to cars when the lower bumper reference line is less than 500 mm above the ground reference level.

The legform impactor consists of two foam covered rigid segments, representing femur (upper leg) and tibia (lower leg), joined by a deformable, simulated knee joint. The overall

length of the legform impactor shall be 926 ± 5 mm, having a required test mass of 13.4 ± 0.2 kg (6.8 in femur and 4.8 kg in tibia). A full description of the legform along with the EuroNCAP procedure is given in EEVC WG17 2002 and EuroNCAP 2001, 2004.

This legform is equipped with a uni-axial accelerometer in the non impacted part of the tibia and two potentiometers, one in the tibia and one in femur to account for shear and bending.

The parameters involved in the legform tests and the stiffness derivation are:

Parameters	Value	How to obtain.
Legform mass (M)	13.4 kg	From the protocol.
Test Speed (V_0)	Measured.	From the test report
Shear displacement (sh)	Channel output.	From the test data output.
Bending angle (Bd)	Channel output.	From the test data output.
Tibia acceleration (A_T)	Channel output.	From the test data output.
Force in the impact (F_L)	*Calculated*	*Derived from the data output.*
Velocity (V_L)	*Calculated*	*Derived from the data output.*
Deflection (D_L)	*Calculated*	*Derived from the data output.*

Table 2-5: Tests parameters for legform tests.

2.1.3.1 Legform tests stiffness calculation.

Considering the channels measured and the real kinematics of the bending, some channels are missing to undertake a fully realistic stiffness derivation.

In order to get some approximate values a simplification is done considering the whole legform as rigid, which is not true, but it may approximate well in cases where knee bending is low. With this assumption, the calculated force is likely to be an overestimate in most cases.

With the assumption of a rigid legform impactor, the following steps have been followed to derive the stiffness.

- Define the t_0 of the test.
- Multiply the tibia acceleration A_T with the impactor mass, M to obtain the force in the impact F_L.

- Double integrate the A_T to get displacement using the V_0 as the initial velocity and making the zero of the displacement in the t_0. This displacement includes the car structure displacement together and the crush of the impactor. (around 20 mm)

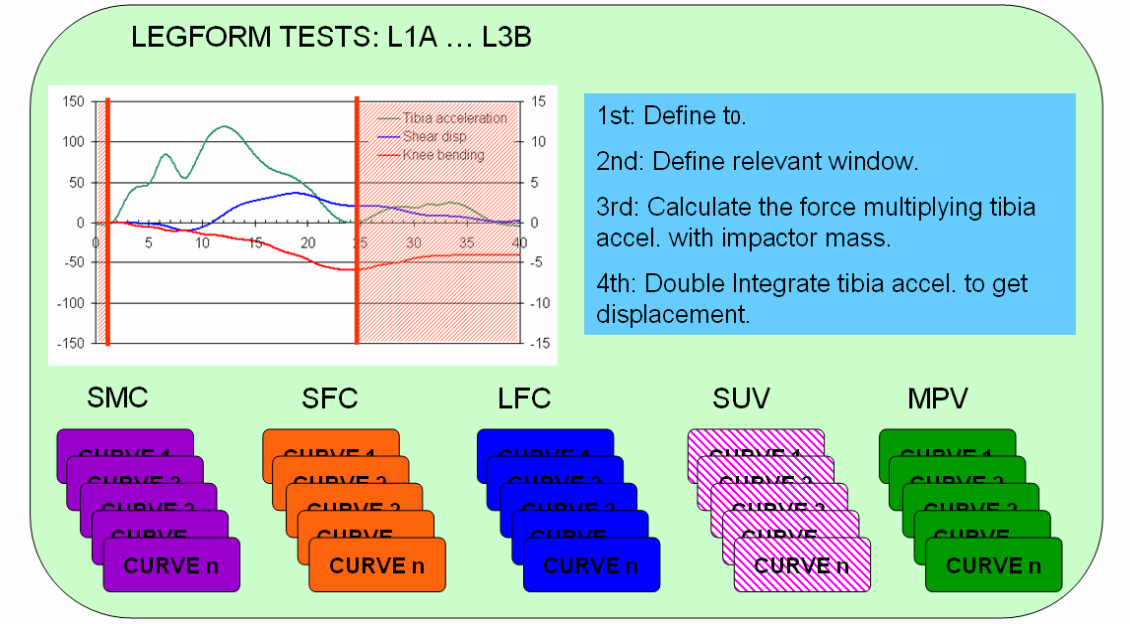

Figure 2-7: Legform tests stiffness calculation.

2.1.4 Methodology applied for upper legform tests.

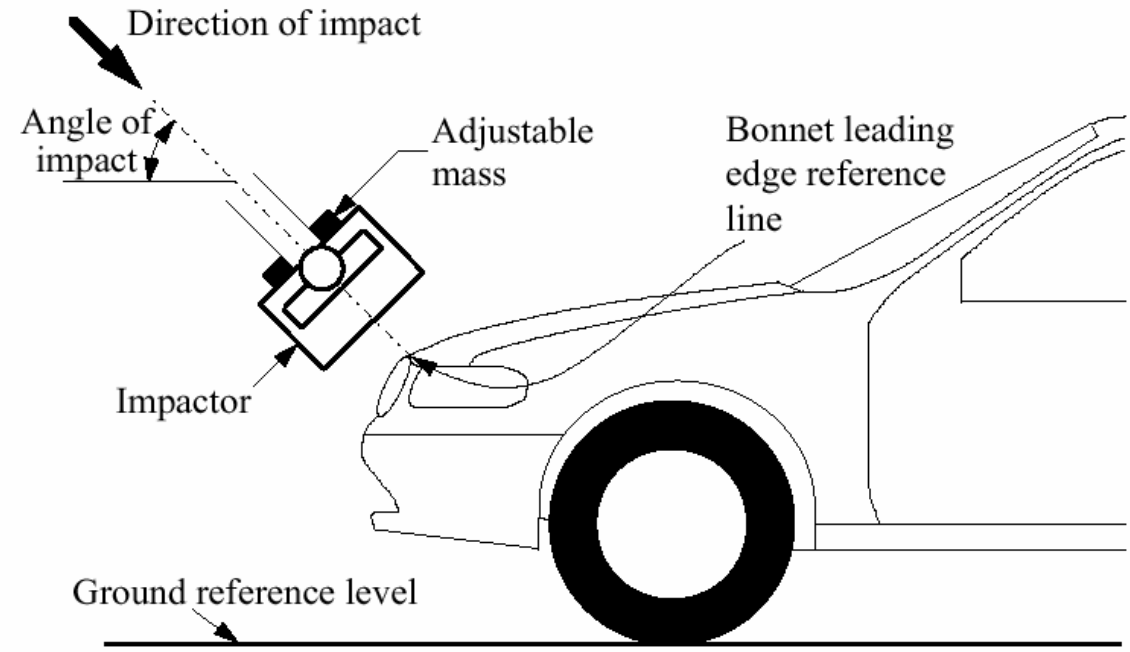

Figure 2-8: Upper legform test configuration.

The legform tests channels data consist of the following parameters:

Parameters	Value	How to obtain.
Upper Legform mass (M_{UL})	Dependent on geometry	From the test report.
Impact angle (α_I)	Dependent on geometry	From the test report
Test Speed (V_0)	Dependent on geometry	From the test report
Force Top	Channel output.	From the test data output.
Force Bottom	Channel output.	From the test data output.
Sum of Forces (F_S)	Channel output.	From the test data output.
Femur upper bend moment	Channel output.	From the test data output.
Femur centre bend moment	Channel output.	From the test data output.
Femur lower bend moment	Channel output.	From the test data output.
Upper Legform mass for the LC (M_{LC})	*M-2.55 kg*	*Derived from the data output*
Acceleration of the upper legform (A_{UL})	*Calculated*	*Derived from the data output.*
Total Force (F_T)	*Calculated*	*Derived from the data output*
Velocity (V_{UL})	*Calculated*	*Derived from the data output.*
Deflection (D_{UL})	*Calculated*	*Derived from the data output.*

Table 2-6: Tests parameters for upper legform tests.

The upper legform impactor is rigid, foam covered at the impact side and 350 ± 5 mm long. Two load transducers are fitted to measure individually the forces applied at each end of the upper legform impactor, plus strain gauges measuring bending moments at the centre of the upper legform impactor and at positions 50 mm either side of the centre line.

The total mass of the front member and other components in front of the load transducer assemblies, together with those parts of the load transducer assemblies in front of the active elements, including the foam and skin, shall be 2.55 ± 0.15 kg. The total mass of the upper impactor, as well as the impact angle and the impact velocity is dependent on

the general shape of the front of the car. Further details on the impactor, the procedure and geometry dependencies are given in EEVC WG17 2002 and EuroNCAP 2001, 2004.

2.1.4.1 Upper legform tests stiffness calculation.

As the upper legform device measures force, only a correction in mass is needed to derive the stiffness. The following steps are followed in these tests.

- Define t_0 of the test.
- Divide the sum of forces (F_S) with the upper legform mass for the load transducer (M_{LC}) obtaining the acceleration of the whole device. (A_{UL})
- Multiply the calculated acceleration with the upper legform total mass (M_{UL}) to get total Force.(F_T)
- Double integrate the A_{UL} to get displacement using the V_0 as the initial velocity and making the zero of the displacement in the very first moment of impact D_{UL}. Again, the displacement obtained through this procedure includes the displacement of the car structure together with the crush in the impactor (typically 40 mm).

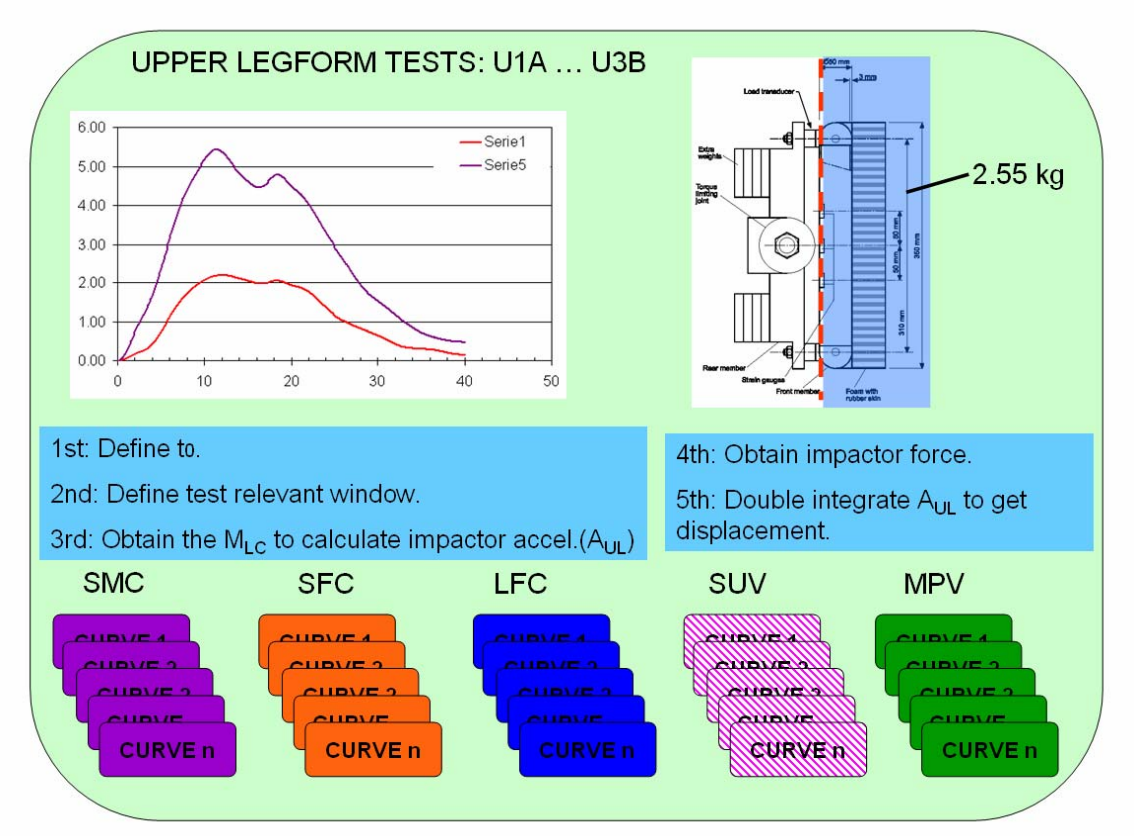

Figure 2-9: Upper legform tests stiffness calculation.

2.2 Pedestrian sub system test analysis.

2.2.1 Sample analysis.

EuroNCAP has made available for this analysis a total of 425 pedestrian sub-system tests, for a total of 26 vehicles, including super mini cars (SMC), small family cars (SFC), large family cars (LFC), multipurpose vehicles (MPV) and sport utility vehicles (SUV). This sample represents hardly 10% of the whole set of vehicles tested by EuroNCAP but it is considered to be large enough for the scope of this task.

The car models considered are included in the Table 2-7.

Segment	Vehicles	Segment	Vehicles
SMC (4)	Citroen C2 (2003) Renault Clio (1996) Rover 25 (2001) Opel Tigra (2004)	LFC (4)	Ford Mondeo (1997) Renault Laguna (1997) Opel Vectra (1997) Mazda 6 (2003)
SFC (9)	BMW Series 1 (2004) Citroen C4 (2004) Honda Civic (2001) Ford Focus (2004) BMW Series 3 (1997) Opel Astra (2004) Renault Megane (2004) VW Golf (2004) Audi A3 (2003)	MPV (5)	Ford Focus Cmax (2003) VW Touran (2003) Renault Kangoo (2003) Renault Scenic (2003) Toyota Corolla Verso (2004)
		SUV (4)	Range Rover (2002) Hyundai Santa Fe (2003) Honda CR-V (2002) Nissan X-Trail (2003)

Table 2-7: Summary of vehicles considered.

As EuroNCAP pedestrian testing has been running since 1996, the sample has included both cars tested with the current procedure from 2002 onwards and rated with green stars as well as cars tested under the former procedure and therefore rated as blue stars.

In the Figure 2-10, it can be seen that 7 out of 26 cars were tested with former EuroNCAP pedestrian protocols while 19 have been tested with the current version of EuroNCAP pedestrian protocol (EuroNCAP 2004). As the testing procedures have been essentially maintained the same but for the impact locations and the rating criteria, there is no problem to put together the older and the newer tests as all the process is performed with the test raw data and all the ratings are performed with the same criteria.

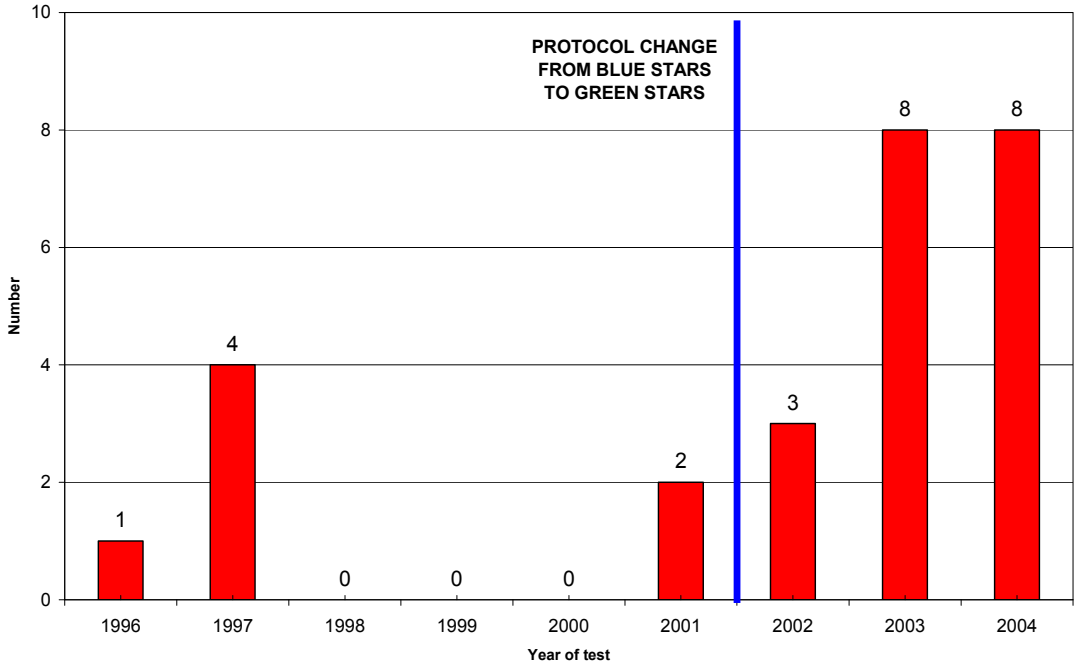

Figure 2-10: Age and vehicle type of the sample.

As defined in the EuroNCAP pedestrian tests protocol (EuroNCAP 2004), a test needs to be performed in the most dangerous points for a pedestrian to hit in each of the 18 areas in which a matrix divides its front part.

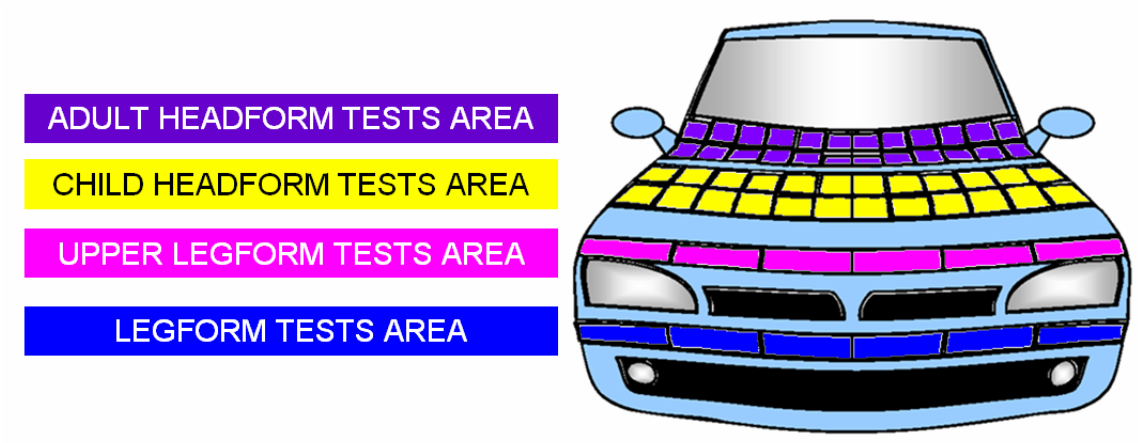

Figure 2-11: EuroNCAP defined matrix on a car.

This matrix (EuroNCAP 2004), defined individually for each car, consists of:

- Three zones for legform impact (L1 to L3) in the bumper, each divided into two (A/B).
- Three zones for the upper legform impact (U1 to U3) in the bonnet leading edge, each divided into two (A/B).

- Six zones for the child headform (C1 to C6) in the bonnet at wrap around distance (WAD) between 1000 and 1500, each divided into four (A to D).
- Six zones for the adult headform (A1 to A6) in the bonnet/windscreen base at WAD between 1500 and 2100, each divided into four (A to D).

The total number of tests analysed in this study is 425. The breakdown according test configurations and vehicle groups is found in Table 2-8. It can be seen that the numbers for each configuration match with the EuroNCAP testing matrix rather closely.

	Legform	**Upper legform**	**Child headform**	**Adult headform**	**TOTAL**
SMC	14	15	25	15	**69**
SFC	24	32	63	34	**153**
LFC	9	12	22	13	**56**
MPV	14	16	39	11	**80**
SUV	8	9	26	24	**67**
TOTAL	**69**	**84**	**175**	**97**	**425**

Table 2-8: Summary of tests considered in the study.

As three legform and upper legform tests are requested in each car, a total of around 80 tests would be expected for each of these configurations. The 69 legform and 84 upper legform tests reflect a small variation due to the symmetric points not tested and the extra test points selected by the manufacturers.

As six adult and child headform tests are requested in each area, a total of around 160 tests would be expected for each of the child and adult headforms. The 175 child tests reflect this with the same small variations than in legform tests. On the other side, the 97 adult tests reflect, along with this variation, the exclusion in the EuroNCAP protocols to test the windscreen middle and the A-pillars.

2.2.2 Force-deflection curves derivation.

Following the methodologies defined in the previous chapter, the post-processing of the EuroNCAP tests have been performed.

Considering the objectives of this chapter, the force deflection curves for each of the five configurations were classified according the vehicle segments, as shown in the next figures (Figure 2-12 to Figure 2-17). In all of them, SMCs are purple, SFCs are orange, LFCs are blue, MPVs are dashed pink and SUVs are green.

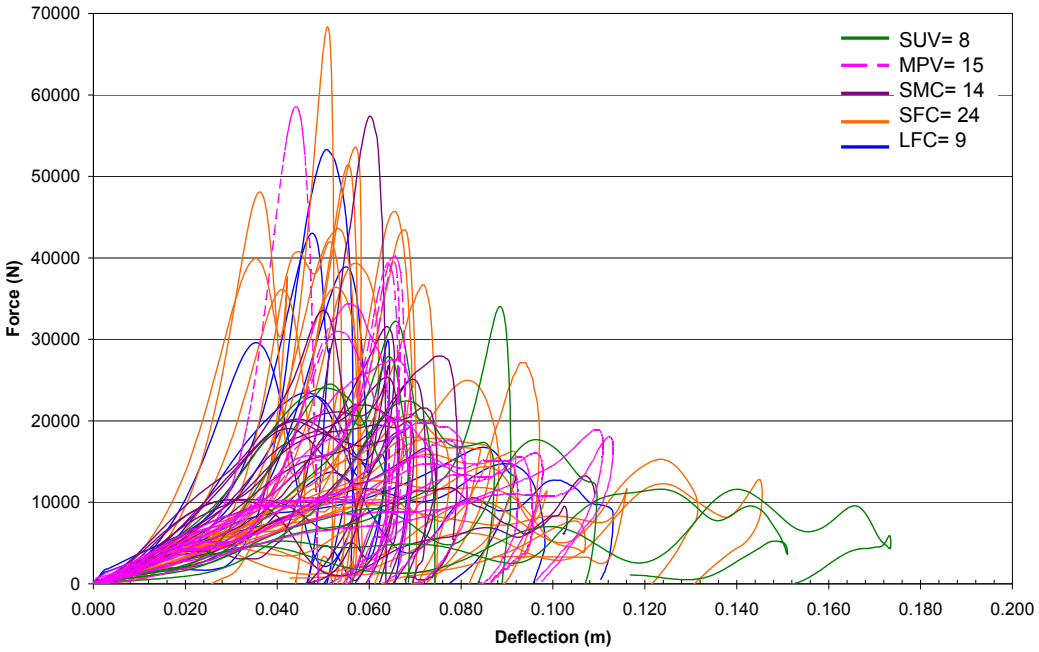

Figure 2-12: Force deflection data for the bumper (from the legform tests).

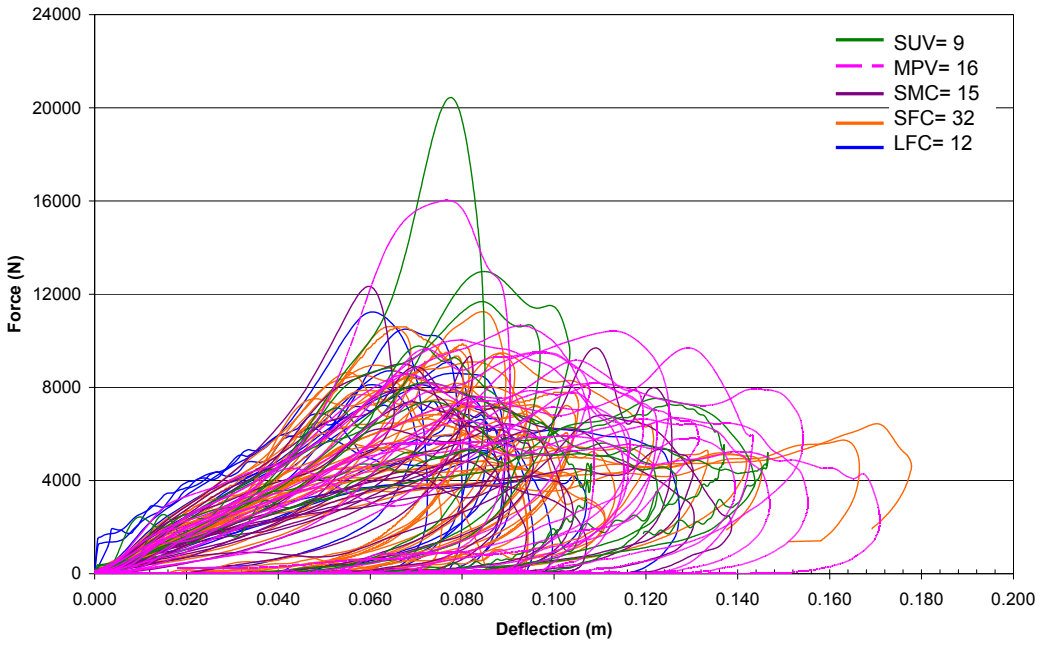

Figure 2-13: Force deflection data for bonnet front (from upper legform tests).

Regarding the bumper area, the Figure 2-12 shows great variation in the maximum peak force as well as a great difference in the maximum deflection reached.

The boundaries of such variations are limited by tests with steep slopes that reach high peak forces, (over 40 kN) in short deflections (0.04 to 0.06 m) and others where the

slopes are rather progressive, the peak forces are kept below 20 kN and the deflection generally exceeds 0.08 m.

In both boundaries, tests from different vehicle groups are found; therefore this parameter does not discriminate between these trends. In terms of unloading, most curves show rather vertical unloading slopes showing little elastic behaviour.

Regarding the bonnet front area, Figure 2-13 shows a rather narrow bunch of curves in the beginning (below 0.03-0.04 m) that start to open up from there leading to a wide range of peak forces and maximum deflections. This range starts in curves with peak force near 12 kN at 0.05 m of deflection and ends with curves with peak force of 6 kN at 0.12 m of deflection.

Again, a clear relationship can not be identified between these trends and the vehicle group as tests from different vehicle segments appears all over this range. Within these curves, the unloading slope after the maximum seems to be higher as the maximum deflection is lower.

With respect the bonnet middle area, Figure 2-14 and Figure 2-15 represent separately the done in this area with the adult headform and with child headform.

In these figures, there are a huge number of curves that reach its peak force near 0.02 m of deflection to start decreasing from then, with some slope to reach a maximum deflection over 0.06 m. This trend completes its unloading with soft slopes.

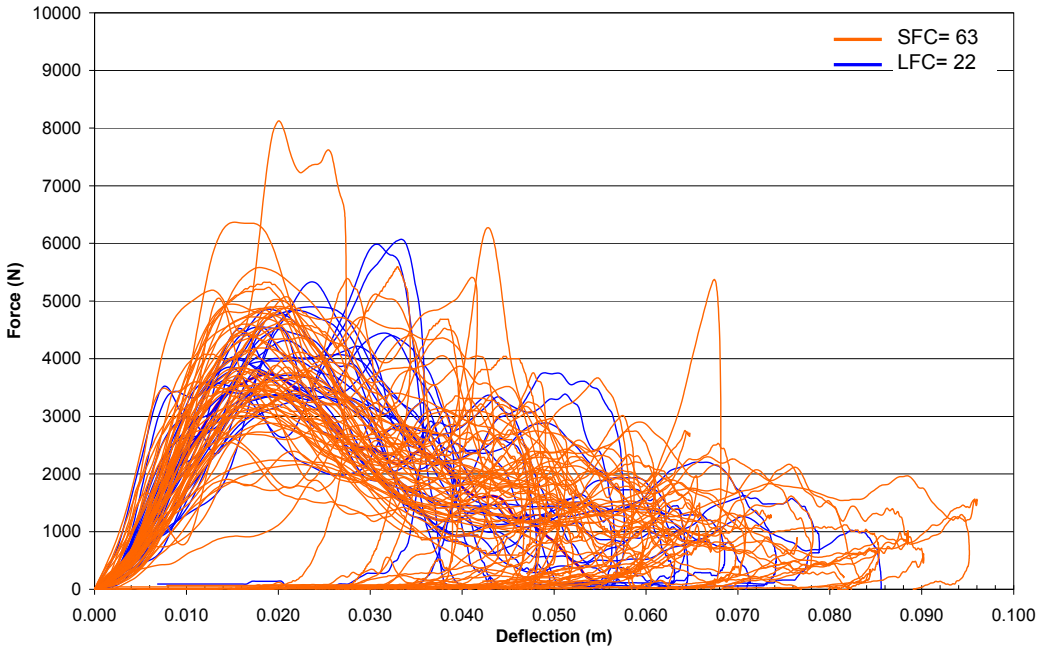

Figure 2-14: Force deflection data for bonnet middle area I(from the adult headform tests).

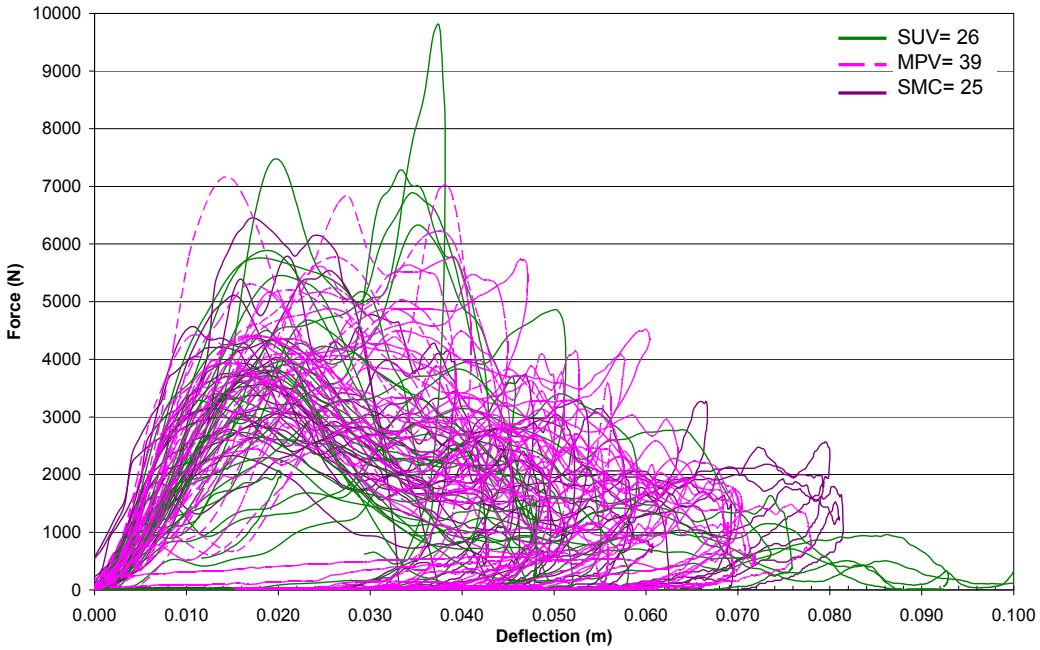

Figure 2-15: Force deflection data for the bonnet middle area II (from the child headform tests).

Finally, Figure 2-16 and Figure 2-17 collect separately the adult impact in the windscreen and the bonnet.

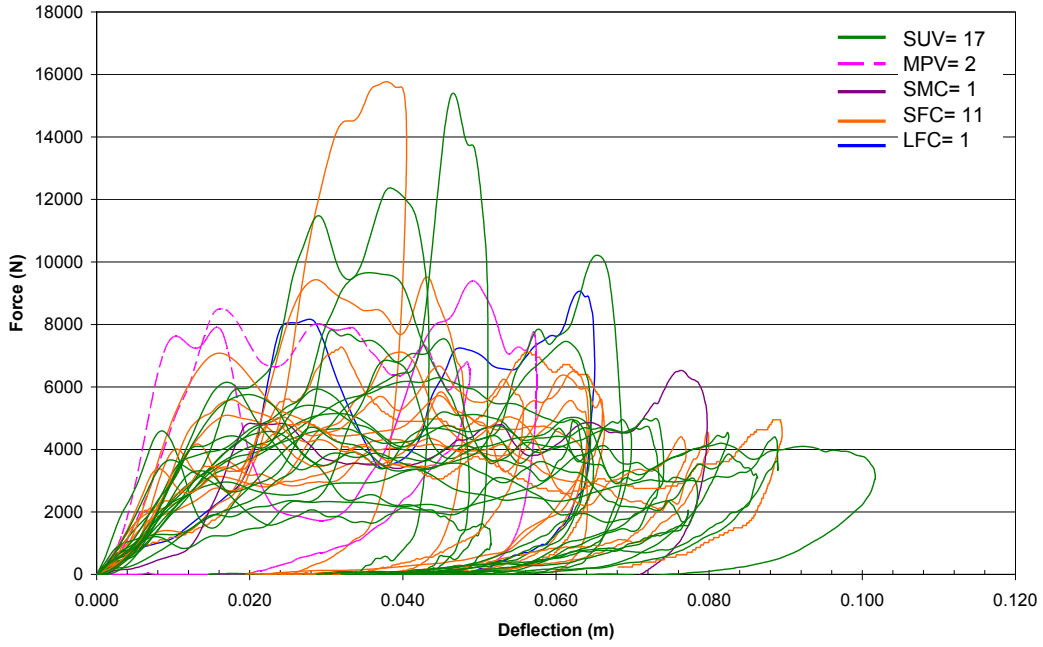

Figure 2-16: Force deflection data for the bonnet rear area (from the adult headform tests).

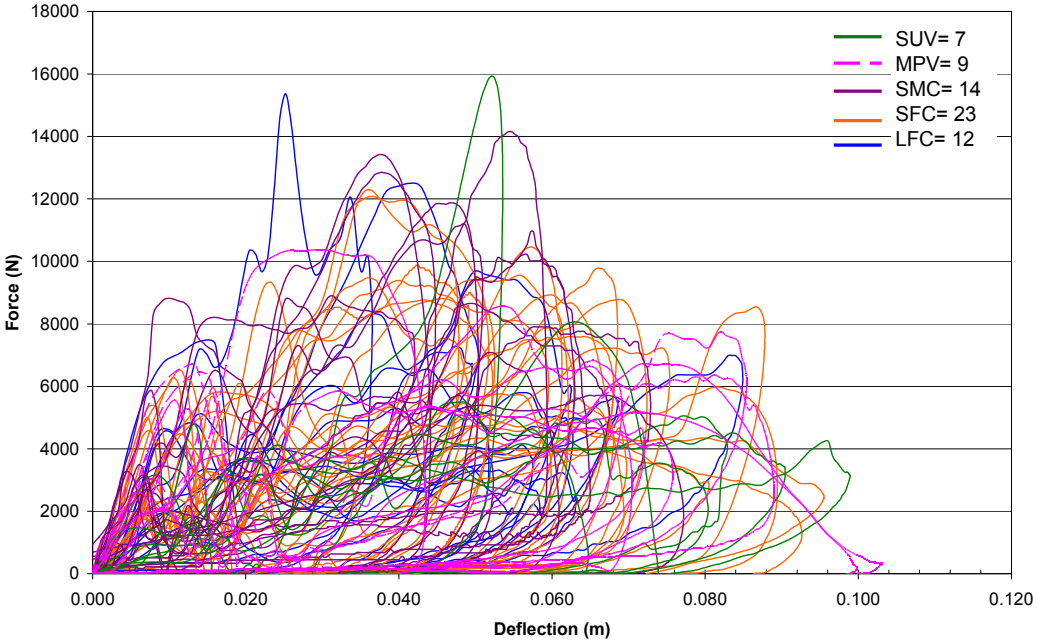

Figure 2-17: Force deflection data for the windscreen base area (from the adult headform tests).

As EuroNCAP skips the tests in the middle of the windscreen, when this document reads “adult tests impacting in the windscreen” it refers to the windscreen part supported by the dashboard and not in the middle of the windscreen. It is relevant to highlight that the number of adult tests impacting in the windscreen base area is rather higher than the number impacting on the bonnet in all segments but SUVs, where the reverse is true.

In the bonnet rear area, it can be seen increasing functions with soft loading slopes in the beginning and sudden steep slopes to get to the maximum and other functions where a plateau close to the maximum level is maintained throughout the deflection range. In terms of unloading slope, great difference appears according the former ways of loading. In this case, again vehicle group parameter does not describe the trend observed.

In the windscreen base impact it is generally observed an initial peak function to describe the breaking of the glass during the impact (independent of the colour) and then, a softer slope to get a second maximum peak force value with no link to the vehicle type. Again, the unloading slopes show a great variation being higher in the curves where higher load appears.

2.2.3 Force-deflection curves ratings.

It can be concluded from the previous figures that the different trends observed are not dependent on the vehicle groups; therefore a different variable needs to be considered to match them. A rating variable has been introduced in the analysis with such purpose.

As EuroNCAP rates each test individually to give a final rating to the car, the rating procedure followed by EuroNCAP (EuroNCAP 2004) has been applied in this point, with some remarks (* and **, see Table 2-9) to the whole set of tests. The rating procedure used is basically the one from EuroNCAP and, in addition, it gives a final colour score of red, yellow or green to each individual test according to the criteria described in the table.

Test	Red score	Green score	Yellow score
Headforms	HIC>1350	HIC<1000	HIC € (1000,1350)
Upper legform*	Max bending>380Nm **Total forces>6.0 kN**	Max bending<300Nm **Total forces<5.0kN**	Max bend € (300-380Nm) **Total Force € (5-6 kN)**
**: As the total force is the parameter considered in the process to get to force-deflection, the rating procedure has only been based on results regarding total force criteria.*			
Legform**	Max shear>7mm Max bending>20º **Max tibia acc>200g**	Max shear<6mm Max bending<15º **Max tibia acc<150g**	Max shear € (6-7mm) Max bending € (15-20) **Max tibia acc € (150-200g)**
*** As the impactor has been considered rigid in the process to get to force-deflection, the rating procedure has only been based on the maximum tibia acceleration criteria.*			

Table 2-9: Rating procedure followed in the tests.

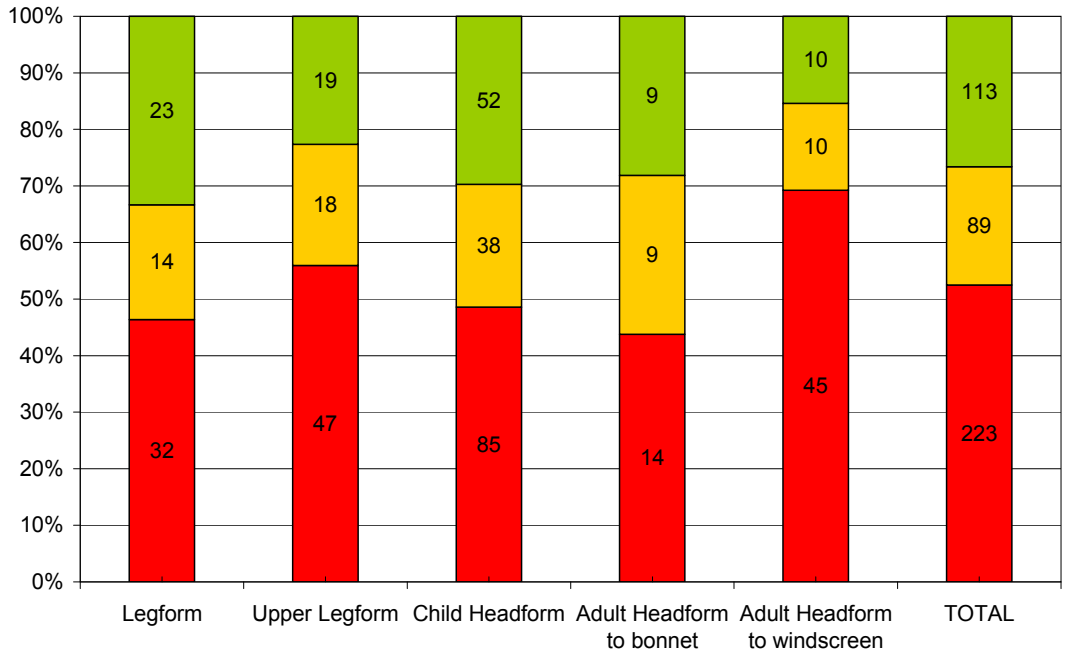

Figure 2-18: Distribution of test ratings along test configurations.

It can be seen in the previous figure that red curves represent in total over the 50% of all the tests, while green curves are near the 30%. Per test configuration, it seems that adult impacting on the windscreen area is the test configuration where red reaches its top value (almost the 70% of all the cases), while if it impacts in the bonnet area it reaches its minimum value (only the 45% of the cases). Regarding the green curves, legform seems to be the test configuration where it reaches its maximum (33%) and the adult impacting on the windscreen where it reaches its minimum (15%).

Figure 2-19 to Figure 2-23 show the whole dataset once rated according the criteria from Table 2-9. In those figures, it can be identified the different trends already suggested in the initial figures. The two trends in the legform tests are clearly highlighted and linked to the red or the green curves group.

Figure 2-19 suggests, for all the segments, the existence of a high stiffness trend characterized by steep slopes that reaches high peak forces, (over 40 kN) in short deflections (0.04 to 0.06 m) and a low stiffness trend were the slopes are rather progressive, the peak forces are keep below 20 kN and deflection stands over 0.08 m or more.

It similarly happens in the upper legform tests. Figure 2-20 shows how the narrow bunch of curves in the start (below 0.03-0.04 m) starts to open up to red curves with peak force over 12 kN at 0.08 m of deflection and green curves with curves with peak force below 6 kN at 0.12 m of deflection. Moreover, in these two configurations the yellow group fits in between the red and the green one, which is rather coherent with the process.

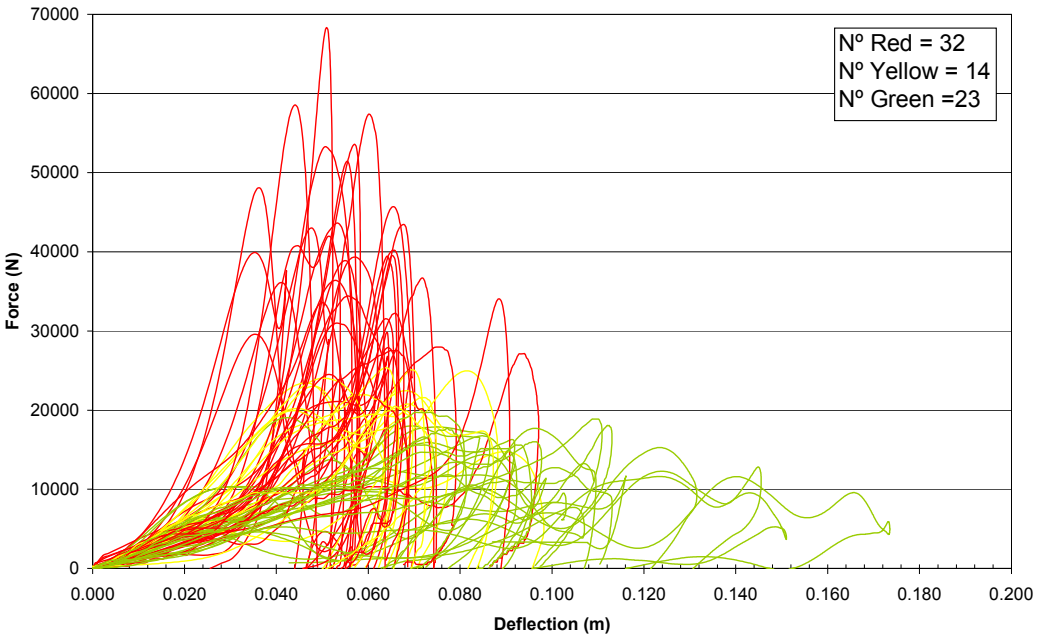

Figure 2-19: Force-deflection data for the bumper rated according Table 2-9.

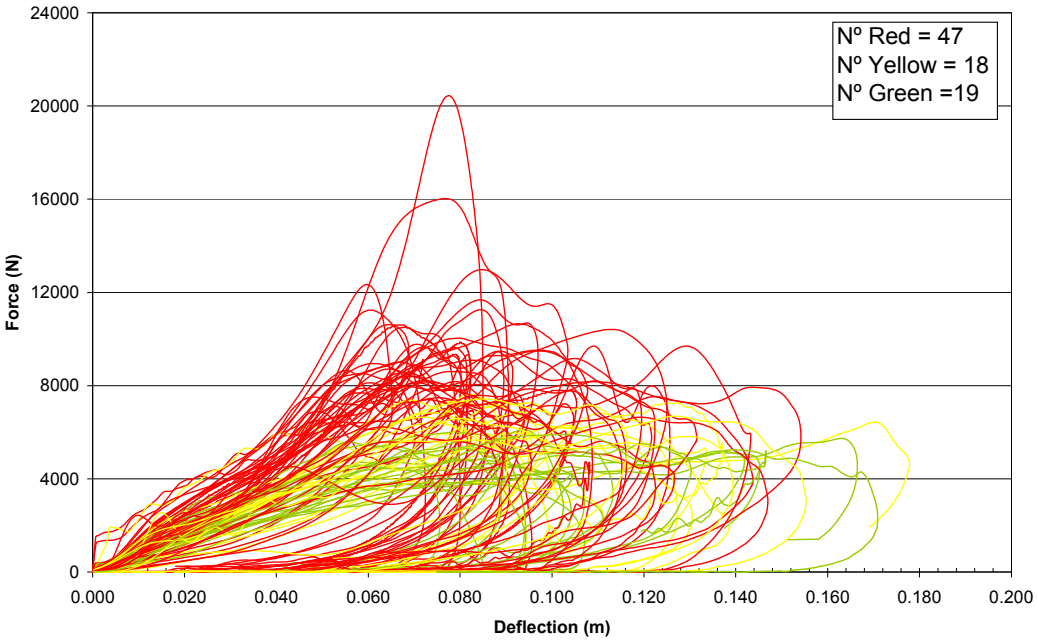

Figure 2-20: Force-deflection data for the bonnet front rated according Table 2-9.

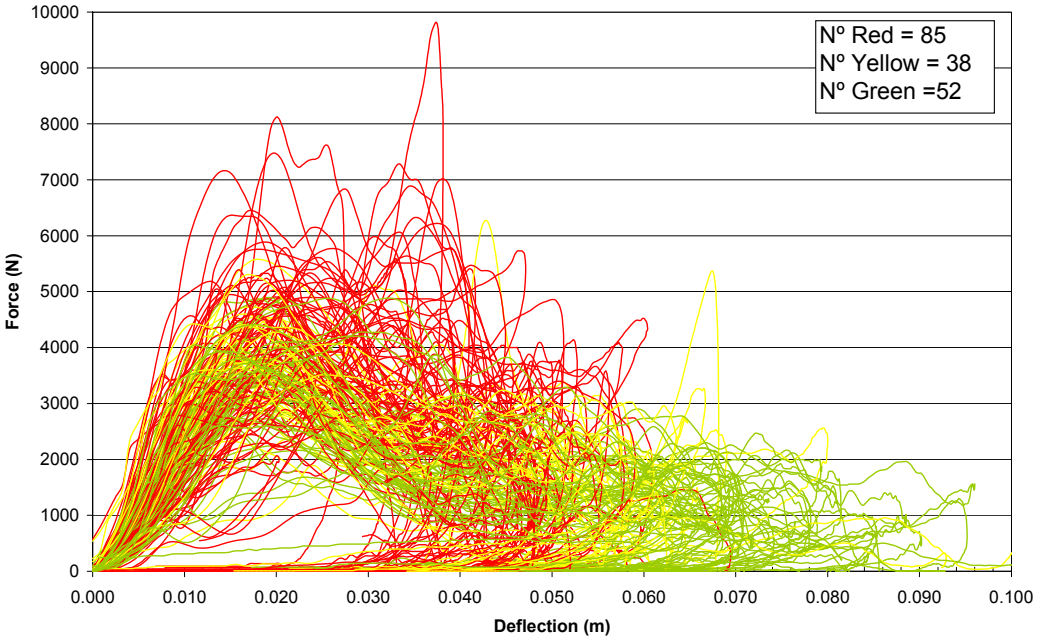

Figure 2-21: Force-deflection data for the bonnet middle rated as Table 2-9.

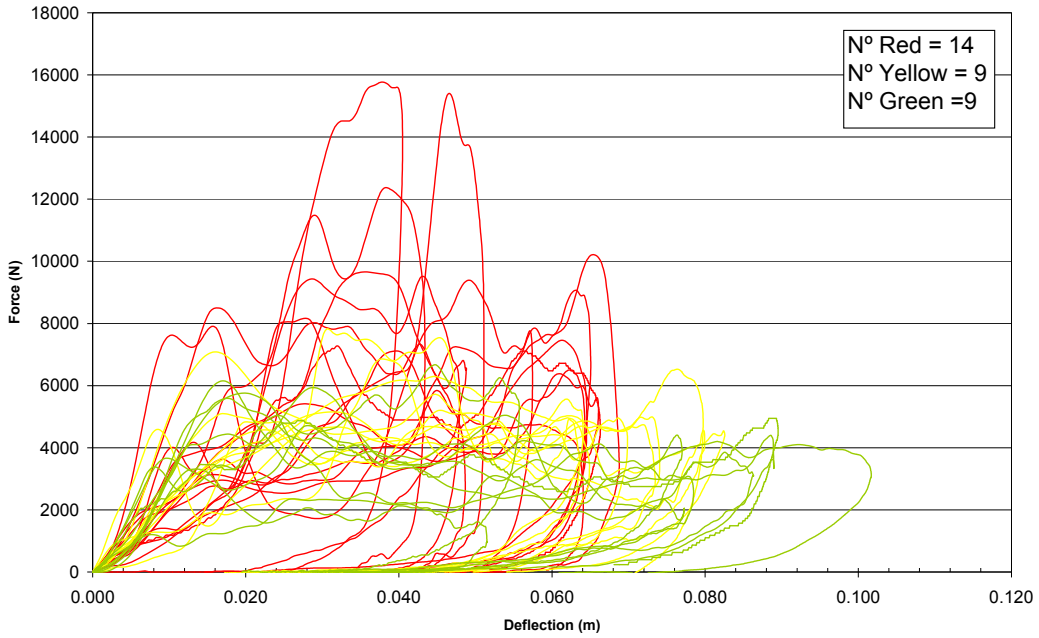

Figure 2-22: Force-deflection data for the bonnet rear rated according Table 2-9.

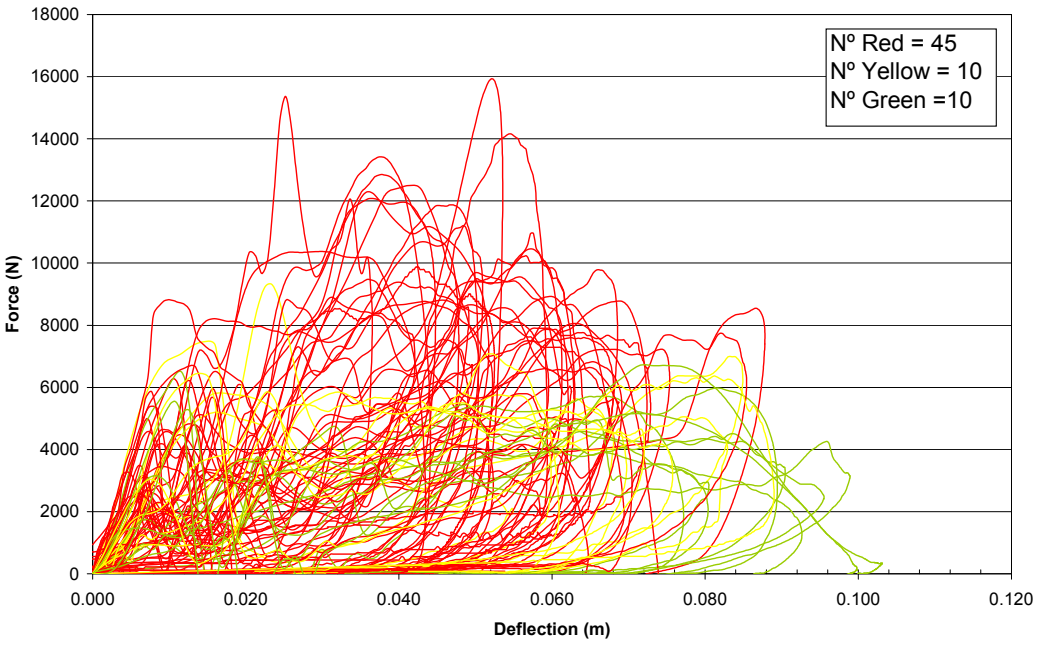

Figure 2-23: Force-deflection data for the windscreen base area rated according Table 2-9.

With respect the bonnet middle area, it can be seen that the trend already identified matches well with the green curves group while a second trend exists where deflection is kept below 0.06 m in all cases and steeper unloading slopes are registered.

Regarding the rated adult impact data, it shows coherence with the boundary trends identified previously in the case of bonnet impact while in the case of windscreen impact, it can be seen a first peak in most tests (independently of the colour rate) and a slight different slope variation in the second loading, linked to the different colours.

2.2.4 Force deflection average curves.

Once rated, average parameters will be calculated for each of the 15 groups (red, yellow and red groups in each of the 5 test configurations defined). To fulfil them, two issues have been taken into account:

- As the force deflection curves come from a cross plot between force-time and deflection-time, they result in curves with different sample rates in deflection in the same group.
- There are force deflection curves in the same group that reaches different maximum deflection levels.

To tackle the first issue, a Visual Basic application has been generated that:

- Calculate the maximum of deflection of the curve as well as the maximum peak force closest to the maximum deflection ($F_{max\text{-}Last}$).
- Cut the curve in the maximum deflection value and re-sampled it in deflection to 0.001 mm.
- Obtain, if it exists, the unloading slope of the curve determined by two points where the force level reaches 90% and 30% of the $F_{max\text{-}Last}$ respectively. In some cases, these two force levels did not represent correctly the unloading slope of the curve. For these cases, the percentages have been modified in order to best fit the unloading part of the curve.

This application has been applied to each curve of the 15 groups and once with this format, average parameters can be calculated.

In order to address the second issue, (different maximum deflection value in the different curves in the same group), and not to penalty the average curves, only the curves with force level different from 0 in each deflection step are considered in the calculation of the averages instead of using the whole set of curves.

Even with this approach, it can be observed in the averages the discontinuities caused by the end of the different curves. If the mean values were used instead, not only were these

discontinuities higher but also, at high deflection levels, the mean curves will be considerably under-estimating the actual curves.

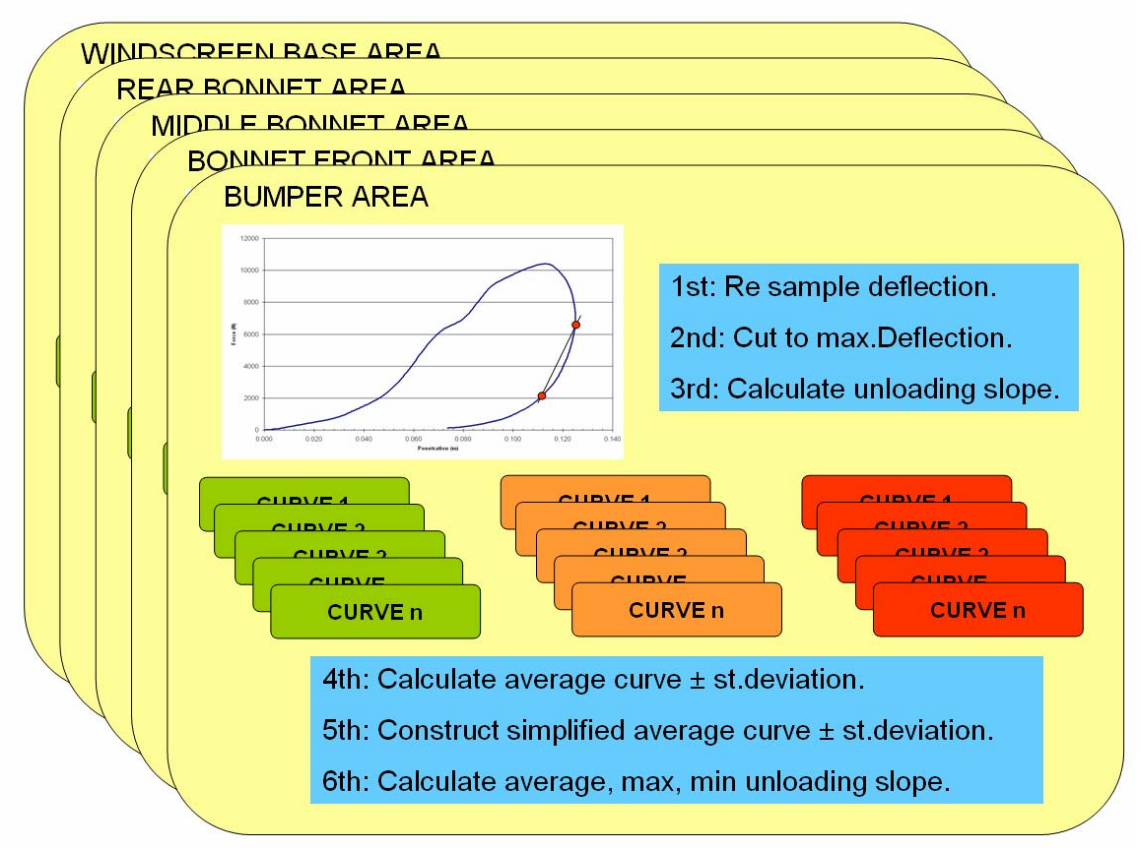

Figure 2-24: Approach to force deflection average curves and corridors.

The Table 2-10 summarizes the average unloading slopes, highlighting the number of curves with unloading with respect the total number of curves, while Figure 2-25 to Figure 2-29 show the average characteristics for the three rating groups in each of the five configurations.

It can be seen that unloading slope is registered in most cases but in bonnet middle, there are a number of cases without slopes. In general, green groups show the lowest slopes in the five configurations while red reach the highest ones, in some cases very similar to the yellow ones.

Regarding the average curves, it can be seen the differences between the behaviour of the three rating groups in the five test configurations. It is relevant to observe that the rating does reflect three significantly different average trends for the legform and the upper legform tests, while this is not so clear in the case of headform tests, where trend differences are not so highlighted.

Units: N/m	Bumper (n=63/70)	Bonnet front (n=83/84)	Bonnet mid (113/175)	Bonnet rear (n=32/32)	Windscreen (n=60/65)
Red	9.61E+07 (n=28)	1.46E+06 (n=47)	2.05E+06 (n=57)	1.32E+07 (n=14)	2.85E+06 (n=42)
Yellow	1.53E+07 (n=14)	1.66E+06 (n=18)	7.50E+06 (n=18)	8.47E+05 (n=9)	1.05E+06 (n=10)
Green	3.29E+06 (n=21)	6.30E+05 (n=18)	4.92E+05 (n=38)	4.81E+05 (n=9)	8.79E+05 (n=8)

Table 2-10: Average unloading slopes for the different groups and vehicle areas.

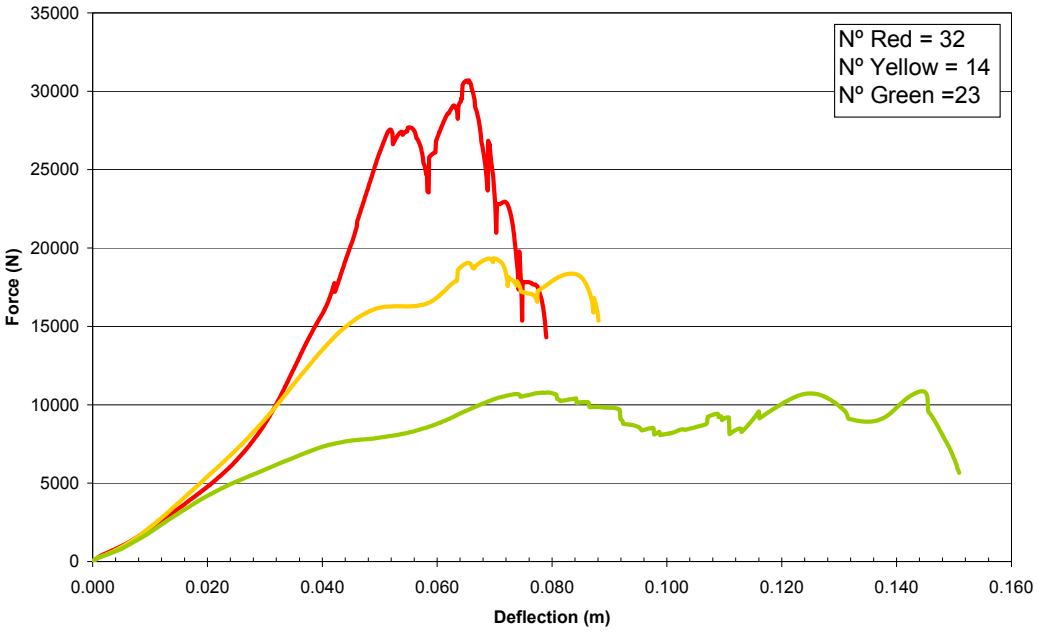

Figure 2-25: Average force deflection curves for the bumper area.

Legform red average curve reaches peak values over 25kN at deformations of 0.06m, while green average curve gets to peak values near 10kN at deformation of 0.08m and a plateau until deformations of 0.15m. In this case, the average yellow curve lies in between, with peak values below 20 kN and maximum deformations in 0.09m.

Upper legform red average curves reach a peak value of 8.5kN at 0.08m of deformation, while green stands below 5.0kN with the same deformation levels. Again, the yellow average curve lies in between with peak values of 6.0kN, although the first slope (deformation<0.06m) is the same as the green curve.

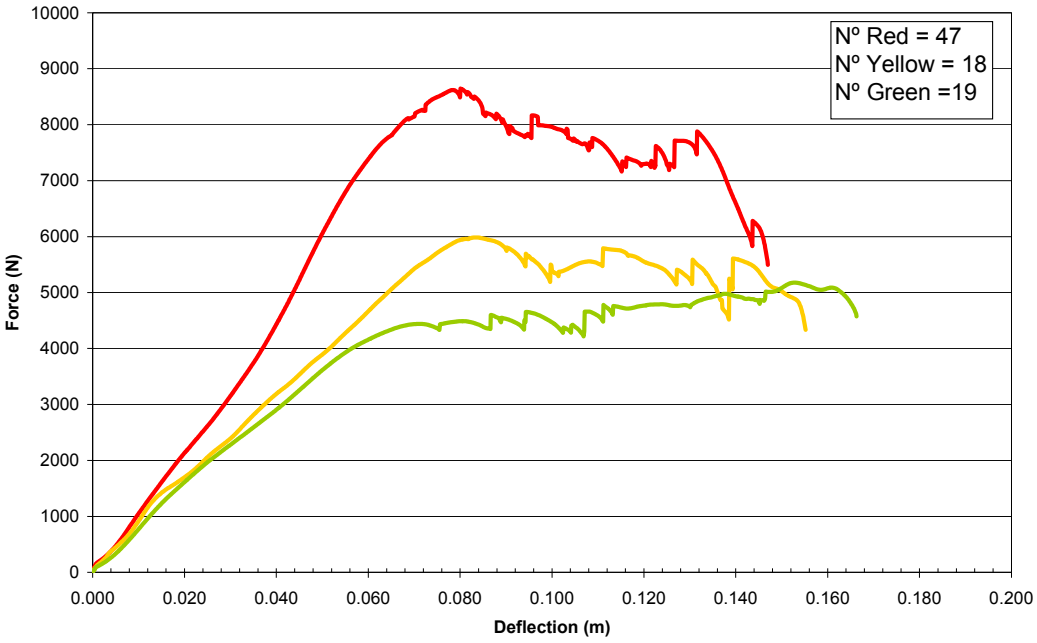

Figure 2-26: Average force deflection curves for the bonnet front.

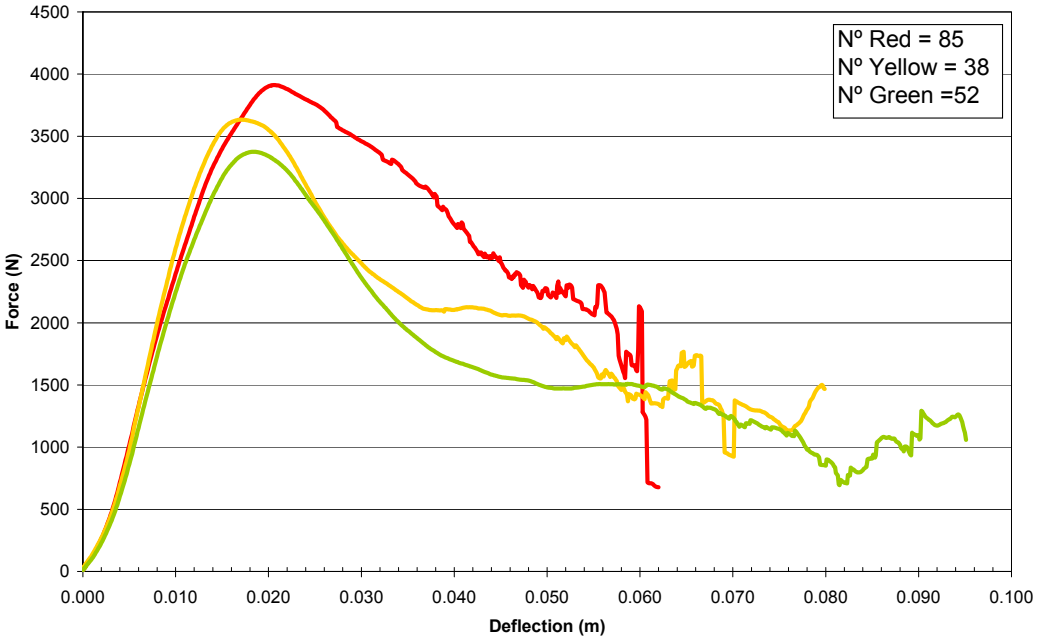

Figure 2-27: Average force deflection curves for the bonnet middle area.

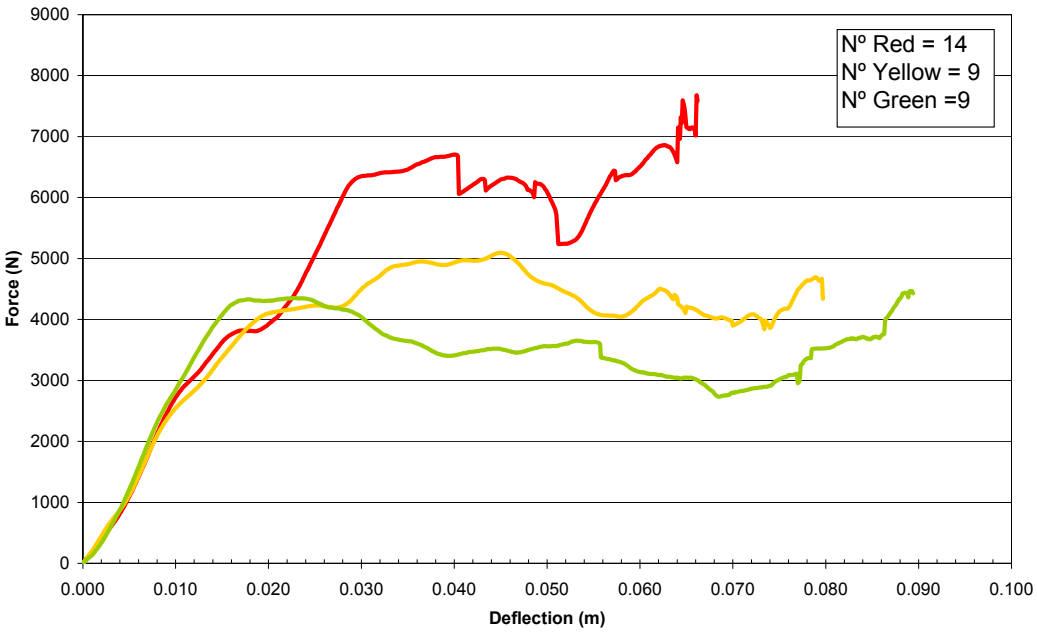

Figure 2-28: Average force deflection curves for the bonnet rear area.

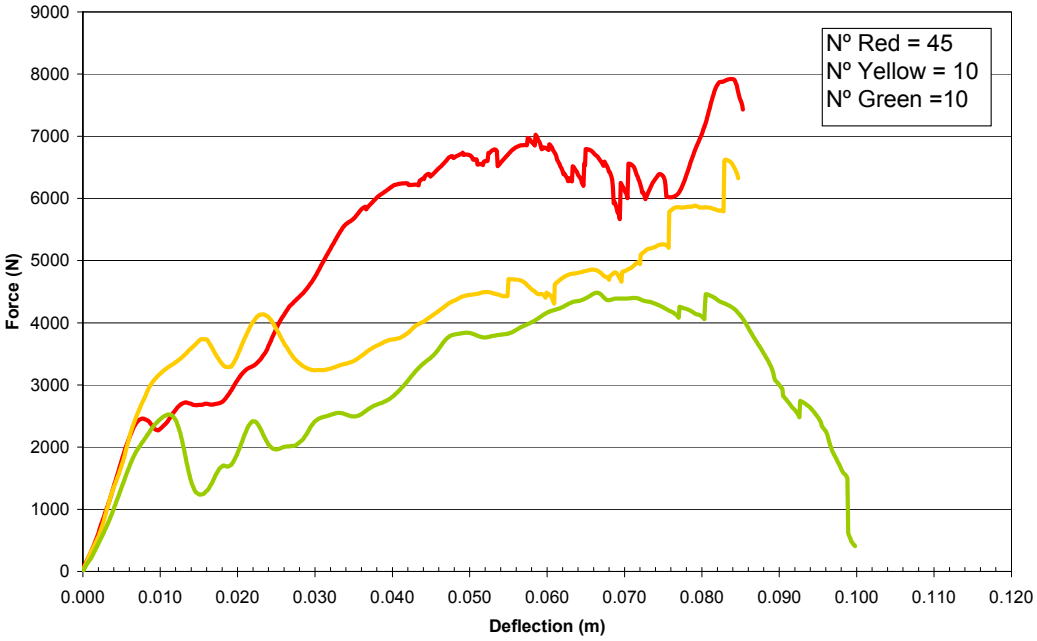

Figure 2-29: Average force deflection curves for the windscreen base area.

Regarding child headform tests, the average red curve reach a peak of 4.0kN at 0.022m of deflection while the green one gets to 3.4kN at lower deflection (0.02m). Moreover, it can be seen that the average red curve maximum deflection is 0.06m, while for the green one, it goes up to 0.100m. The yellow curve stands in between red and green (peak value of 3.6kN and maximum deflection of 0.08m). It is remarkable in this case that the initial slope (deformation<0.015m) is the same for the three average curves.

In the case of the adult headform tests on the bonnet, red trend seems to deviate from the green-yellow one only after 0.01m of deflection. Only then, the red curve continues increasing until values of 7.0kN, the green curve loads up to 4.3kN at deflection 0.018m and start decreasing from then and the yellow curve reaches its maximum also in 4.3kN but with an increasing slope until 0.05m of deflection.

Finally, the adult headform tests on the windscreen show the effect of glass breaking. The red average curve reflects it with a short plateau at deformation values of 0.01m and 2.5kN and then it continues increasing to 7.0kN at 0.06m. The green curve shows it with a first peak of 2.5kN at 0.01m and then, following an unloading phase, a moderate increasing phase until 4.5kN at 0.08m. Finally, the yellow curve, again mostly between the red and green curve, increase to values of 4.0kN at 0.02m, maintains similar values up to 0.03m, and then continues increasing up to 6.0kN at 0.08m.

2.3 Proposed stiffness corridors.

There are several options commonly used to derive corridors out of a sample of curves, as collected in Hynd 2005. The most relevant are:

- Average ±25% of the peak average value.
- Average ±1 standard deviation of the average peak value.
- Average ±1 standard deviation on each point.

Considering the great variation in force and deflection level of the peak value, the average force ±1 standard deviation at each point in deflection is the method preferred to derive the contact characteristics corridors as it describes better the local behaviour of the curves.

However, due to that great variation, an overlapping between rating groups in some of test configuration appears, especially for the cases of the headform impactor.

With these premises the corridors are built and shown in Figure 2-30 to Figure 2-34.

For the case of unloading curves, it is analysed more as a range of variation (maximum-minimum) than as a corridor format, and as this, is presented in Table 2-11.

Units: N/m	Bumper	Bonnet front	Bonnet mid	Bonnet rear	Windscreen
Max	7.07E+08	1.70E+07	2.63E+07	1.38E+08	1.84E+07
Average	9.61E+07	1.46E+06	2.05E+06	1.32E+07	2.85E+06
Min	1.58E+06	1.45E+05	4.031E+04	6.63E+04	1.6E+05
Max	1.35E+08	1.04E+07	8.82E+07	1.85E+06	6.0E+06
Average	1.53E+07	1.66E+06	7.50E+06	8.47E+05	1.05E+06
Min	9.73E+05	9.00E+04	5.85E+04	1.40E+05	7.71E+04
Max	2.17E+07	2.08E+06	4.68E+06	1.51E+06	4.00E+06
Average	3.29E+06	6.30E+05	4.92E+05	4.81E+05	8.79E+05
Min	2.51E+05	1.39E+05	2.85E+04	7.96E+04	2.01E+05

Table 2-11: Maximum, average and minimum unloading slopes for the different groups and impacted vehicles area.

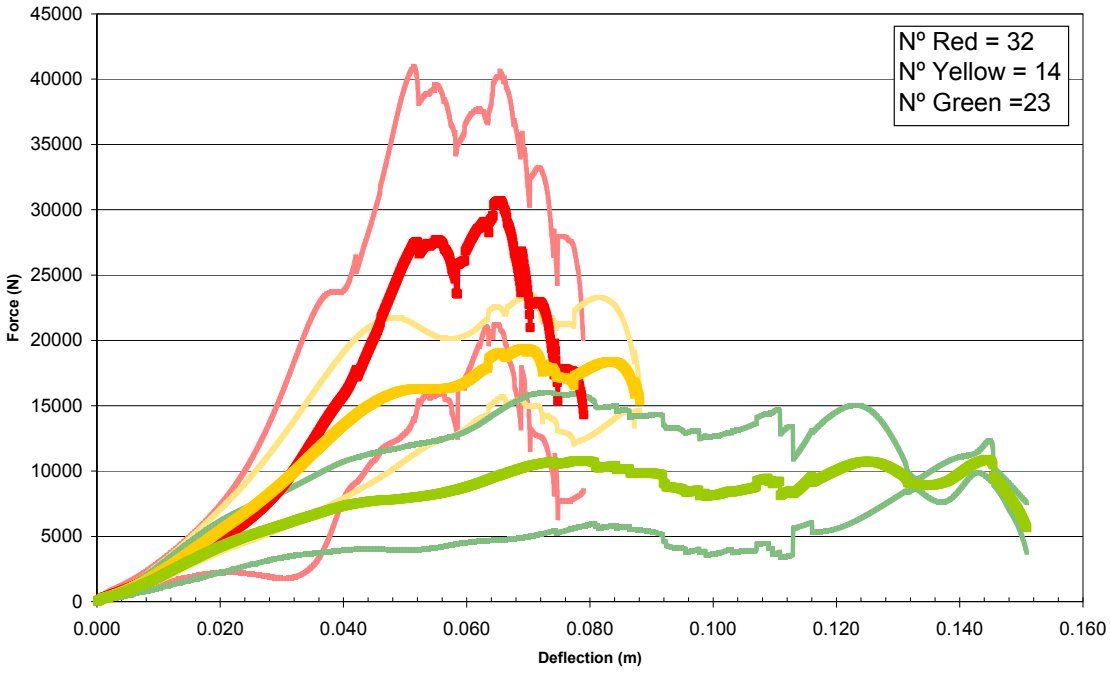

Figure 2-30: Force deflection data for the bumper.

It can be seen in the Figure 2-30 that the corridor for the red group is broader than the green and yellow ones, especially in the areas of maximum forces and considerably shorter in deflection, so, a significant difference is seen between the three behaviours.

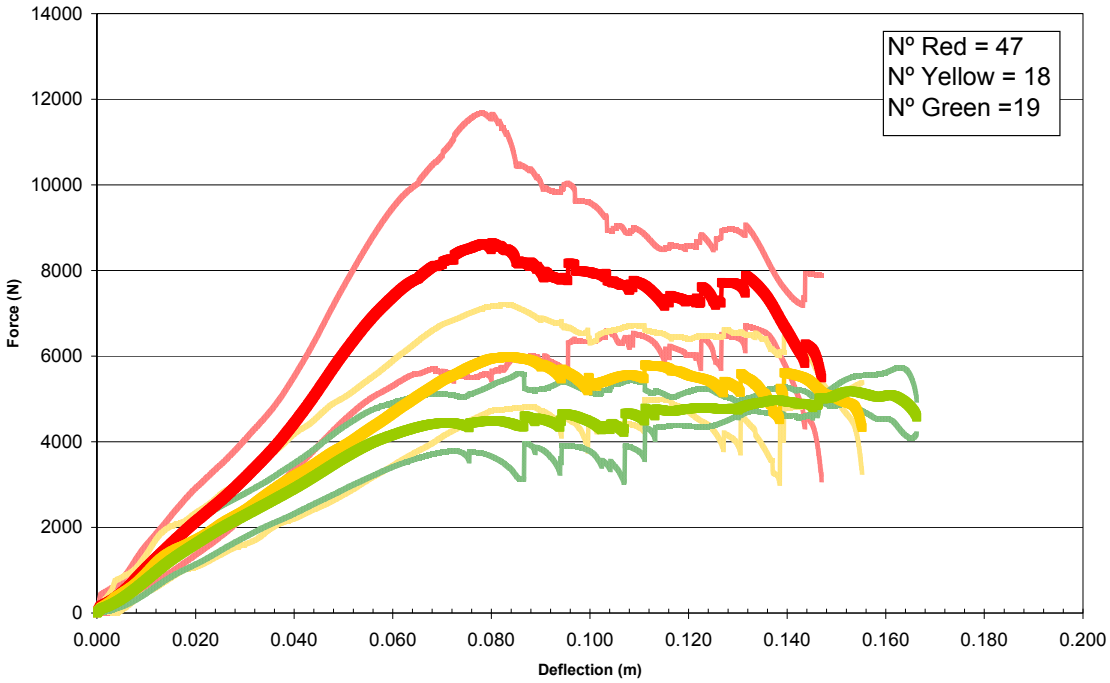

Figure 2-31: Force deflection data for the bonnet front

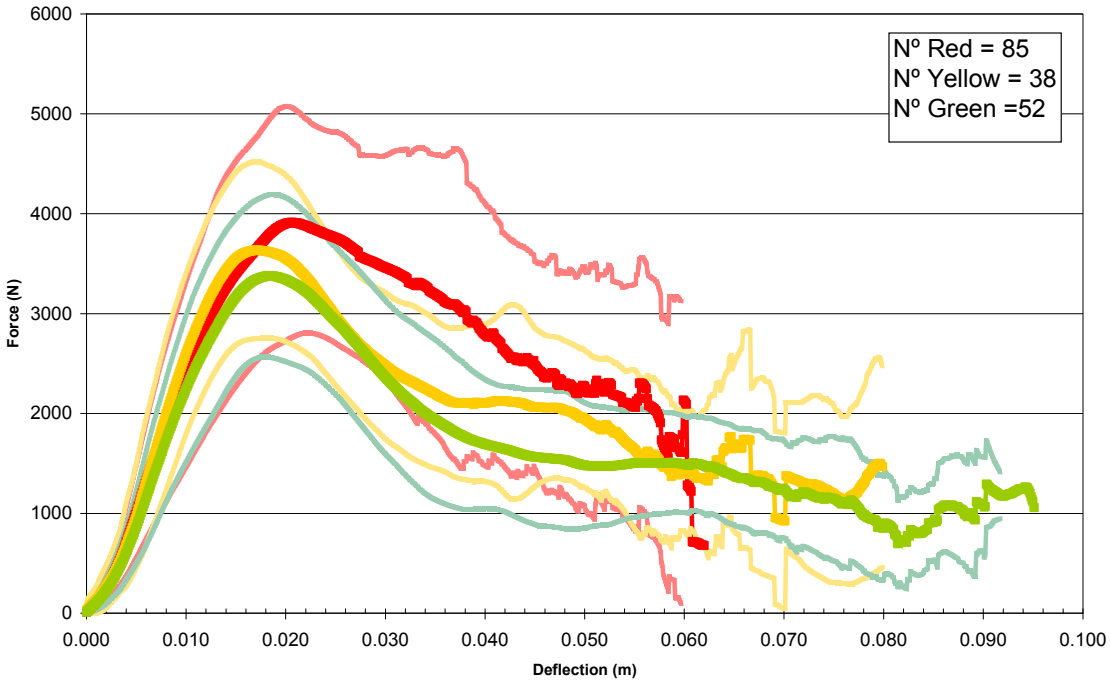

Figure 2-32: Force deflection data for the bonnet middle

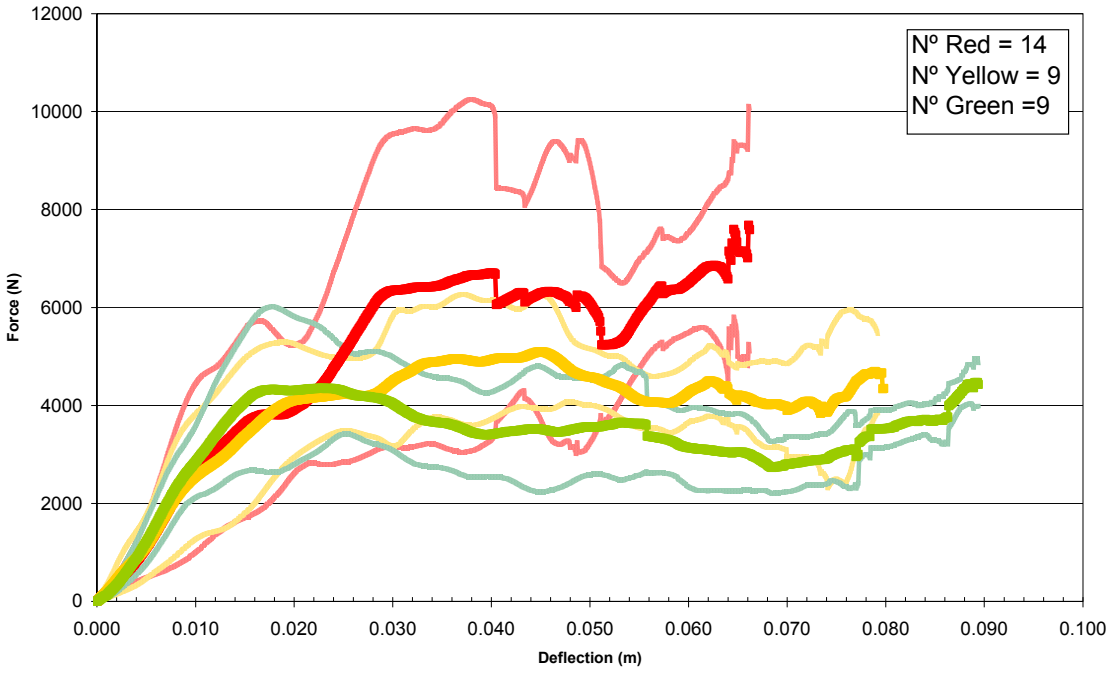

Figure 2-33: Force deflection data for the bonnet rear area.

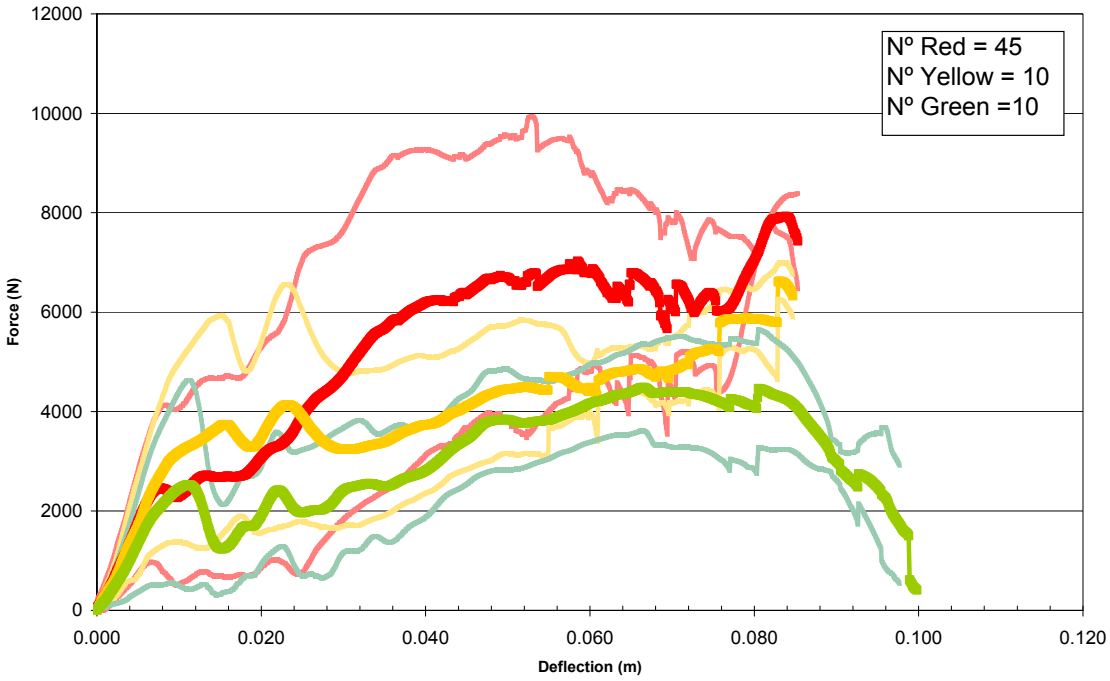

Figure 2-34: Force deflection data for the windscreen base area.

In the case of upper legform, the red corridor width is again higher than for the yellow and green corridors, but the deflection ranges are rather similar. In any case, the overlap between the three corridors is clear, especially for the yellow and the green one, as it can

be seen in the Figure 2 31. In the case of headforms, the corridors overlap considerably, especially the green and yellow ones. Moreover, for the three configurations, the lower half red corridor is partially contained in the yellow or green corridors while the upper half red corridor stands differentiated.

In order to ease handling and dissemination of these corridors into pedestrian simulations, a simplified version of them has been built and showed in the next figures. With this approach, these curves can be easily implemented into a simulation model. The similarity of the simplified curves with the real curves has been ensured by restraining the difference in area below each curve to less than 1‰ difference in all cases.

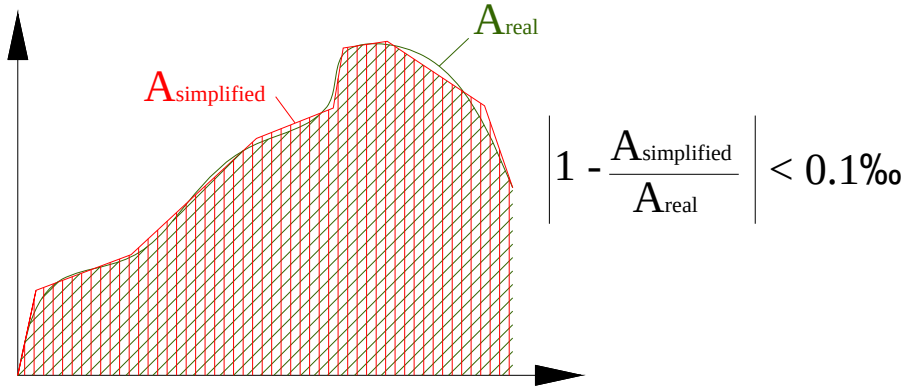

Figure 2-35: Area coverage between the simplified curve and the real curve.

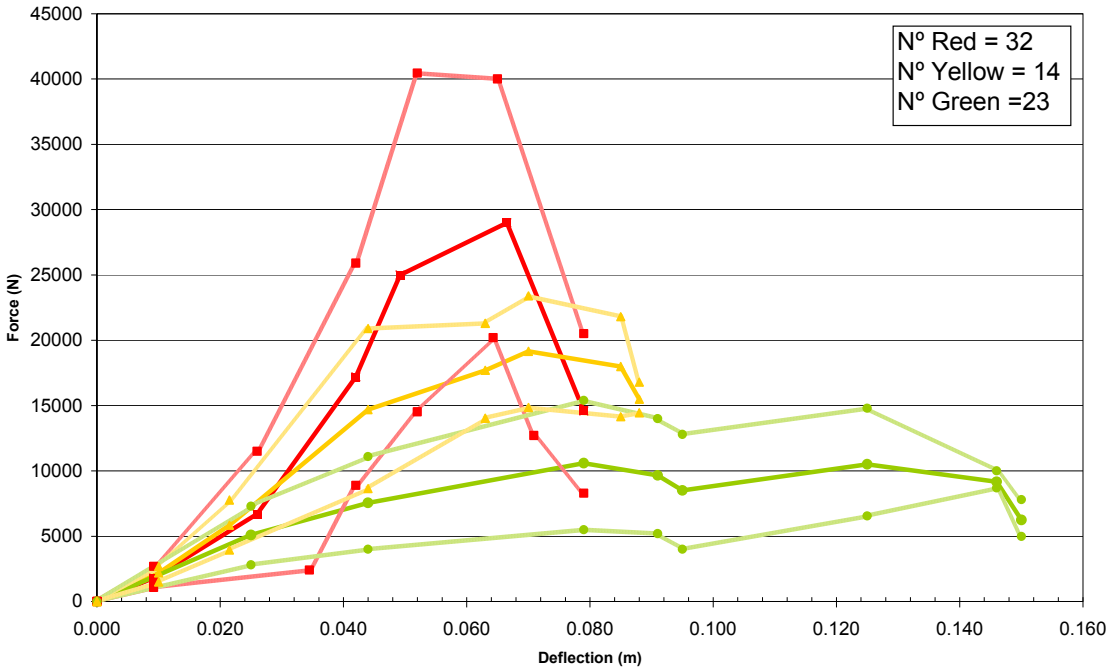

Figure 2-36: Simplified force deflection data for the bumper area.

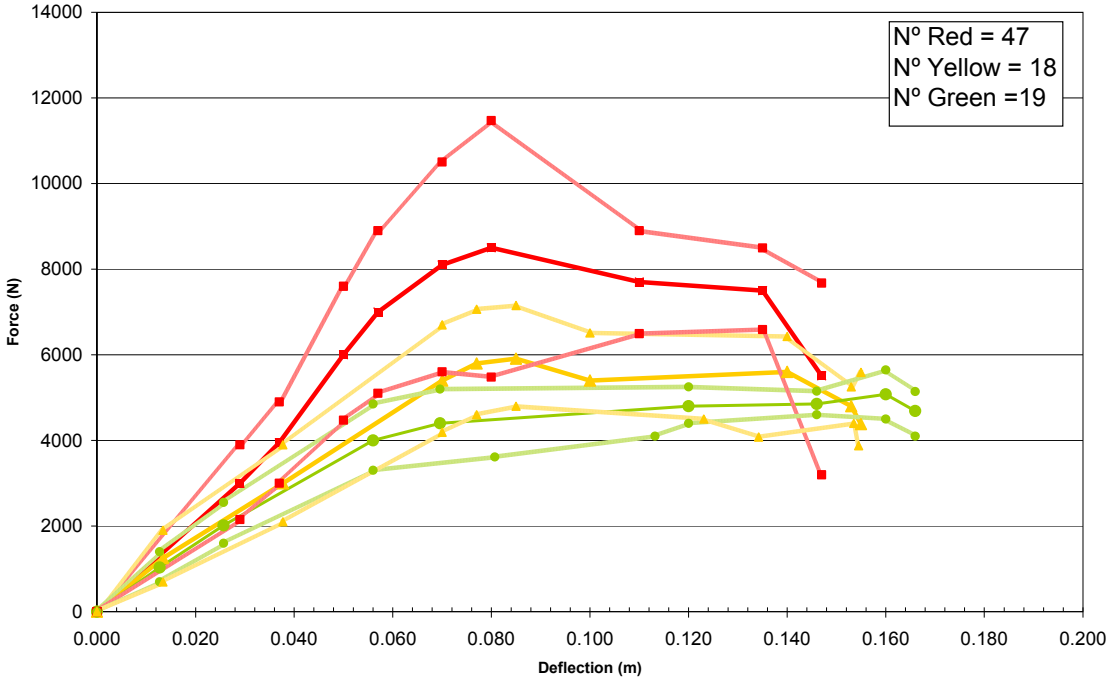

Figure 2-37: Simplified force deflection data for the bonnet front area.

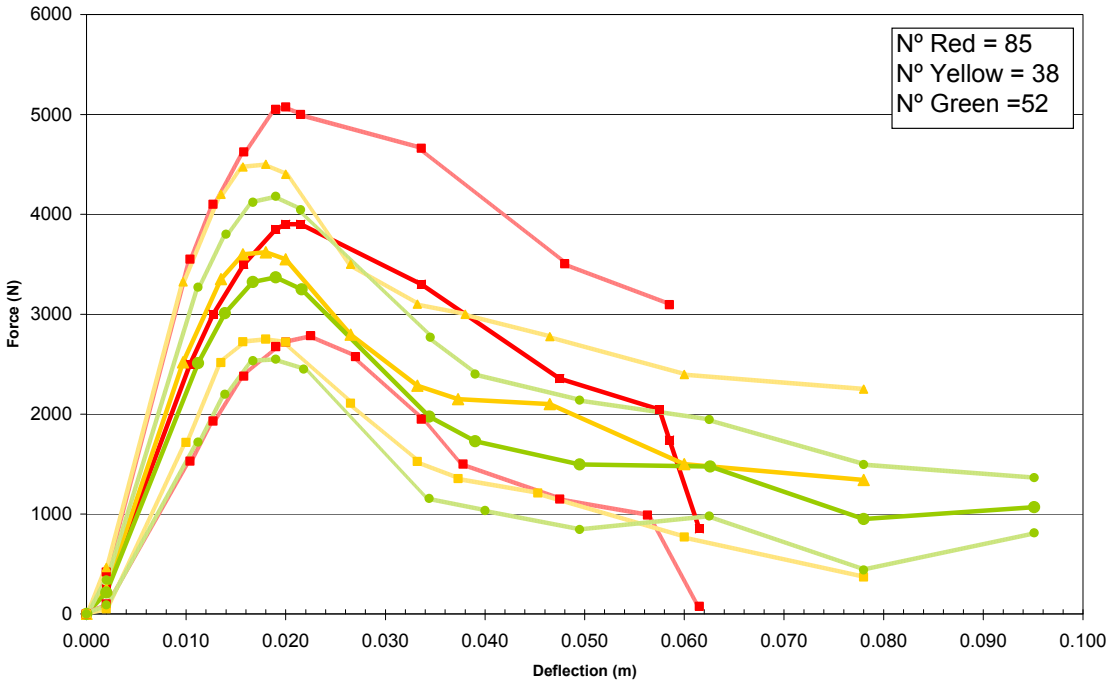

Figure 2-38: Simplified force deflection data for the bonnet middle area.

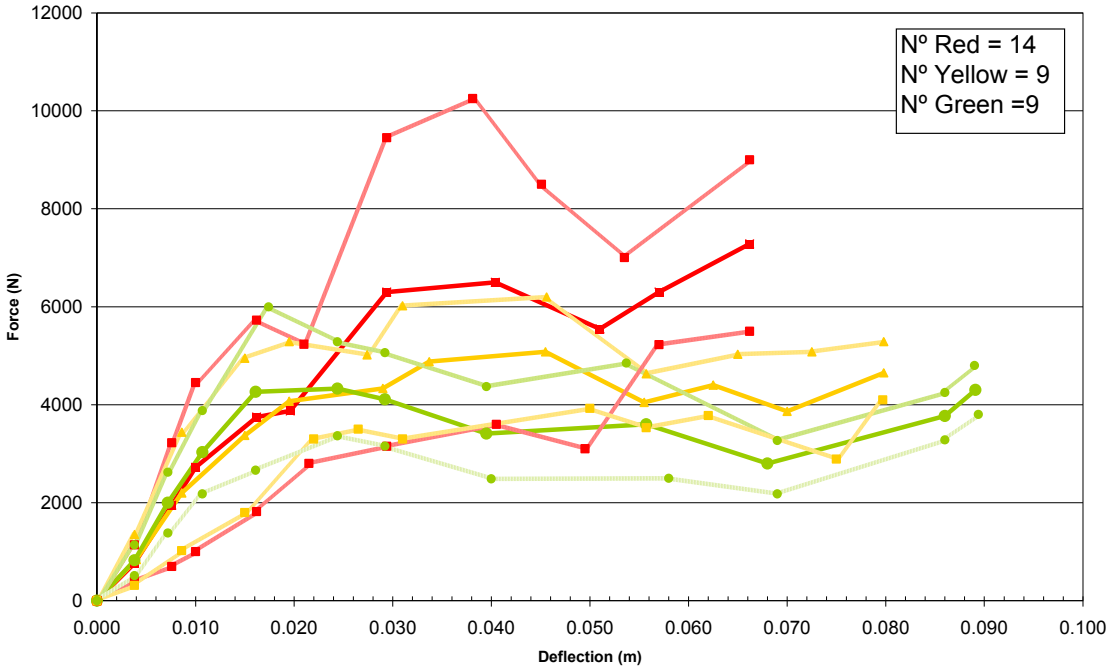

Figure 2-39: Simplified force deflection data for the bonnet rear area.

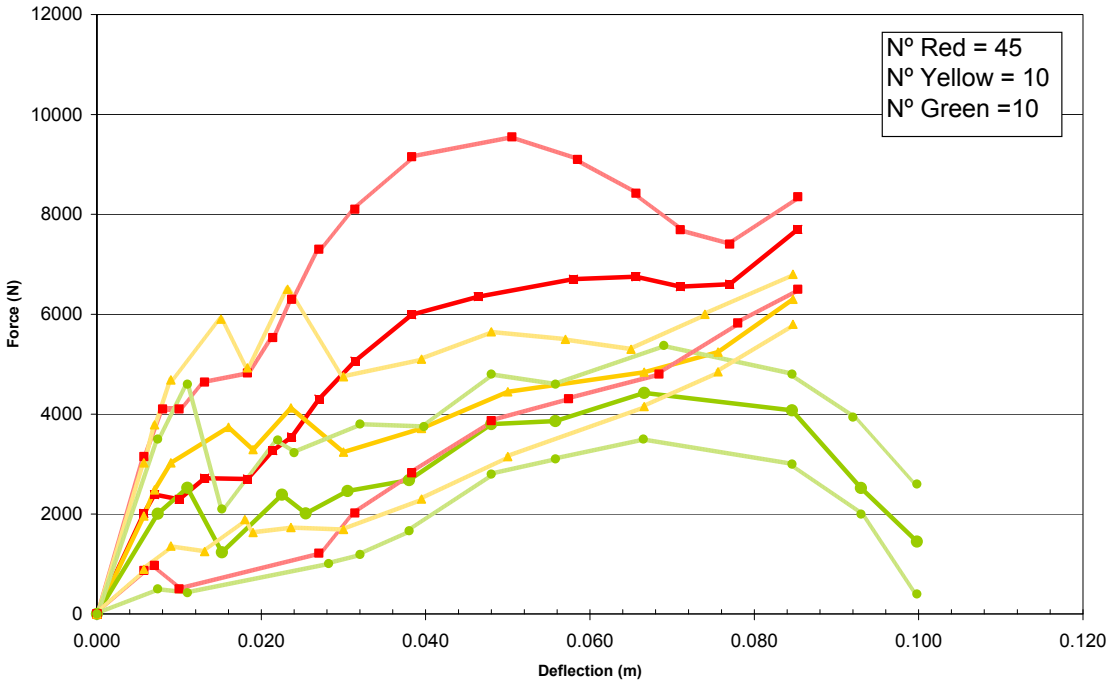

Figure 2-40: Simplified force deflection data for the windscreen base area.

The next tables present the same information in tabular way considering that:

- The points selected in the simplified curves will describe the actual details of the average and the ± 1 standard deviation corridors obtained from the 425 force-deflection data set.
- The difference in area covered by real and the simplified curves is below 0.1 ‰.

BUMPER																	
AVERAGE						TOP						LOW					
Red		Yellow		Green		Red		Yellow		Green		Red		Yellow		Green	
0	0	0	0	0	0	0	0	0	0	0	0	0	0	0	0	0	0
9.2	1794	10	2183	25	5100	9	2685	10	2670	25	7300	9	1080	10	1500	25	2800
26	6699	22	5844	44	7560	26	11500	22	7765	44	11090	35	2399	22	3950	44	4000
42	17195	44	14700	79	10595	42	25900	44	20900	79	15400	42	8900	44	8650	79	5495
49.2	25000	63	17700	91	9650	52	40450	63	21300	91	14000	52	14520	63	14026	91	5200
66.5	29000	70	19150	95	8500	65	40000	70	23400	95	12800	64	20200	70	14850	95	4000
79	14595	85	17995	125	10500	79	20500	85	21800	125	14800	71	12700	85	14150	125	6550
		88	15485	146	9160			88	16800	146	10000	79	8289	88	14450	146	8690
				150	6250					150	7800					150	4985

Table 2-12: Simplified force deflection data for the bumper.

BONNET FRONT																	
AVERAGE						TOP						LOW					
Red		Yellow		Green		Red		Yellow		Green		Red		Yellow		Green	
0	0	0	0	0	0	0	0	0	0	0	0	0	0	0	0	0	0
29	3000	13.4	1250	12.7	1030	29	3900	13.4	1900	12.7	1400	29	2150	13.4	695	12.7	700
37	3946	37.7	3000	25.7	2015	37	4900	37.7	3900	25.7	2550	37	3000	37.7	2100	25.7	1600
50	6000	70	5400	56	4000	50	7600	70	6700	56	4850	50	4475	70	4190	56	3300
57	7000	77	5800	69.6	4400	57	8900	77	7065	69.6	5200	57	5100	77	4600	80.7	3615
70	8100	85	5910	120	4800	70	10500	85	7150	120	5250	70	5600	85	4800	113.2	4100
80	8500	100	5400	146	4850	80	11470	100	6511	146	5150	80	5480	123.1	4500	120	4400
110	7700	140	5600	160	5075	110	8900	140	6425	160	5645	110	6495	134.2	4080	146	4600
135	7500	153	4800	166	4690	135	8495	153	5250	166	5142	135	6590	153.5	4400	160	4500
147	5510	155	4380			147	7675	155	5590			147	3197	154.5	3875	166	4100

Table 2-13: Simplified force deflection data for the bonnet front.

BONNET MIDDLE																	
AVERAGE						TOP						LOW					
Red		Yellow		Green		Red		Yellow		Green		Red		Yellow		Green	
0	0	0	0	0	0	0	0	0	0	0	0	0	0	0	0	0	0
2	250	2	250	2	215	2	420	2	465	2	340	2	99	2	50	2	90
10.4	2500	9.7	2520	11.2	2510	10.4	3550	9.7	3325	11.2	3270	10.4	1530	10	1715	11.2	1720
12.7	3000	13.5	3350	13.9	3010	12.7	4100	13.5	4199	14	3800	12.7	1930	13.5	2515	13.9	2200
15.8	3500	15.7	3600	16.7	3323	15.8	4625	15.7	4475	16.7	4120	15.8	2380	15.7	2725	16.7	2535
19	3850	18	3620	19	3370	19	5050	18	4500	19	4180	19	2675	18	2750	19	2550
20	3900	20	3550	21.6	3250	20	5075	20	4400	21.5	4045	20	2720	20	2720	21.8	2450
21.5	3900	26.5	2795	34.4	1975	21.5	5000	26.5	3500	34.5	2770	22.5	2785	26.5	2110	34.4	1155
33.6	3300	33.2	2285	39	1730	33.6	4660	33.2	3100	39	2400	27	2575	33.2	1525	40	1034
47.5	2355	37.3	2150	49.5	1495	48	3505	38	3000	49.5	2140	33.6	1950	37.3	1355	49.5	845
57.5	2045	46.5	2100	62.6	1475	58,5	3095	46.5	2775	62.5	1945	37.8	1500	45.3	1210	62.5	980
58.5	1740	60	1500	78	950			60	2397	78	1495	47.5	1150	60	770	78	440
61.5	853	78	1341	95.1	1068			78	2250	95.1	1364	56.3	990	78	369	95.1	810
												61.5	75				

Table 2-14: Simplified force deflection data for the bonnet middle.

BONNET REAR																	
AVERAGE						TOP						LOW					
Red		Yellow		Green		Red		Yellow		Green		Red		Yellow		Green	
0	0	0	0	0	0	0	0	0	0	0	0	0	0	0	0	0	0
3.8	765	4	840	3.8	825	3.8	1140	3.8	1350	3.8	1140	3.8	400	3.8	310	3.8	510
7.6	1950	8.6	2200	7.2	2000	7.6	3225	8.6	3440	7.2	2620	7.6	700	8.6	1020	7.2	1380
10	2723	15	3375	10.7	3030	10	4450	15	4950	10.7	3880	10	1000	15	1800	10.7	2180
16.2	3750	19.5	4070	16.1	4265	16.2	5725	19.5	5290	17.4	6000	16.2	1820	22	3300	16.1	2665
19.6	3875	29	4334	24.4	4330	21	5235	27.4	5020	24.4	5285	21.5	2800	26.5	3500	24.4	3365
29.4	6300	33.7	4880	29.2	4110	29.4	9450	31	6020	29.2	5060	29.4	3150	31	3300	29.2	3155
40.4	6500	45.5	5080	39.5	3410	38.1	10250	45.6	6200	39.5	4370	40.5	3600	50	3925	40	2485
51	5550	55.5	4050	55.7	3600	45.1	8500	55.7	4630	53.7	4850	49.5	3100	55.7	3530	58	2500
57	6300	62.5	4400	68	2800	53.5	7005	65	5030	69	3271	57	5225	62	3780	69	2180
66.2	7283	70	3865	86	3774	66.2	8999	72.5	5080	86	4250	66.2	5500	75	2890	86	3280
		79.8	4650	89.1	4300			79.8	5290	89	4800			79.7	4100	89.4	3802

Table 2-15: Simplified force deflection data for the bonnet rear.

WINDSCREEN BASE																	
AVERAGE						TOP						LOW					
Red		Yellow		Green		Red		Yellow		Green		Red		Yellow		Green	
0	0	0	0	0	0	0	0	0	0	0	0	0	0	0	0	0	0
5.7	2015	5.7	1960	7.4	2004	5.7	3150	5.7	3025	7.4	3500	5.7	870	5.7	890	7.4	500
7	2388	7	2485	11	2525	8	4100	7	3785	11	4600	7	970	9	1360	11	425
10	2295	9	3027	15.2	1235	10	4100	9	4685	15.2	2100	10	500	13.1	1250	28.2	1010
13.1	2715	16	3735	22.5	2385	13.1	4640	15.1	5900	22	3480	27	1215	18	1890	32	1190
18.3	2700	19	3290	25.4	2012	18.3	4825	18.3	4925	24	3230	31.4	2020	19	1630	38	1665
21.4	3271	23.6	4125	30.5	2460	21.4	5530	23.2	6500	32	3799	38.3	2825	23.6	1730	48	2800
23.7	3545	30	3240	38	2680	23.7	6300	30	4750	39.8	3750	48	3870	30	1690	55.8	3105
27	4300	39.5	3715	48	3800	27	7300	39.5	5100	48	4800	57.4	4308	39.5	2300	66.5	3500
31.4	5060	50	4447	55.8	3860	31.4	8100	48	5650	55.8	4600	68.4	4800	50	3150	84.6	2999
38.3	5990	66.6	4840	66.6	4425	38.3	9150	57	5497	69	5375	78	5825	66.6	4150	93	2000
46.4	6350	75.6	5240	84.6	4075	50.5	9550	65	5300	84.6	4800	85.3	6500	75.6	4845	99.8	399
58	6700	84.7	6300	93	2520	58.5	9100	74	6000	92	3941			84.7	5800		
65.6	6749			99.8	1447	65.6	8420	84.7	6798	99.8	2599						
71	6550					71	7690										
77	6600					77	7400										
85.3	7699					85.3	8351										

Table 2-16: Simplified force deflection data for the windscreen base.

2.3.1 Corridor interpretation.

As it is seen in the Figure 2-30 to Figure 2-40, overlaps between the corridors of the different rating exist due to the nature of the corridor construction and the sample variation. This variation may induce some problems in the corridor interpretation if corridors are expected to univocally define red, green or yellow areas.

However, considering how the corridors have been constructed, they aimed to represent the mean value of the sample with an indication of its variability through the standard deviation. This indicates that the upper and lower boundaries of the corridors do not envelope the whole set of data of the sample, but represent the variability in each point of the mean value. In fact, an analysis of the sample variation according formula 2-1 highlights its importance in most of the cases. (see Table 2-17)

$$CV = \frac{\sum_{i=1}^{n} Sx_i / \overline{X}_i}{n} \times 100$$

Formula 2-1

CV (%)	Bumper	Bonnet front	Bonnet mid	Bonnet rear	Windscreen
	51.65 %	29.6 %	47.6 %	42 %	48.2 %
	29.8 %	27 %	45.1 %	28.7 %	34.6 %
	42.5 %	18.9 %	38.5 %	25.6 %	40.6 %

Table 2-17: Coefficient of Variation of the data in each configuration.

It can be seen that the variation of the sample is quite high, being in most groups the CV over 30%. In some cases, as all bonnet middle cases or windscreen base cases, the CV exceeds the 40% which lead to corridor overlaps rather more important than in the rest of cases. Therefore, in order to use these corridors properly in simulations, it is generally suggested to use the average curves obtained rather than the boundary curves or any self-constructed curves within the corridors.

3 PEDESTRIAN ACCIDENT ANALYSIS

As the current pedestrian test procedures have been wisely based on sub-system test which try to translate the infinite number of pedestrian accident scenario into a reduced set of “worse cases” with pre-defined impact conditions, it is very important to keep a permanent link to the reality where these infinite pedestrian cases may occur to ensure that this translation is still relevant. For that, not only fatal scenarios but also those causing long term disabilities need to be approached.

With this objective, this thesis has performed an in-depth analysis of the Spanish database ABIDA (Aparicio, 2005) that has gathered detail information on the scene of 108 pedestrian accidents (involving 118 pedestrians) occurring in Madrid from November 2002 to November 2004, thanks to the joint collaboration from the Municipal Police of Madrid, the SAMUR ambulance service, the 12-Octubre Hospital and the in-situ accident group from UPM-INSIA. To complete this in-situ data collection a post-process phase has followed the collecting phase in order to get extra information on the accident scene and on impact velocities.

This in-depth analysis has consisted of looking in details on trends of the different variables of the accidents but also, which is more relevant, in looking for the injury patterns for fatal accidents and non fatal accidents related with age and gender, which can make a difference in the human body response to impact.

A first part of the analysis has looked to all variables linked to the accident itself including the vehicle parameters and a second one is just focused on the pedestrian injuries. Finally

a third part is included highlighting the relevance of the findings with respect to the different test procedures and drafting paths for the continuation of the work of this thesis.

3.1 Accident scenarios analysis.

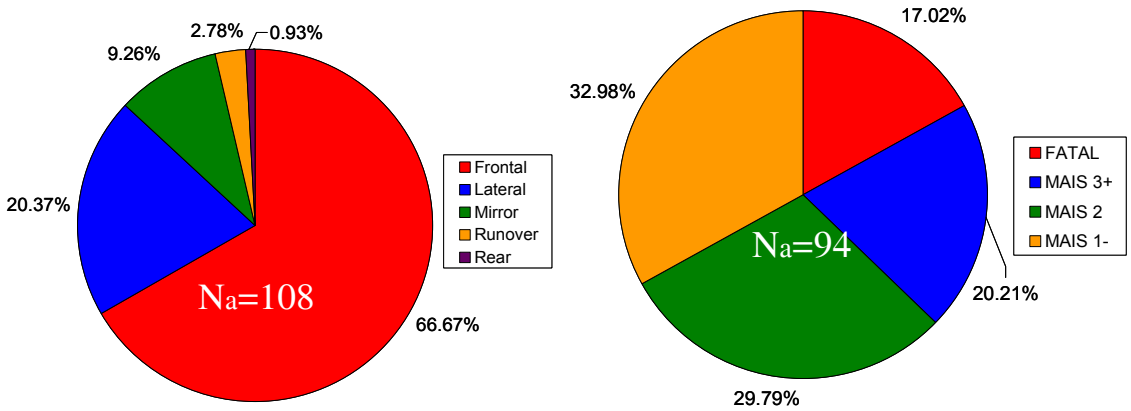

Figure 3-1: Accident type and severity of the pedestrian accident sample.

As previously commented, a total of 108 pedestrian accidents were included in the ABIDA database. From them, only scenarios where the pedestrian hits the frontal or fronto-lateral part of the vehicles are relevant for this study, since cases where the pedestrian is hit by the mirror or totally runover by the vehicle are typically out of the scope of the pedestrian testing procedures.

Looking in the figure, these scenarios are 94 out of the 108 cases, and these 94 will be the relevant sample for our study. As the injuries are AIS-coded, these 94 accidents are classified according to the maximum AIS of the injuries sustained by the pedestrian involved in them. This break-down is also shown in the next figure and suggests that 2/3 of them show injuries MAIS2+ and in the 17% of the cases these injuries are fatal.

Looking in detail what were the typical impact locations of these accidents, it turned out that in 69 cases the accident caused permanent damages on the car, while in 25 cases no damage was registered in the car. Distributing the 183 permanent damages along the different parts of the vehicle, as indicated in Figure 3-2, it shows that permanent damages in bonnet and windscreen are by far more common than in the bumper or other surrounding areas, although no distinction is done with respect the severity of the accident. In any case, this would lead to the conclusion that even when the impact with the bumper occurs, (from the kinematics point of view it is rather improbable a pedestrian impact without an impact in the bumper) the main structures of the current vehicles absorbing energy through deformation are the bonnet and the windscreen.

Obviously, the relative positions of these structures with respect to the ground as well as their pedestrian friendliness had an influence in its interaction with the pedestrian and as such it will be studied further. A first step on that is shown in Figure 3-3, where the

impacting vehicles are classified based on their vehicle type according EuroNCAP (Super-mini cars (SMC), Small family cars (SFC), Large family cars (LFC), Multi-purpose vehicles (MPV), Sport Utility vehicles (SUV), Vans or Heavy vehicles (HV).

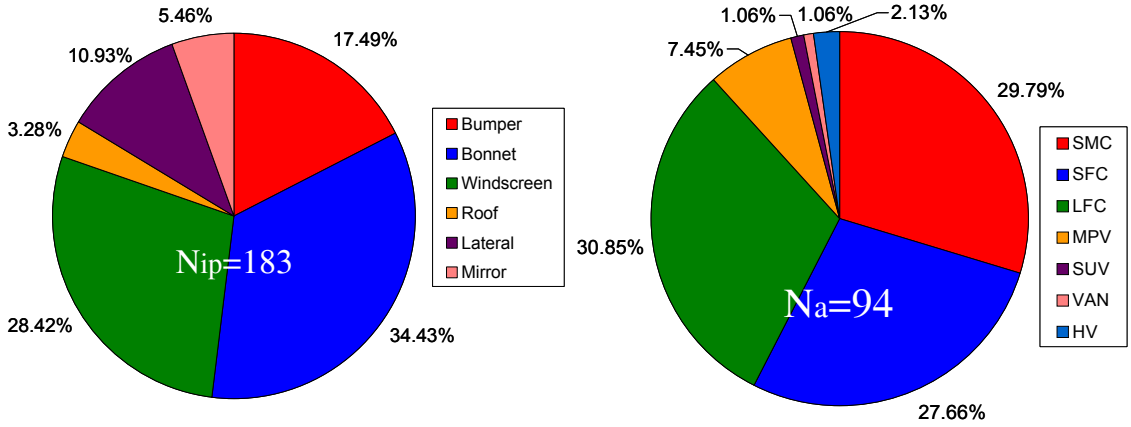

Figure 3-2: Impact location distribution on the vehicle structures of frontal and fronto-lateral accidents and the classification per vehicle segment.

This figure shows that in 90% of the cases, the impact with the pedestrian occurred with a "typical" sedan passenger car as those considered directly on the development of the pedestrian testing procedures, and the number of cases in the database with "conflictive vehicles" (high bumper vehicles, very short bonnet vehicles (Smart-type), flat heavy vehicles...) are very limited, which will somehow determine the future paths for this thesis, as the analysis of these geometries would need a separate approach.

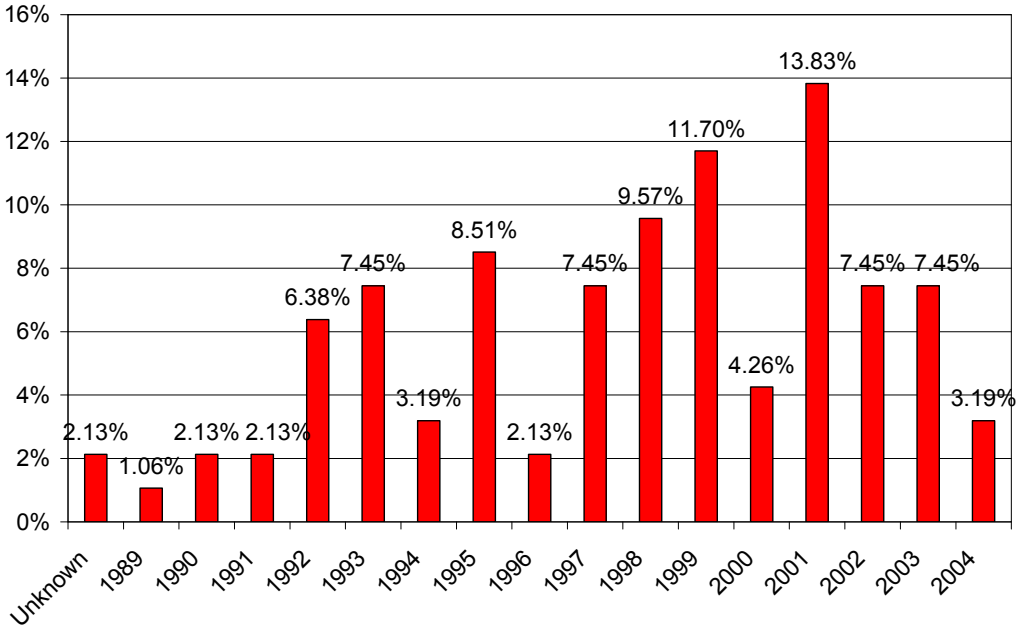

Figure 3-3: Segment and age distribution of the vehicles involved in the accidents.

Moreover, the Figure 3-3, that shows the age of the vehicles involved, highlights that 35% of the cars are from 2000 or newer, and only the 25% were from 1995 or elder, which means that most of the vehicles involved in the accidents were manufactured within the years where the original EEVC pedestrian testing procedures were developed and most of them were tested under them in any of the extensive testing programmes performed by EEVC or EuroNCAP from 1995 to 2004.

Accident speed was one of the parameters calculated during the post process of the scene data by using PC-CRASH to reproduce all the cases and estimate the impact speed of the accident (Aparicio, 2005). The speed distribution and cumulative frequency is observed in the Figure 3-4 while it is decoupled according to accident severity in Figure 3-5.

It can be seen that 30-40 km/h is the most frequent speed collision interval in the sample, with over the 25%, being 20-30 km/h interval also near the 25%. The cumulative frequency curve shows that the 73% of the accidents happen at speeds below 40 km/h, and almost 50% below 30 km/h.

Since the sample has been recorded almost exclusively in urban environment, this curve is underestimating typical fatal scenarios occurring on non urban road at higher speeds, as seen in Neal-Sturgess (2007). This is confirmed when accident severity is considered jointly with speed, as 40 km/h accounts for over the 70% of the MAIS1, MAIS2 and MAIS3+ accidents, but accounts for less than the 30% of the fatal cases, which reach the cumulative 70% of cases at the speed of 60 km/h.

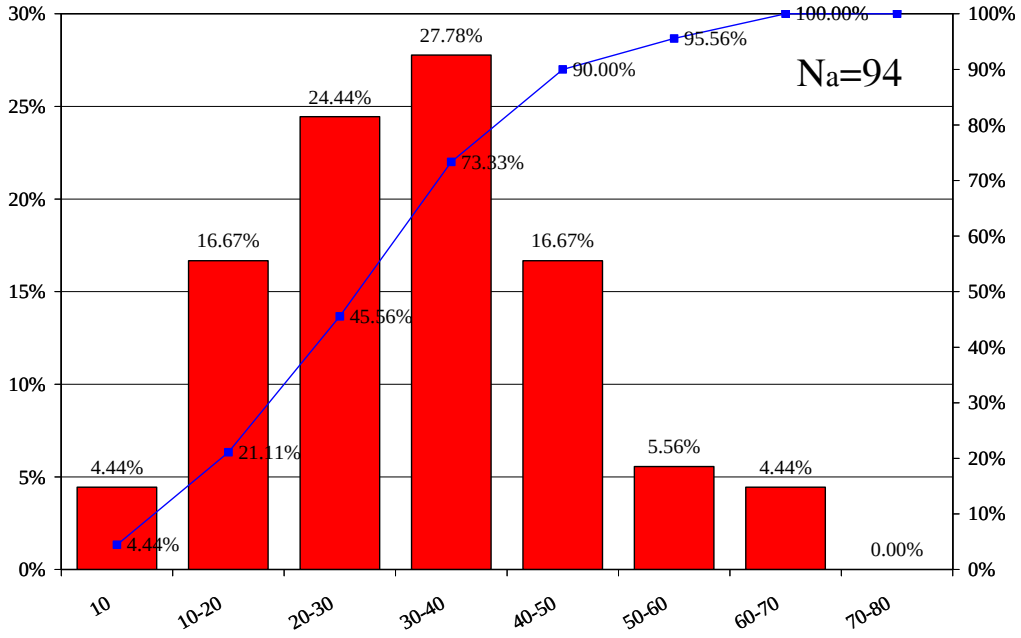

Figure 3-4: Accident speed distribution and cumulative frequency.

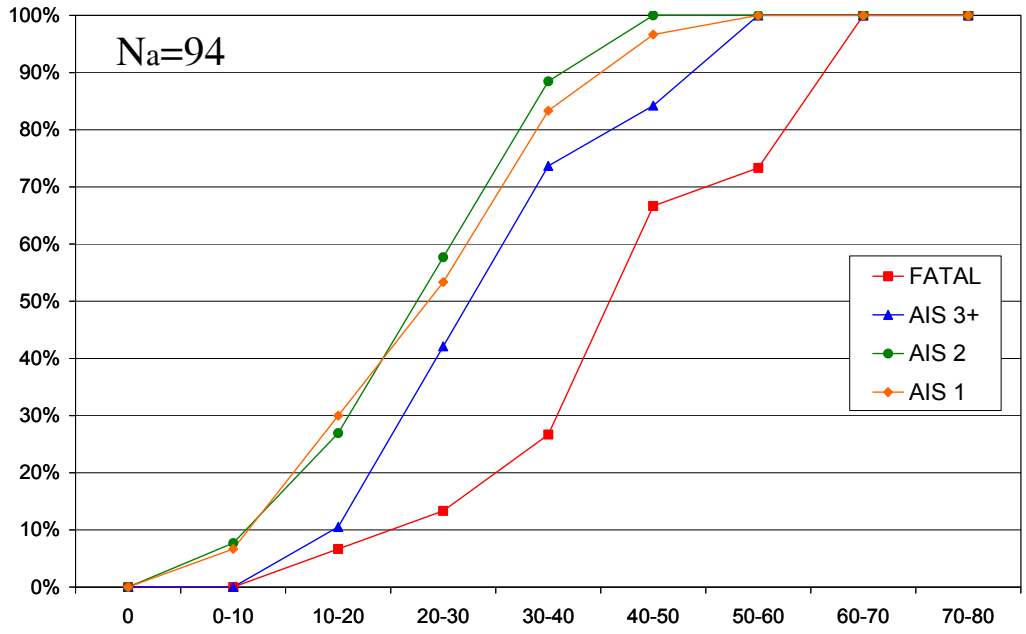

Figure 3-5: Accident speed considering the accident severity.

3.2 Pedestrian analysis.

The 94 accidents considered involved a total of 103 pedestrian of which typically, pedestrian movement, age, gender and injuries were recorded for each accident.

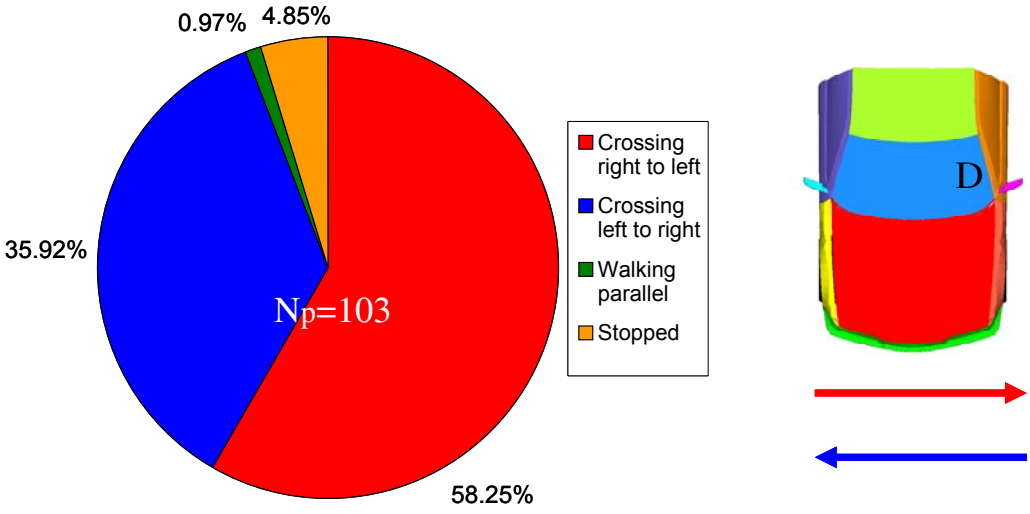

Figure 3-6: Pedestrian movements prior to the impact.

A first analysis on the pedestrian movement suggests that, in 95% of the cases, the accident occurred when the pedestrian was crossing the street. Although in the sample significant difference is highlighted regarding direction: 58% of cases the pedestrian

crossed from the right to the left side of the vehicle, while in the 36% of the cases occurred from the left to the right, it seems that no evidence of such tendency is found in larger samples (Neal Sturgess, 2007). What it is really remarkable is that in most cases, the initial pedestrian position can be concluded to be a walking posture, therefore receiving the impact from the vehicle laterally.

Although this finding was expected, it is very relevant to understand the latter kinematics during the impact of the different body parts, since this lateral aspect of the impact is indeed considered in the legform tests but it is not in the headform tests.

Among the 103 pedestrian, there were 18 fatalities, 33 pedestrian casualties with MAIS 1 injuries and 52 with MAIS2+ injuries although in total there were 431 injuries reported distributed as shown in the table.

AIS Level	1	2	3	4+	9	TOTAL
Injuries	226	112	40	10	43	431

Table 3-1: Summary of injuries and severities in the database.

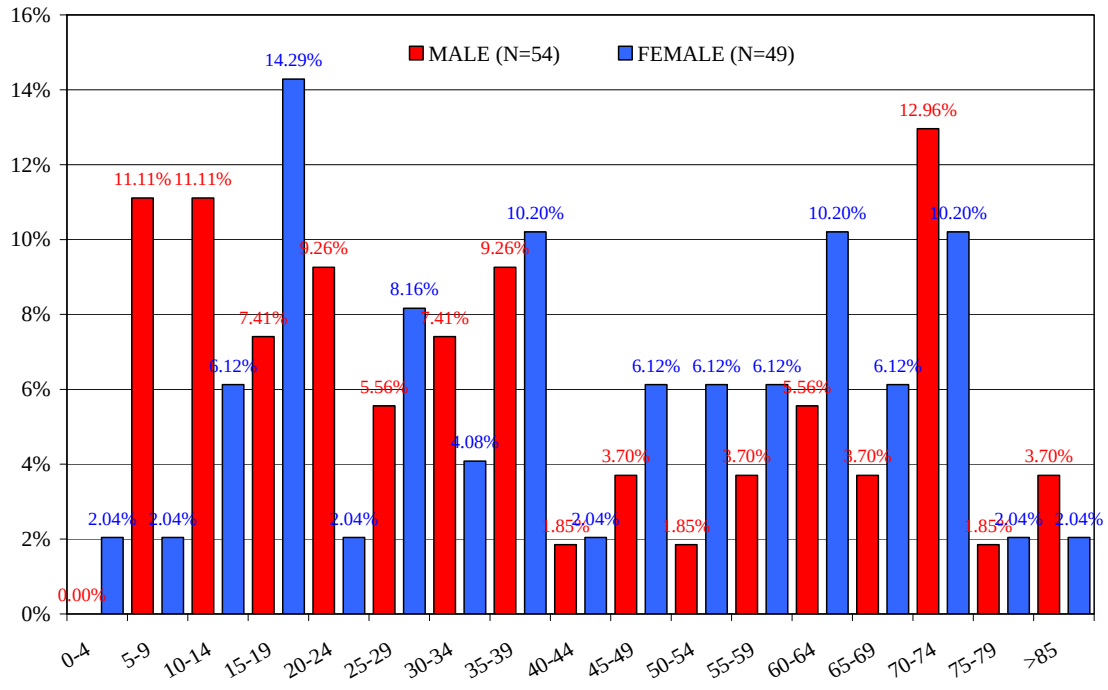

Figure 3-7: Age distribution of pedestrian casualties.

Looking in detail into age and gender, it is found an equal distribution of casualties in the sample (54 males and 49 females) as well as a similar age distribution. While for females, teenagers (15-19) are the group more involved in the accidents (14.3%), and elder people (>65) represent about 20% of the total female sample, in males, elder people also

represent around 20% of the sample with children and young boys accounting for other 20% together. So in this sense, the basic “double hill” topology is presented in both cases.

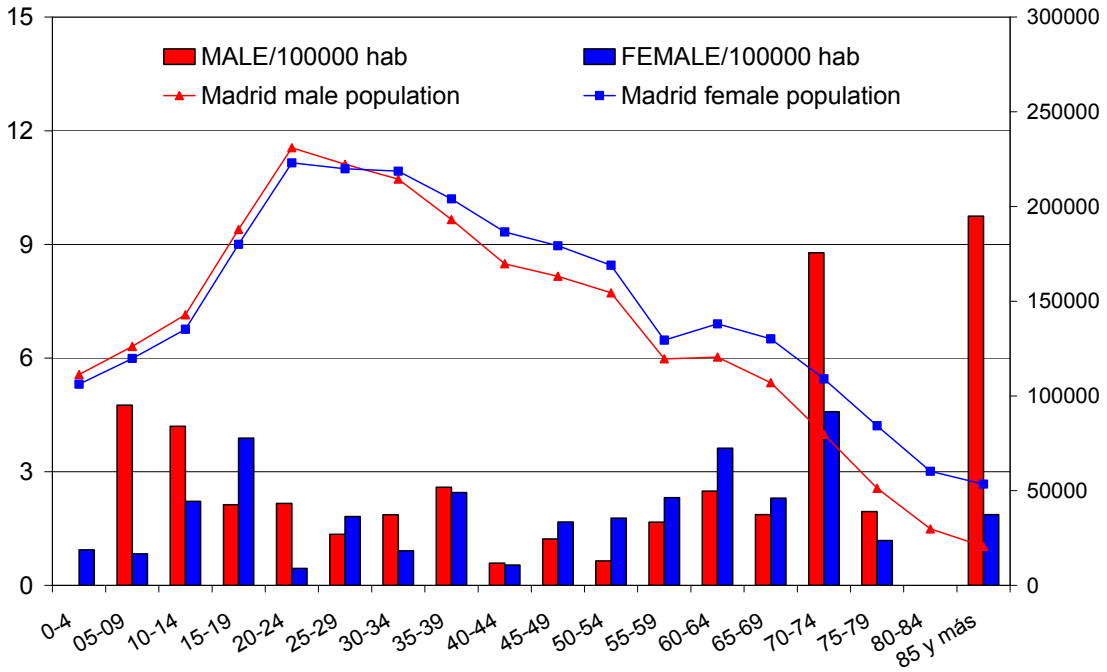

Figure 3-8: Age distribution of pedestrian casualties.

Dividing the accidents per the population from Madrid, estimations of accidents/per 100,000 inhabitants is given highlighting even more that elder people seems to be of higher risk than younger people, for both genders. Making further analysis on that and plotting the injury distribution relative to the pedestrian age, the following figures are obtained in terms of injuries/pedestrian.

In the male distribution, elderly (over 70) show the highest number of injuries per pedestrian (4.5 injuries per pedestrian), with high proportion of AIS2+ injuries, while children (0-10) and young adults (20-30) hardly reach 2.5 injuries per pedestrian.

Regarding severity, AIS 3 and AIS4+ injuries are hardly found in male young pedestrian, while they occur often over 40 years old, especially for elder pedestrians. If AIS 9 injuries are separated into slight or severe according the subjective medical injury description, 40-50 age range becomes important as its proportion of AIS3 and AIS 9 severe is the highest of all age ranges.

The female distribution indicates that the age range of 50-60 years old shows the highest number of injuries per pedestrian (almost 6), although they are only AIS1, AIS 2 and slight AIS 9, followed by the 40-50 and the 10-20 age range. Regarding AIS 3 and AIS 4+ injuries, again they are hardly found in young pedestrians, while they are important along the adult range. Only when AIS 9 severe is considered, the elderly group becomes

important and shares with the 20-30 range the highest proportion for AIS3+AIS9 severe injuries.

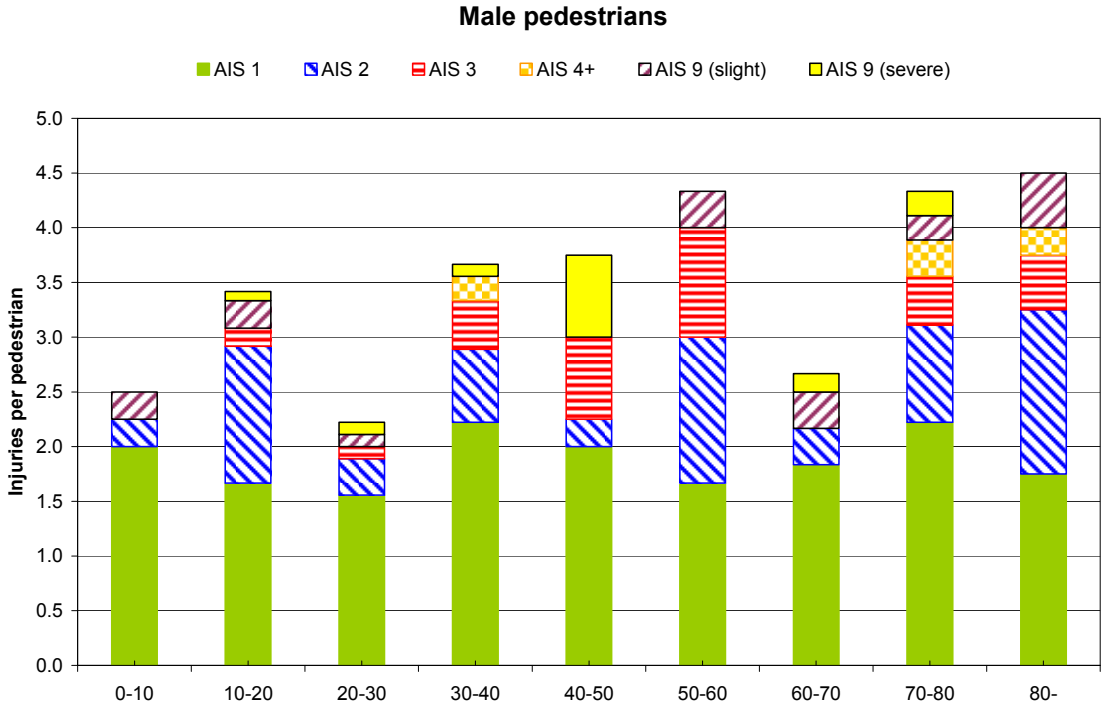

Figure 3-9: Injury severity distribution with respect pedestrian age for males.

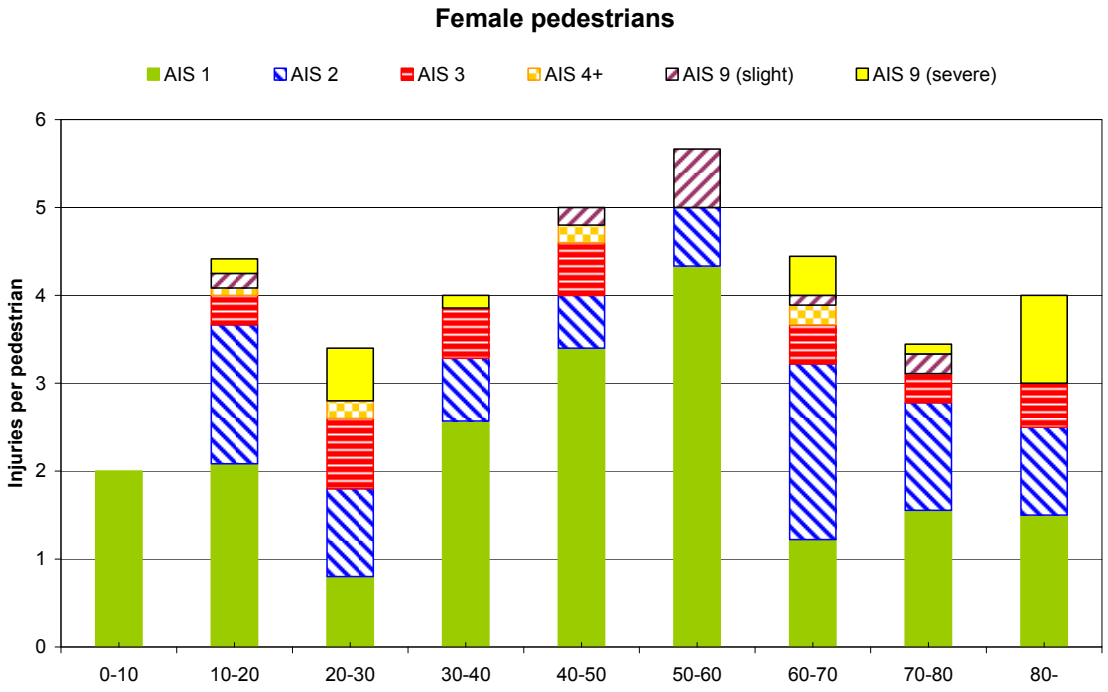

Figure 3-10: Injury severity distribution with respect pedestrian age for females.

Although these two graphics have shown higher number of injuries per pedestrian in elder cases for both genders, it has not shown significant differences in the severe injury ratios from elder pedestrian and the rest of the adult ages. This high number of injuries per accident in elder pedestrians demonstrates their special characteristics in pedestrian scenarios and requests to dedicate further attention to this issue along this thesis.

AIS	Head	Face	Spine	Thorax	Abdomen	Upper extremity	Lower extremity	Total
1	1	6	0	1	1	1		10
2			0	1	2	5	7	15
3	6	1	0	4	2		4	17
4+	3		0	3		AIS 3 is the maximum		6
9	14		0	1	4			19
Total	**24**	**7**	**0**	**10**	**9**	**6**	**11**	**67**

Table 3-2: Injury distribution in fatal pedestrian.

Apart from age and gender, it is worth to look into the different body regions considering separately the injuries found in non fatal pedestrians and those found in fatal pedestrian. The Table 3-2 shows the injuries per each body region found for fatal pedestrian. It is remarkable that head injuries are the ones most frequent (37%), followed by lower extremity (16%). In this case, thorax and abdomen injuries occur more frequently than for non fatal pedestrians, representing for fatal pedestrian the 15% and 13% of all the injuries, respectively. For fatal pedestrian, injuries in the spine and face are the one least frequent.

Regarding the severity of the injuries, the Figure 3-11 describes it in each body region, showing in most regions obvious high shares of AIS 3 and AIS 4+ frequencies. In fact, in these terms, the thorax (70%) is the body part where the highest proportion of AIS3+ injuries is found, while head (37%) and lower extremity (36%) are the next ones, although taken into account also the global numbers, the order of importance should be reversed.

Making a further analysis on AIS 9 injuries based on their description from the hospital, it turns out that all abdominal and thorax AIS 9 injuries are described as “severe”, while in the head, 85% of the AIS 9 cases are described as “severe”. (See next figure). Considering these “severe” cases as AIS3+, AIS3+ head injuries proportion increases up to the 87%, being the highest proportion of AIS3+ of all body parts, while the thorax proportion remains in the 80% and the abdomen proportion raises to the 66%, leaving the rest body parts rather below.

These findings suggest that, for fatal cases, head injuries are the critical injuries.

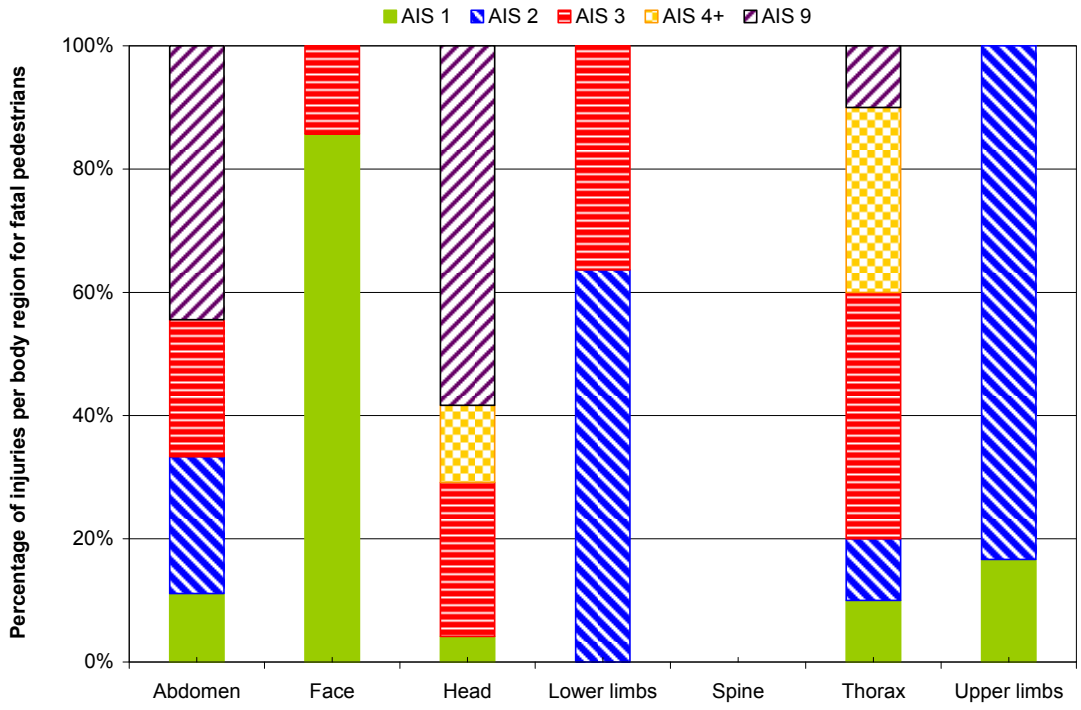

Figure 3-11: Frequency distribution of injuries in fatal pedestrians.

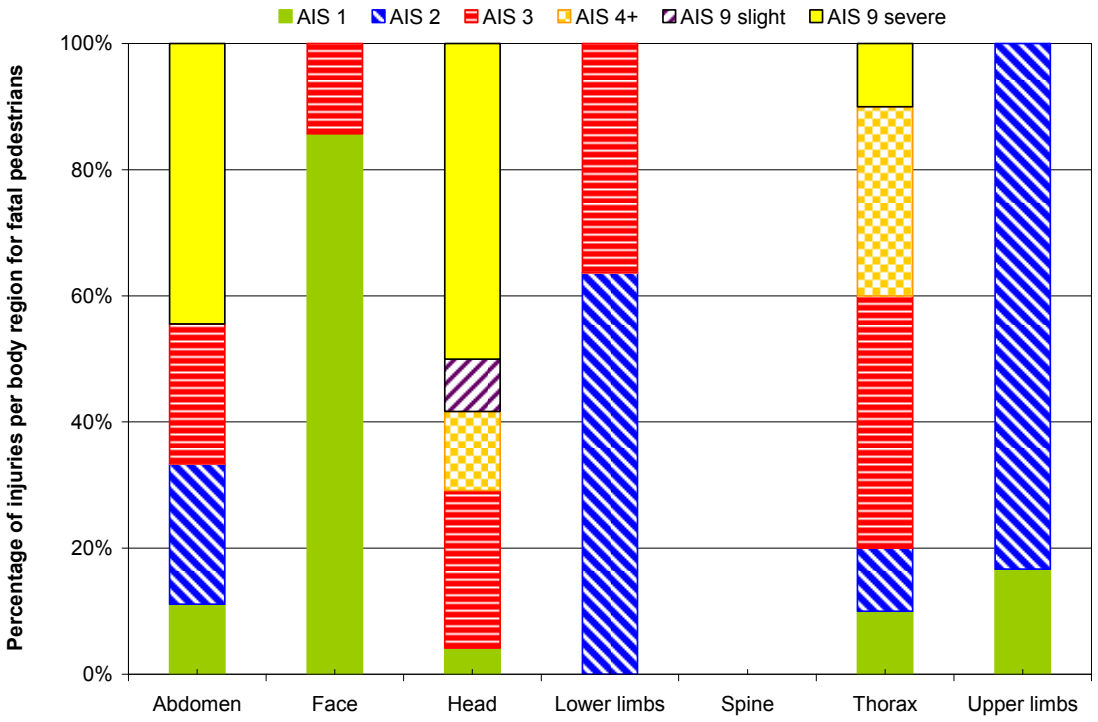

Figure 3-12: Frequency distribution of injuries in fatal pedestrians (AIS 9 separated).

Analysing the injuries found in non fatal pedestrians, it seems that head and lower extremity (including pelvis bone as defined is the AIS 90 code) are the most frequent injured areas, accounting together with almost the 60% of all injuries. On the other hand, abdomen and thorax are the body region least injured in non fatal pedestrians.

AIS	Head	Face	Spine	Thorax	Abdomen	Upper extremity	Lower extremity	Total
1	58	44	19	9	4	33	49	216
2	21	1	3	4	1	20	47	97
3	6		1	3		2	11	23
4+	2			2		AIS 3 is the maximum		4
9	22				2			25
Total	**109**	**45**	**23**	**18**	**7**	**55**	**107**	**364**

Table 3-3: Injury distribution in non fatal pedestrian.

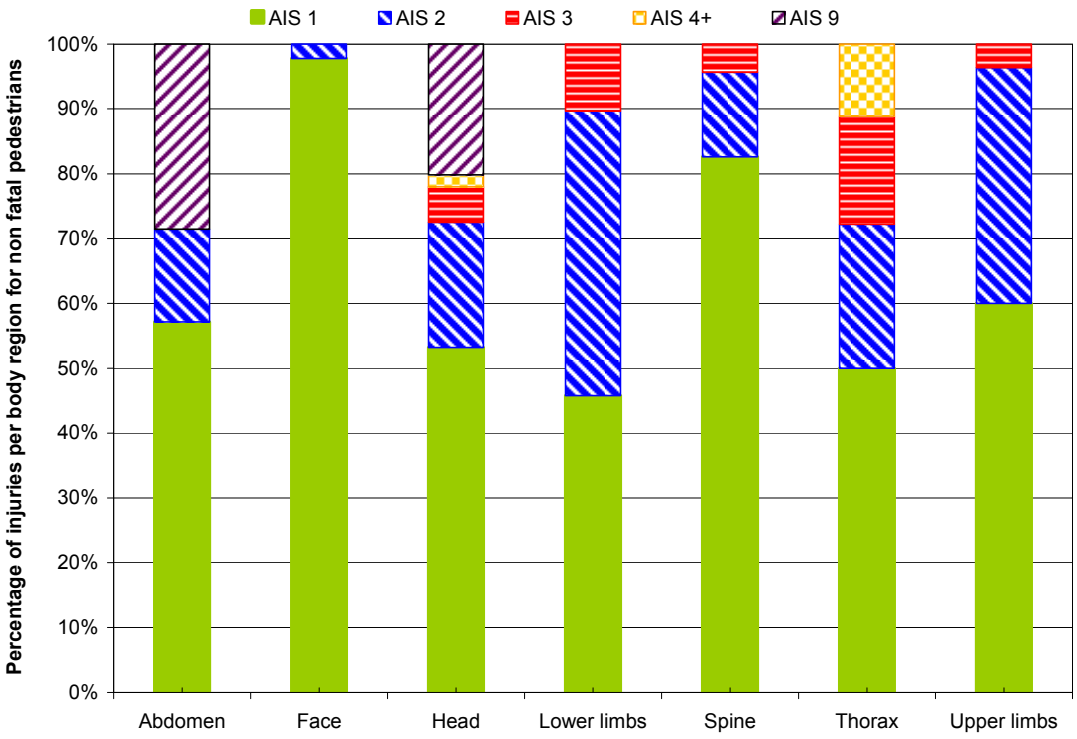

Figure 3-13: Frequency distribution of injuries in non fatal pedestrians.

The figure shows, in percentages, the severity of the injuries found in each body region for non fatal pedestrians. This figure highlights that lower extremity as well as being the most frequent, it also show the highest proportion for AIS 2+ injuries for all the body regions (54%), while head injuries, with similar frequency values, show a AIS2+ injuries proportion (excluding AIS 9) relatively lower (near the 26%). Thorax severity distribution also shows high proportion in AIS2+ injuries (50%), even with a higher AIS 3 proportion than the one from the lower extremity. However, from the numbers shown, the thorax injuries occurrence is very limited. These figures may indicate that, for non fatal pedestrian, lower extremity injuries are the most relevant.

To further gain insight into this data, the distribution of the lower extremity injuries in the different leg parts has been analysed grouped into:

- Foot (that includes foot and ankle)
- Lower leg (that includes tibia and fibula)
- Knee
- Upper leg (femur)
- Pelvis (pelvis bones).

It can be seen that the lower leg injuries represent almost the 35% of all leg injuries, followed in frequency by the knee ones with near 25%, with pelvis and upper leg injuries accounting each for less than 15%.

At different AIS levels, it is significant that AIS 2 injuries are more frequent than AIS 1 injuries, being together accounting for almost 90% of the injuries.

Regarding regions, the lower leg accounts for more than half of all AIS 2 injuries, and represents the 23% of all the leg injuries, while in AIS 3, upper legs injuries are the most important.

	Foot	Lower leg	Knee	Upper leg	Pelvis	Total
AIS 1	6.8%	6.8%	17%	6.8%	4.2%	41.5%
AIS 2	5.9%	22.9%	7.6%	0%	9.3%	45.8%
AIS 3	0%	5.1%	0%	6.8%	0.8%	12.7%
Total	**12.7%**	**34.8%**	**24.6%**	**13.6%**	**14.3%**	**100% (n=118)**

Table 3-4: Distribution of injuries in the different leg parts (fatal and non fatal pedestrian).

Making focus on AIS 2+ injuries, the injury description of the 69 AIS 2+ injuries from the database are summarized in the figure. Distinction is done between bone fractures (Fx),

ligament ruptures or joint dislocations, according to the description of each injury from the medical experts.

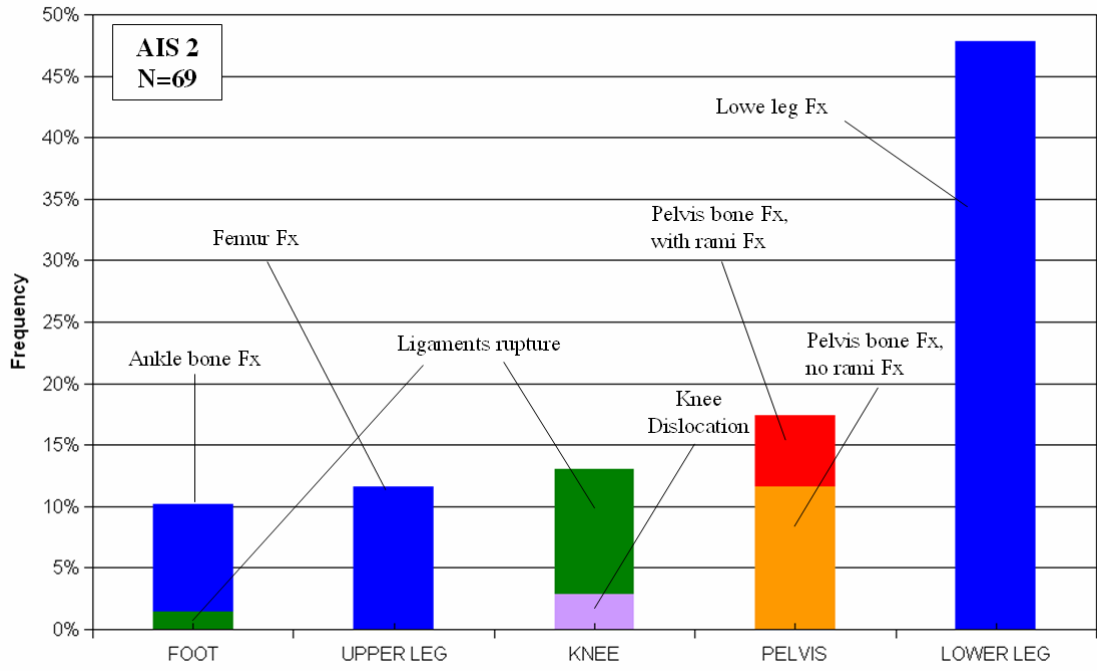

Figure 3-14: Leg injury descriptions for AIS2+ injuries in the legs.

Looking at the frequency they occur, it seems that lower leg fractures and pelvis fractures are the injuries which more often appear in pedestrian accidents, being knee ligaments rupture in a lower stage. Regarding upper leg, there is no injury reported as AIS 2 as all AIS2+ upper leg injuries are femur fractures, which are coded as AIS 3.

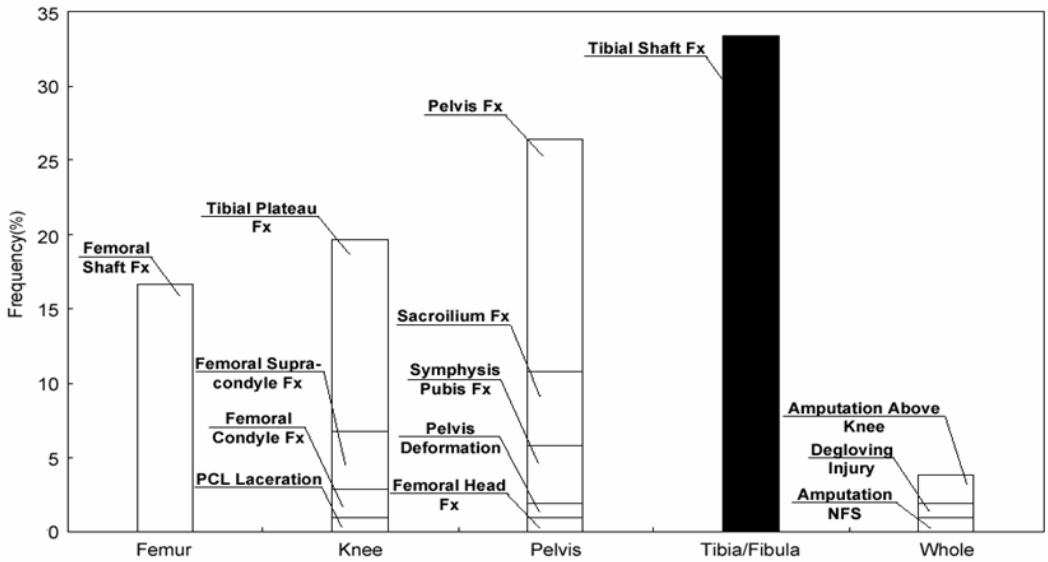

Figure 3-15: Leg injury descriptions for AIS3 injuries in the legs from PCDS database (Takahashi 2000).

This trend can be compared with the one for AIS 3 injuries obtained from the Pedestrian Crash Data Study (PDCS, NHTSA 2000). In this figure, tibia fractures are on the top (33% approx.), followed by pelvis fractures with inherent instability (26% approx.) and knee injuries (20%). Behind, with less importance the femoral shaft fractures.

Both figures show a similar priority order in both AIS 2 and 3 injuries:

- Lower leg fractures.
- Pelvis fractures, being the most frequent the pelvis bone fractures.
- Knee injuries, with ligaments ruptures as well as condyles fractures as most common injuries.
- Femur fractures.

To further investigate on the causes of the AIS 2+ injuries sustained in the legs, the interaction between each pedestrian and the corresponding impacting vehicle has been analyzed. This analysis aims to evaluate how the first impact location with the vehicle (above or below the knee height) may promote lower leg injuries or upper leg injuries and in which extend the bonnet leading edge may be the cause of upper leg injuries. For this analysis, only AIS 2+ injuries sustained in accidents where the pedestrian is hit by the front part of the car are included in this analysis (49 injuries from 27 accidents).

Two parameters are needed to locate the pedestrian with respect its impacting vehicle mean profile:

- Estimated knee height. The estimated knee height has been calculated following the methodology described in Matsui (2003) using the mean and standard deviation for the 50% percentiles measurements for males and females from the UMTRI anthropometry set (Schneider 1983) for the tibialis. Assuming a normal distribution in total body height, a normalized total body height and knee height can be calculated as shown in the formula 1 and 2. If they are considered equal, the knee height estimation can be cleared as shown in formula 3. Moreover, a shoe sole of 25 mm is added to the obtained height, as proposed by Matsui (2003), as typically pedestrian are impacted with their shoes on.
- Vehicle 2D profile. The vehicles 2D front profiles have been digitalized from the available commercial brochures of the cars involved in the accidents to locate the height of the first point of the impact, defined as the uppermost forward point in the front part of each car.

With these data, the next distribution of injuries is observed based on the estimated height of the knee of the pedestrians with respect the first point of contact in the front of each car.

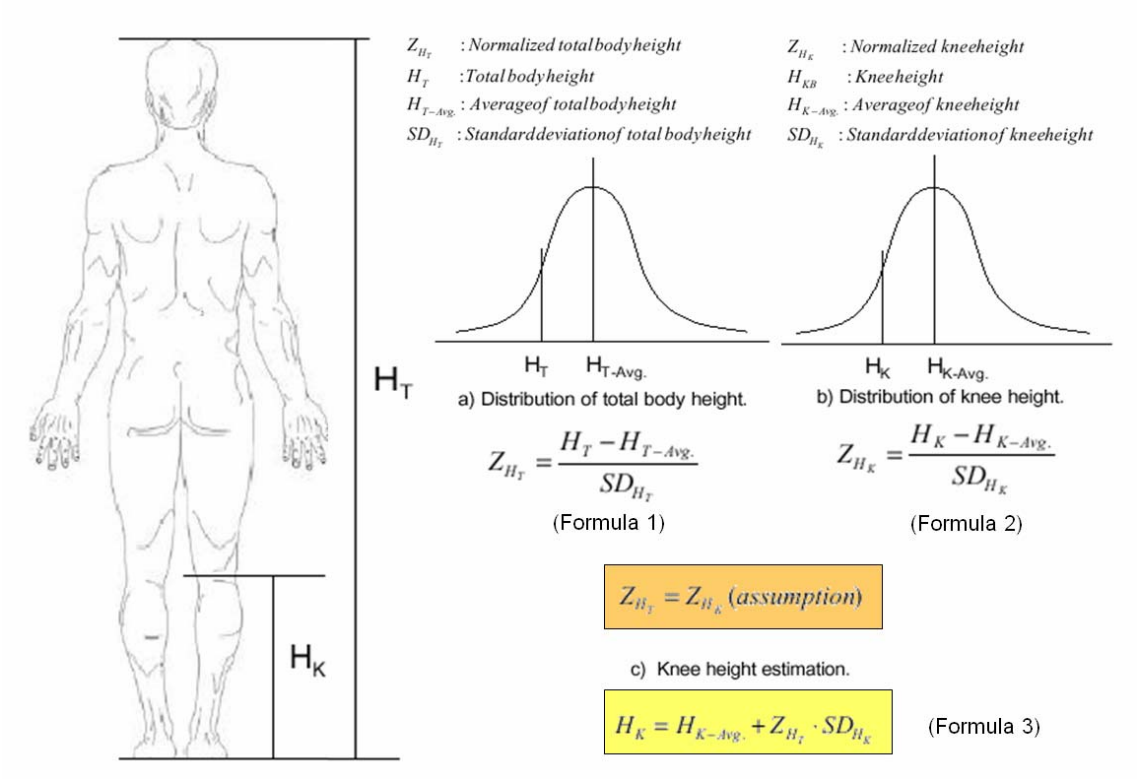

Figure 3-16: Methodology to estimate knee height.

According to Schneider (1983) and adding the sole, the knee height for a 5% female is 0.435 m, for the 50% male is 0.508 m and for a 95% male is 0.566 m.

In terms of knee height, variation from 0.35 to 0.63 m is observed due to the differences in height found in the pedestrians. The minimum knee height belongs to a 9 years old pedestrian, 1.15 m tall and the maximum is found in a 1.88 m male 18 years old pedestrian. It is remarkable that in 77% of the cases the knee height is below that from the 50%ile.

Regarding the height of the first contact point, the subset does not cover SUVs, as there is not any accident with this type of car in this dataset. With these limitations, the highest contact points identified in the sample belong to MPV vehicles (over 0.55 m) while, the rest of vehicles first impact points lay between 0.4 and 0.55 m, being only the 20% below 445 mm.

In terms of the priority injuries identified in the figure, it can be observed that:

- Tibia fracture occurs in impacts below the knee as frequent (48%) as in impacts above the knee (52%), however, when they occur above the knee they are hardly found alone.

- Pelvis fracture occurs more often in impacts above the knee (81%). Moreover, the higher over the knee the impact occurs, the more frequently these injuries are found alone.
- Knee injuries can be found at both impacting zones (50%), so no conclusions can be derived from the figure.

Femur fractures occur if the first impact point is placed above the knee. There are no cases where this injury appears when the car impacts below the knee in the analysed data.

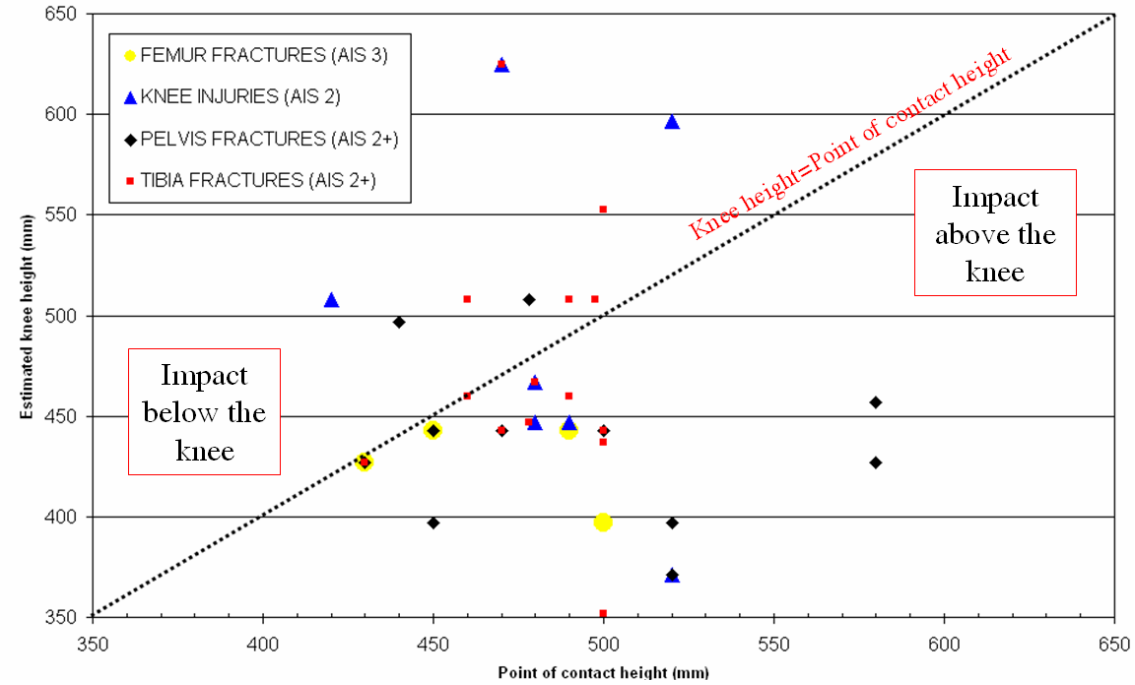

Figure 3-17: AIS 2+ injuries in the legs with respect the impact point.

SECTION I: CONCLUSIONS

Section I has set the basis of the framework of this thesis, showing the first important outputs and obtaining relevant topics to be consolidated further in this thesis.

It has shown firstly the background of the pedestrian testing procedures, analysing the evolution of the pedestrian test procedures recommended by EEVC WG17 (2002) to those finally included in Regulation 2009/78 EC.

Comparing each of these tests individually, it can be concluded:

- Regarding the legform test procedures, it can be concluded that it is still considered to be a very relevant test. The procedure has not been changed in the process but only their threshold limits, therefore demonstrating that it was conceived very robustly. This robustness would allow making minor modifications in the test procedure if the core is maintained and therefore it is worth to concentrate efforts in this thesis in that direction.
- In terms of the upper legform test procedure, it can be seen that within the process the relevance has been lost with the new car designs and it has been kept only for monitoring purposes in the Directives, so it is not of high interest unless the accidentology analysis would indicate the contrary, which has not.
- Finally, regarding the headform test procedures, it can be seen strong modifications of the injury thresholds and the test severity from the EEVC proposals to the current Regulation, with many feasibility issues taken into account in between. This shows that the final solution is a compromise of many

negotiations and therefore the room for further modification in the current environment is reduced. However, these variations along the time would also suggest that the test procedure does not fit 100% its purpose and that there are many other factors not considered that influence significantly this test. This conclusion would encourage working on that direction with an open perspective, adding research based evidence of the influence of some of these factors but being conscious of the limited contribution of this thesis on that topic and the reduced scope for proposing feasible short terms improvements for this test procedure.

Following this interesting comparison between the pedestrian test procedures recommended by EEVC WG17 (2002) and those finally included in EC Regulation 2009/78, a link to real life is mandatory to understand it and to define the issues where this thesis can really add value.

From this accidentology based analysis presented in Chapter 3, the following conclusions can be obtained that will be consolidated further along this thesis.

- The age distribution of the pedestrian casualties and the number of injuries per pedestrian has shown that elder pedestrian would need a special attention when talking about pedestrian protection. Although this effect is seen also in larger pedestrian accident databases it has never been taken into account from a legislative perspective, so it would make sense for this thesis to deepen into the consequences of this consideration from a research basis perspective.
- The relevant injury patterns found for non fatal pedestrian suggest that AIS 2-3 lower extremity injuries are the most important in both frequency and severity, although non fatal head injuries are also typically occurring. The rationale of these findings is explained, for most pedestrian accidents, by the fact that the vehicle impacts first the pedestrian legs and after that, depending on the trajectory and energy, the head impacts with more or less severity on the different vehicle structures. This first impact typically causes femur fractures, knee injuries or lower leg fractures, basically depending on the impacting vehicle geometry and stiffness. This finding supports the relevance of a good legform procedure within the Directive valid for all EU fleet segments ensuring that an appropriate correlation exists between the test requirements and the typical leg injury patters of bone fracture and ligament ruptures. This is not already solved in the current Regulation, and therefore it is worth that this thesis will examine further this issue providing improvements valid for the whole European fleet.
- The latter impact of the head with the car is highly influenced by the outcome of the former impact and, of course, on the stiffness of the impacting structure. In this case, the real world possibilities are infinite but in 95% of the cases, as the

accidents occur with pedestrian in walking position, the head impact has a significant lateral component and a high rotation induced from the first impact. This lateral impact is indeed considered in the legform test but it is not in the headform tests, so this thesis will investigated further which effect can have this rotational acceleration in the outcome of head injuries. Moreover, as the variety of head injury patterns is rather wider than in the legs, as it includes not only bone fracture but also all injury patterns related to neurological injuries, the relevance of the correlation between the test requirements and the real head injury prediction is rather more critical, especially in the non fatal cases. Although it has not been the core work of this thesis, a number of real cases have been analysed regarding head impact scenarios, in joint collaboration with ULP and TNO to gather evidence on appropriate injury prediction criteria for these different head injury patterns, as it seems obvious that HIC criterion alone cannot account properly for all of them.

To consolidate these conclusions along the thesis a number of tools are needed and this Section I presents in Chapter 2 the first one developed in the framework of the thesis, closely link to the test procedures themselves.

Taking advantage of the “learn by doing” process undertaken in the pedestrian test procedures by EuroNCAP during its maturation form EEVC proposal to current Directive, part of the raw data of these test has been used to conduct the first large scale study defining the stiffness characteristics of the European fleet frontal part relevant for pedestrian protection, the first important output as result of this thesis.

In a first phase, the kinematics of the different test configurations have been analysed to identify a set of assumptions to define a unique methodology to obtain the force-deflection characteristics for the different impactors (headforms, legform and upper legform). These methodologies, once proved, have been applied extensively to the whole set of tests available (425), differentiating the adult headform tests impacting on the bonnet from the ones impacting on the windscreen base.

The responses have been grouped for each test configuration (legform tests, upper legform tests, child headform tests, adult headform tests on the bonnet and adult headform tests on the windscreen base) following EuroNCAP rating protocols to define the red, yellow and green groups in each test configuration.

Average parameters (average curves, standard deviation and average unloading slopes) have been calculated for each of the 15 groups (red, yellow and green groups in each of the 5 test configurations defined) leading to a set of corridors, which have been simplified into straight lines to ease handling and dissemination and referred as a stiffness mapping tool.

This stiffness mapping tool, in whatever its form, has resulted to be an important source of data for pedestrian simulation purposes as it represents widely the European fleet

stiffness ranges in the front part of the vehicle. Moreover, although newly tested cars may change the average green, yellow and red curves of the fleet herein obtained, since the corridors have been constructed gathering red, yellow and green curves, their validity as estimates will be maintained while the EuroNCAP rating of the tests is maintained.

The development of these corridors opens high possibilities to the research community as well as facilitates the work to be done in the rest of the thesis as they allow an easy integration on demand with vehicle mathematical models for pedestrian accident reconstruction or parametric studies. In fact, in the long term, they can be easily transferred to accident reconstruction software to be used as robust stiffness estimates for the whole EU fleet.

SECTION II: MULTIBODY ANALYSES OF PEDESTRIAN SCENARIOS.

II

At the sight of the conclusions observed in the accident statistics analyses, this Section looks more in detail in real world scenarios to collect further information regarding the significance of the age in the occurrence of pedestrian injuries and at which extent this effect could be considered from a testing perspective. With this objective, four accident cases, representative of typical pedestrian accident scenarios have been selected and mathematically modelled, making use of a pedestrian and a vehicle model with the following requisites:

- A validated pedestrian model capable of being scaled in size and age. An upgrade of the MADYMO pedestrian model, (already scalable in size and which main features are presented in the Chapter 4), has been developed within this thesis to allow the model to be also scalable in age based the results of an extensive study conducted that quantifies how age influence the human body tissues and translate this to the MADYMO pedestrian model.
- A vehicle mathematical model with detailed geometry and stiffness characteristics representing the same vehicle make and model of those from the real world scenarios. Although there are reported a number of case by case basis approaches, this thesis has enhanced this process developing a cost effective methodology, (Chapter 5), that integrates the generation of the detailed geometry of the vehicles, with the previously developed stiffness mapping tool and a parametric construction of the multibody frame.

With these models in place, the four scenarios have been simulated in MADYMO and its results reported in the Chapter 6. In addition, a parametric study is also presented in this chapter to complement these results and quantify more precisely the relevance of age in these accidents in order to derive conclusions on the feasibility to take into account age as an extra variable in the pedestrian test procedures.

4 SCALABLE PEDESTRIAN MODEL IN SIZE AND AGE

As the objective of this section of the thesis is to reproduce real pedestrian scenarios, a pedestrian model capable to reproduce any typology of adult human being possibly involved in a pedestrian accident is needed. This premise is overambitious and there is not currently any pedestrian model capable of such coverage.

The current pedestrian model that best fits these requirements, at least partially, is the MADYMO scalable multibody pedestrian model developed by TNO (2003), which has three reference sizes, the 5% female, the 50% male and the 95% male. There are other ellipsoid pedestrian models available in MADYMO, as those created by Chalmers (Yang, Lovsund et al. 2000), JARI (Neale, Hardy et al. 2003) and the Road Accident Research Unit from Univ. Adelaide (Garrett, 1998) showing some specific differences with the TNO model, as has been reported in literature (Mizuno, 2003, Neale, Hardy et al. 2003, and Linder, Clark et al. 2004). However the latest improvement of the TNO model, taken into consideration a number of aspects highlighted with the other models, as well as their new functionality of scaling, has made the TNO MADYMO model the preferable to be used in this thesis.

This functionality enables the model to be scaled to the specific height and weight of the pedestrian in question – or even to 35 anthropometrical parameters if these are known. The MADYSCALE software scales the model's geometry, mass and inertial properties, joint characteristics, contact characteristics, force models, sensor locations, fracture levels and Viscous Criteria (V*C) criterion (van Hoof, 2003). This MADYSCALE has been

verified in an extensive validation with Post Mortem Human Surrogates (van Hoof, 2003) and in real world accident reconstructions (Coley, 2001).

The extensive validation of these MADYMO MB pedestrian human models has made them a very useful tool to simulate the motion of pedestrians in real world accidents. In fact, it is generally accepted their usefulness in predicting the kinematic responses of pedestrian impacts and the validity of using their outputs regarding load values and injury criteria for qualitative analysis (Happee 1999; McLundie 2002). However, it is also accepted its limitations in making actual injury or force predictions from the models.

These characteristics are highlighted again in van Hoof (2003), where the accuracy of the MADYMO predictions relative to a set of PMHS full pedestrian tests is evaluated. They showed that the head impact location of the pedestrian with the vehicle is predicted with a correlation score of over 90%, and similarly occur with the head impact velocity. However, in terms of acceleration, the correlations achieved were lower, reaching an acceptable 76% for the legs acceleration, but an inacceptable 40-50% for the pelvis and the head. These results suggest that HIC values obtained with this pedestrian are just useful for qualitative purposes, but leg fractures can be evaluated at some extend if the accurate vehicle contact characteristics are considered.

4.1 Description of MADYMO MB pedestrian models.

The MADYMO user manual (TNO 2004) describes that the MADYMO MB model consists of 64 ellipsoids that represent the outer surface of an average Western European human being according to the anthropometry data of RAMSIS software (Speyer and Seidl 1997). The different body regions of the model are assigned with the inertia values calculated based on the ones from UMTRI (Schneider 1983) for the different percentiles, 50% male, 95% male and 5% female.

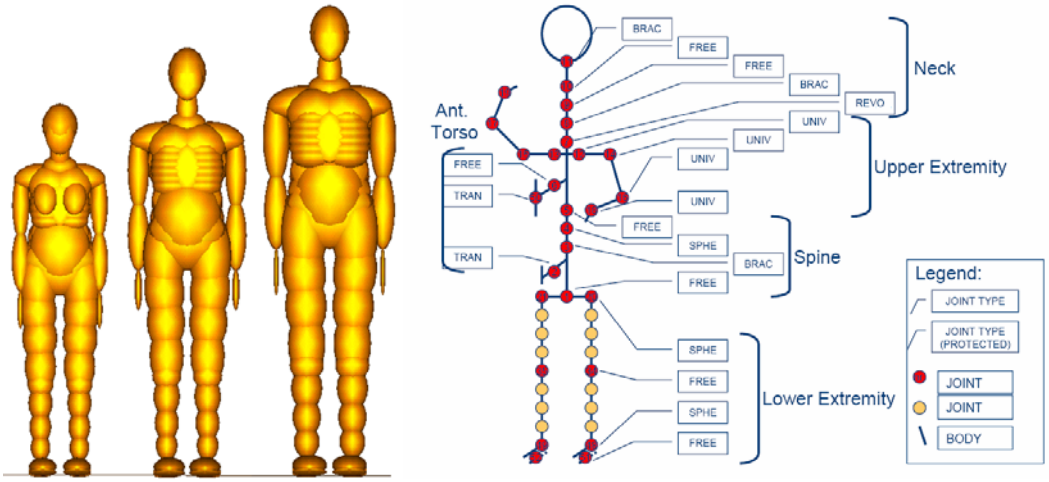

Figure 4-1: Structure of the MADYMO multibody model (Van Rooij, 2003)

The skeletal structure of the human body is modelled with 52 rigid bodies, which geometry is defined through ellipsoids representing most of the bony parts of the skeleton. They are interconnected by kinematic joints, representing the articulations, as seen in the Figure 4-1. MADYMO MB human models output the acceleration, velocity and displacement, both lineal and angular, for any of the ellipsoids conforming the body as well as force and torque (in any direction) in any of the joints.

Moreover, it is equipped with the injury parameters typically used in crashworthiness scenarios as HIC, peak 3ms acceleration or Viscous Criteria although not all of them are applicable for pedestrian scenarios.

- The spine and the neck of the models are modelled by 4 kinematic joints: (1 free joint at lower lumbar location, 1 spherical joint between the lumbar and thoracic spine (L1-T12), 1 free joint at the lower neck (T1-C7) and1 free joint at the upper neck (C1-Head OC). These free joints allow elongation and the stiffness in the different directions was modelled by six-DOF (Degree of Freedom) restraints at the joint locations. The rotational stiffnesses in the spine were based on Yang (2000). The translational stiffness in z-direction was based on the resultant elongation stiffness of the MADYMO occupant model (Happee et al., 2000), while the translational stiffnesses in x- and y-direction were chosen higher than in z-direction to prevent lateral translation. In the head, MADYMO models output the HIC as the head injury criteria for pedestrian scenarios, correlated with head injuries by Prasad-Mertz (1998) as shown in the figure.

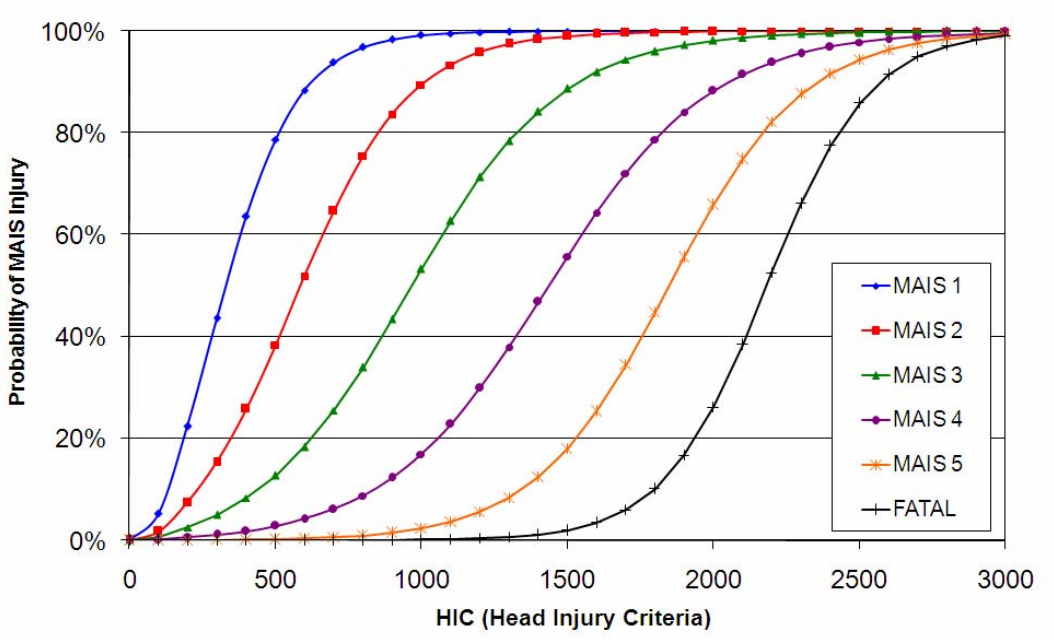

Figure 4-2: Correlation Head Injury Criterion - MAIS injuries in the head.

- Thorax and abdomen are represented by a number of ellipsoids (pelvis, abdomen,

ribs, shoulders and chest) superimposed in order to avoid discontinuities in the outer surface of the model. Their contact characteristics (stiffness, hysteresis, and damping) from the lateral load on pelvis, abdomen, ribs and shoulders have been taken from the biofidelity requirements for the EuroSID-1 dummy (ISO-N455, 1996) and validated with lateral impact against Post Mortem Human Subject (PMHS) tests (Kajzer 1990, Yang 1995, Kajzer 1993, Roberts 1991).

- The hip joint was modelled by a spherical joint with joint stiffness characteristics taken from Frankel & Nordin (1980). These joint stiffnesses were found to agree well with ranges of motion of the RAMSIS human model (Speyer and Seidl, 1997).
- The knee is modelled with a kinematic free joint. Linear and nonlinear joint resistance functions have been implemented based on data available from literature, optimized for an approximately extended position, as this position is most relevant for pedestrian loading. The linear lateral bending stiffness in the knee joint was based on the dynamic data of Kajzer (1997). This dynamic stiffness is significantly larger than the quasi-static values reported by Piziali & Rastegar (1997) but comparable to EEVC requirements (EEVC, 1994). For knee lateral shear, the EEVC (1994, 1998a) has defined an injury tolerance level of 4 kN force and 6 mm displacement. This results in a linear stiffness of 6.7E5 N/m, which has been applied in the pedestrian model. For pedestrian applications, forward/rearward shear is considered of minor importance and, therefore, the stiffness selected for lateral shear has also been applied for forward/rearward shear. Results from Piziali & Rastegar (1997) indicate that this is acceptable for conditions with an extended knee. The knee flexion/extension stiffness has been implemented using volunteer data (Engin, 1979a; Ma et al. 1995) and the axial compression stiffness based on PMHS data from Walker & Hajek (1972).
- The legs are implemented with bending and fracture properties at several locations in the femur and tibia using bending/fracture joints. The location of the middle bending joint in the femur corresponds with the location of the femur load cell in the Hybrid III dummy. The positions of the upper and lower bending joints in the tibia correspond with the positions of the tibia load cells in the Hybrid III dummy.
- Cardan restraints have been implemented at the bending joints to model the bending stiffness of femur and tibia. Angular stiffness functions were derived from simulations of the quasi-static bending tests in anterior-posterior and lateral-medial directions by Yamada (1970). The angular stiffness was assumed to be equal throughout one long bone. Therefore, the same characteristics have been used for all three Cardan restraints within one segment.
- A spherical joint is used for the ankle, which rotational stiffness for dorsiflexion and inversion/eversion was derived from volunteer data (Crandall et al., 1996). Since

both volunteer and PMHS experiments have shown that the ankle dorsiflexion stiffness depends on the knee flexion angle, inward rotation of the foot has been implemented as a combination of knee and ankle rotation using data from Engin (1979b).

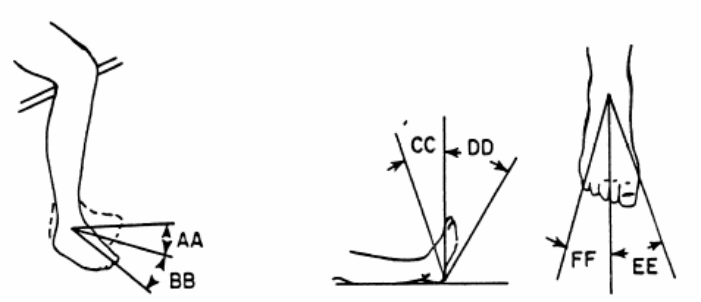

AA- Knee medial rotation

BB- Knee lateral rotation

CC- Ankle dorsiflexion

DD-Ankle plantar flexion

EE- Ankle inversion

FF-Ankle eversion

Figure 4-3: Knee and ankle range of motions.

Fracture of the femur and tibia has been implemented through fracture joints, which are spherical joints that are initially locked until a pre-defined fracture trigger signal exceeds the fracture tolerance level. Bending moments and shear forces were used as fracture trigger signals in these models, so when any of the trigger signal exceeds its threshold, the joint is unlocked.

Once the fracture tolerance is exceeded, the angular resistance in the fracture joint is set to zero and both parts of the fractured bone are free to rotate relative to each other.

The fracture limits selected for an average male are:

Part	Shear Force	Reference	Bending	Reference
Femur	6,3 kN	EEVC (2002)	430 Nm	EEVC (2002)
Tibia	4,0 kN	Yang (1997)	285 Nm	Nyquist (1985)

Table 4-1: Summary of injury thresholds in the male average MADYMO pedestrian model.

The robustness of these fracture tolerances for the MADYMO pedestrian model were analysed thoroughly in Van Hoof (2003). In this analysis, 3 different sets of thresholds were selected covering the whole range of femur and tibia fracture tolerances found in the literature in terms of shear force and bending moment.

For each of them, its capacity to predict the severity and the timing of the injuries reported in 4 full pedestrian PMHS test (INRETS, 1997) is analysed modelling this set of tests with MADYMO. These PMHS tests were conducted at impact velocity range from 32 km/h to 40 km/h with PMHS subjects ranging from 75 to 94 years old and positioned laterally with

respect to the vehicle. The three sets of injury thresholds selected are shown in the Table 4-2 and the results of the analysis in terms of injuries reported and injuries predicted is shown in Table 4-3.

	U-Leg force (kN)	U-Leg bend. (Nm)	L-Leg force (kN)	L-Leg bend. (Nm)
Set 1 (Original)	6.3 (EEVC, 2002)	430 (EEVC 2002)	4.0 (Yang, 1997)	285 (Nyquist, 1985)
Set 2 (low)	2.6 (Yamada, 1973)	224 (Yamada, 1973)	2.7 (Yamada, 1973)	194 (Yamada, 1973)
Set 3 (high)	6.3 (Rodmell 1998)	430 (Rodmell 1998)	5.0 (Nyquist, 1985)	328 (Nyquist, 1985)

Table 4-2: Injury threshold sets analysed in Van Hoof (2003).

It can be seen that the original set and the one based on the high fracture tolerance only diverge in the tibia fracture threshold while the set based on the low fracture limits has thresholds 50-60% lower than the other two sets.

	Injuries reported	Set 1 (Original)	Set 2 (Low)	Set 3 (High)
T00	R: knee ACL rupture	FX R L-leg (up)	FX R L-leg (up) FX L U-leg (low) FX R U- leg (low)	FX R L-leg (up)
T01	R: fibula FX & ankle ligament rupture L: femur fracture at femoral head and knee, ankle fracture	No fracture	FX L U-leg FX R L-leg (up) FX R U-leg FX L L-leg (up)	No fracture
T02	R: fibula fracture at head & neck. L: Femur fracture & FX fibula head	FX R L-leg (up) FX L L-leg (up)	FX L U-leg FX R L-leg (up) FX L L-leg (up) FX R U-leg	No fracture

T03	R: upper & lower tibia fracture, upper fibula fracture	FX R L-leg (mid)	FX R L-leg (mid) FX L U-leg (low) FX R U-leg FX L L-leg (mid)	No fracture
T04	R: Tibia & fibula fracture at ~1/3 from top	FX R L-leg (mid) FX L L-leg (mid)	FX R L-leg (mid) FX L U-leg (low) FX L L-leg (mid) FX R U.leg	FX R L-leg (mid)

Table 4-3: Analysis of the injury prediction of the different sets of leg injury thresholds analysed (Van Hoof, 2003)

From this analysis a number of conclusions are worth to highlight, especially to deal with elder pedestrians:

- The set of thresholds based on the lowest value for fracture are too low to give confident results for pedestrian scenarios as they predict upper and lower leg fracture in all cases.
- In environments where only ligament rupture occurs, as MADYMO knee ligament do not break an unrealistic load path take place and tibia fracture is likely to occur.
- In the tests involving femur fractures, neither the original nor the high set of thresholds provide confident results, suggesting that these limits for elder pedestrian are too high and are underestimating the real injuries sustained.
- In the test involving tibia fractures, it seems that the high set of thresholds underestimates the occurrence of these injuries and that the original set of thresholds only works well in the multiple severe tibia fracture cases, being less confident in cases with isolated tibia fractures. This would suggest that, again using these thresholds for elder pedestrian the capacity of predicting injuries is not adequate enough.

From these conclusions it is clear that age dependency fracture limits are necessary to predict accurately leg injuries and deriving them will be the objective of the following parts of this chapter.

4.2 Literature review on age effect in human body tissues.

In order to define how age affects the behaviour of the human body tissues, an extensive search into the current state of the art has been undertaken. The data collection has been based on tissue level to allow the characterization of the material models typically used to

model human body tissue in FE models. For that reason, not only data on bone is collected but also information on other tissues, going far beyond the strictly necessary data to consider age in the MADYMO MB but presenting a coherent and complete state of the art in this area. Unfortunately, the quantity and homogeneity in the data has been found to be much dependent on the tissue and in many cases, it would not allow to consider age clearly as a variable on their different characteristics.

4.2.1 Bones.

Bone is a hard material that has a stress-strain relationship similar to many engineering materials (Fung, 1993). It is known that dry bone is brittle and fails at a strain of 0.4 %; but wet bone is less fragile and fails at a strain of 1.2 %.

Fung (1993) explains that a long bone is non homogeneous and consists of a shaft (diaphysis) with an expansion (metaphysis) at each end. A long bone diaphysis is a hollow tube which walls are composed of dense cortex (compact or cortical bone), which is thick throughout the extent of the diaphysis but becomes a thin shell at each metaphysis. The central space (medulla) inside the diaphysis contains the bone marrow.

There are two main types of bone, compact bone (cortical) and trabecular bone (cancellous).

- The cortical bone appears solid except for microscopic spaces. Its crystalline structure gives it hardness and rigidity forming the structural shell of most bones and nearly all of the diaphysis of long bones.
- Cancellous bone is continuous with the inner surface of the cortical shell. It consists of slender, irregular trabeculae (bars) of compact bone which branch between them to form intercommunicating spaces that are filled with bone marrow.

The classification of bone tissue as cortical or cancellous is based on porosity, which is the proportion of the volume occupied by non-mineralised tissue. Cortical bone has a porosity of approximately 5 to 30 %, whereas cancellous bone porosity may range from approximately 30 to more than 90 %. The distinction between very porous cortical bone and very dense cancellous bone is somewhat arbitrary.

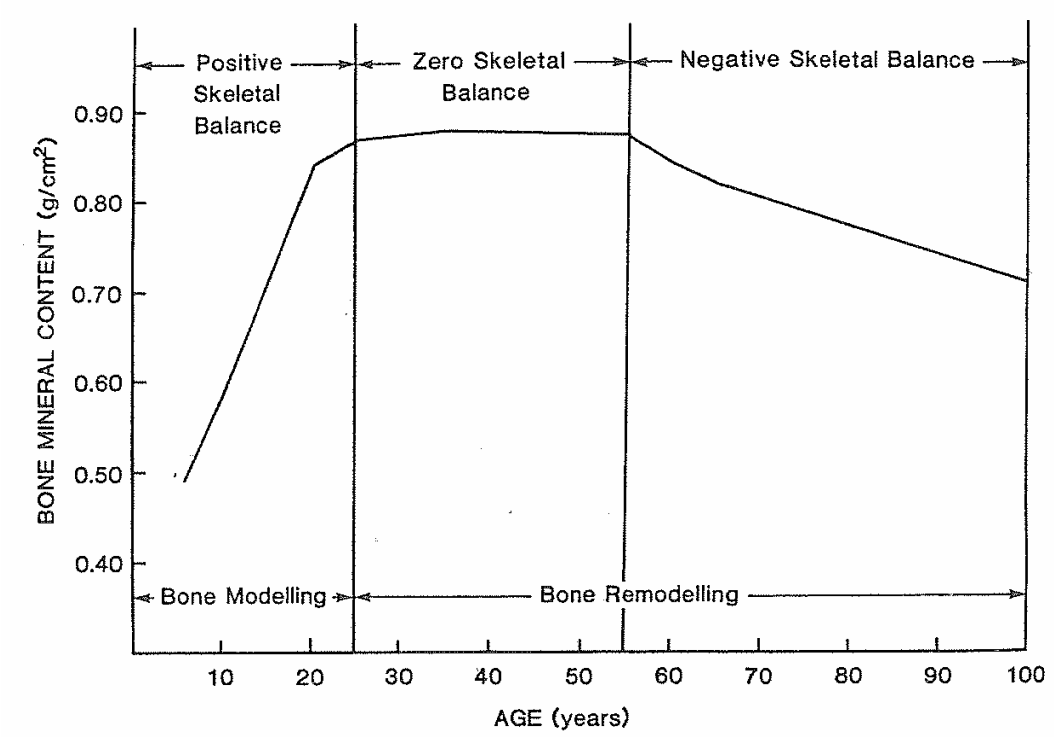

Figure 4-4: Skeletal balance with age (Kleerekoper *et al.*, 1986).

In a growing person, the end of the long bone is separated from the main bone by a layer of cartilage, a cartilaginous growth plate (epiphyseal plate). The epiphyseal plate allows the diaphysis of the bone to increase in length until early childhood. As a child grows, cartilage cells are produced on the epiphyseal side of the plate. They are then destroyed and the cartilage is replaced by bone on the diaphyseal side of the plate. In this way the bone on the diaphyseal side increases in length. When the epiphyseal cartilage stops dividing and bone replaces the cartilage the fusing of the diaphysis and the epiphysis occurs (approx. at 25 years old) and the growth of the bone finishes.

While bones grow in size, the mineral content of the skeleton increases progressively (childhood and adolescence), and there is a 'positive skeletal balance' on the body. However, throughout the rest of the adult life, old bone is removed and new bone is deposited at the same site. During the period of 'zero skeletal balance', the amount of old bone removed matches exactly with the new bone replaced. If there is an excessive removal of old bone or deficient replacement of new bone, the skeletal balance in the body becomes negative (approx from 55 years old). In general, bone loss leads to both trabecular bone atrophy and cortical thinning (Horikoshi 1999, Pistoia 2003) although this effect is partially compensated by an increase in cortical diameter (Koshla 1994), which means that the torsional stiffness increases while buckling resistance reduces. (Beck 2001)

In general, bones are modelled in FE models as piecewise lineal plasticity material or elastic plastic materials. In the reference strain rate, this material model behaves elastically until it exceeds the yield stress. From them, it follows a hardening function until it reaches its ultimate stress where the material fails. Therefore, to define the stress-strain curve (at reference strain rate level) the elastic modulus (E), the yield stress (σ_y), the hardening function and the ultimate stress (σ_u) and strain (ε_u) are needed.

In cases where there is dependency on the strain rate, when it increases, the slope and the limit of the elastic part also increase. Regarding the plastic part, the initial plastic strain is reached earlier but the ultimate stress is commonly reduced, so there are strain rates where the global plastic deformation is higher than in the reference strain rate and cases where it is lower. To include the strain rate dependency effects in the material there are several mathematical models that could be used, as described further in this chapter.

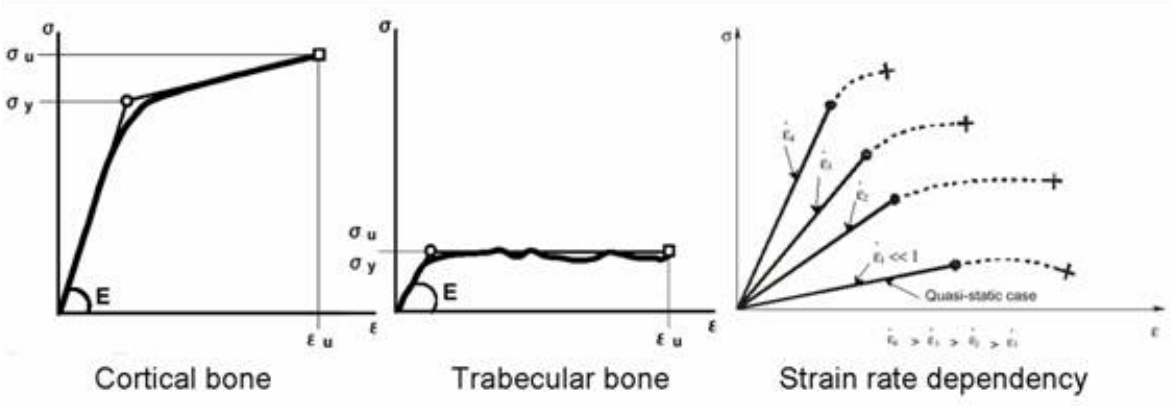

Figure 4-5: Bone stress-strain typical behaviour.

The relevant literature analysed for the age dependency of bone properties is included in the Table 4-4 including several parameters that define each dataset.

Reference	Properties	Test	Specimen	Strain rate (s^{-1})
Bayraktar (2004)	E	Tension Compression	Femur cortical and cancellous bones	0.5
Burstein (1976)	E, σ_u, σ_y, E_p	Tension Compression	Cortical and cancellous bones.	2
Dalstra (1994)	E	Tension	Pelvis cortical and cancellous bone	Quasi-static
Ding (1997)	E, σ_u, ε_u	Tension Compression	Cancellous different bones	0.002

Ducheyne (1977)	E, σ_u	Compression	Femur cancellous bone	0.002-9.16
Evans (1973)	E, σ_u	Tension Compression	Femur cortical bone	Quasi-static
Imperial College (2004)	E, σ_u	Compression	Femur cortical bone	0.8-17
Leung (1983)	σ_u	Compression	Femur cortical and cancellous bones.	0.001
Li (2007)	E	Tension	Hip cortical and cancellous bone	-
McElhaney (1966)	E, σ_u	Compression	Femur cortical bone	0.001-300
Morgan (2003)	E	Tension Compression	Cancellous bones	0.1
Mosekilde (1987)	E, σ_u	Tension	Vertebral cancellous bone	-
Rohlmann (1980)	E, σ_u	Tension	Femur cancellous bone	-
Saha (1976)	E, σ_u	Tension	Femur cortical bone	133
Stitzel (2003)	E, σ_u, ε_u	Bending	Ribs cortical bone	5
Wall (1972, 1974)	E, σ_u	Tension	Femur cortical bone	0.08-45
Yamada (1970)	E, σ_u	Tension Compression Bending	Cortical/cancellous bones.	Quasi-static

Table 4-4: Relevant literature for bone properties: Elastic modulus (E), plastic modulus (E_p) yield stress (σ_y), ultimate stress (σ_u) and ultimate strain (ε_u)

Within these references, elastic modulus (E), ultimate strength ($\sigma_{u,}$), yield stress (σ_y) and plastic modulus (E_p) are analysed taken into account age and strain rate. The first two properties are investigated in-depth in a first qualitative analysis for femoral sample datasets (the most frequent) to then add a quantitative approach to understand the anatomical variation of each property along the human body.

As it was observed by Fung (1981) that the non-homogeneous anisotropic composite structure of bones causes that the mechanical properties in tension and in compression to differ, the elastic modulus and ultimate strength derived from tension and compression tests are analysed together in the next figures and in them it can be highlighted the differences.

On the other hand, the other two material parameters age dependencies, yield stress and plastic modulus, are analysed only based on Burstein (1976).

Figure 4-6 and Figure 4-7 show respectively the different trends observed for the elastic modulus found in the literature with respect age and strain rate for femoral samples.

As commented by Fung (1981), these two figures highlight that tension and compression moduli show discrepancies and depend on the loading conditions. In the compression area, the elastic modulus for the cancellous bone (Ding, 1997) and the one from cortical bone (Burstein, 1976) are shown. It is remarkable that the elastic modulus in compression for the cancellous bone is 15 times smaller than that from the cortical bone samples.

Regarding the evolution with age, it seems that the cortical bone series show decreasing elastic modulus with increasing age, after a peak value in the age range of 40 to 50 years old.

In its variation with strain rate (Figure 4-7), the elastic modulus in compression from McElhaney (1966) and Imperial College London (2004) show agreement, confirming that the elastic modulus in compression seems to increase with increasing strain rate.

In the positive part of the figure, Burstein (1976) and Evans (1973) data for the elastic modulus in tension show similar trends and values, with a decline in the modulus of elasticity with increasing age after reaching a peak in the adult age range (20-49).

Wall data (1974) also show this trend but with unexpected lower values, even considering that they were performed at lower strain rate, since it seems that for Wall data (1974) the elastic modulus does not increase with strain rate. However, in more recent tests conducted at the Imperial College London (2004), an increase in the modulus of elasticity was observed in tensile tests at two different strain rates.

On conclusion, it seems that the elastic modulus, both in tension and compression, increases with age until a peak in the adult age is reached and from then, it declines with age. Regarding its evolution with varying strain rate, the higher it is, the higher also becomes the elastic modulus for all ages and both tension and compression.

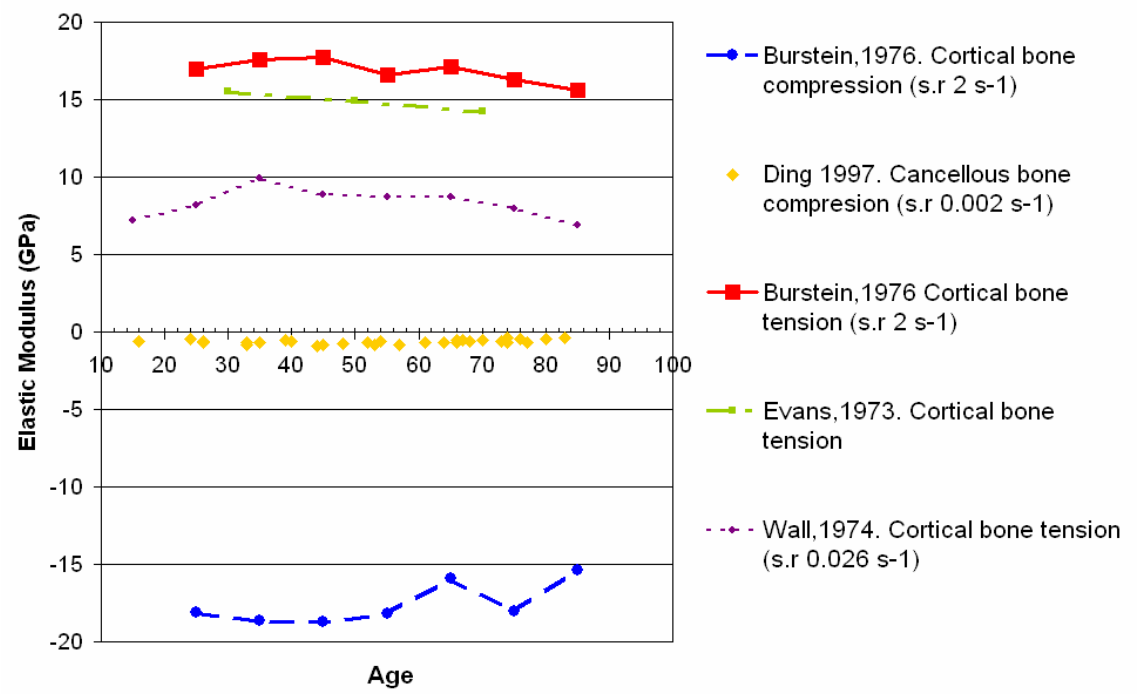

Figure 4-6: Elastic modulus variation with age (negative values are compression test and positive values are tension tests).

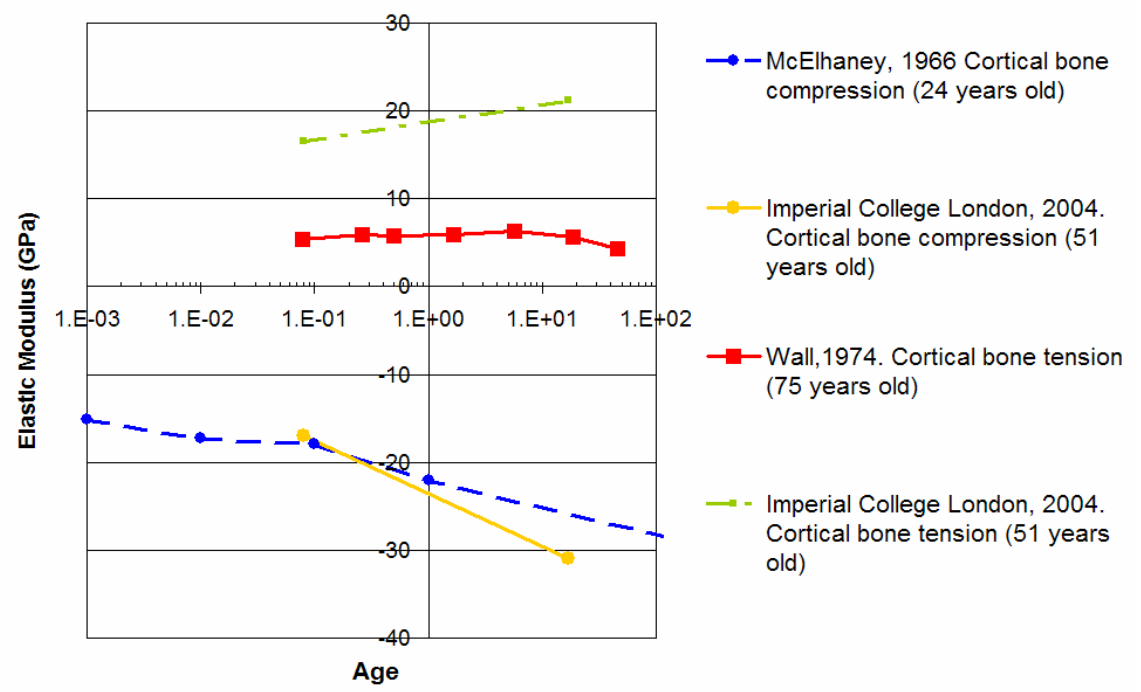

Figure 4-7: Elastic modulus variation with strain rate (negative values are compression test and positive values are tension tests).

Regarding the values, the figures have shown the ones corresponding to femoral samples, however, others for different bones are summarized in the Table 4-5.

Bone	Elastic modulus (GPa)	
	Tension	Compression
Femur (cortical)	17.26 [1]	18.35 [2]
Tibia (cortical)	18.05 [1]	32.95 [2]
Fibula (cortical)	18.54 [1]	-
Humerus (cortical)	17.16 [1]	-
Ulna (cortical)	18.44 [1]	-
Radius (cortical)	18.54 [1]	-
Ribs (cortical)	-	7.5-10.7 [3]
Hip bone (cortical)	-	17 [4]
Femur (cancellous)		0.441 [5]
Tibia (cancellous)	-	0.635 [6]
Vertebra (cancellous)	-	0.068-0.088 [1]

Table 4-5: Reference values for elastic modulus in different bones. [1] Yamada (1970), [2] Burstein (1976), [3] Stitzel (2003), [4] Li (2003), [5] Rohlmann (1980), [5] Ding (1997).

Figure 4-8 and Figure 4-9 show the different datasets found in literature for the ultimate strength in function of age and strain rate for femoral samples. These figures emphasize more the previous comment by Fung (1981) as in this case, the difference between tension and compression values is more obvious. The compressive strength values from the cortical bone in the Yamada data (1970) are similar for both the 20 to 29 and 30 to 39 year-old groups and from then, there is a general trend for strength to decrease with increasing age. The general trend observed by Yamada for decreasing compressive strength with increasing age can be seen from the Burstein data also. However, each point from Burstein is approximately 40 MPa above those from Yamada since Burstein tested at strain rate of 2 s^{-1} while Yamada tests were quasi-static. Taking this loading rate into account, the ultimate compressive strength from Burstein may match Yamada dataset.

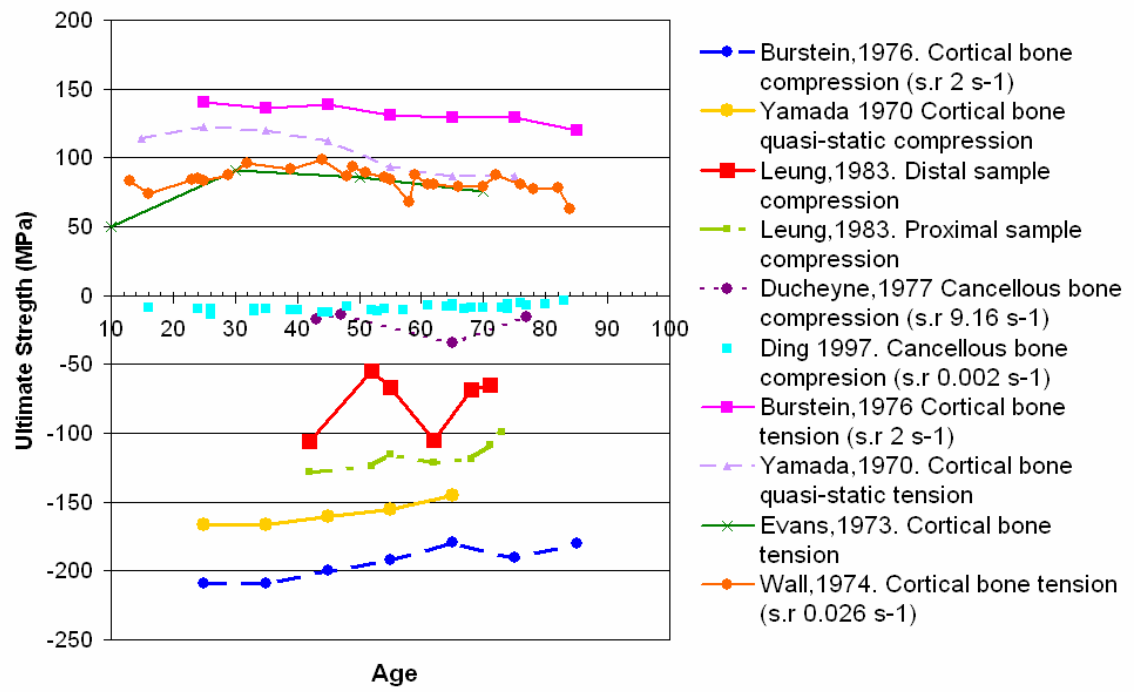

Figure 4-8: Ultimate strength variation with age (negative values are compression test and positive values are compression tests).

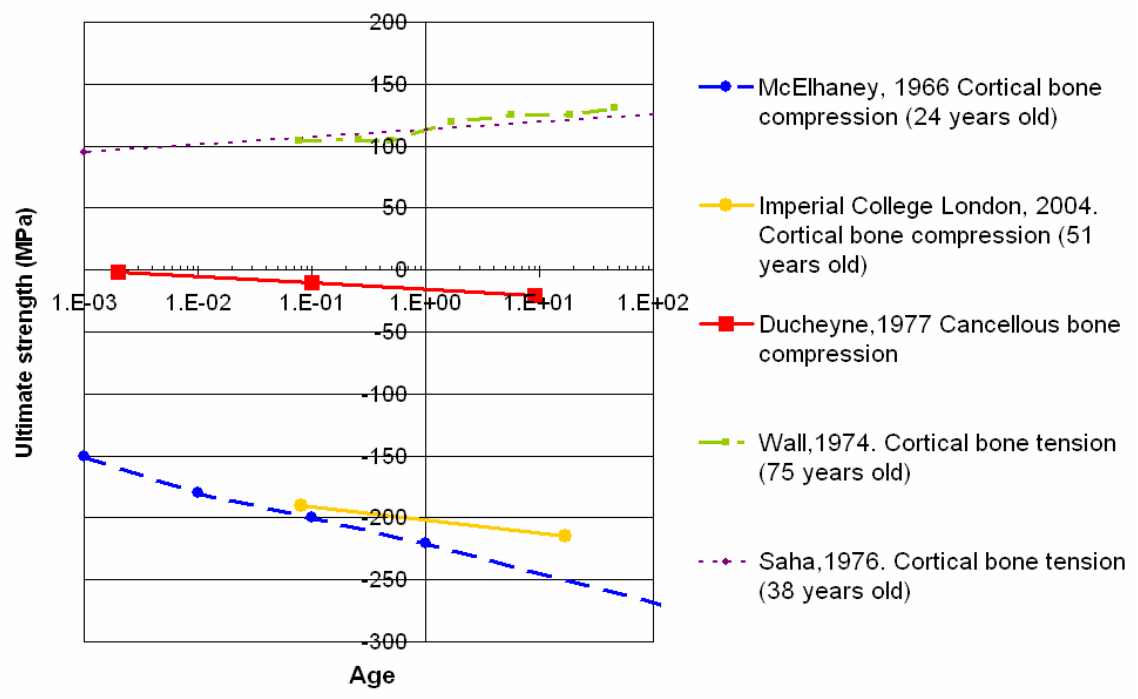

Figure 4-9: Ultimate strength variation with strain rate (negative values are compression test and positive values are compression tests).

Regarding cancellous bone, data from Ducheyne (1977) show that cancellous bone has much lower ultimate compressive strength, compared with cortical bone. Ding (1997) also reported on tests of specimens of cancellous bone. Ducheyne tested at higher strain rate and therefore it makes sense its higher values with respect Ding data.

The data from Leung (1983), conducted on mixed cortical and cancellous bone, falls between the purely cancellous and cortical samples, showing also a trend of decreasing strength with increasing age, as commented with the cortical bone.

Moreover, this data are similar to those reported by McElhaney (1966) at the lowest strain rate. This agrees with a hypothesis that at low strain rates, such as that used by Leung, the response of bone specimens containing both cortical and cancellous bone would be dominated by the cortical bone properties.

Regarding its variation with strain rate, McElhaney (1966) and Imperial College London (2004) data, corresponding to cortical bone, show close agreement in the evolution and in the values at the strain rate level of Burstein (1976).

McElhaney and Imperial College London test data show that the ultimate compressive strength tends to increase with increasing strain rate, which is in agreement with some of the observations already done.

For cancellous bone, Ducheyne (1977) data variation with strain rate show similar slopes to the ones from the Imperial College London (2004), with the corresponding shift in value due to the difference between cortical and cancellous bone.

In case of ultimate tensile strength, Yamada (1970) data shows a peak in tensile strength in the age range of 20 to 29, decreasing from this age onwards.

The test data from Wall (1974) show a similar trend to that shown by the Yamada data. That is a decrease in tensile strength, with increasing age after peak strength has been reached. A difference in this trend is that the peak value from the Wall data occurs at the age of about 40 years, as opposed to being in the range of 20 to 29 years, as it was in the Yamada data.

The test data from Evans (1973) agrees well with that from Wall (1974). It is remarkable that Yamada data agrees with the Wall (1974) and Evans (1973) data with older subjects, but the difference between Yamada and the other sources increases at earlier ages.

As noted earlier, Burstein (1976) tested at strain rates above those of quasi-static loading. This explains the difference in ultimate tensile strength from the values reported by Wall (1974) and Evans (1973); however the trend of the three sets closely resembles.

For its relationship with strain rate, the data from Wall (1974), and Saha (1976) show an increase in the tensile strength with increasing strain rate similar to the one seen for the ultimate compressive strength.

On conclusion, it seems that the ultimate strength in tension and compression increases with age until a peak in the adult age is reached, and from then, it decreases with age. With respect the strain rate, increasing strain rate leads to increasing ultimate strength levels.

As occurred with the elastic moduli, the values shown as far as now are valid for femoral samples. For other bones, reference values are given by Yamada (1970) and are summarized in the Table 4-6.

Bone	Ultimate strength (MPa)	
	Tension	Compression
Femur (cortical)	121.64 [1]	154.02 [1]
Tibia (cortical)	140.28 [1]	151.08 [1]
Fibula (cortical)	146.17 [1]	122.62 [1]
Humerus (cortical)	122.62 [1]	125.57 [1]
Ulna (cortical)	148.13 [1]	117.72 [1]
Radius (cortical)	149.11 [1]	114.77 [1]
Femur (cancellous)		10-17 [2]
Tibia (cancellous)		8.8 [3]
Vertebra (cancellous)		0.8-7 [4]

Table 4-6: Reference values for ultimate strength for different bones. [1] Yamada (1970), [2] Ducheyne (1977), [3] Ding (1997), [4] Mosekilde (1987).

Regarding the plastic modulus and the yield stress, only Burstein (1976) analyses these properties and its variation with age.

The dataset from his work is presented in the Figure 4-10.

It can be seen in both cases that the age has an influence in the values of these properties. While the age makes the yield stress to decrease with an average rate of 2% per decade, the plastic modulus is increasing with age with a higher average rate per decade (near 8%).

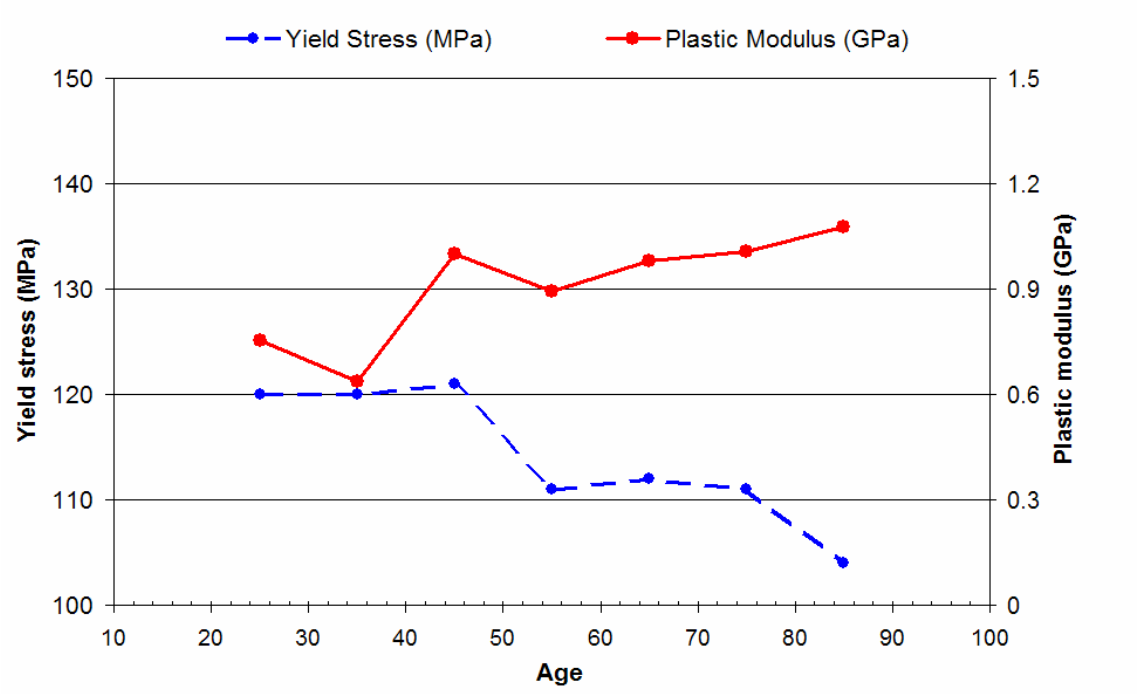

Figure 4-10: Bone plastic modulus and yield stress variation with age. (Burstein 1976)

4.2.2 Ligaments and tendons.

Ligaments and tendons are soft collagenous tissues. Ligaments connect bone to bone and tendons connect muscles to bone playing both a significant role in musculoskeletal biomechanics.

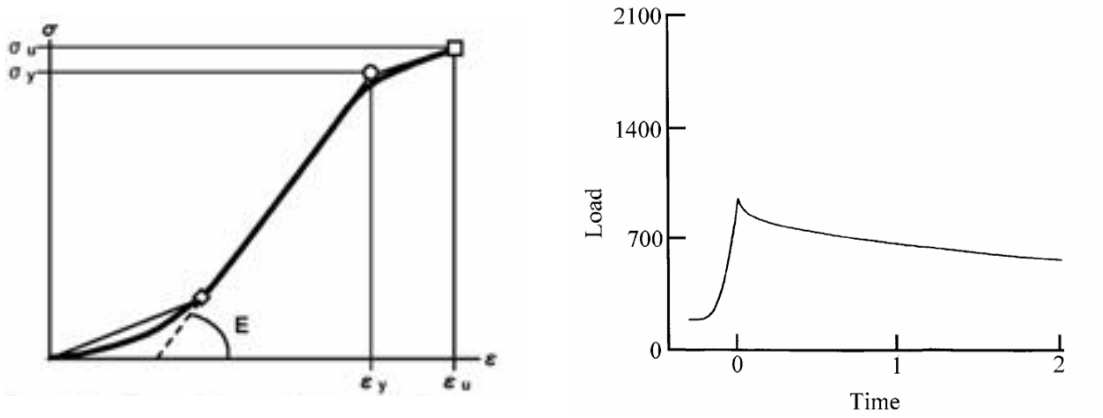

Figure 4-11: Ligaments and tendons stress-strain curves.

Ligaments are defined as dense bands of collagenous tissue (fibres) that span a joint and then become anchored to the bone at either end. They vary in size, shape, orientation and location. Their unique and complex bony attachments are called insertions and they often involve unusual shapes on the bone that are likely critical to how the fibres within the

ligament are recruited as the joint moves. Ligaments have a fibrous architecture which is further organized hierarchically into groups of parallel fibres known as bundles that are difficult to separate suggesting that they are interconnected in some point (Frank, 2004). One of the main functions of ligaments is mechanical as they passively stabilize joints and help in guiding those joints through their normal range of motion when a tensile load is applied.

A tendon is a tough band of fibrous connective tissue that connects muscle to bone and is built to withstand tension. Tendons and muscles work together and can only exert a pulling force. The origin of a tendon is where it joins to a muscle. Collagen fibres from within the muscle organ are continuous with those of the tendon. A tendon inserts into bone at an enthesis where the collagen fibres are mineralised and integrated into bone tissue. While they exert no pulling force of their own, tendons transfer the contractions of muscles and can exert an elastic force if forcibly stretched.

Ligaments and tendons exhibit nonlinear anisotropic mechanical behaviour and under low loading conditions they are relatively compliant, perhaps due to recruitment of "crimped" collagen fibres as well as to viscoelastic behaviours and interactions of collagen and other matrix materials. Continued tissue loading results in increasing stiffness until a stage is reached where they exhibit nearly linear stiffness. Beyond this, the ligament/tendon continues to absorb energy until tensile failure (disruption). To describe this behaviour linear elastic or hyperelastic material models are used.

These tissues show relaxation when they are pulled to constant deformations, decreasing the applied loads/stresses within the ligament/tendon and creep, which is defined as an increase in the deformation (or elongation) under a constant or cyclically repetitive load. Creep is particularly important when considering joint injury or reconstructive surgery as excessive creep could result in laxity of the joint thus predisposing it to further injury.

Ligament and tendon viscoelasticity does play a role in the response of joints to high-rate loading or impact scenarios. This behaviour is not taken fully into account in the material definitions used for ligaments and tendons in THUMS FE model (elastic material, strain rate dependent plasticity material or seatbelt material) since neither creep nor relaxation are considered. The relevant references investigated in the literature review are summarized in the next table.

Reference	Properties	Specimen
Blanton (1970)	σ_u	Tendons (upper and lower limbs)
Blevins (1994)	E, σ_u, stiffness	Patella tendon
Butler (1986)	E, σ_u, ε_u	Patella tendon

Eppinger (1998)	E, σ_u, ε_u	Spine ligaments
Funk (2000)	Stiffness	Ankle ligaments
Hewitt (2001)	E, σ_u, $\varepsilon_{u,}$	Pelvis ligaments
Johnson (1994)	E, σ_u, ε_u	Patella tendon
Kerrigan (2003)	E, σ_u, $\varepsilon_{u,}$ stiffness	Knee ligaments
Koh (2004)	E, σ_u, ε_u	Shoulder ligaments
Lemosse (1998)	Load to failure	Sterno-costal and costo-vertebral ligaments
Lewis (1997)	E, σ_u, $\varepsilon_{u,}$ stiffness	Achilles tendon
Noyes (1976)	E, σ_u, $\varepsilon_{u,}$ stiffness	Knee ligaments
Noyes (1984)	Load to failure, stiffness	Knee ligaments, Patella tendon
Nowak (1998)	σ_u, ε_u	Wrist ligaments
van Dommelen (2005)	E, σ_u, relax, creep	Knee ligaments
Woo (1991)	Stiffness	Knee ligaments
Wren (2001)	Load to failure	Achilles tendon
Yamada (1970)	σ_u	Calcaneal tendon
Zander (2004)	Stiffness	Spine ligaments

Table 4-7: Relevant literature for ligaments and tendon properties. Elastic modulus (E), ultimate stress (σ_u) and ultimate strain (ε_u)

Within these references, elastic modulus (E), stiffness and ultimate tensile strength ($\sigma_{u,}$) are analysed taken into account age and strain rate. To find the trend for these dependencies, a qualitative analysis is done for knee ligaments and patella and Achilles

tendons to then add a quantitative approach to understand the anatomical variation of each property.

Figure 4-12 presents the modulus of elasticity for patella-patella tendon-tibia complex specimens from subjects of a range of different ages, determined by Butler (1986), Blevins (1994) and Johnson (1994) along with the corresponding one for Achilles tendon specimens from Lewis (1997) for males (M) and females (F).

It appears that the results obtained by Butler and Johnson are comparable between them. The Johnson data show a decrease in the elastic modulus with the increasing age of the subjects and similarly occurs with Lewis data. However, Blevins results are less than half of those of Butler and Johnson likely due to, as explained by Blevins, to differences in specimen preparation and test procedures.

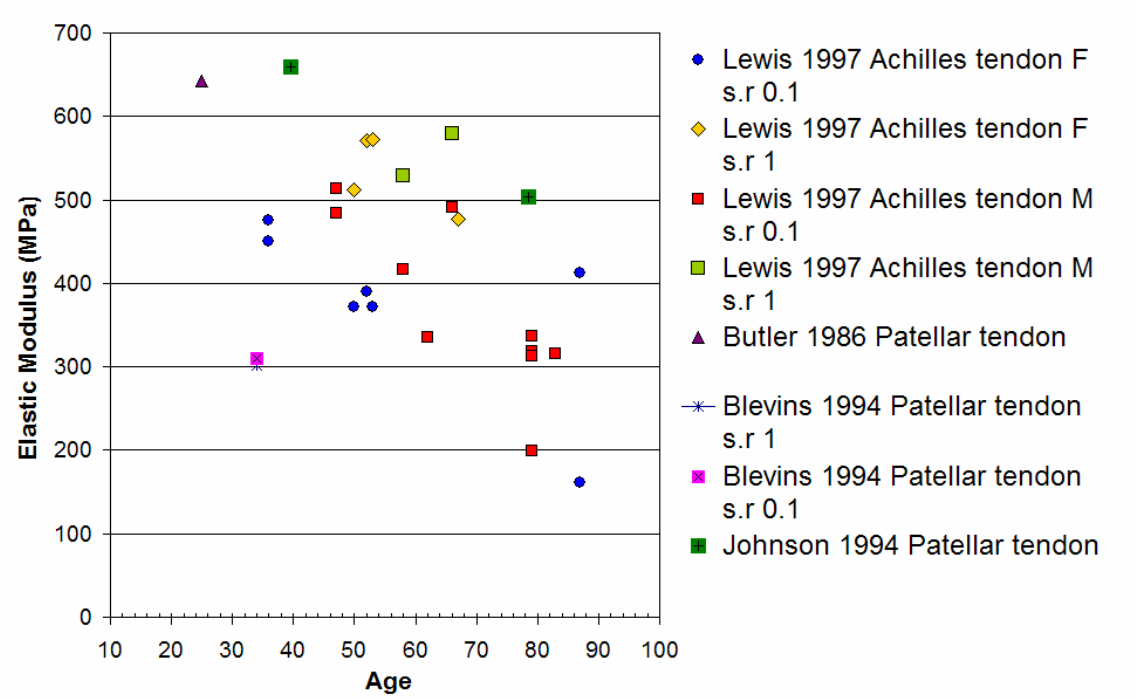

Figure 4-12: Elastic modulus of tendon specimens from subjects of different ages.

The ultimate tensile strength for tendon complex specimens is shown in Figure 4-13. In this figure it can be seen that the two values taken from Noyes (1984) are similar to those determined by Butler (1986), being in both case subjects of similar ages. The tests by Johnson (1994) were conducted on specimens from older subjects. Despite a larger variability in age and maximum stress, that had been found in Noyes (1984) or Butler (1986), the mean values from Johnson (1994) show a trend for decreasing maximum stress with increasing age.

Yamada (1970) also analysed the variation of ultimate tensile strength with age. This is an interesting set of data as it includes values for foetal tissue, from six to ten months of

pregnancy. Yamada reports that the ultimate strength in the sixth month of pregnancy corresponds to about one third of that in the tenth month, which is about two thirds of that in adults.

Regarding the dependency on the strain rate, Lewis data shows that a ten-fold increase in the strain rate produced a significant increase in both the modulus of elasticity and the ultimate strength of tendons.

In the case of ligaments, only Noyes data (1976) have been found to relate age with the elastic modulus and maximum stress values. These data conclude that the mean value of the elastic modulus of the ligaments from younger adult humans (mean age of 21) is 1.7 times that of the ligaments from older humans (mean age of 67), being 2.8 times for the case of maximum stress values.

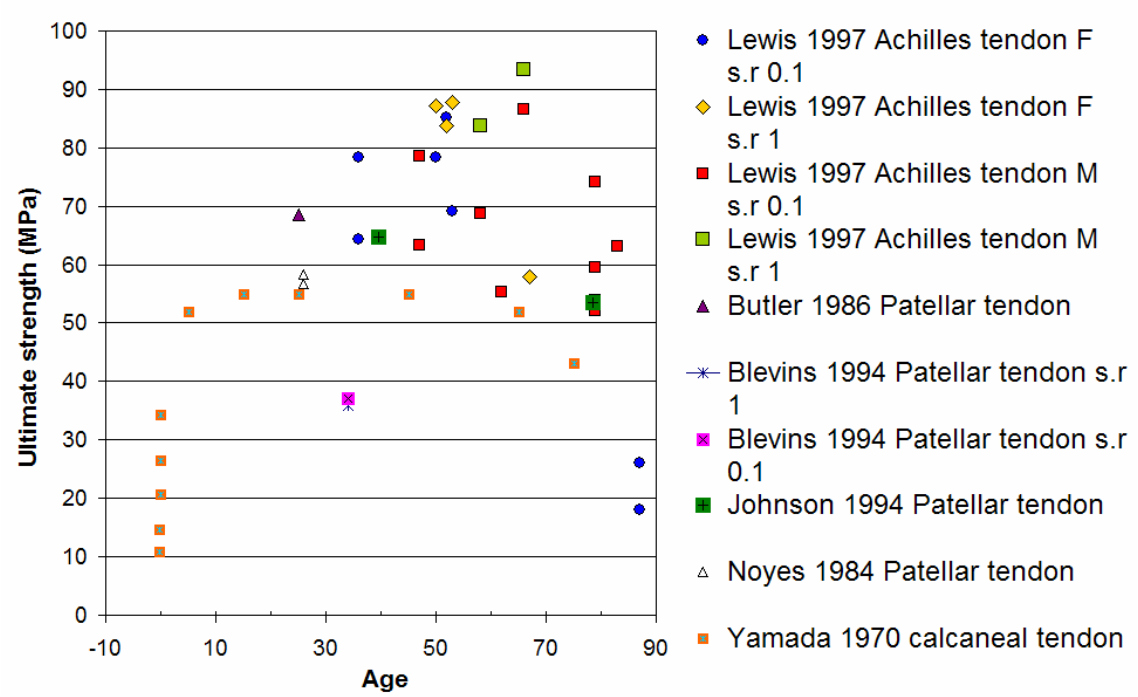

Figure 4-13: Ultimate strength of tendon specimens from subjects of different ages.

In the rest of the literature references, the lineal stiffness and the failure load values were recorded and they are shown in Figure 4-14 and Figure 4-15.

It can be seen in Figure 4-14 that the effect of age in the stiffness is very patent in ACL ligament, showing all authors similar decreasing trends and values, while the Figure 4-15 highlights the general agreement in maximum force values between the authors. Moreover, the general trend for decreasing maximum force with increasing age is clearly evident. The extent of this trend indicates that the maximum force required for failure of knee ligaments at the age of 75 may be one third of that force at the age of 30 years.

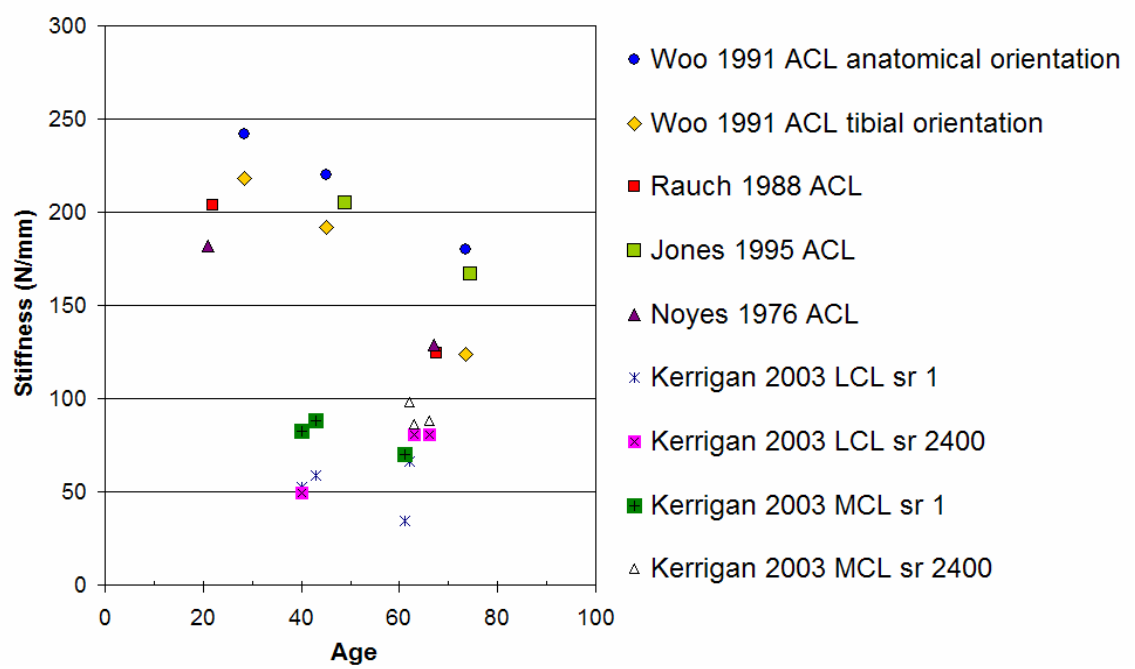

Figure 4-14: Stiffness of knee ligament specimens of different ages.

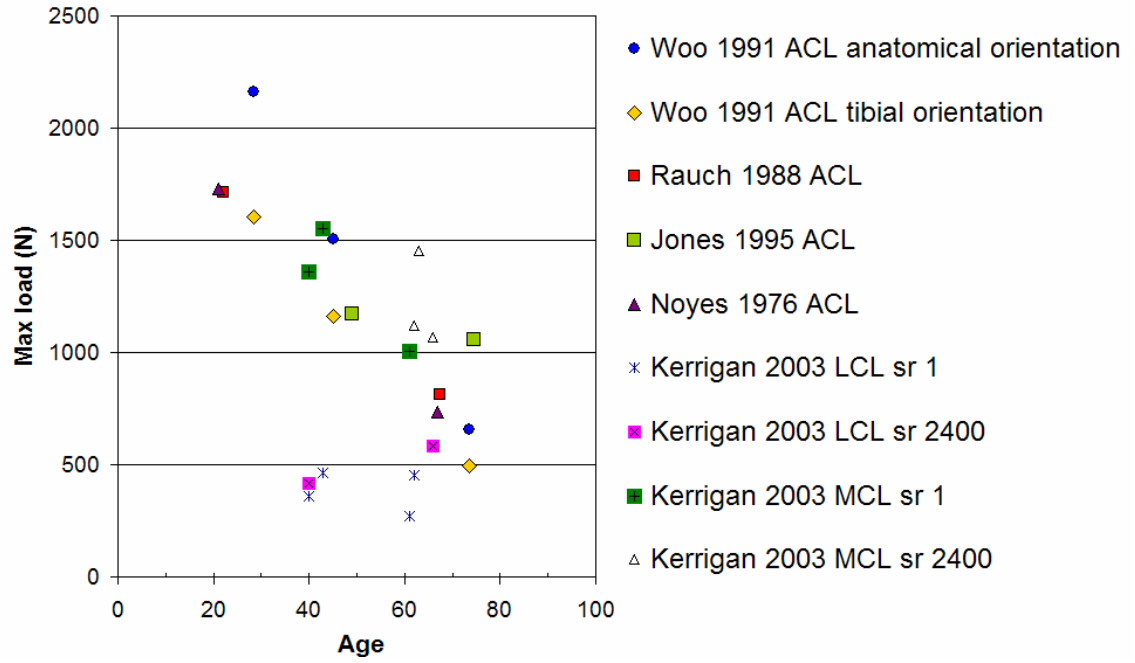

Figure 4-15: Failure load of knee ligament specimens of different ages.

For strain rate dependency, Kerrigan (2003) data have been analysed. He concluded that the stress at a particular strain in an average high rate test is significantly greater than the stress at the same strain in an average low rate test, therefore implying that ligaments have rate-dependent properties.

4.2.3 Cartilage.

Cartilage is a type of dense connective tissue. It is composed of collagenous fibres and/or elastic fibres, and cells called chondrocytes, all of which are embedded in a firm gel-like ground substance called the matrix.

Cartilage serves several functions, including providing a framework upon which bone deposition can begin and supplying smooth surfaces for the movement of articulating bones. Cartilage is found in many places in the body including the joints, the rib cage, the ear, the nose, the bronchial tubes and between inter vertebral discs.

There are three different types of cartilage, each with special characteristics adapted to their function.

- The hyaline cartilage is the most abundant type of cartilage. It is avascular and it is made predominantly of type II collagen. Hyaline cartilage is found lining bones in joints (articular cartilage) and is also present inside bones, serving as a center of ossification or bone growth. In addition, hyaline cartilage forms most of the embryonic skeleton.
- The elastic cartilage (also called yellow cartilage) is found in the pinna of the ear and several tubes, such as the walls of the auditory (Eustachian) tubes and larynx and especially in the epiglottis. Cartilage is present to keep the tubes permanently open. Elastic cartilage is similar to hyaline cartilage but contains elastic bundles (elastin) scattered throughout the matrix. This provides a tissue which is stiff but yet elastic.
- The fibrocartilage (also called white cartilage) is a specialized type of cartilage found in areas requiring tough support or great tensile strength, such as inter vertebral discs, the pubic and other symphyses, and at sites connecting tendons or ligaments to bones. The fibrocartilage found in inter vertebral disks contains more collagen compared to hyaline. In addition to the type II collagen found in hyaline and elastic cartilage, fibrocartilage contains type I collagen that does form fibres bundles seen under the light microscope.

Much like other connective tissue, cartilage is composed of cells, fibres and a matrix. In general, tensile properties of the cartilage are determined by the solid matrix of the cartilage while the compression properties are associated to the permeability and the load sharing between the solid and fluid components (Hui, 2004).

- Cells: The chondrocytes and their precursors, known as chondroblasts, are the only cells found in cartilage. Chondrocytes occur singly or in groups within spaces called lacunae. Chondrocytes are responsible for the secretion and maintenance of the matrix.

- Fibres: Cartilage is composed of collagen (type II) and elastic fibres. In hyaline cartilage, type II collagen makes up 40% of its dry weight and is arranged in cross-striated fibres, 15-45 nm in diameter that do not assemble into large bundles. Elastic cartilage also contains elastic fibres and fibrocartilage contains more collagen than hyaline cartilage.
- Matrix: The matrix is mainly composed of proteoglycans, which are large molecules with a protein backbone and glycosaminoglycan (GAG) side chains. The main proteoglycan in articular cartilage is aggrecan. This molecule fills all the spaces between the collagen fibres and holds water, thus giving to the articular cartilage its resistance to compression and its resilience (ability to spring back into shape after load).

The two most common ways of modelling cartilages are a single phase, isotropic, homogeneous linear elastic solid model and a biphasic model consisting of an isotropic, homogeneous viscoelastic solid and an incompressible, inviscid fluid model (Mak, 1986).

(i.e. THUMS FE model uses the single phase model approach with elastic or plastic material model for hyaline cartilage and elastic or viscoelastic material model for the fibrocartilage. Due to the simplifications of the interior organs of the human body, the elastic cartilage is not modelled in THUMS FE model.)

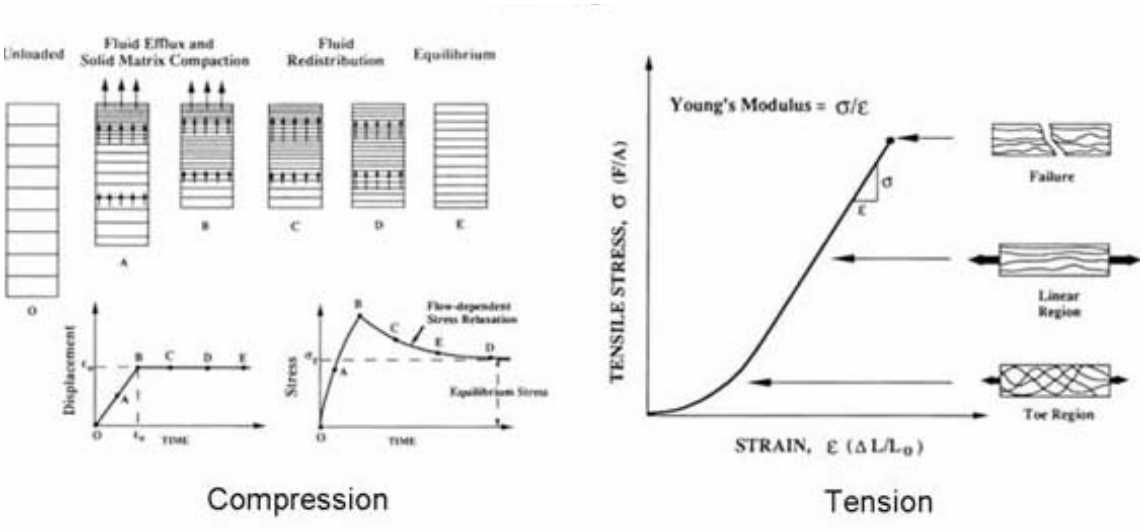

Figure 4-16: Cartilage stress-strain behaviour.

Unlike the previous tissues, cartilage literature is much more reduced and few references have been analysed. Yamada (1970) and Guo (2007) have been investigated for hyaline cartilage while Yin (2005) has been analysed for fibrocartilage.

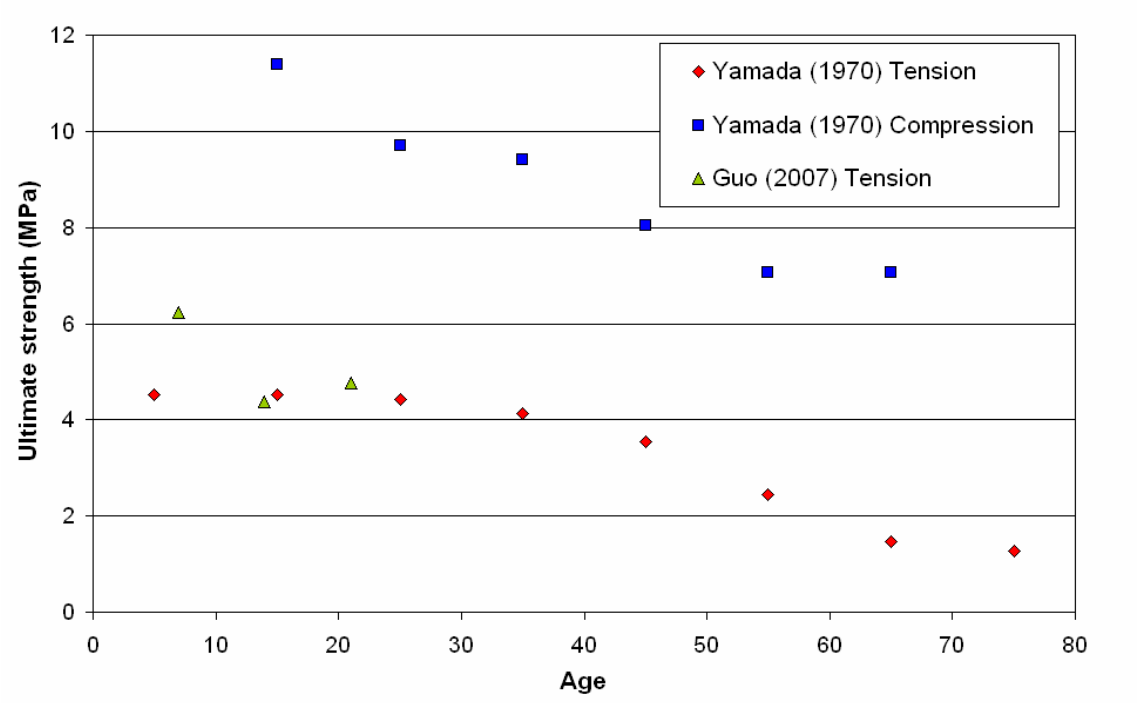

Figure 4-17: Hyaline cartilage ultimate strength in tension and compression.

Yamada (1970) and Guo (2007) give information on the ultimate strength for the costal cartilage, considering the variation with age. Yamada gives information in the whole age range (10-80 years old) while Guo is focused in younger specimens (5-25 years old). These data is shown in the Figure 4-17.

Yamada (1970) and Guo (2007) also give some reference values for the elastic moduli of this tissue. The mean elastic modulus was reported to be 24.5 MPa in tension and 490 MPa in compression by the former while the latter found elastic modulus in tension of 10-15 MPa.

Regarding fibrocartilage, Yin (2005), Lu (1998) and Elliot (2001) give reference values for the vertebrae cartilage but they make no dependency analysis on age, reporting just mean properties for the annulus fibrosus cartilage as well as for isolated fibers and matrix that forms it.

4.3 Algorithms to consider age influence in human tissue.

Considering the data collection presented in the previous heading and also the overall objective of the thesis, the study of age dependency has been limited to the lower limbs region.

With this premise, the most complete series from the ones presented in the previous heading have formed the basis to consider age effect in any of the tissues of the legs, and they are summarized in Table 4-8.

Body region	Age dependency reference
Limbs cortical bones	Burstein (1976), McElhaney (1966), Wall (1974), Imperial (2004)
Limbs spongy bones	Ding (1997), Ducheyne(1977)
Knee ligaments	Noyes (1976), Kerrigan (2003), van Dommelen (2005), Woo (1991)
Patellar tendon	Noyes (1984), Johnson (1994)
Achilles tendon	Lewis (1997)

Table 4-8: Reference datasets to derive age dependency functions for human tissues.

Based on these datasets, regression analysis has been used to examine the relation of the different material properties (response variable) to age or strain rate (explanatory variables).

The mathematical model of their relationships is the regression equation. Each response variable is modelled as a random variable and it is explained with the regression equation that contains estimates of one or more hypothesized regression parameters ("constants"), and includes a “noise” term, which picks up the unpredictable part of the response variable.

An example will be used to illustrate the process that has been followed for each material parameters age or strain dependency function in order to obtain the best regression equation. The data used for this purpose is based on Burstein (1976) and related Elastic modulus in tension with age.

As it can be seen in the Figure 4-18, there are many possible regression equations that might be superimposed upon a dataset (in fact, they are infinite), so it is the function of the regression analysis to define a criterion to evaluate the quality of the estimation. This criterion is the estimator.

Each parameter estimate that an estimator produces can be viewed as a random variable drawn from some probability distribution. If the mean of that probability distribution is equal to the true value of the parameter that it is being estimated, then the estimator is said to be unbiased. In comparing different unbiased estimators, the one with the lowest variance for a given sample is termed efficient (Sykes, 1993).

An estimator is termed consistent if it yields estimates that converge on the true value of the parameter as the sample size gets larger and larger (Sykes, 1993). Thus, the

probability distribution of the estimate for any parameter has lower variance as the sample size increases, and in the limit (infinite sample size) the estimate will equal the true value.

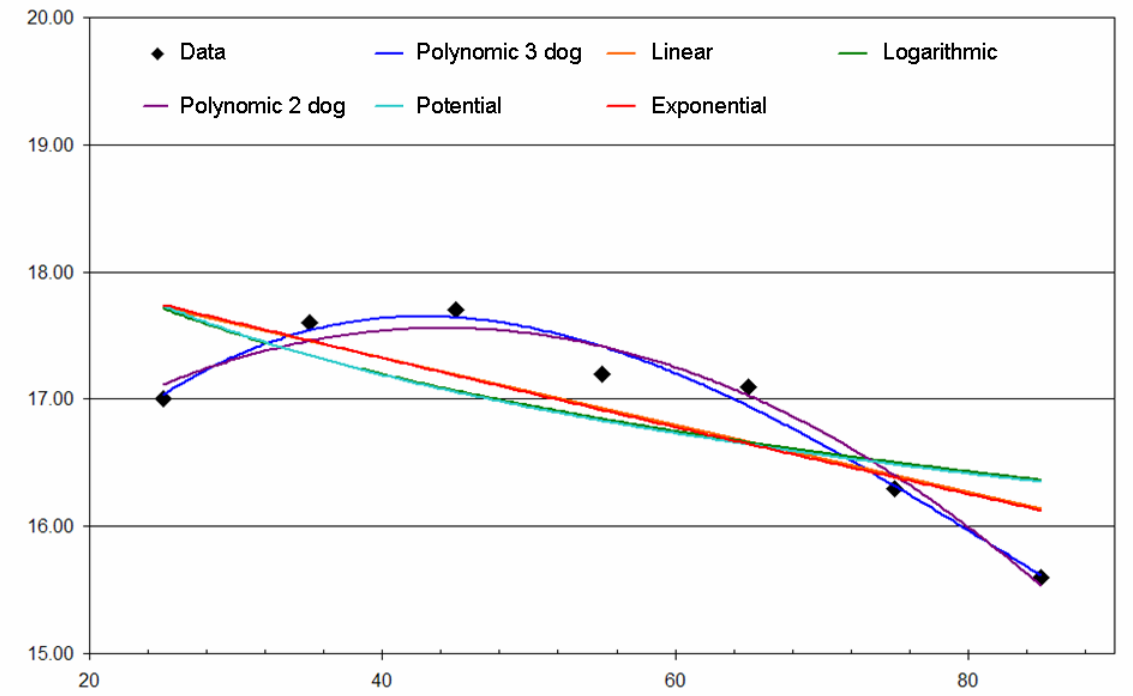

Figure 4-18: Example dataset and different trends to analyse it.

The regression analysis generally uses as estimator, due to its special properties, the minimum sum of squared errors (minimum SSE) criterion. This criterion, under certain assumptions, has the characteristics of unbiasedness, consistency and efficiency (Kennedy 1985). These assumptions are as follows:

- If the noise term for each observation is drawn from a distribution that has a mean of zero, then the minimum SSE criterion generates estimates that are unbiased and consistent.
- If the distributions from which the noise terms are drawn for each observation have the same variance, and the noise terms are statistically independent of each other than the minimum SSE criterion gives the most efficient estimates available from any linear estimator (defined as an estimator that computes the parameter estimates as a linear function of the noise term, which the SSE criterion does). If this assumption is violated, the SSE criterion remains unbiased and consistent but it is possible to reduce the variance of the estimator by taking into account what it is known about the noise term.

Once defined a regression function and its estimated parameters with the SSE criterion, different methods are available to analyse the good fit of this function to the data.

The most common statistic associated with regression analysis is the R^2. It is equal to one minus the ratio of the sum of squared estimated errors (the deviation of the actual value of the dependent variable from the regression line) to the sum of squared deviations about the mean of the dependent variable.

Intuitively, the sum of squared deviations about its mean is a measure of the total variation of the dependent variable while the sum of squared deviations about the regression line is a measure of the extent to which the regression fails to explain the dependent variable. Hence, the R^2 statistic is a measure of the extent to which the total variation of the dependent variable is explained by the regression.

A high value of R^2, suggesting that the regression model explains the variation in the dependent variable is obviously important if one wishes to use the model for predictive or forecasting purposes.

The summary of R^2 from the previous analysis is shown in the next table.

Regression type	Regression Function	R^2
Linear	Et=-0.0264*AGE+18.382	0.59
Logarithmic	Et=-1.1047*LN(AGE)+21.272	0.58
Potential	$Et=0.935*AGE^{3.0900}$	0.42
Exponential	$Et=0.998*e^{18.462*AGE}$	0.59
Polynomial 2 dof	$Et=-1.21E-03*AGE^2+0.107*AGE+15.194$	0.96
Polynomial 3 dof	$Et=1.38E-05*AGE^3-3.5E-03*AGE^2+0.223*AGE+13.418$	0.97

Table 4-9: Summary of R^2 in the different regression functions.

In this case, it seems that neither the linear or logarithmical nor the exponential or the potential accurately explain the dependency of the dependent variable, whereas, both polynomial regression address it very closely.

However, $R^{2,}$ is not conclusive to affirm that the third order polynomial fits better the dataset than the two order one and a further global statistic test needs to be conducted. This test is the F test that is this global statistic test associated with regression analysis. It is a measure of the significance of the regression as a whole as it tests the null hypothesis that all of the coefficients are insignificant against the alternative hypothesis that at least one of the coefficients is significant.

Null hypothesis:	H_0: $C_1=C_2=...=C_k=0$
Alternative hypothesis:	Ha: At least one $C_j \neq 0$

The statistic to test this hypothesis is called the F-statistic and it is calculated as:

$$F = \frac{R^2/k}{\left(1-R^2\right)/\left[n-\left(k+1\right)\right]}$$ **Formula 4-1**

This F statistic is the ratio of the explained variability (as reflected by R^2) and the unexplained variability (as reflected by $1-R^2$), each divided by the corresponding degrees of freedom. This F statistic, or observed F-value of the regression is then compared against a critical F-value, F(α, v1, v2), where α is 1 - the level of significance we are interested in, and v1 =n–k–1 and v2 = k.

The null hypothesis, that all the parameters are zero, is rejected if the calculated F is greater than the F given by the critical value of F for some desired rejection probability (e.g. p = 0.05); therefore, if the observed F-value is greater than the critical F-value, it means the regression as a whole is significant and the larger the F statistic, the more useful the model is.

Regression function type	Observed F-value	Critical F value (95% confidence)
Linear	7.197686646	6.607890969
Logarithmic	3.616708066	
Potential	3.652957523	
Exponential	7.270871813	
Polynomial 2 dof	53.23809524	
Polynomial 3 dof	41.3100304	

Table 4-10: Summary of the F test for the different regression functions

It can be seen in the Table 4-10 that the logarithmic and the potential regressions lack of any statistical significance as their F statistic is lower to the critical one. Moreover, it can be seen that the polynomial 2 dof has a larger F statistic than the 3 dof one, which may mean that the 2 dof regression function is better than the 3 dof one, even with lower R^2.

As the result of this test, it is concluded that at least one of the coefficients is significant for the lineal, the exponential and the polynomial regression functions but it is unknown which of them are and which of them are not. To identify them, individual t tests are applied to each of the regression coefficients to analyse its significance individually.

As the parameter estimates are themselves random variables, each estimate can be thought to be drawn from some underlying probability distribution, without a specified nature. Assuming that the noise terms are all drawn from the same normal distribution, it is possible to show that the parameter estimates have a normal distribution as well (Hogg 1978). The variance of this normal distribution, however, depends upon the variance of the distribution from which the noise terms are drawn. This variance is unknown in practice and can only be estimated using the estimated errors from the regression to obtain an estimate of the variance of the noise term. The estimated variance of the noise term in turn can be used to construct an estimate of the variance of the normal distribution for each coefficient. The square root of this estimate is called the "standard error" of the coefficient (s).

It is also possible to show that if the parameter estimate (p) is normally distributed with a mean of m, then (p–m)/s has a "Student's t" distribution (Hogg 1978), which mean is zero. Using this result, it can be set as null hypothesis that the true value of a parameter in the regression model is m.

Null hypothesis.	H_0: p=m

Because the minimum SSE criterion is an unbiased estimator, it can be deduced that the parameter estimate (p) is drawn from a normal distribution with a mean of m if the null hypothesis is true (Sykes 1993). If then subtract m from our actual parameter estimate (p) and divide by its standard error (s), we obtain a number called the t-statistic which behaves as a t-distribution.

$$T = \frac{(p - m)}{s}$$ **Formula 4-2**

This t-statistic can be positive or negative as the parameter estimate from which it is derived is greater or less than the hypothesized true value of the parameter. Recalling that the t-distribution is much like a normal with mean of zero, we know that large values of the t-statistic (in absolute value) will be drawn considerably less frequently than small values of the t-statistic. And, from the construction of the t-statistic, large values for that statistic arise (in absolute value), other things being equal, when the parameter estimate on which it is based differs from its true (hypothesized) value by a great deal.

This insight is turned on for hypothesis testing taken into account that a large t-statistic (in absolute value) will arise fairly infrequently if the null hypothesis is correct. Hence, when a

large t-statistic does arise, it can be concluded that the null hypothesis is false. The essence of hypothesis testing with a regression coefficient, then, is to formulate a null hypothesis as to its true value, and then to decide whether to accept or reject it according to whether the t-statistic associated with that null hypothesis is large enough that the plausibility of the null hypothesis is sufficiently in doubt.

More precisely, the null hypothesis is implausible if the t-statistic associated with the regression estimate lies so far out of its t-distribution that such a value or larger would arise less than a given percent of the times. This percentage is generally fixed to 10%, 5%, or 1%. When the t-statistic does not arise more than this percentages, the null hypothesis is rejected with a significant level of 90%, 95% or 99%.

To make this operational, it is necessary to compute the exact probability of a t-statistic as large or larger in absolute value as the one associated with the parameter estimate at issue. In turn, it is necessary to know exactly how “spread out” is the t-distribution from which the estimate has been drawn. A further parameter that it is needed is then the shape of the t-distribution, which, in this respect, is based on its “degrees of freedom,” defined as the number of observations in the sample less the number of parameters to be estimated. The fewer the degrees of freedom, the more “spread out” is the t-distribution and thus the greater is the probability of drawing large t-statistics.

This process is interestingly applied considering as null hypothesis that the true value of a coefficient is zero.

Under this hypothesis, m in the notation above is equal to zero, and hence the t-statistic is simply p/s, the coefficient estimate divided by its standard error. If the t-statistic value obtained in this case, or one even larger in absolute value, would not arise more than 10 percent, 5 percent, or 1 percent, then, the null hypothesis is rejected, and therefore, the coefficient in question is said to be “statistically significant”.

This process has been applied to all the coefficients of the linear, the exponential and the polynomial regressions that have already shown statistical significance as a whole and the summary of this process is shown in the Table 4-11.

Regression function type	Coefficients	Observed t value	Critical t value (95% confidence)
Linear (A1x+A0)	A1	2.68285047	2.57058
	A0	31.88516204	
Exponential (A1*e^A0x)	A1	2.696455416	
	A0	84.38114284	

Poly (A2x2+A1x+A0)	A2	6.425396041	
	A1	5.09133175	
	A0	28.57316411	
Poly (A3x3+A2x2+A1x+A0)	A3	1.263227882	
	A2	1.92351207	
	A1	2.373449544	
	A0	9.000216537	

Table 4-11: Summary of t test for the different regression functions coefficients.

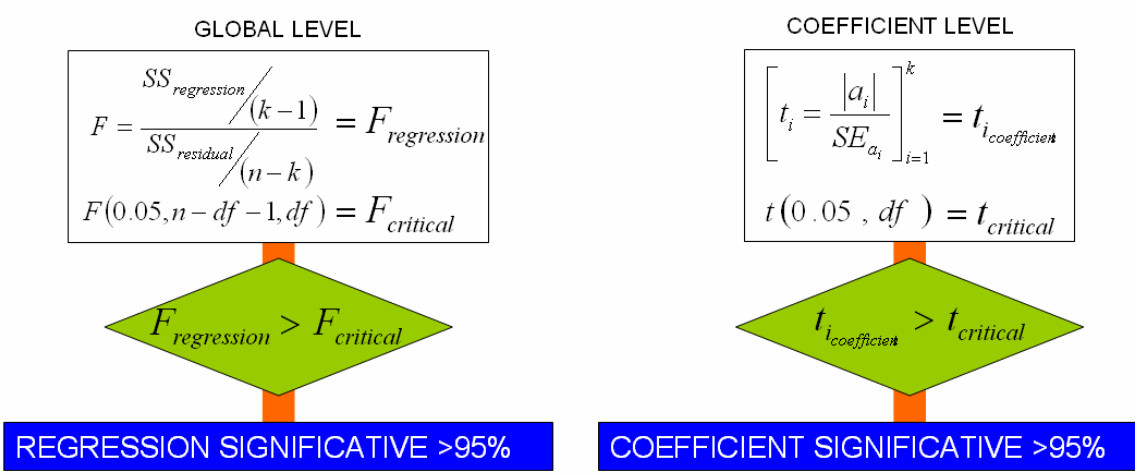

Figure 4-19: Statistic tests done to ensure the significance of the regression.

As it can be seen in the Figure 4-19 graphically, F and t test have been performed on each dataset analysis to complement the information obtained with the R^2. The example selected to illustrate the process has shown that these two analyses are indeed necessary.

In this example, 3 dof polynomial regression had higher R^2 than the 2 dof polynomial regression, however, some of the coefficients of this 3 dof polynomial regression lacked of statistical significance and therefore, they were unnecessary, which may indicate that if this regression were selected just based on R^2, the estimation would have been wrong.

The same process to the one shown as an example has been followed for all the different material properties of each human tissue for which data was available to determine age or strain rate dependency according to Table 4-8.

The material properties analysed in any of the human tissues were:

- Ultimate Compression Strength (*UCS*): The maximum stress a material is able to withstand axially directed pushing forces before crushing.
- Elastic Modulus in compression (*Ec*): This measurement determines the stress-strain relationships in the linear-elastic portion of the stress-strain curve in compression. The linear-elastic region is taken to be between 0 and 0.2% strain, and is defined as the region of strain in which no permanent deformation occurs.
- Ultimate Tensile Strength (*UTS*): The maximum tensile stress a material can withstand. In the case of ligaments, the property considered is the ultimate Load since the area of the ligaments was unknown in the data.
- Elastic Modulus in tension (*Et*): The same definition than for *Ec* but in the stress-strain curve in tension.
- Ultimate Strain (*Ustrain*): The % of change per unit of length in the tested specimen at the maximum strength level. Strain as used with most mechanical tests is based on original length of the specimen.
- Yield strength (*YS*): The stress a material can withstand without permanent deformation. This is not a sharply defined point. Yield strength is the stress which will cause a permanent deformation of 0.2% of the original dimension.
- Elastic Modulus of plasticity (*Ep*): After the yield point, it follows a period of strain hardening, in which the stress increases again with increasing strain up to the ultimate strength. If this hardening function is approximated to a lineal function, the elastic modulus of plasticity is the strain-strain relationship in this linear-plastic portion of the stress-strain curve.

The next table summarises all the regression analyses performed.

In the cases where statistical significant regressions (meeting F and t tests) were obtained, the highest R^2 value are included in the cell for the age and the strain rate, while in the cases where any of the regressions turned out not to be significant, the dependence is discarded and no aging process and/or strain rate dependency was applied to the property, being the cell shadowed in yellow.

The successful regressions from the previous table have been programmed into a software application, called AgedMAT, to allow an automatic calculation of the different human body properties for different ages.

For the cases where both age and strain rate dependency have been found, both regressions have been combined to create best fit surfaces, based on the perpendicular sections defined by the different regression function, and limited by the definition interval of the strain rate range, as the one shown in Figure 4-20.

Significant R^2	UCS	Ec	UTS	Et	Ustr	YS	Ep
Limbs cortical bones	0.98, 0.98	0.93, 0.89	0.61, 0.88	0.98, 1.0	0.89, --	0,71, --	0,71, --
Limbs spongy bones	1.0, --	1.0, --					
Knee ligaments			*0.99, --	*0.99, --			
Patellar tendon			0.99, --	1.0, --			
Achilles tendon			0.90, 0.98				

**In ligaments, ultimate load and stiffness are computed instead of UTS and E_t.*

Table 4-12: Summary of the successful regression built that considered age or strain rate effect into human tissues.

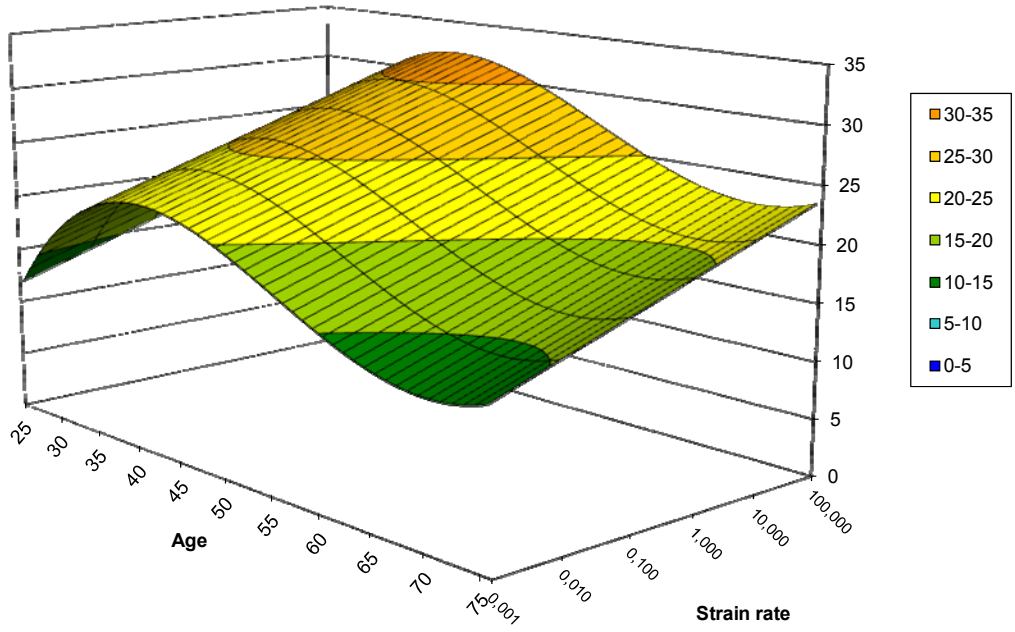

Figure 4-20: Surface constructed to define age and strain rate joint dependency

The resulting surfaces are implemented into the software, and a process is programmed to fit the resulting stress-strain curve of a tissue, at a given age and within a strain rate

range, with two strain rate dependency models. These two models are a Cowper-Symonds model and a Johnson-Cook model.

The Cowper-Symonds (CS) equation is a potential based equation which needs two parameters to be defined. This equation cannot accurately predict stresses for a broad range of strains unless its coefficients change, but it is enough precise for the typical strain rates in vehicle collisions (10^{-1} to 10^{2} s^{-1}).

The Johnson-Cook (JC) equation is a logarithm based equation with only one parameter needed to be defined. The Johnson-Cook equation is only capable of describing material with diverging flow curves (i.e., those where the strain rate hardening increases with the strain level) but it covers accurately broad high rate intervals. (10^{-4} to 10^{4} s^{-1}).

$$1+\left(\frac{\dot{\varepsilon}}{K_1}\right)^{\frac{1}{K_2}}$$

Formula 4-3: Cowper-Symonds formulation

$$1+C_1\cdot LN\left(\frac{\dot{\varepsilon}}{\dot{\varepsilon}_0}\right)$$

Formula 4-4: Johnson-Cook formulation

The parameters of these models are calculated in AgedMAT allowing the user to choose between both models to consider the strain rate effect in the selected property.

4.4 Implementation of algorithms in a software tool: AgedMAT.

AgedMAT is the software tool that integrates the different successful algorithms developed in this thesis, allowing the user to consider easily the age of the subject as an important variable affecting significantly the different human tissues. With this tool, the users can output the estimates for the different human tissues properties in function of the age, required to model the human body in vehicle safety environments. Therefore, this scaling tool is designed to cover, with different degrees of definition, the influence of age and strain rate in bones, cartilage, ligaments, tendon and skin.

The scaling tool is structured in three parts:

- The Input panel, where the user defines the age of the subject to calculate the different material properties.
- The Results panel, where the calculations are displayed to the user in different forms.
- The Output panel, where the user defines which output the tool will generate into disk.

The user can navigate through them as shown in the Figure 4-21, going from the input forward to the result panel, from the result panel back to the input or forward to the output

panel and from the output panel back to the result or the input panels. The current panel is shown in all the caption bars of the different forms.

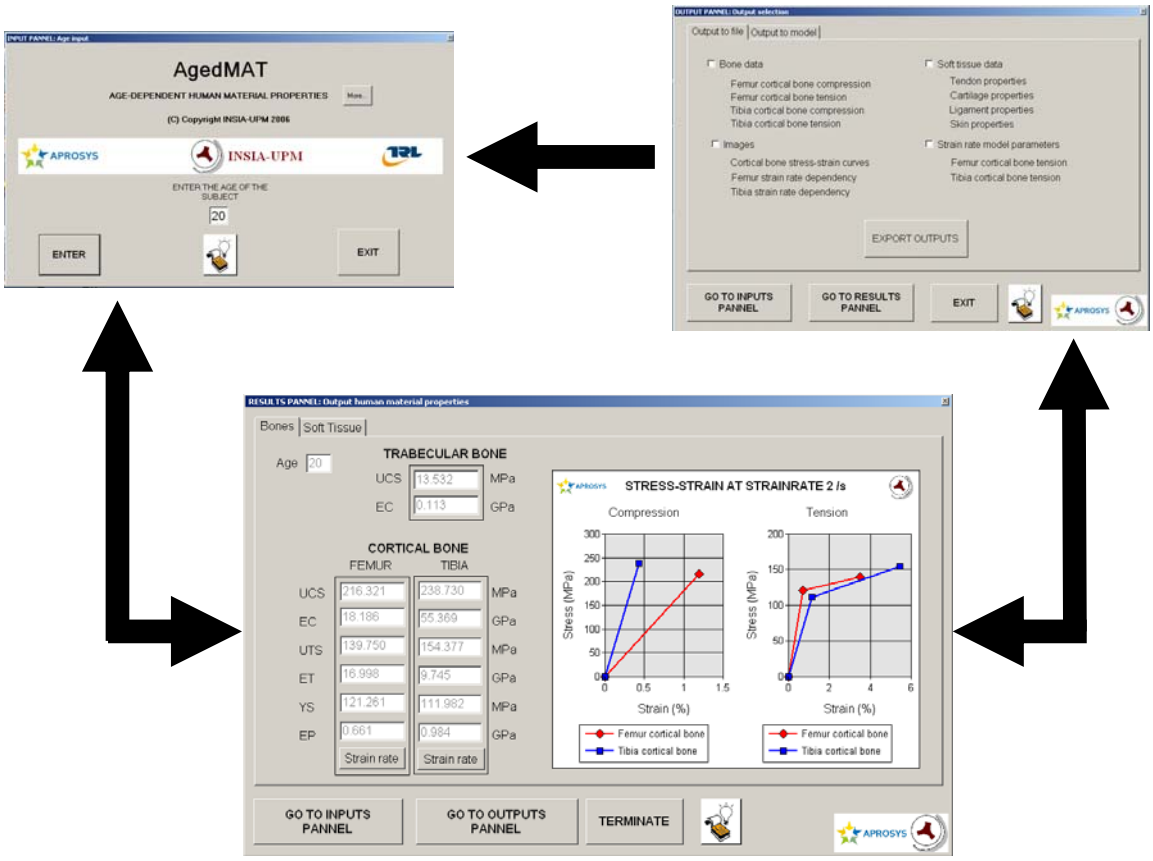

Figure 4-21: Navigation options between panels of AgedMAT.

The input panel welcomes the user to the application giving the basic information about the tool, allowing the user to start the application once the input box is filled with the age of the subject (left), enter into the application tutorial (middle) or exit the application.

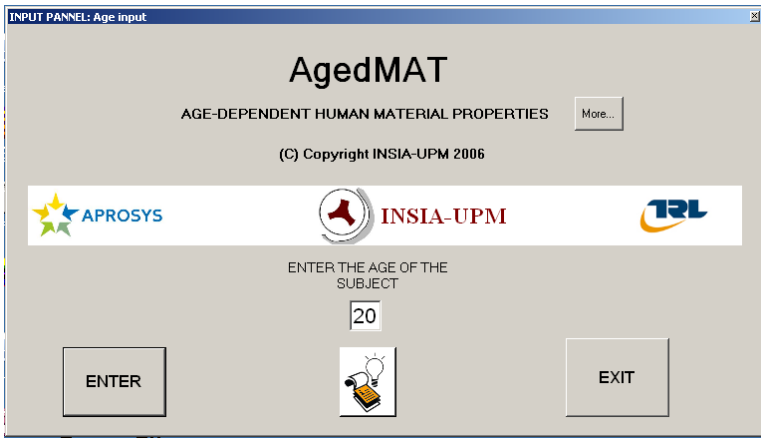

Figure 4-22: Input panel of AgedMAT.

Parameter	Units	
	Bones	Soft tissue
Ultimate strength	MPa	MPa
Yield stress	MPa	MPa
Elastic modulus	GPa	MPa
Ultimate Load	--	N
Strain	%	%

Table 4-13: Units used for AgedMAT©.

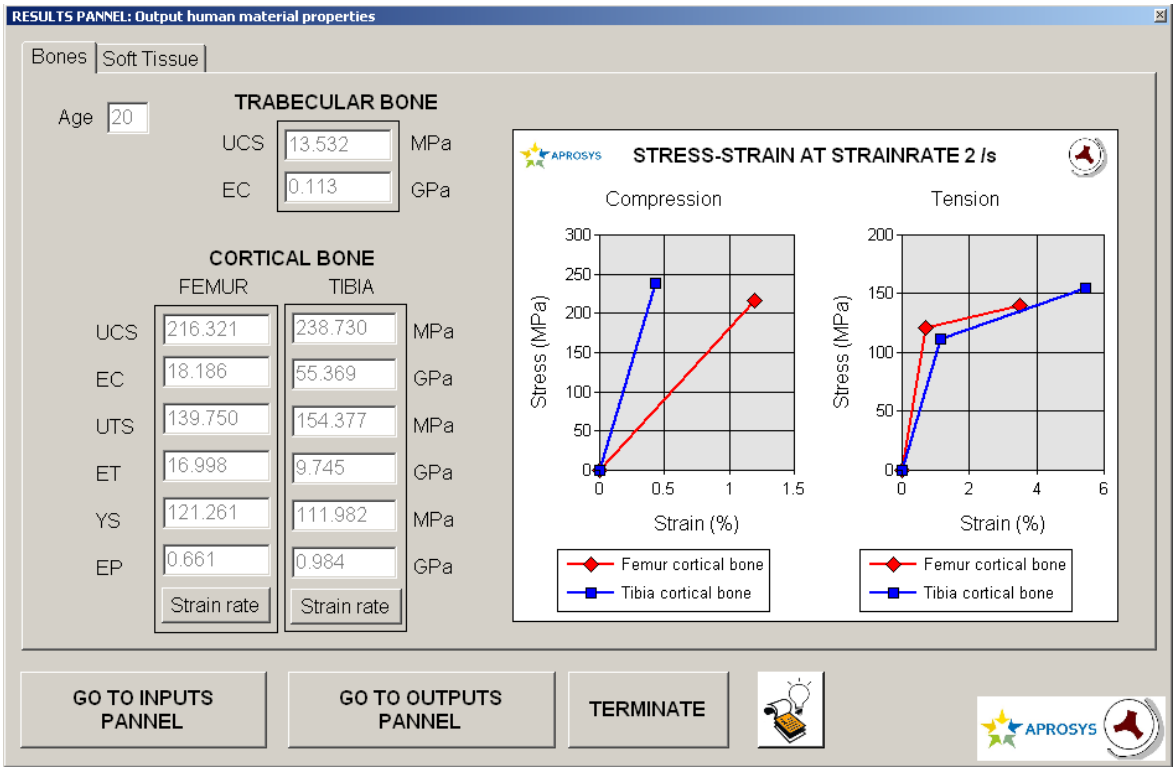

Figure 4-23: Results panel for bones.

The results panel aims to present the user the whole set of material parameters for a human subject of the different ages, using as units for each of them the ones summarized in the Table 4-13. It is divided into two sub-folders:

- The bones properties folder, which has two parts: On the left part, the bone properties folder shows the numerical value of the Ultimate Compression Strength

(*UCS*), Elastic Modulus in compression (*Ec*): Ultimate Tensile Strength (*UTS*), Elastic Modulus in tension (*Et*) Ultimate Strain (*Ustrain,* Yield strength (*YS*), Elastic Modulus of plasticity (*Ep*) for different cortical bones. On its right part, the user can see the stress-strain function in tension and compression resulting from these parameters at the reference strain rate. Extra buttons named “strain rate” into each cortical bone areas lead to pop-up forms that show the behaviour of the stress strain curve at different strain rates (shows slices of the surfaces shown in Figure 4-20) and calculate the parameters for Johnson-Cook and Cowper-Symonds models for strain rate dependency. Under these parameters, a note reads informing about the maximum and minimum strain rate considered to fit the strain rate dependency models.

- The soft tissue folder, where the material parameters for tendon, ligaments, cartilage and skin are shown. Tensile material properties are given for all the soft tissues (tendons, ligaments, cartilage and skin) (Ultimate Tensile Strength, Elastic modulus in Tension and Ultimate Strain) while compression properties are only found for cartilages (Ultimate Compression Strength, Elastic modulus in Compression). Only the numerical values given into white background do depend on age. The bold yellow values are only recommended range values, as there were not enough data to build an age dependent functions for them.

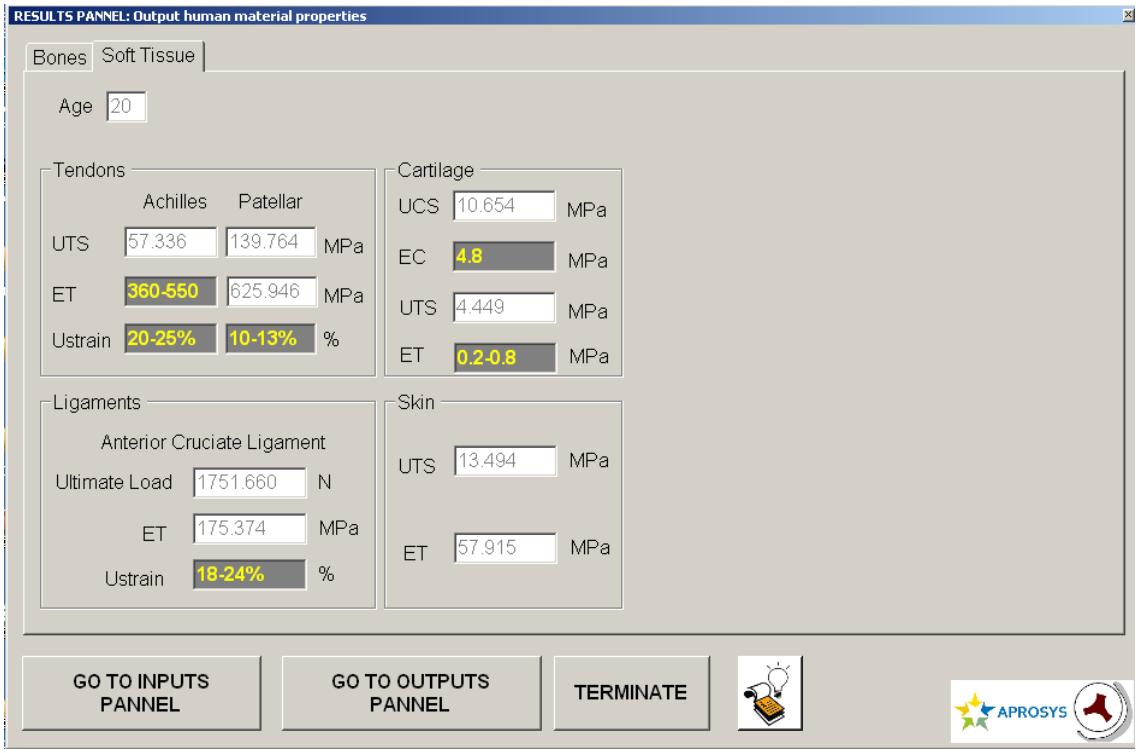

Figure 4-24: Results panel for soft tissues.

Additionally to these two folders, navigation buttons to go back to the input panel or to go forward to the output panel, along with the help button and the exit button, are available in the bottom part of the panel.

Finally the output panel gives the user the interface to define the outputs from the application as well as it presents similar navigation capabilities than the previous panels. There are two options to output from the tool, each of them available in each of the two folders of the panel.

In the “output to file” folder, the user can define the parameters to output from the tool between the whole set of parameters calculated to be exported into a user-defined folder. The output to file folder allows the user to select which data output to a file by a checkbox. (Bone properties data, strain rate dependency model parameters, soft tissue data and images). When click to the export outputs button, the user is asked to select a folder. In this folder, the application creates the files where the data is exported:

- If the images are exported, each one is exported as jpeg file in this folder.
- If any of the datasets are exported, a text file named **props_at_age_of_(input age).txt** is created. This file contains the information regarding each data set selected in the checkboxes: (bone data, soft tissue data and strain rate dependency model parameters).

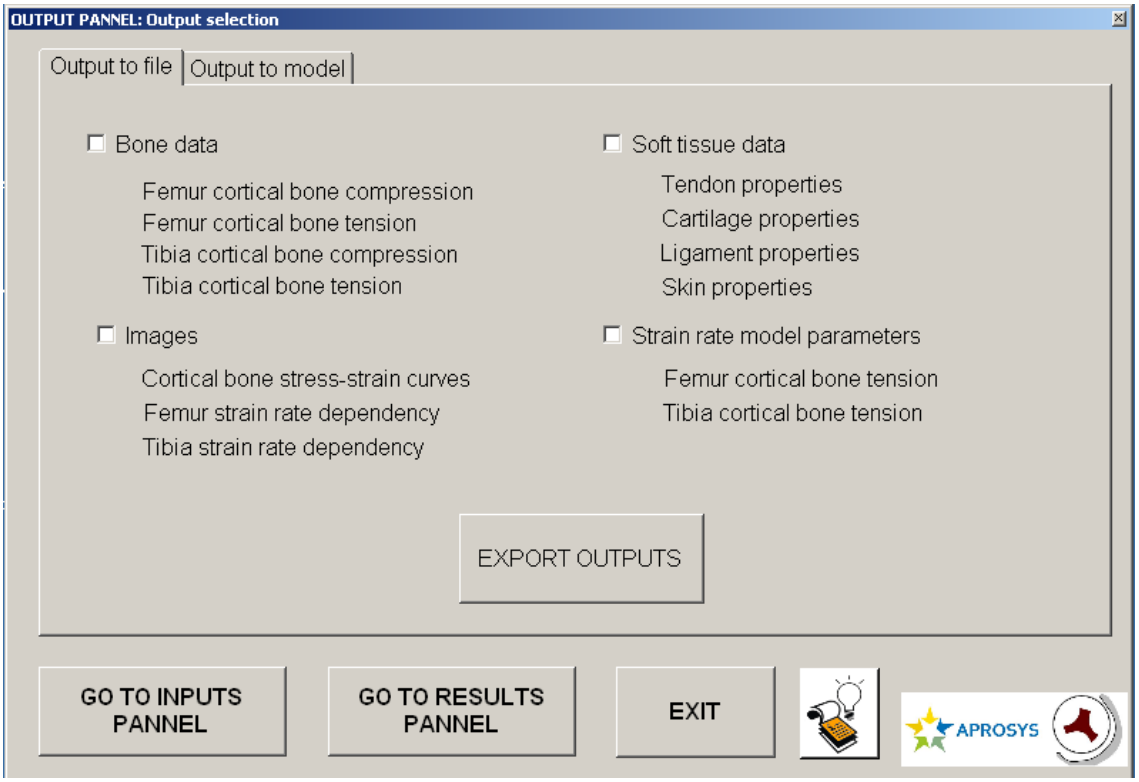

Figure 4-25: Output panel: export to file folder.

The “output to model” folder was included in AgedMAT in order to automatically update mathematical FE models to a selected age; however, this automatic generation of an elder pedestrian model has not been programmed in the current release.

4.5 Implementation of age in the MADYMO pedestrian model.

Taken into account the previous features, the next approach is followed to implement the age effect in the MADYMO MB pedestrian.

Regarding ligaments and tendons, although good correlations are found for some of them in AgedMAT, it is not possible to consider the effect of age in them since they are not individually considered within the MADYMO multibody model. This is particularly the case of the knee, where its lateral stiffness in defined as a function based on dynamic data of Kajzer (1997) and not as the result of the joint effort of the different knee ligaments. With this definition, it is not possible to consider the age effect found for any of the knee ligaments and neither to derive any direct transference function from AgedMAT.

Regarding the long bones, properties under tension and compression have been obtained within AgedMAT with the objective to consider the material characteristics of the bone, typically defined as elastic plastic material with strain rate dependency in FE models. However, since the MADYMO MB model does not consider material models but load values, the outputs from AgedMAT cannot be used and stress and stiffness in bending scenarios are needed instead to transform them into force and torque.

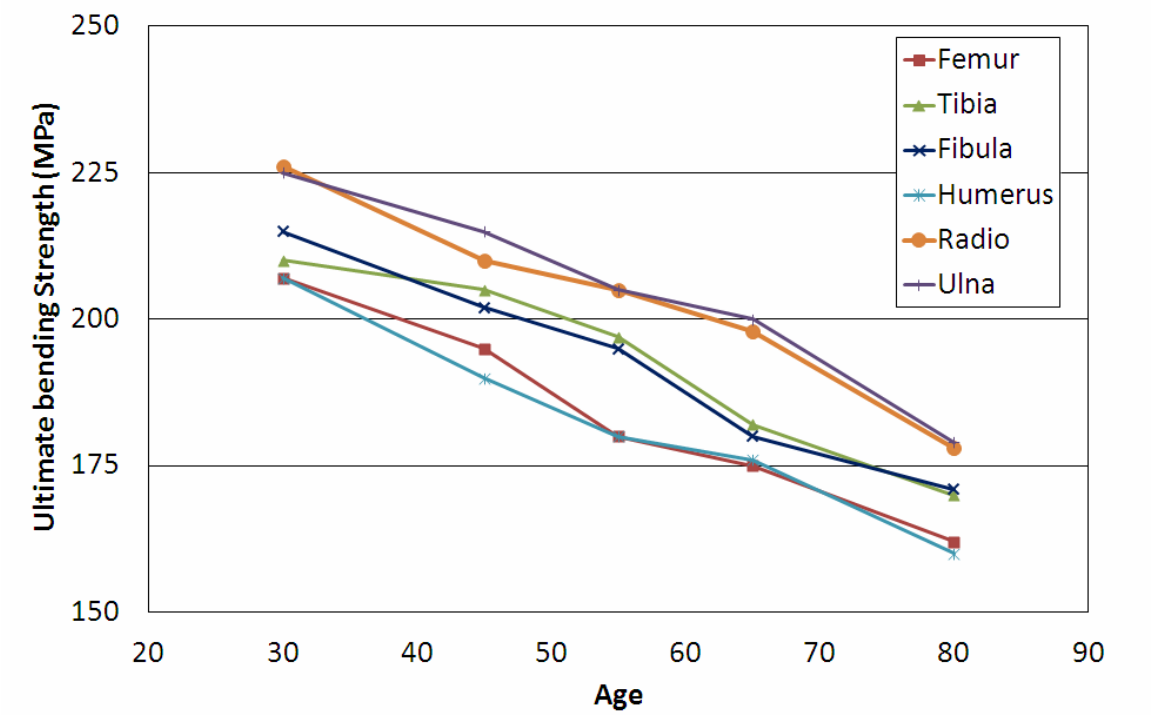

Figure 4-26: Ultimate bending strength variation with age for different long bones (Yamada, 1970).

To take this into account an extra analysis on bone ultimate bending strength is needed, following the same procedure already presented previously to obtain a statistically significant relationship between ultimate bending strength and subject age. Data from Yamada on different bones (1970) is used for that purpose and it is summarized in the figure.

It can be seen that the data on bending strength show a similar pattern to its compression and tension results, as bending strength decreases with the age of the subject and this appears to be very similar regardless of which long bone the specimen came from. In terms of value, the ultimate bending strength values of Yamada are greater than those of ultimate compressive strength and also from those of ultimate tensile strength.

Making use of the simple beam´s theory in pure bending, the fracture of the femur or tibia will occur when the maximum stress is reached in the tensile fibres of the outer part of the beam section with a maximum value that depends linearly with the applied load and the section modulus (Z), which is a purely geometrical parameter.

With these assumptions, a transference function can be obtained from the bending to obtain maximum force and torques, considering how the section modulus varies with age if it is the case.

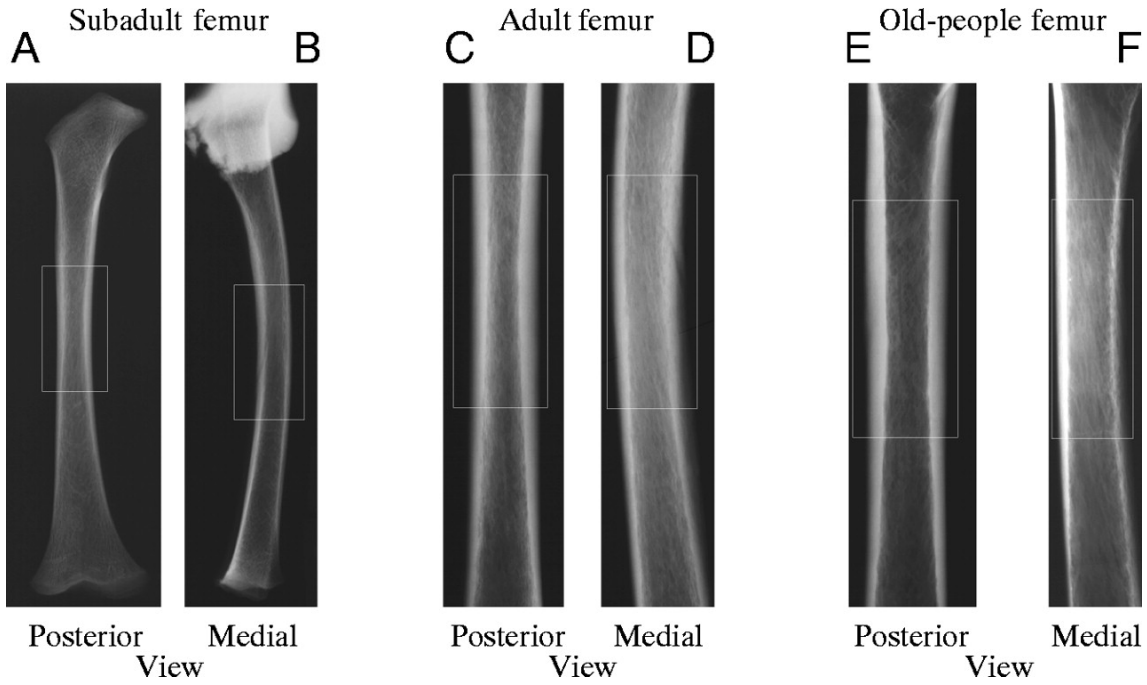

Figure 4-27: Evolution of femur section with age. Évinger et al. (2005)

In a simplified manner, the section of a long bone can be assumed to be a hollow cylinder with an external diameter d and internal diameter d_0 neglecting the contribution of the marrow to the stiffness of the bone. With this approach the section modulus is just dependent on these two diameters and their evolution with age, being aware that the

same section modulus can be achieved increasing the outer diameter and reducing the thickness of the wall of the cylinder, as the contribution of this bone area to the section modulus varies exponentially with distance from the centre of mass of the cross-section. As outer diameter is increased, less material is needed for the same bending stiffness.

A number of references (Woodhead 2001, Lindahl, 1967, Gomberg 2000, Bryon 2005) have already shown that adult bones continually expand in diameter throughout adult life in adaptation to the changing mechanical demands but decrease in thickness with age as the resorption from the marrow space is more rapid than the periosteal growth on the surface. The resulting effect of combining both, as shown in Lindahl (1967), is that the femur section decreases with age in a statistically significant way at similar rate for both male and female, as shown in the figure. Moreover, as already presented in Figure 4-4, (Kleerekoper,1986) the bone skeletal balance becomes negative approx at 55 years old, reducing the BMC of the bones approximately 5-6% per decade and therefore reducing the "solid part" real contributions of the bone to the section. The combination of these two effects needs to be considered to define the transference function for the geometry to obtain the MADYMO MB fracture level inputs.

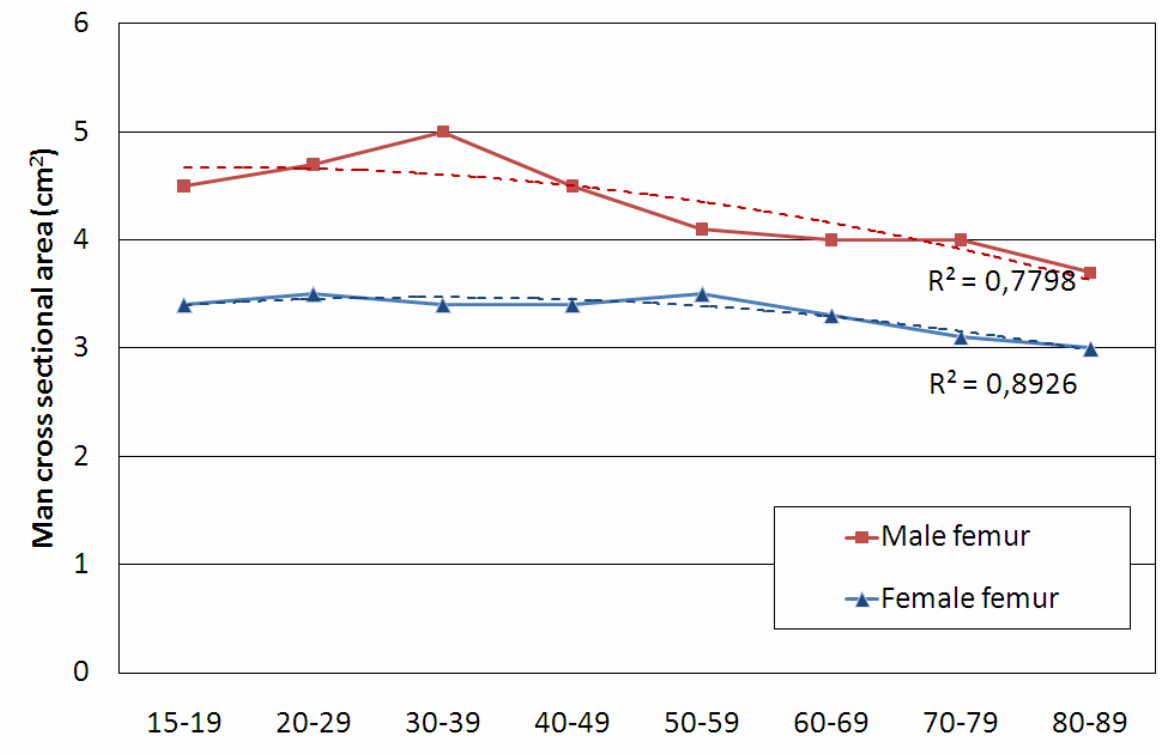

Figure 4-28: Mean cross sectional area variation with age (Lindahl, 1967)

So, in general terms five steps are needed to scale the reference MADYMO pedestrian model to the desired geometry and age to be used to reconstruct pedestrian accidents. As in chapter 6 the selected accident reconstructions involved pedestrians from different age,

size and gender, the development of a scaled model for one of these scenarios (an elder female 1,58m tall and aged 65) is presented here to illustrate this five-steps process.

1. Select the reference MADYMO pedestrian model (5% female, 50% male or 95% male) closer to the real pedestrian characteristics. As in this case, it is a female 1,58m tall, the closer MADYMO pedestrian model is the 5% female (1,53m). This model has as reference fracture limits 5500N and 380Nm, for the femur and 3040N and 190 Nm for the tibia for shear force and torque respectively.
2. Scale the pedestrian in size using MADYSCALE©, if needed, to fit the data on the scene. Considering that the height difference n the example is less than 3%, no geometrical scaling needs to be applied in this model.
3. Obtain the material parameters from the legs for the selected age in bending scenarios. To calculate the relative change in the fracture limits on the model, the percentage variation in ultimate bending strength is obtained between the reference adult model and the one scaled in age. The variation in this case from the standard adult female (aged typically 35 as defined in Van Hoof (2003)) and the needed at 65 years old is 13.5% for the femur and 12.1% for the tibia.
4. Calculate the transference function to consider geometry and gender to convert stress into force and torque. The cross section reduction is obtained from the previous figure considering the pedestrian gender while the BMC decays 5% per decade starting at 55 years old. In the example, the reduction in cross area for females is just 3%, while the reduction in the BMC is expected to be around 5% for a 65 years old female.
5. Transform ultimate stress into force and torque. With all these considerations, the original fracture limits of 5500N and 380Nm for the femur and 3040N and 190 Nm for the tibia for shear force and torque respectively are scaled in age with a factor of (1-0,135)*(1-0,03)*(1-0,05)=0,797 for the femur and (1-0,121)*(1-0,03)*(1-0,05)=0,81 for the tibia resulting in 4383N and 303Nm for the femur and 2462N and 154Nm for the tibia.

5 DETAILED GEOMETRY & STIFFNESS VEHICLE MATHEMATICAL MODELS

There are two technologies available to develop mathematical models for automotive vehicles: Finite element (FE) modelling or multibody (MB) modelling.

FE models usually have a very detail description of the geometry and material characterization of all the parts of the model, which, in the case of a full scale car, means extraordinary complex FE models with thousands of parts and materials.

Therefore, they have the advantage to represent accurately the car geometry and all the local stiffness variations due to the bumper and bonnet underlying parts as well as their deformations during the impact. However, they have the inconvenience that they require very high CPU time to run and they are very complex to develop and not easy to modify in their local behaviour.

Moreover, as these FE models are generally owned by car manufacturers and their contents are confidential, there are very limited public domain models detailed enough (NHTSA 1998) or representative enough (APROSYS SP7 2007) that could be available for this thesis. Furthermore, in these cases, the validation is generally limited to the chassis crashworthiness and the occupant safety but not for pedestrian safety.

On the other hand, multibody models allow having a geometrical description sometimes as accurate as the FE models but simplify the FE models material characterization with the implementation of the stiffness in the contact surfaces. This simplification has the disadvantage that there is not deformation in the models and the stiffness distribution over

the car is not as accurate as the one from the FE models. However, it increases the models flexibility and drastically reduces the CPU time needed for simulation, (Yang 2000, Yao 2005). Moreover, these models can be built from scratch for any vehicle if its stiffness, its outer geometry and its mass distribution are available (Martínez 2007, Bovenkerk 2007).

Taking into account these arguments, this thesis will use MB technology to develop car models in such a flexible and accurate way to be valid to study, analyse and improve pedestrian safety. This thesis proposes a three steps methodology to develop these vehicle models:

- Define the dynamic behaviour of the car and its multibody frame.
- Build in detail the vehicle front end geometry.
- Map the local stiffness along the vehicle front.

This third step is the most critical aspect, since in most cases it is unknown. This thesis has dealt with this aspect in detailed, having defined in Section I a stiffness mapping tool that supply appropriate and wide test based estimates on the stiffness of most of the European vehicles front parts.

5.1 Definition of the vehicle multibody frame.

The first step of the methodology is to set the model structure in the space, together with its dynamic behaviour. The chassis of the vehicle is represented by a simple multi-body frame consisting of a chassis body, linked with a free joint to the inertial space, plus four bodies representing each of the tyres, linked to the chassis body through a translational-revolute joint to allow the front and rear suspension work independently, letting the car to pitch if braking is considered or when it impacts the pedestrian.

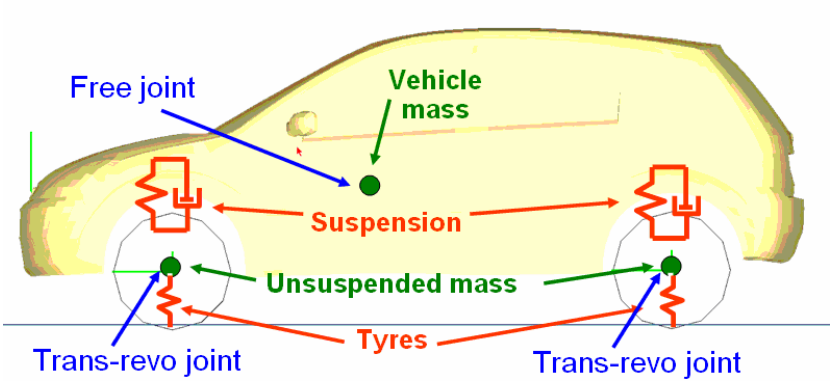

Figure 5-1: Overview of the multibody frame of the vehicle.

The suspended mass of the vehicle is assigned to the chassis body, while the unsuspended mass is assigned to each of the four tyre bodies, each located according the wheelbase and track data of the vehicle. The inertial properties of both the chassis

and the tyres are calculated according McInnis formulas (1997), that take into account the overall dimensions of the vehicles together with its mass and centre of gravity location, which can be obtained knowing the car mass distribution in the front and the rear axle.

The front and rear suspension stiffnesses are calculated with a simplified two degrees of freedom model of a quarter of the vehicle (Figure 5-2 model A). This model is typically used for pre-designs in suspensions and it can give good estimates for all the vehicles without diving into their specific suspension details. In these pre-designs, the target for suspensions natural frequency is 1 Hz; since it is found that human being tolerate best this frequency (Vera, 2003). To achieve this target, the natural frequency should be 1-1.2 Hz for the suspended mass and, around 10 Hz, for the unsuspended mass.

To start the pre-design process, the suspended mass (per tyre) is supposed to be much higher than the unsuspended one.

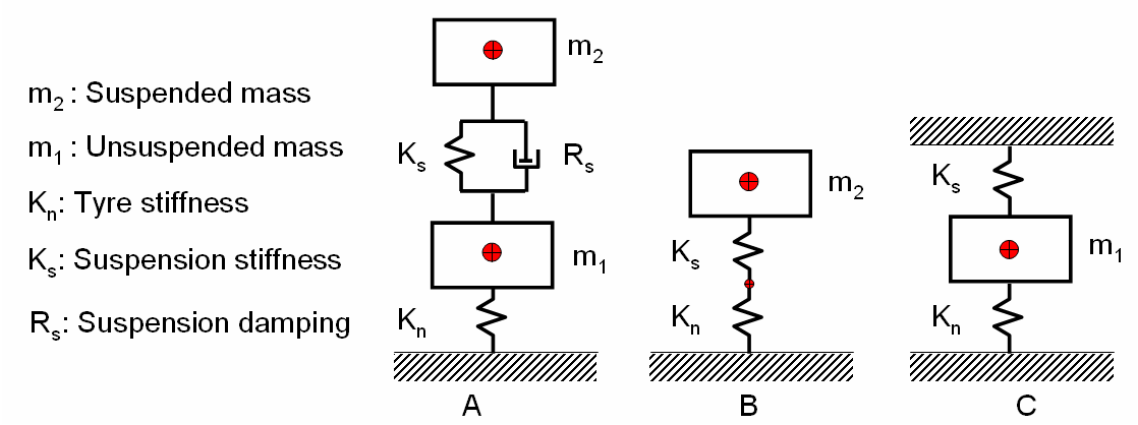

Figure 5-2: Simplified two degrees of freedom model of a quarter of a vehicle.

With this hypothesis, the model A in Figure 5-2 is simplified into model B for the suspended mass and into model C for the unsuspended mass.

With model B together with a target natural frequency of 1 Hz for the suspended mass, the equivalent stiffness can be obtained via Formula 5-1.

$$K_{eq} = \frac{K_s \cdot K_n}{K_s + K_n} \qquad w_{m2} = \frac{1}{2\pi}\sqrt{\frac{K_{eq}}{M_2}}$$ **Formula 5-1:**

With model C the natural frequency of the unsuspended mass can be calculated using Formula 5-2.

$$K_{eq} = K_s + K_n \qquad w_{m1} = \frac{1}{2\pi}\sqrt{\frac{K_{eq}}{M_1}}$$ **Formula 5-2:**

In both cases, the tyre stiffness value is needed and it has been calculated applying Hooke's Law, considering the tyre loaded radius as the 90% of its nominal radius (Vera 2003).

The front and rear suspension stiffnesses are calculated separately and implemented as characteristic load functions in the translational part of the translational revolute joints of the model, while the tyre stiffness is implemented as contact characteristic in their contact with the ground.

In order to initialize the model, the initial deflection of the suspension model is determined in a pre-simulation study with only gravity acting on the vehicle. With this preload of the suspension and the orientation of the chassis free joint as inputs, the vehicle is positioned with respect to the ground.

In the cases where the vehicles were to be used for reconstructing pedestrian accidents with braking, a braking pre-simulation is needed to re-calculate the orientation of the chassis free joint and locate correctly the vehicle orientation due to the braking in the real accident scenario.

5.2 Development of the vehicle front end geometry.

The vehicle geometry can be implemented in detail as a mesh (facet surface) or using ellipsoids. The implementation of the geometry of the vehicle as a facet surface allows the most accurate definition of the front end geometry of the car; however, in some cases it is more convenient to define the vehicle geometry using ellipsoids taking into account how the interacting object is defined.

In fact, in the cases where the vehicle model is to be used with a pedestrian model in FE (i.e. THUMS FE model), it is recommended to have the vehicle defined as a facet MB model, that is, a geometrical mesh representing the car geometry, because the contact characteristics between meshes of similar sizes work more efficiently that contact characteristics between ellipsoids and meshes. For that reason, if the vehicle model is to be used with an ellipsoid pedestrian model, such as the MADYMO pedestrian model, it is preferred to define the vehicle model geometry in terms of ellipsoids, which simplify significantly the geometrical definition, and increase the accuracy in the contact algorithms between the vehicle and the pedestrian.

In any of the cases, the first step to obtain the car geometry is to scan it with a 3D scanning device. As a result of this process, splines of the vehicle outer geometry front end are obtained.

If ellipsoid geometry is used, ellipsoids are placed according these splines to create the outer geometry, but if a facet model is the target, the splines need to be transformed into surfaces through a post process in CAD and a further process in ANSYS to generate the final mesh of shell elements of the car geometry.

A detailed description of these steps is given in the next headings.

5.2.1 Scanning of the vehicles.

Considering the needs of this analysis, only the outer geometry where pedestrians may impact in front accidents have been considered and the scan of the vehicles have been limited to front parts, including the front doors and roof. The scanning process has followed three steps:

The first step aims to define a robust coordinate system for all vehicles as well as to define important reference points in the vehicles as ground reference points or tyre centres. To ease the process the same coordinate system definition is used for all vehicles. This system is defined linked to the vehicle geometry and with the origin of the coordinate system placed in the centre of the vehicle brand logo.

- The XZ plane in the vehicle is defined by a perpendicular line to the supporting surface of the measurement device and the mean point (x1) of a line defined between two symmetrical points in the vehicle (typically the wiper washers), being the Z axis the perpendicular line from the supporting surface plane to the coordinate system origin.
- XY plane is determined by a plane parallel to the ground through the origin, being the X axis the line from the origin to the projection of point x1 in the plane XY.
- YZ plane in the plane perpendicular to the other two planes through the origin, being the Y axis the intersection of this plane with the XY plane.

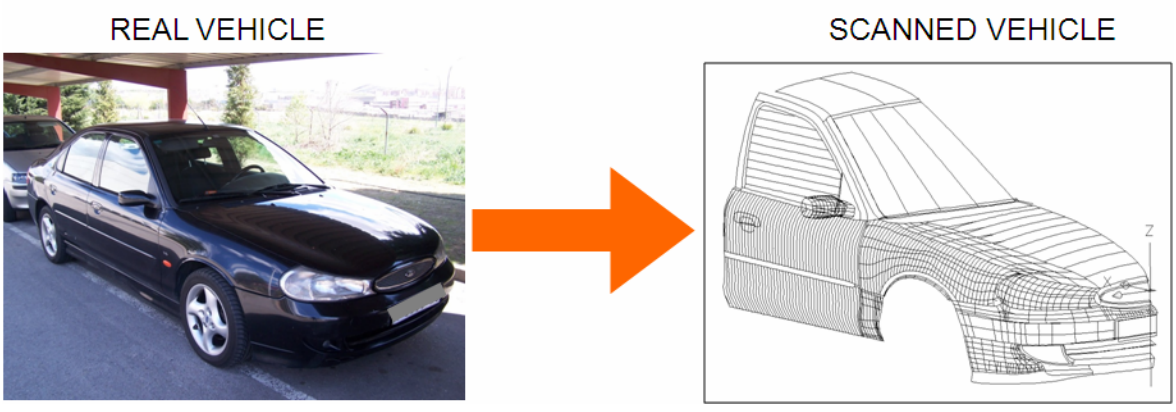

Figure 5-3: Scanning process of the vehicles geometry.

The second step is defining the edges in the vehicle. The edges of the vehicle define the different parts in which the vehicle is divided. The definition of the vehicle edges will determine the different surfaces to be defined within the vehicle geometry that will be constructed later separately. Moreover, these edges are not only the physical edges that separate the different components but also the edges needed, in a later stage, to map the stiffness into the vehicle, as those defining the different “wrap around distances” (WAD).

Finally, the last step scans the intermediate splines to construct the surfaces. Each individual part of the vehicle, with the different edges as boundaries, is scanned to obtain the intermediate splines that best define each surface. Depending on the curvatures, different densities of splines are applied to the different parts of the vehicle in order to minimize the effort in the next post process.

The final files containing this information is exported as IGES file and imported into CAD for the post-process and the surfaces generation, or directly into the MADYMO pre-processor to locate the ellipsoids that define the geometry.

5.2.2 Post process in CAD.

Mechanical Desktop offers a wide number of options to create complex surfaces from splines. However, some of the splines obtained in the scanning are not valid to create surface and needs some previous refinements.

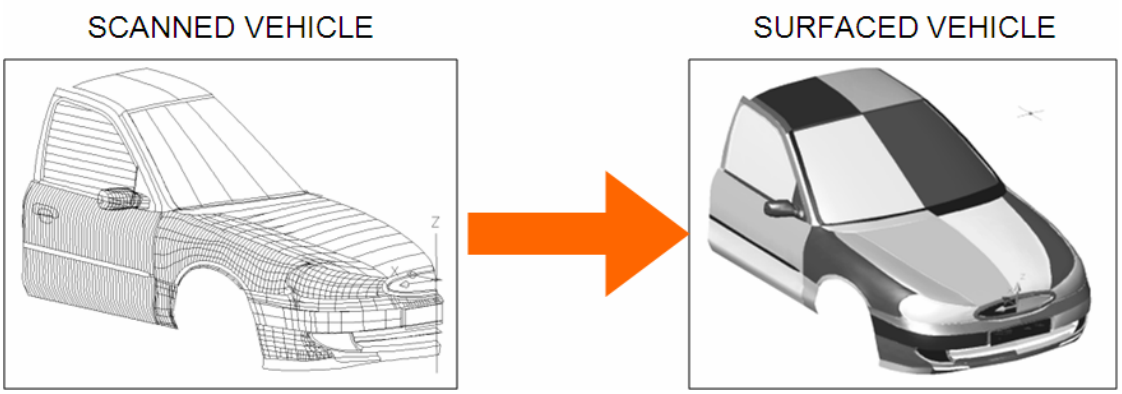

Figure 5-4: Post-process of the splines to convert them into surfaces.

The following operations have been done or checked in all vehicles before the generation of the car surfaces:

- Refine the start and end points of the edge splines. As the real edges have, in some cases, a significant width, the scanning process did not select the same points as common start or end of different edges, therefore, a merge of these points needs to be done to make common start or end points to coincide.
- Define finite edges limiting each surface. In order to define properly a surface, the edges needs to define a closed boundary and, therefore, individual edges need to be split to close the different car surfaces.
- Refine the intermediate splines to make them start and finish into an edge. In order to build a surface, U and V wires that define its curvature must start and end into an edge of the contour, therefore, the intermediate splines needs to be conditioned and modified in order to fit to these needs.
- Due to symmetry, only half of the vehicle was scanned. At this point, as final step

in the refinement process, the other part of the vehicle is built with a XZ symmetry and the converging edges are joint in order to create continuous surfaces at both sides of the XZ plane.

The car geometry, already into surfaces format, is exported as IGES file and imported into ANSYS for meshing.

5.2.3 Mesh generation.

The ANSYS meshing tool for shell modelling has been used to generate the meshes of the surfaces since it contains numerous approaches to provide the mesh that best meets the needs of the different parts of the car, whether it is a very simple mesh, as happens in the windscreen, or a very complex one, as happens in the bumper, where a tailored mesh is needed in order to select or neglect the details of the geometry.

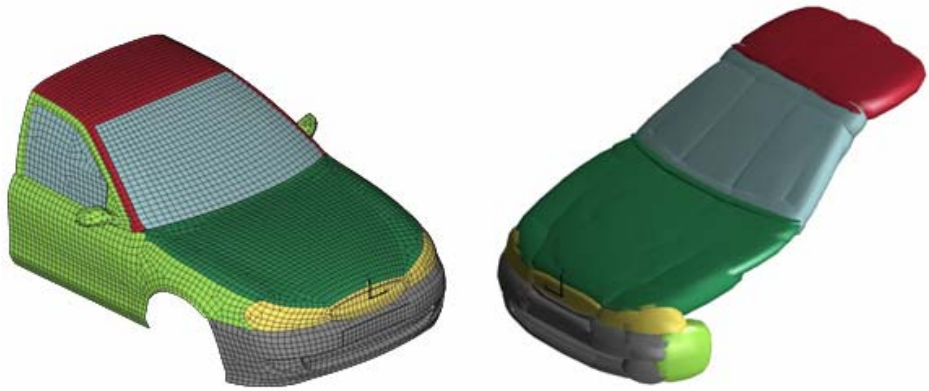

Figure 5-5: Detailed geometry of the vehicle model in facet surfaces or ellipsoids.

The element length has been selected to be very similar to the models to which the cars are to interact (THUMS FE human model, pedestrian sub-system FE impactors) and geometrical checks as well as connectivity checks have been performed during the meshing in order to ensure a high mesh quality.

The result of the meshing for one of the vehicles is seen in the Figure 5-5 together with the equivalent in ellipsoid format (to be used with MADYMO multibody pedestrian models) to highlight that, in both cases, the geometry of the vehicle is described in detail.

5.3 Map the local stiffness along the vehicle front.

The stiffness of the different parts of the meshes is implemented as contact characteristics in a force-deflection format, but to map correctly the different stiffnesses into the vehicle geometry, it needs to be defined the exact location where to apply them. There are two strategies to approach it depending on data availability and the objectives to address with the vehicle mathematical model.

a) In accident reconstruction cases, with typically known vehicle make and model, it is preferable to derive stiffness directly from the actual test data for the vehicle

make and model involved in the accident, using the methodology shown in Section I to obtain the force-deflection functions. If this is not possible, the stiffness corridors obtained in Section I are good estimates to be used.

b) In more generic studies where there is not a need of a concrete vehicle make and model, the stiffness of the vehicles is mapped making use of the stiffness corridors derived from the EuroNCAP pedestrian sub-system tests presented in Section I depending on the need of red, yellow or green behaviour of their different front parts.

Considering that EuroNCAP impact point selection is performed on an individual vehicle based matrix (Figure 5-6), and this matrix is also the basis for the EuroNCAP ratings, it is coherent to use this matrix as a template to apply the proposed characteristics. With this approach, sixty different zones can be mapped in each car with a correct estimate of their local stiffness. To take into account the areas not covered by this matrix, basically parts of the windscreen and the A-pillar, the values obtained by Mizuno (2000) are used for these two zones.

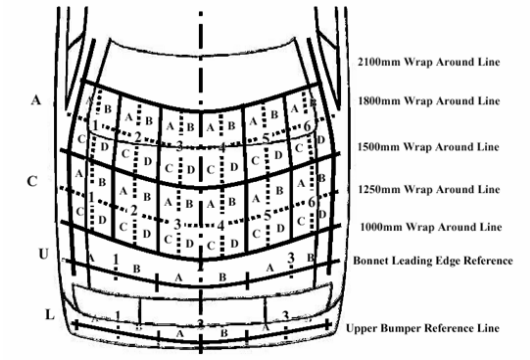

Figure 5-6: EuroNCAP labelling of impact zone and typical matrix for the different segments. (SMC, SFC; LFC; MPV and SUV respectively).

In this mapping, two approaches can be followed depending on the objective of the vehicle model:

- If the vehicle model is to be used to represent a single car, its EuroNCAP stiffness map should be applied to locate its stiffnesses,
- However, if the vehicle model is to be used as a representative car of any segment, a “standard” stiffness map should be applied to set its stiffness properties.

For the first case, EuroNCAP gives, from phase 14 onwards, not only the pedestrian stars for the vehicles it tested, but also the pedestrian ratings in the pedestrian test matrix, therefore, they are a valuable source of data to guide the vehicle front end stiffness distribution.

For the second case, “standard” stiffness maps needs to be developed. As it can be observed in the Figure 5-6, the coverage of the pedestrian impact matrix differs between the vehicle types, therefore, a “standard” stiffness map has to be derived for each of them (Super mini cars SMC, small family cars, SFC, large family cars LFC, multipurpose vehicles MPV and sport utility vehicles SUV). Two approaches have been considered to find a “standard” mapping for each segment:

- An average approach that considers the results of all the vehicles from each segment and find an average map for each of them.
- A best map approach that select the car which best scores in the EuroNCAP pedestrian tests.

In both cases, the sample used in these two approaches has been extended from the 26 vehicles used to derive the stiffness corridors from the previous Section to 69 vehicles, including all the vehicles tested in EuroNCAP and rated in the pedestrian test matrix map

format (vehicles tested until September 2006; distributed in 18 SMC, 13 SFC, 12 LFC, 12 MPV and 14 SUV).

5.3.1 Average mappings.

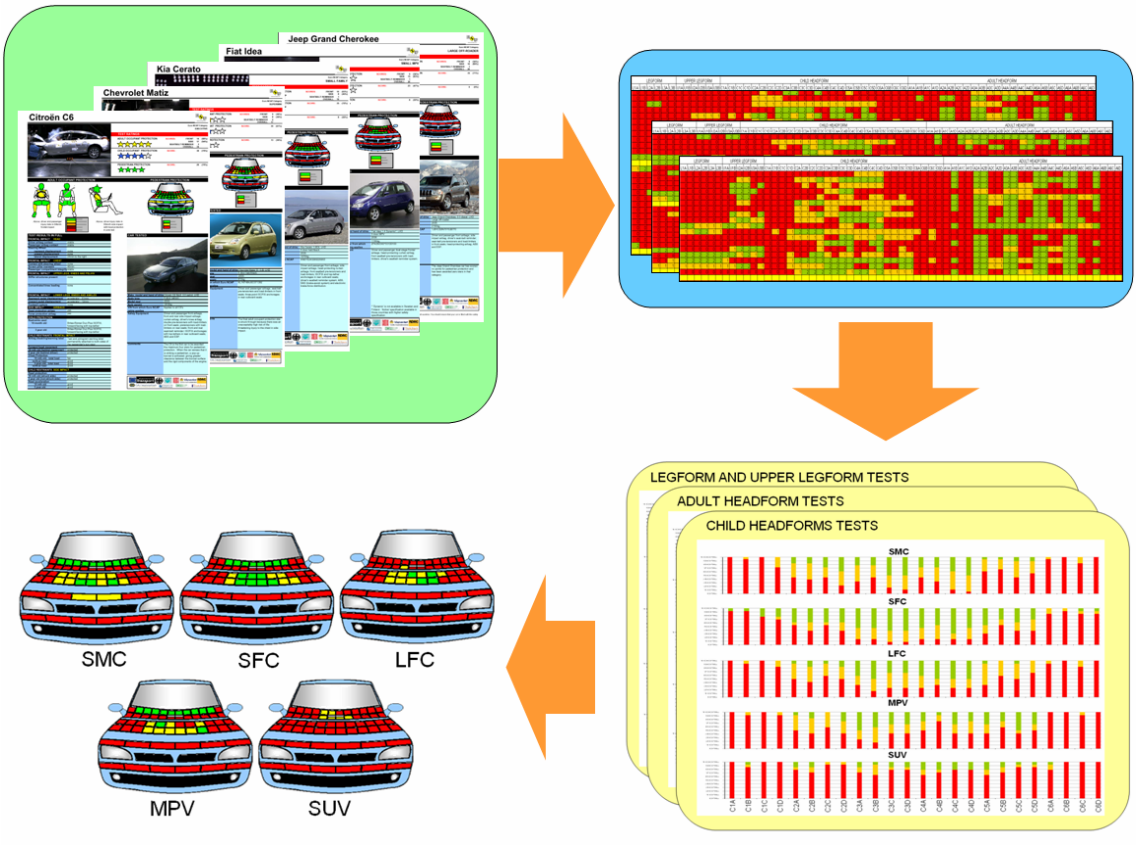

Figure 5-7: Approach to the definition of the vehicle segments typical mapping.

The 60 areas EuroNCAP gives a rating for each vehicle have been account and grouped for the different vehicle segments. A frequency analysis has been performed on each of these areas to define an average mapping for each vehicle segment. To build these mapping the distribution of red, yellow and green scores for every area has been computed and, based on them the average mapping have been built with the following criteria in each impact test area:

- If a colour rate represents more than a 50% in an impacting zone, the area is coloured in such colour.
- If there is not any colour rated with more than a 50%, yellow colour is applied.

It can be seen in the Figure 5-8 the distribution of red, yellow and green ratings over the bumper and the bonnet leading edge areas. In both cases, the sample size is 414 tests (6 zones x 69 vehicles).

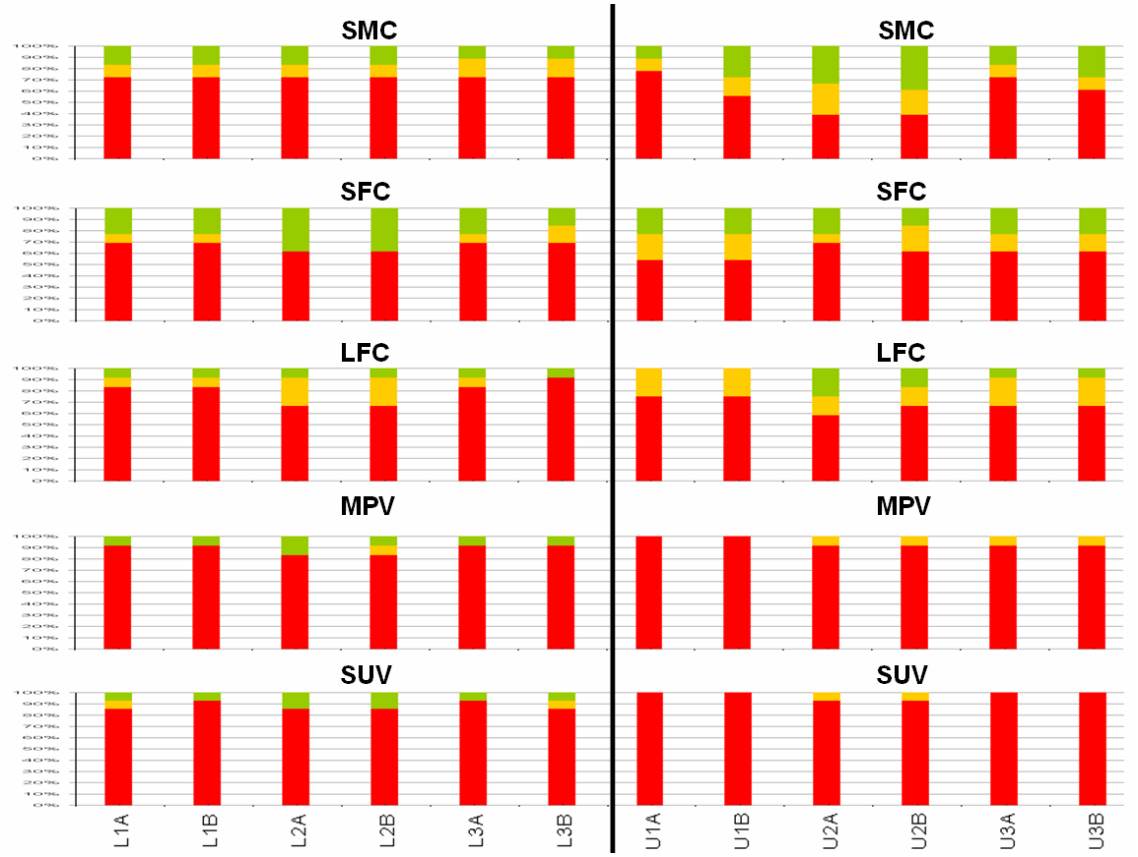

Figure 5-8: Legform and upper legform testing area ratings for the different car segments.

Regarding the former, it can be seen that red percentages are rather constant for SMC, MPV and SUVs with values over the 70-80% in all the areas. On the other hand, SFC and LFC show more dependency on the impact area.

For SFC, green reaches 40% in the middle of the bumper and around 25% in the sides while in LFC, red percentage decrease especially in the middle of the bumper (65%) while it is maintained in 80% for the sides. In the non red part, green is the dominant colour in SFC and yellow in LFC.

Regarding upper legform tests, current SUV and MPV are almost always rated red while the trend is rather different for the other segments.

LFC and SFC show similar trends for red percentages; in both it is maintained around a constant value for all the areas (70% for LFC and 50-60% for SFC), while the green and yellow diagrams show some differences. In SFC green is maintained close to 20% in all areas while it shows this behaviour only in the middle part for LFC.

Regarding the SMC, they show differentiated trends in the middle, where green and yellow accounts for the 60%, and the sides, where red is again the predominant colour.

It can be seen in Figure 5-9 the distribution of red, yellow and green rates over the child test area, which covers the bonnet area between WAD 1000 and WAD 2100 and includes around 1600 ratings.

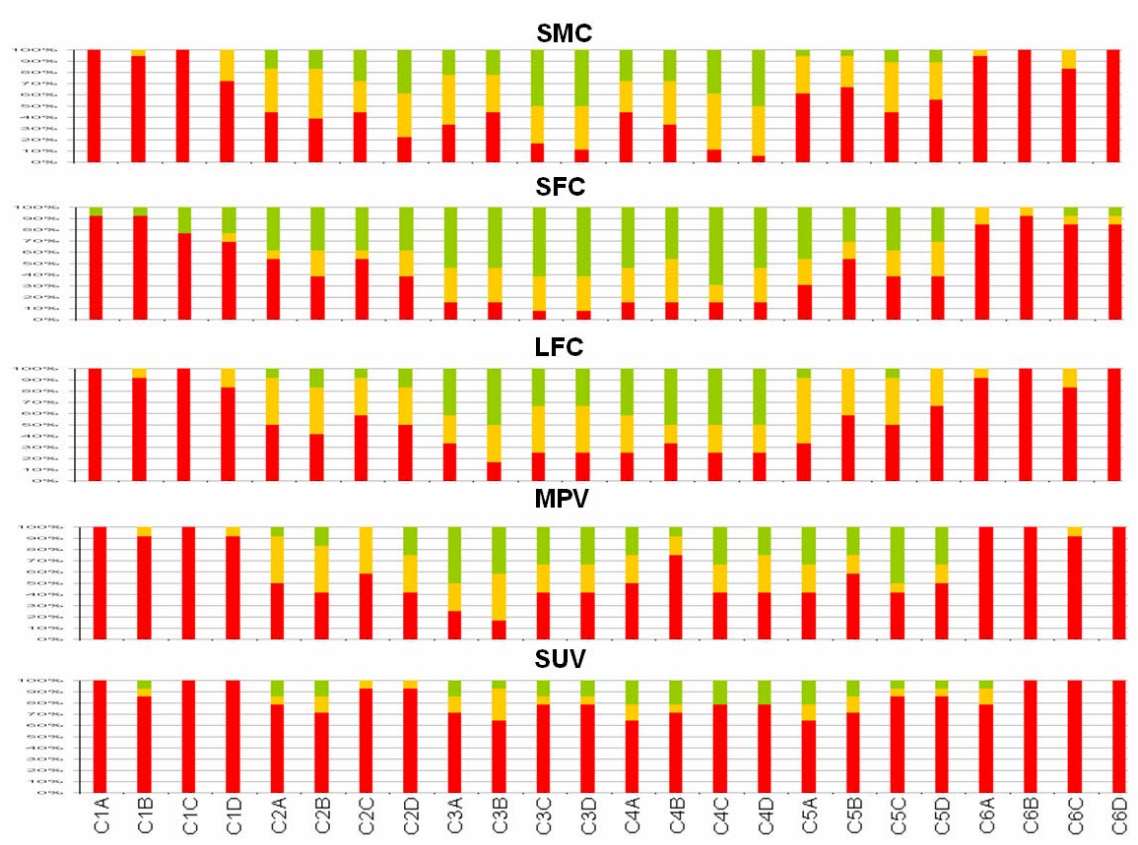

Figure 5-9: Child headform testing area ratings for the different car segments.

It can be observed a similar trend in the child impact zone corners for all the segments and different distributions in the middle part depending on the vehicle segment.

It can be seen that the SUV middle child impact area remains commonly red rated while this is not the case for the rest.

SFC and LFC red parts are reduced to a constant value less than 10% for the former and 20% to the latter reaching the green percentage constant values near 60% and 45% respectively in the C3 and C4 areas. Moreover, it is also relevant that for areas C2 and C5 green predominates for SFC and yellow predominates for the LFC.

For the case of SMC, similar tendencies to SFC and LFC are found in C3CD and C4CD but due to the shorter bonnet C3AB and C4AB tests are performed close to the rear part of the bonnet and the results are not so positive. In these parts, red percentage increases near 40% and yellow is more predominant in the non-red part.

Finally, MPV show an intermediate behaviour between the SUVs and the family cars with moderate importance of green and yellow in the middle (together hardly represents the 60%) which is rather maintained also to C2 and C5 with the exception of the C4B where red shows a sudden peak.

Figure 5-10 shows the mapping of the adult headform impact zone of the different segments including the green rate given to windscreen impact and the red rate given to A-pillar impact (both without testing).

Red scores due to A-pillar impact in A1A and A6B were given to all cars, but the green score for middle windscreen impact (commonly A2AB, A3AB, A4AB and A5AB) are only extensively given to SMC, SFC and MPV groups. In these three groups, C and D part, show some variations although commonly red rates are again over the 50%.

In the case of LFC most of adult tests impacted on the windscreen base and not in the windscreen middle, therefore the red rating is maintained over 60% but in the A3C and A3D, where yellow is more predominant.

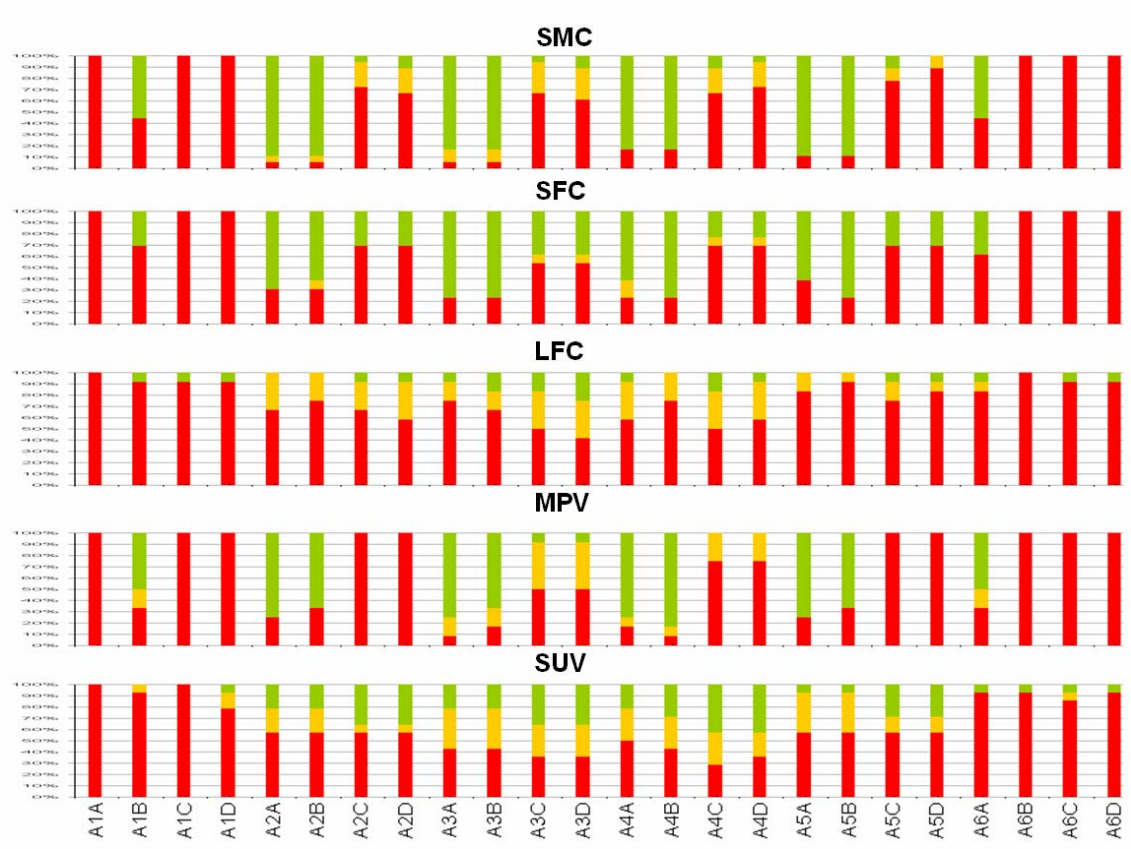

Figure 5-10: Adult headform testing area ratings for the different car segments.

Finally SUVs show a different trend as they present a rather constant behaviour in A3 and A4 zones with red percentages around 50% and a bit higher, but also rather constant in the A2 and A5 zones, near 70%.

As a result of the analysis of Figure 5-8 to Figure 5-10, Figure 5-11 shows the average mappings for the different five segments.

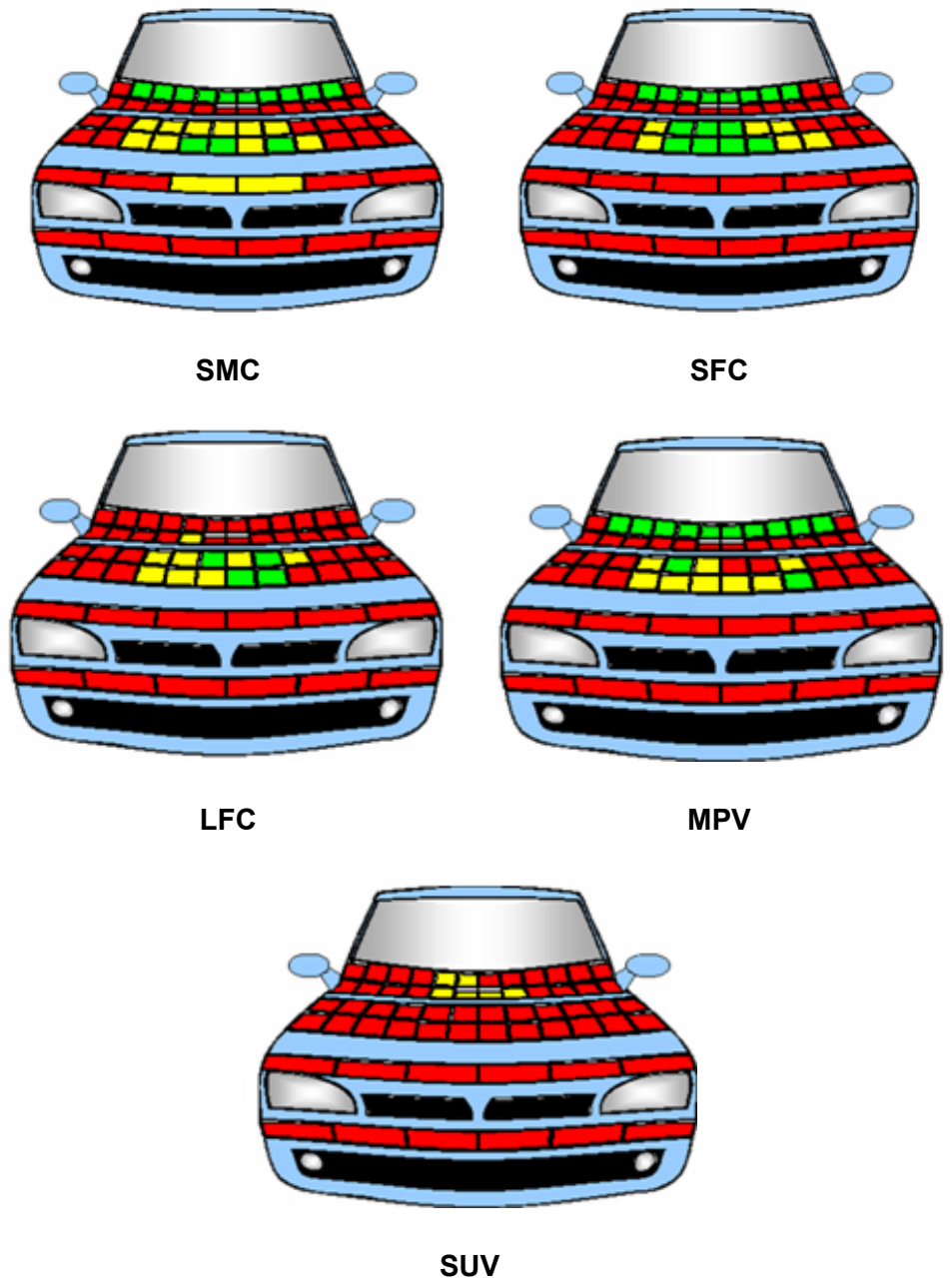

Figure 5-11: Average mappings of the different vehicle segments.

5.3.2 Best mappings.

The 69 vehicles considered have been ordered according the score obtained in EuroNCAP and the best car of each segment has been selected.

In case of the same score, priority has been given to the car where more points have been gained through testing and not by excluding windscreen areas. The five mappings in this approach are shown in Figure 5-12.

Comparing the Figure 5-11 of the average cars and the Figure 5-12 of the best rated cars it can be highlighted a number of interesting differences:

- Regarding the bumper, the average mappings show all red zones in this area while it seems that the current status in pedestrian safety of best rated cars has already addressed this issue for pedestrians showing green scores in most cases.
- Regarding the bonnet leading edge, the average mappings are all rated in red, while it is only the case of the best scored SUVs, since best scored SMC, SFC and LFC are predominantly green and MPV is mainly yellow.

Regarding the bonnet, the child zone was the one with best results in the average mappings. The improvement in this zone is remarkable in the case of the best rated SUVs, MPV and LFC while it is not so important for SMC and SFC since the average mappings were already rather yellow and green.

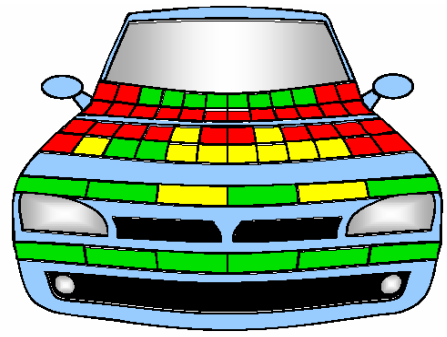

SMC (Peugeot 207)

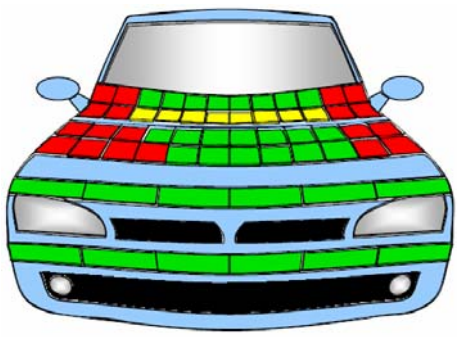

SFC (Honda Civic)

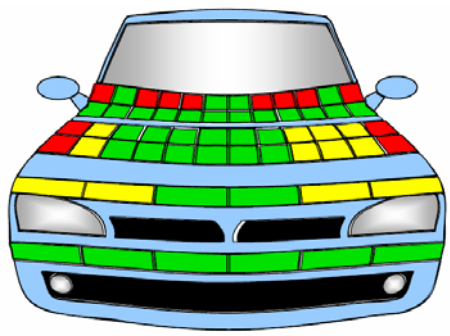

LFC (Citroen C6)

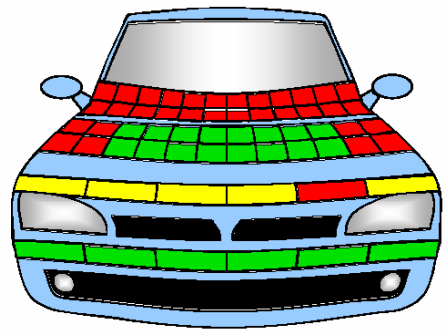

MPV (C4 Picasso)

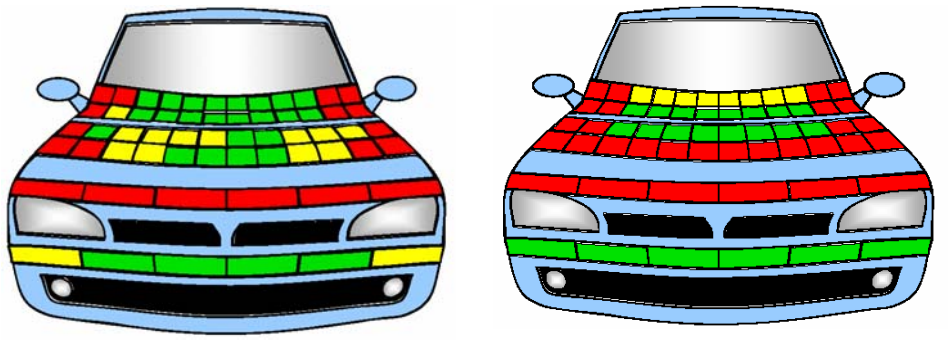

Small SUV (Toyota RAV 4) **Large SUV (Audi Q7)**

Figure 5-12: Best mapping of the different segment.

- In the case of the adult impact area, the average mapping and the best rated mapping are very similar in all case but for the SUVs and LFC, where the best rated improves significantly the red scores of the average mapping, turning most of them into green and yellow areas. In the case of SUVs the improvements have been based on a wise packaging below the hood to allow enough deformation travel for the impactors, while in the case of LFC, the pop up bonnet system has worked effectively to achieve the green scores.

Considering these items, the best rated maps per segment are preferred to be used within this thesis when a "standard" stiffness map per segment is needed, since they take into account the current status of pedestrian safety solutions and any derived recommendation would be a step forward to improved cars already pedestrian friendly.

5.4 Methodology validation.

In order to validate this methodology, a sedan vehicle mathematical model has been constructed in MADYMO with the following set of characteristics.

Weight	Wheelbase	Track (F-R)	Height	Length	Width	Tyres
1295 kg	2512 mm	1513mm-1494mm	1431mm	4507mm	1731mm	195 65 R15

Table 5-1: Vehicle characteristics.

Chassis	Ixx	Iyy	Izz	Wheel	Ixx	Iyy	Izz
1165 kg	444.1	1880.3	1950.3	32.4 kg	2.34	1.865	1.865

Table 5-2: MADYMO vehicle model mass and inertia properties.

% mass distribution	K_n (N/m)	K_s front (N/m)	K_s rear (N/m)	W_{m2} frontal (Hz)	W_{m2} rear (Hz)
60/40	190170	15181	9388	12.68	12.50

Table 5-3: MADYMO vehicle model joint stiffness.

With the geometry and the multibody frame in place, whole red, yellow and green stiffness is implemented in all the vehicle structures and a matrix of pedestrian sub-system tests is simulated including 4 tests configurations: the adult headform impacting in the windscreen and in the bonnet, the child headform impacting in the bonnet and the lower legform impacting on the bumper, all at the test conditions defined in the EuroNCAP pedestrian testing pedestrian procedures.

As headform impactors, the EEVC WG17 MADYMO FE headform models have been used with the initial test conditions from the EuroNCAP pedestrian protocol: Impact velocity of 40 km/h at 65º with the ground for the adult and 50º for the child. In the case of the legform, the MADYMO FE model of the EEVC WG17 legform impactor is used, with its corresponding initial test conditions: Impact velocity of 40 km/h horizontally.

The measurements that EuroNCAP uses to rate each impact point, HIC, in case of the headforms, and tibia maximum acceleration, in the case of the legform, are obtained from each simulation and compared with the average ones obtained in the red, yellow and green test groups in each of the test configurations (adult impactor in the bonnet, adult impactor in the windscreen, child impactor in the bonnet and lower legform impactor in the bumper), that were used to derive the corridors (Figure 5-13).

It can be seen that HIC output from the models in all cases is rather similar to the mean HIC value obtained from the tests. It is remarkable that red behaviours are very close with their targets and very well distinguished from the other two rankings.

Regarding the yellow and green best fit, they are also considerably close to the target. However, the output of these two models has been found to depend on the variation of the hysteresis slope and the friction coefficient, showing cases where green and yellow behaviour are exchanged, especially in the bonnet impacts. This behaviour is not surprising as the average curves in these two configurations show a significant overlap.

In the case of the legform, the differences in the expected output and the obtained one are always within the acceptable interval. As in this case, the acceleration directly is the computed output the remarkable differences shown in the stiffness are directly translated into the tibia acceleration results showing no overlapping between the colours.

As in the process of obtaining the bumper stiffness corridors the knee bending angle and the knee shear displacement measured in the legform tests were not considered, neither are used in this stage as they are more geometry dependant than stiffness dependant.

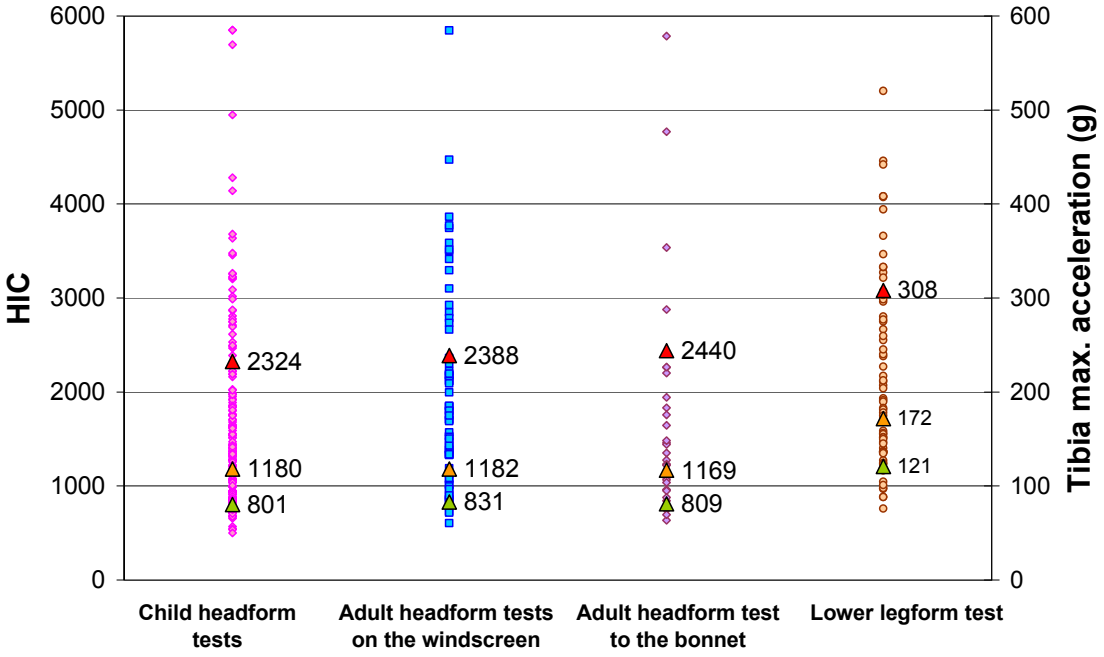

Figure 5-13: HIC and tibia acceleration average values from the test sample.

		Child headform on bonnet (HIC)	Adult headform on bonnet (HIC)	Adult headform on windscreen (HIC)	Lower legform to bumper (Tibia acc, g)
Red	Expected	2324(±1014)	2440(±1306)	2388(±961)	308(±80)
	Obtained	2356	2444	2430	303
Yellow	Expected	1180(±108)	1169(±106)	1182(±140)	172(±15)
	Obtained	1273	1287	1255	174
Green	Expected	801(±114)	809(±109)	831(±115)	121(±21)
	Obtained	909	920	913	120

Table 5-4: Comparison of the obtained values vs. calculated average values.

Having seen these results, it can be concluded that the proposed methodology is suitable for pedestrian analyses and also that in most cases, there are clear correlations between the stiffness corridors levels and the injury outputs they lead to. Nevertheless, caution should be considered if the results are extrapolated to locate an isolated result into the

corridor to conclude univocally that it will result either in green, yellow or red EuroNCAP rating.

6 REAL WORLD ACCIDENT RECONSTRUCTIONS

Making use of the tools already delivered in this Section II, this chapter looks closer to real world scenarios in order to analyse the significance of the age in the occurrence of pedestrian injuries as well as the feasibility to consider its effect from a testing perspective.

With this objective, four accident cases, from the ABIDA project database (ABIDA 2004) and representative of typical pedestrian accidents have been selected and mathematically modelled in MADYMO.

The selected four cases cover the whole age range of adult pedestrian, include injuries in the critical body areas identified in the accidentology analyses (head and legs, mainly) and have enough information on the scene to validate the kinematics derived from the mathematical simulations.

As the selected cases are also expected to serve as valuable source of information for looking in detail the occurrence of injuries in the two areas mentioned (head and legs) some other extra requisites have been considered in the selection process to ease them.

With respect to head injuries, the accidents selected have included cases where the pedestrian head impacted the vehicle (windscreen or bonnet and but not A-Pillars) and resulted with and without head injuries. These scenarios have output very valuable information regarding the impact conditions of the pedestrian head with the vehicle that has been integrated with FE human models in the Section III in collaboration with ULP

and TNO, and has allowed investigating the relevance in injury causation of the different initial kinematics parameters.

In the case of legs injuries, the accidents selected have involved pedestrian of a wide age range where the vehicle impacted the pedestrian legs above or below its knee level, resulting with and without upper leg /lower leg injuries. The output of the reconstructions of these different scenarios have been used firstly, to prove the suitability of the previously developed aging functions to scale leg fractures limits and, secondly, to define the critical geometrical aspects in the pedestrian-car interaction leading to leg injuries.

Together with these strategic requisites, for practical reasons, cases have involved vehicles tested under EuroNCAP pedestrian protocols (to use real front end stiffness) and occurring at impact speed where the injuries on the pedestrian are not so severe and massive that it was not possible to identify pedestrian injuries univocally and separately.

With these premises, the selected four scenarios main characteristics are summarized in the table.

Pedestrian				Vehicle model	Estimated impact speed
Age	**Gender**	**Height**	**Injuries**		
55	Male	1.75m	Head injuries	BMW 325	28 km/h
19	Female	1.60m	Leg injuries	Ford Mondeo	27 km/h
21	Male	1.69m	Head and leg injuries	Renault Clio	31 km/h
65	Female	1.58m	Head and leg injuries	Skoda Octavia	28 km/h

Table 6-1: Summary of real world scenarios.

For simulating these scenarios, the vehicle models have been constructed according to the procedure described in the previous chapter; that is, the vehicle characteristics in terms of mass, inertia and joint stiffness have been calculated and integrated into the underlying MADYMO multibody frame of the vehicle models and the vehicle front geometry has been scanned and an ellipsoid-based geometry has been constructed on top.

The models have been initialized with only gravity acting on the vehicle to preload the suspension and in cases where braking was reported, a braking pre-simulation is also performed to orientate adequately the chassis free joint prior to the pedestrian impact.

Vehicle	Chassis (kg)	Ixx	Iyy	Izz	Wheel (kg)	Ixx	Iyy	Izz
BMW 325	1156	382.4	1977	2050.5	32,1	1.32	1.11	1.11
Ford Mondeo	1297	488.2	2245.6	2322.8	32.1	1.32	1.11	1.11
Renault Clio	877	285.7	1146.5	1189.1	24.3	0.91	0.65	0.65
Skoda Octavia	1165	444.1	1880.3	1950	32.4	1.63	1.225	1.225

Table 6-2: Vehicle model mass and inertia characteristics.

Vehicle	% mass distribution	K_n (N/m)	K_s front (N/m)	K_s rear (N/m)
BMW 325	51/49	227666	13715	13146
Ford Mondeo	60/40	190170	15181	9388
Renault Clio	62/38	138759	11639	6909
Skoda Octavia	62/38	190170	14533	8152

Table 6-3: Joint stiffness characteristics of the vehicle models frame.

Regarding stiffness, as real world scenarios are analysed, real EuroNCAP tests have been used to derive the stiffness map in each vehicle as summarized in the next table.

	Lower legform tests	Upper legform tests	Child Headform tests	Adult headform tests
BMW 325	R1, R3	R4, R5, R6	R7, R8, R9, R10, R11, R12	R13, R15, R16, R17, R18
Ford Mondeo	R1, R2	R4, R5, R6	R7, R8, R9, R11, R12	R15, R17, R18
Renault Clio	R1, R3	R4, R5	R7, R8, R9, R10, R11, R12	R13, R15, R17
Skoda Octavia	R1, R2, R3	--	R7, R8, R9, R10, R11, R12	R13, R14, R15, R16, R17, R18

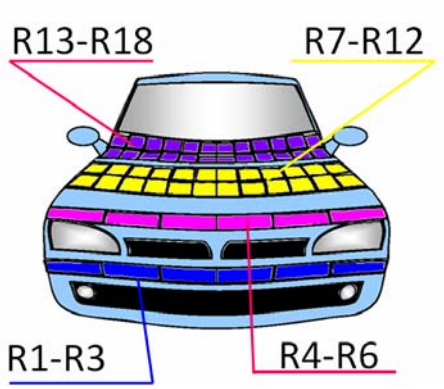

R13-R18: Adult headform test areas

R7-R12: Child headform test areas

R4-R6: Upper legform test areas

R1-R3: Lower legform test areas

Table 6-4: Summary of EuroNCAP tests used for mapping vehicle stiffness.

Force-deflection curves have been derived from these tests following the procedure described in Section I and its allocation of the different vehicle structures has done according to the results of these tested areas.

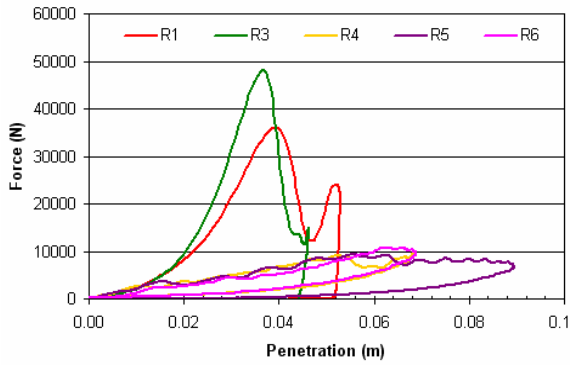

BMW 325

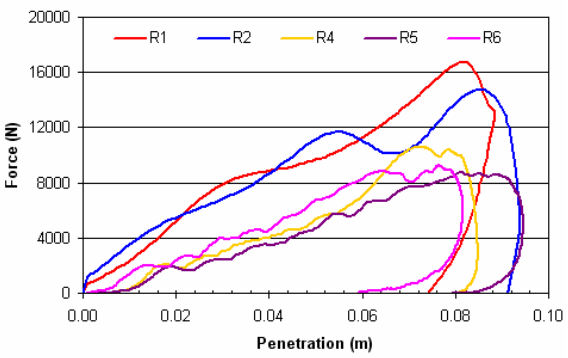

Ford Mondeo

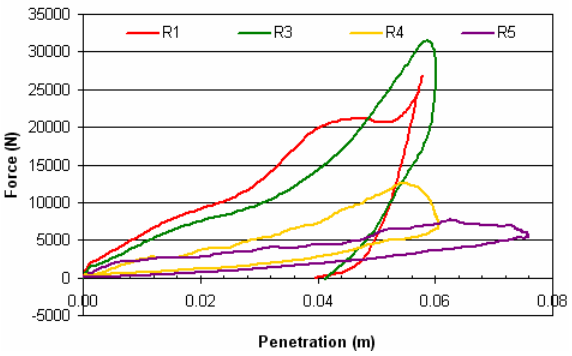

Renault Clio

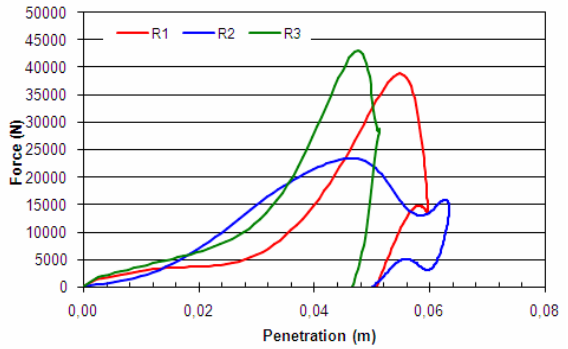

Skoda Octavia

Figure 6-1: Bumper and BLE stiffness derived from EuroNCAP legform tests

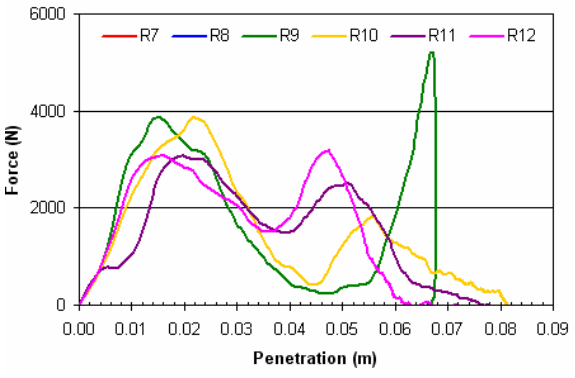

BMW 325

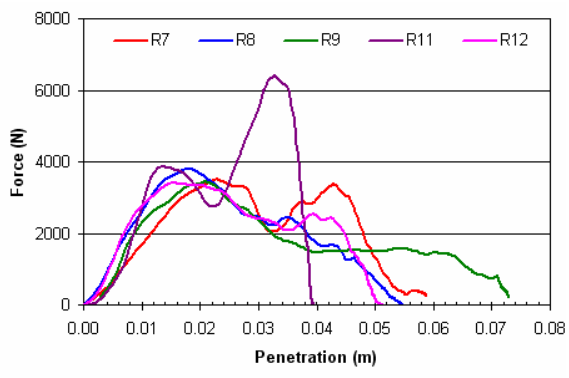

Ford Mondeo

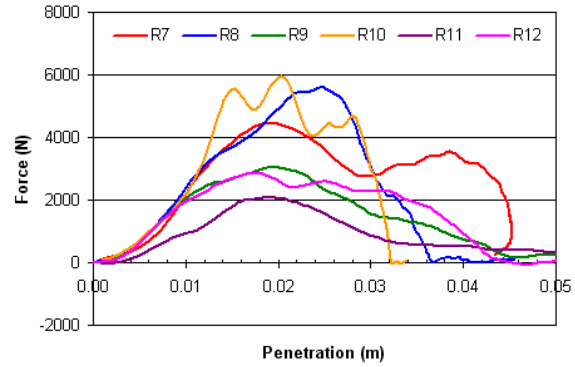

Renault Clio

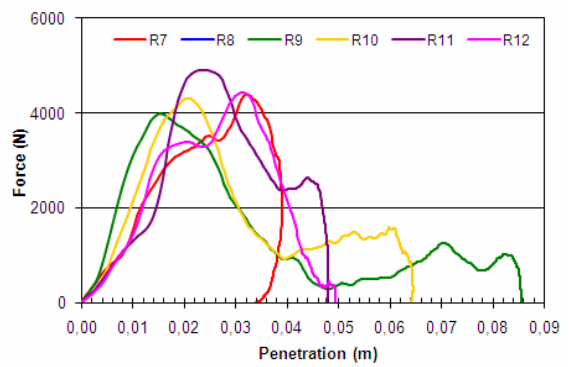

Skoda Octavia

Figure 6-2: Bonnet stiffness derived from EuroNCAP child headform tests.

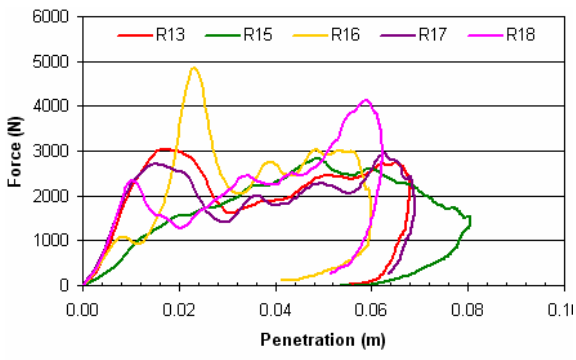

BMW 325

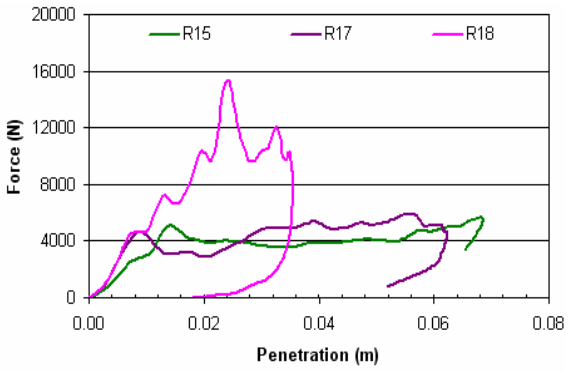

Ford Mondeo

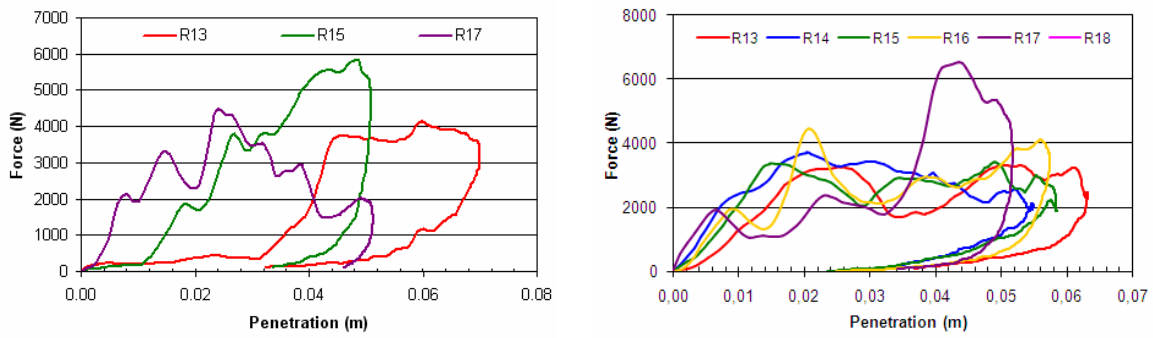

Renault Clio

Skoda Octavia

Figure 6-3: Summary of vehicle stiffness obtained from EuroNCAP adult headform tests.

A brief description of the scenarios is given in the next heading, along with the outputs of each reconstruction case that assess their validity.

6.1 Summary of the accident reconstructions.

6.1.1 Pedestrian Case IP002.

A 55 years old male pedestrian (1,75 m, 75 kg) was crossing the street in a crosswalk regulated by traffic lights, from the right to the left when a BMW 325 1998 impacted him.

There were no parked vehicles in the cross, although it was wet and it was late evening. The car brake without avoiding the impact with the pedestrian, in the right outer third of the car and in the windscreen. The impact speed was estimated in 28 km/h, and the impact on the windscreen was measured on the scene (WAD 183cm, R34 cm).

The reconstruction model in MADYMO have been developed using the geometry of the MADYMO 50% pedestrian male model, (since the overall dimension of the pedestrian was very similar to the one in this model) scaled in age to 55 years old, and a vehicle model representing a BMW 325 from 1998.

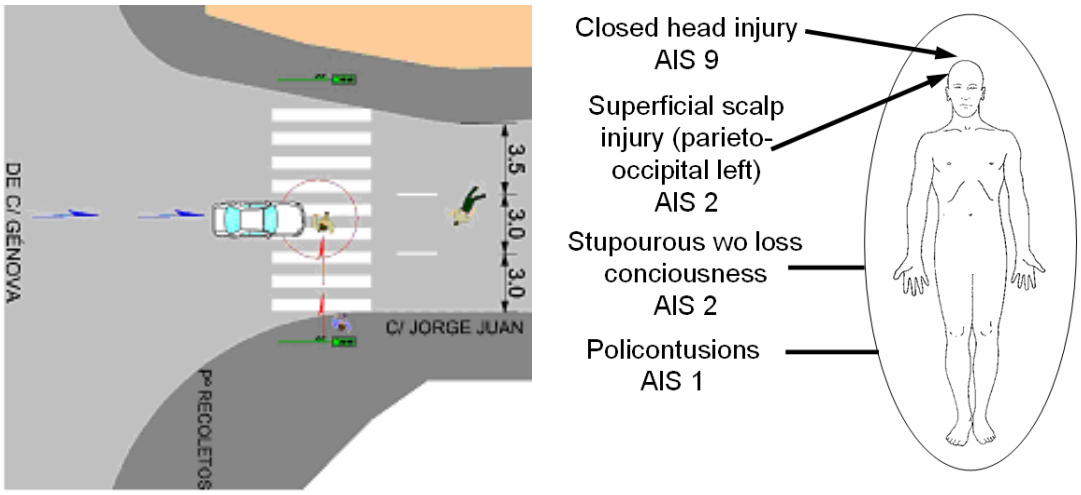

Figure 6-4: Case IP002 accident information (ABIDA, 2004).

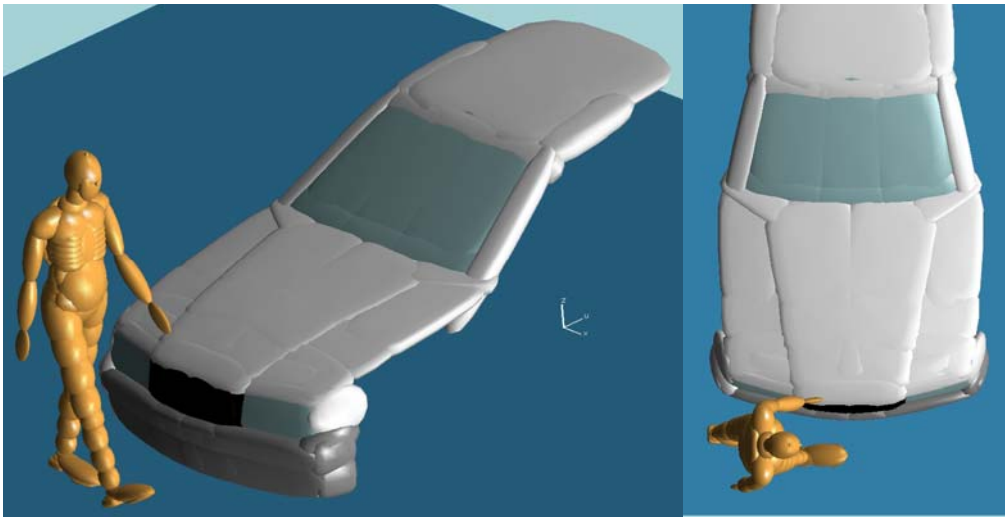

Figure 6-5: MADYMO accident reconstruction model IP002 (pedestrian + vehicle).

The best match to the simulation with the accident evidence is achieved with the pedestrian in walking position at speed of 1.1 m/s.

The Figure 6-6 shows the kinematics of the accident.

It can be seen that the car impacts the pedestrian with the bumper area below the right light lamp. It impacts first on the leg (time 25 ms) and then in both legs (time 40 ms).

This impact made the pedestrian to bend over the bonnet, contacting the left part of the pelvis and the left upper extremity on the bonnet (time 105-135) to lead the head impact on the windscreen lower part (time 205 ms-420 ms). This impact point matches the target impact point measured in the real accident scene and the severity, through HIC, seems to be appropriate to the injuries sustained by the pedestrian.

From then, the pedestrian is thrown forward due to the car braking and slides over the bonnet until it falls from the front of the vehicle.

The final position of the pedestrian in the accident was recorded. In this case, the final position obtained in the simulation from the pedestrian (8.1 m) and the one recorded (7.5 m) is rather similar, which supports the feasibility of this simulation.

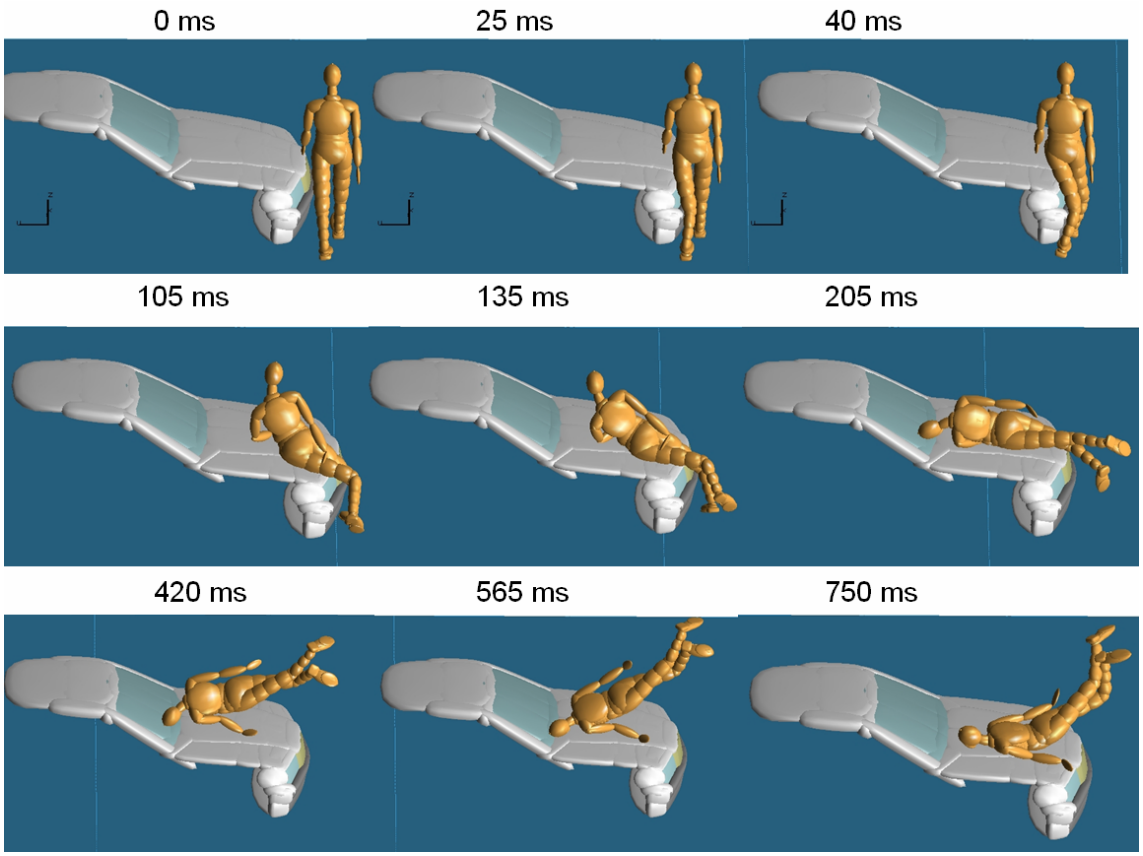

Figure 6-6: Sequence of special time points at accident case IP002.

Figure 6-7 shows the comparison between the real case and the simulation.

The red marked points are documented in the real case as impact points in the car, and the yellow marked ones have been obtained in the simulation.

It can be seen that the impact in the windscreen is reproduced accurately in the model. Moreover, the simulation indicates that impact in the bumper occurred in the legs and some others occur in the bonnet with the pelvis and the arm; however, there was neither permanent deflection nor evidence in the accident scene.

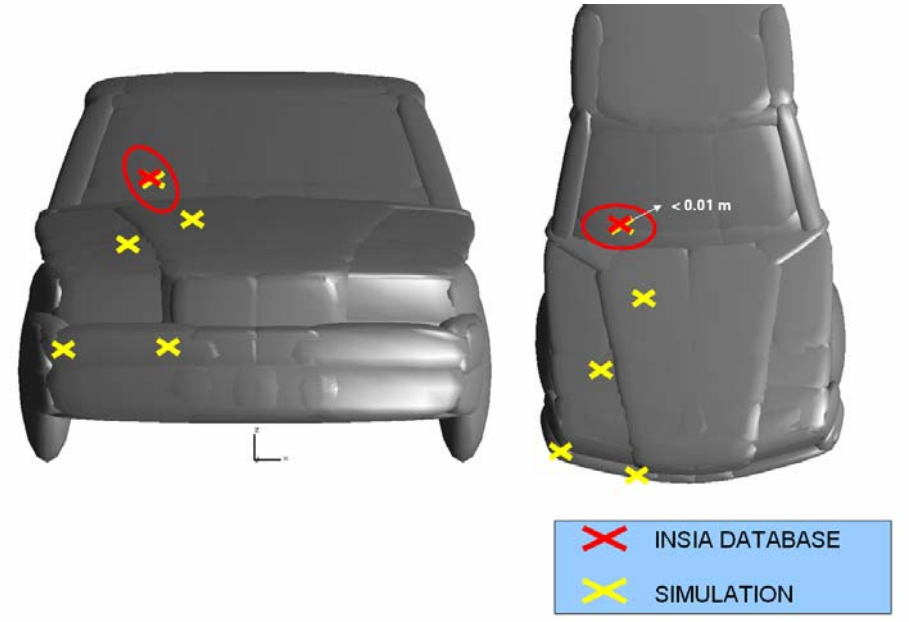

Figure 6-7: Impact positions from the real case and the simulation IP002.

The injuries sustained by the pedestrian are matched to the kinematics and summarized in the next table along with the observations from the outputs from MADYMO.

Injury	Timing	Kinematics	Observations
Closed head injury, superficial scalp and stuporous without loss consciousness (MAIS 2)	185 ms	The head impacts the windscreen	The head maximum acceleration is 81.3 g at time 205 ms with a HIC of 1105.6 (62% risk of MAIS 3, Prasad-Mertz 1997)

Table 6-5: Injury information on the simulation.

6.1.2 Pedestrian Case IP003.

A 19 years old female pedestrian (1,60m and 59 kg) was crossing quickly a dual carriageway with 2 lanes in a pedestrian crosswalk regulated with traffic lights in green for cars. The vehicle involved, a Ford Mondeo 1997 braked but hit the pedestrian with its outer right third. The estimated impact speed of the car in this point was 27 km/h.

The car showed the evidence of the impact in the bonnet, above the right lamp, with a small dent (WAD=94 cm, R53 cm) and with sliding marks along the bonnet (approx. length 80 cm, with the starting point on the dent and the ending point near the bonnet rear right corner).

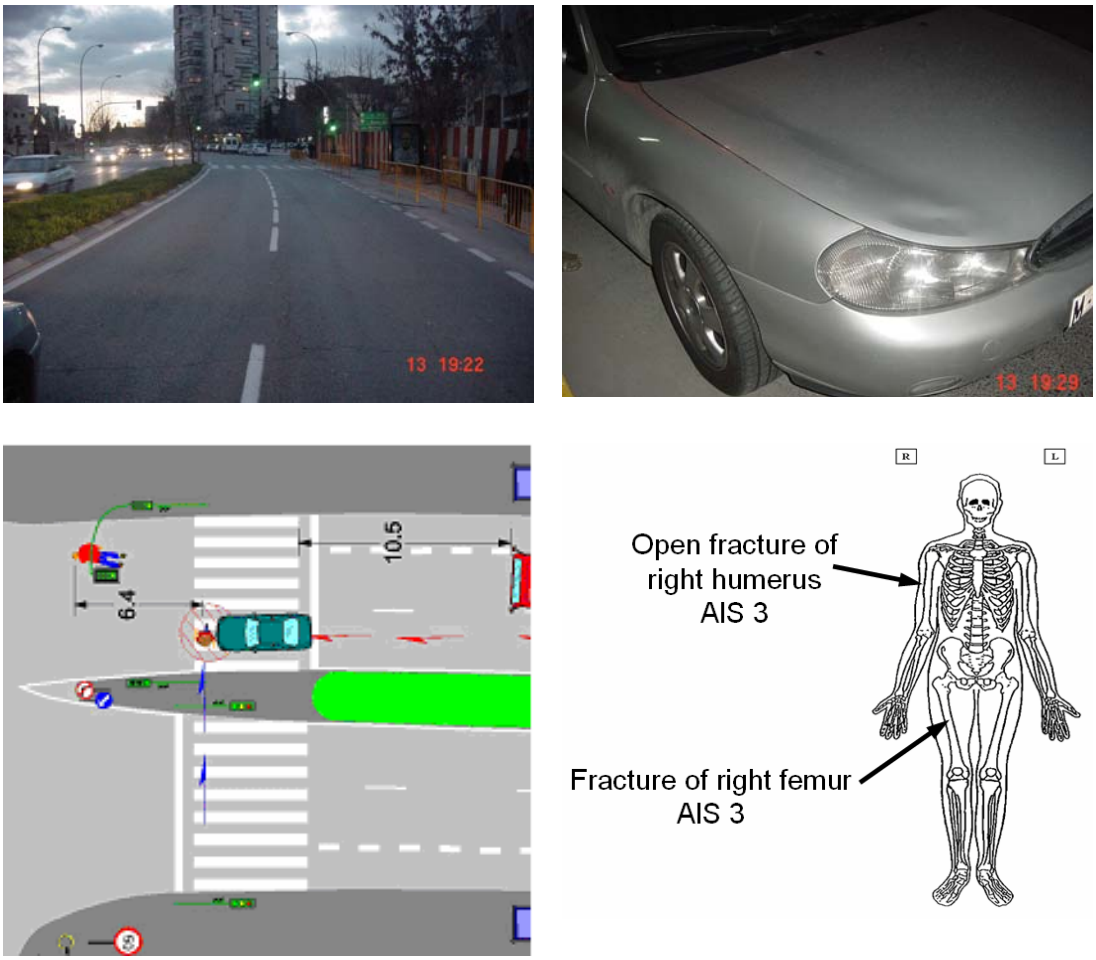

Figure 6-8: Case IP003 accident information (ABIDA, 2004).

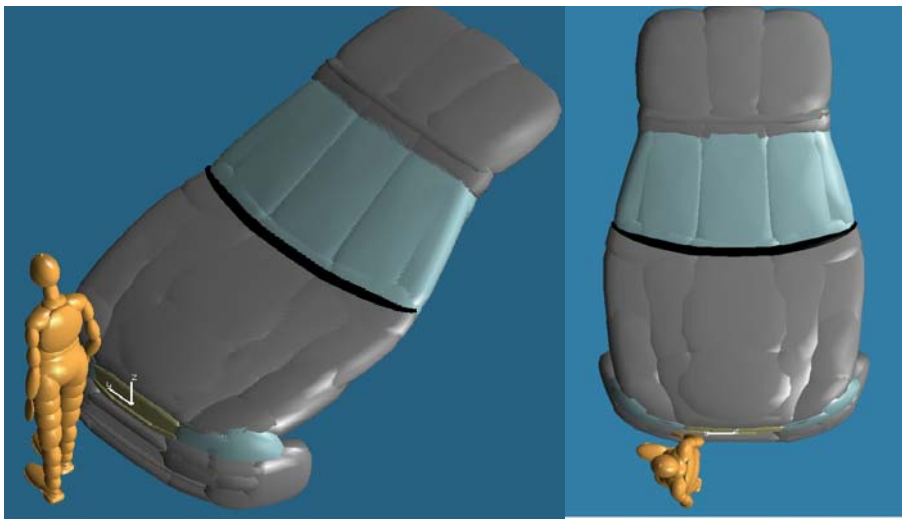

Figure 6-9: MADYMO accident reconstruction model (pedestrian+vehicle).

The reconstruction model in MADYMO have been developed using the MADYMO 5% pedestrian female model as basis for the geometry, scaled in age to make it younger, and a vehicle model representing a Ford Mondeo from 1997.

The best results for this reconstruction have been obtained with the pedestrian speed at 1.5 m/s and the right foot in front. With this initial posture and speed, the pedestrian hits the impact point from the vehicle and reproduce the marks recorded.

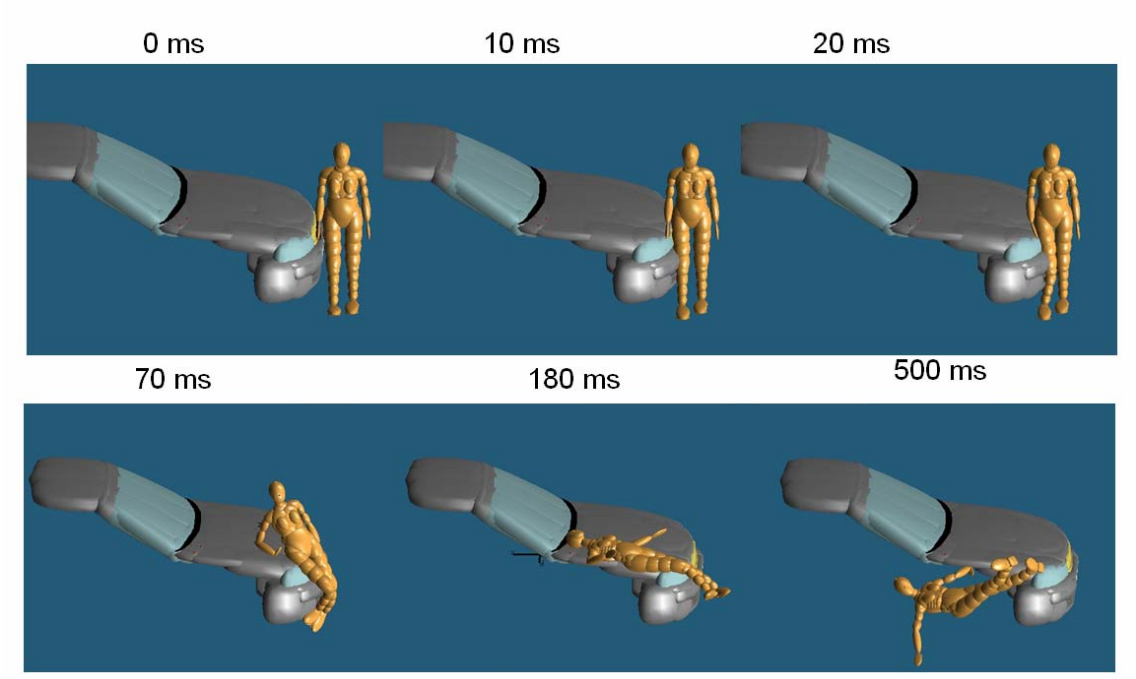

Figure 6-10: Sequence of special time points at accident case IP003.

The accident kinematics is shown in Figure 6-10 representing the primary impact with the vehicle.

At 10-20ms the pedestrian upper leg is struck by the bumper. At 70-90 ms, the pedestrian upper leg and pelvis have been impacted with the vehicle light lamps and the pedestrian elbow is hitting in the bonnet.

At 180 ms, the sliding phase of the pedestrian onto the bonnet, in which the left arm also impact in the bonnet, is finishing with a slight impact of the head in the top of the bonnet. Finally, at 500ms the pedestrian is ready to land in the ground.

The simulation has been evaluated with the available information on the evidence of the accident. The figure shows the comparison between the real case and the simulation. The red marked points are documented in the real case as impact points in the car, and the yellow marked ones have been obtained in the simulation.

It can be seen that the upper leg-pelvis impact point location in the car is matched and the length of the sliding marks on the car is a bit higher (86 cm in simulation vs. 82 in the real

case). These differences may be due to the real deformation occurring around the impact point together with the actual surface curvature of the bonnet which eases the body to be thrown out of it. This effect may also influence the fact that the simulation leads to a head impact in the bonnet when in the real case, there is not even an AIS 1 injury reported in the head.

Moreover, the final position of the pedestrian in the accident was recorded. In this case, the final position obtained in the simulation from the pedestrian (5.67 m) and the one recorded (6.4 m) is within 1m, which supports the feasibility of this simulation.

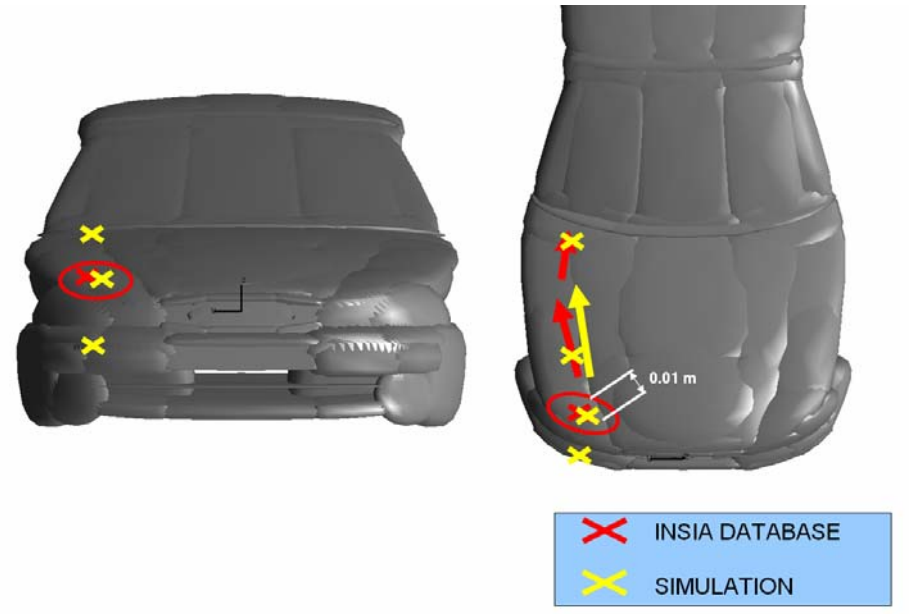

Figure 6-11: Impact positions from the real case and the simulation IP003.

The injuries sustained by the pedestrian are supported by the kinematics and summarized in the next table along with the observations from the outputs from MADYMO.

It seems that the simulation does predict femur fracture but the humerus fracture reported in the real case can not be attributed to the car direct impact.

Taken into account the landing of the pedestrian on the ground, it is feasible that humerus fracture may occur in this secondary impact.

Injury	Timing	Kinematics	Observations
Fracture of right femur AIS 3	18 ms	Leg impact on the light lamp and bumper.	The maximum shear force limit was exceeded and the femur fracture joint is unlocked at 18 ms indicating femur fracture.

Open fracture of humerus AIS 3	80-90 ms	Impact with the elbow on the bonnet	The values of axial 1504 N, shear 404 N and torque 41.4 Nm compared to the limits 3600 N, 1700 N and 85 Nm respectively (Yang 2002) suggest no fracture
No head injury	180 ms	Impact of the head in the upper part of the bonnet	The HIC value of this impact is 132. (10% risk of MAIS 1, Prasad-Mertz 1997)

Table 6-6: Injury information on the simulation.

6.1.3 Pedestrian Case IP006.

A 21 years old male (1.69 m, 75 kg) pedestrian was crossing running a pedestrian cross when a Renault Clio 1996 hit him. The driver said that the sun dazzled her and he did not react to avoid the accident.

The pedestrian was hit with the right outer third of the car, impacting the windscreen (WAD 209cm, R50cm).

The estimated impact speed of the car was 31 km/h.

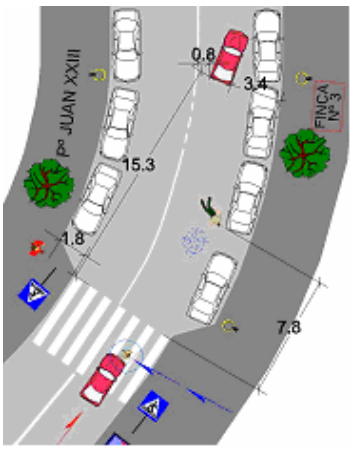

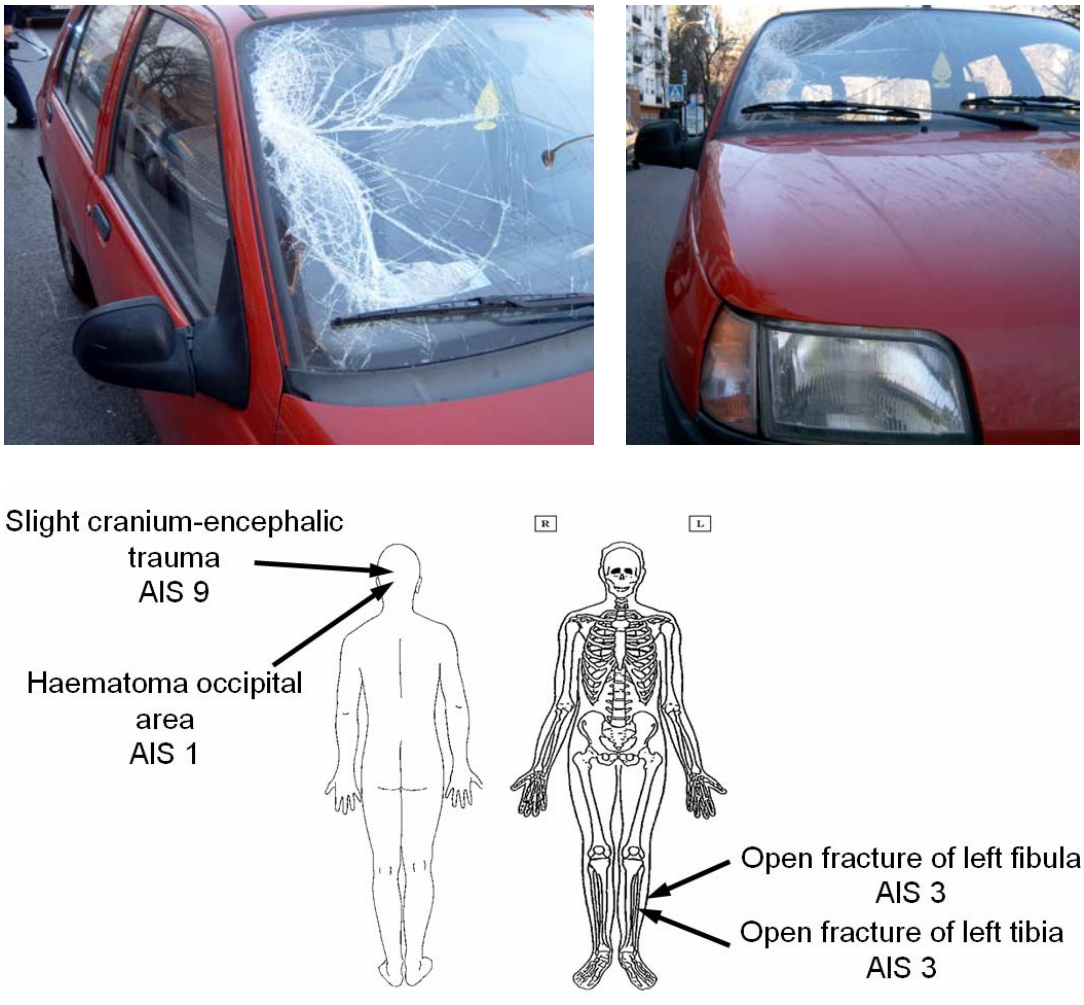

Figure 6-12: Case IP006 accident information (ABIDA, 2004).

Figure 6-13: MADYMO accident reconstruction model IP006 (pedestrian+vehicle).

Taken into account the real pedestrian figures, the MADYMO 50% pedestrian male model has been used in the reconstruction, aged accordingly.

The best reconstruction results have been obtained with the pedestrian in running position and at speed of 1.5 m/s. The Figure 6-14 shows the kinematics of the accident reconstruction.

The impact of the corner of the bumper to the left leg of the pedestrian (time 10 ms to 60 ms) is believed to cause the leg injuries to the pedestrian. As this impact hardly affect the right leg, the pedestrian is rotated around the vertical axis to land with the occipital part of the head into the windscreen (time 160ms to 250 ms). This impact to the windscreen may cause the scalp haematoma of the head.

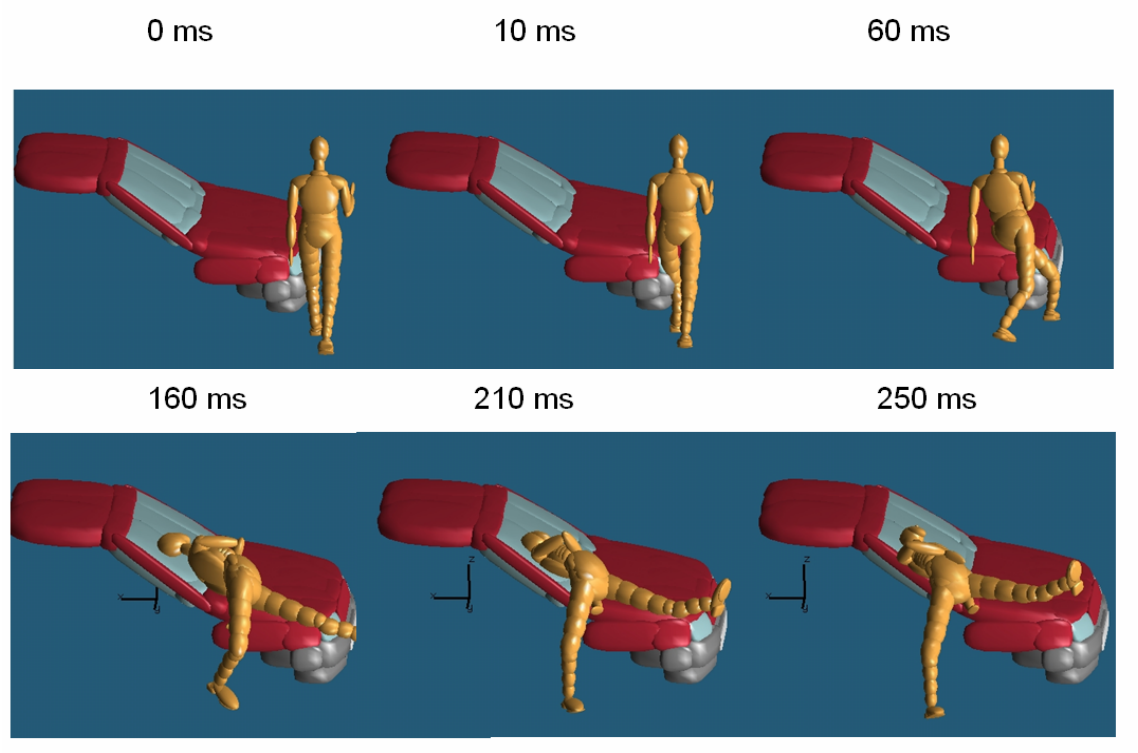

Figure 6-14: Sequence of special time points at accident case IP006.

Figure 6-15 shows the comparison between the real case and the simulation impact points. The red marked points are documented in the real case as impact points in the car, and the yellow marked ones have been obtained in the simulation.

It can be seen that the impact point in the windscreen is reached within 3 cm. Moreover, the simulation highlights the impact of the left leg of the pedestrian in the bumper and light lamp corner of the vehicle although there was no deformation evidence in the actual accident scene.

The throw distance was estimated to be around 7 m and the simulation results in 6.7 m.

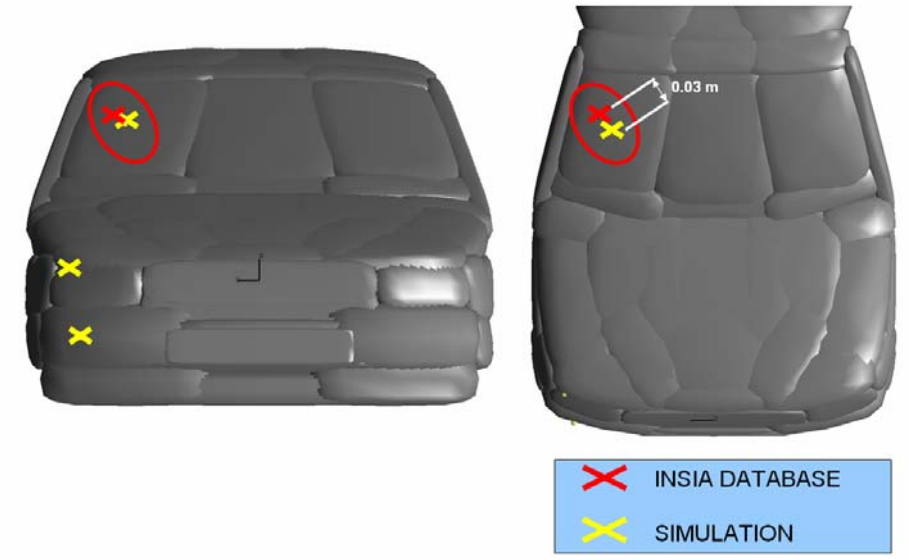

Figure 6-15: Impact positions from the real case and the simulation IP006.

The injuries sustained by the pedestrian are matched to the kinematics and summarized in the next table along with the observations from the outputs from MADYMO. The output values are given in order to roughly indicate the severity of the impact.

Injury	Timing	Kinematics	Observations
Open fracture of left tibia and fibula	7-10 ms	The left leg, which goes in front, is impacted by the corner of the bumper of the car	The maximum shear force in the lower leg is exceeded and the fracture joint is unlocked at 7 ms. These values suggest that the lower leg is fractured
Slight closed head injury and occipital haematoma in scalp	150-160 ms	The head is impacting the windscreen with the occipital part first	The head acceleration reaches a maximum of 119 g at that point with a HIC value of 722.6. (25% risk of MAIS 3, Prasad-Mertz 1997))

Table 6-7: Injury information on the simulation.

6.1.4 Pedestrian case IP012.

The accident happened in a street with two directions, and one lane for each of them. The scene is close to an X junction, regulated by traffic lights and a pedestrian crossing on the pavement.

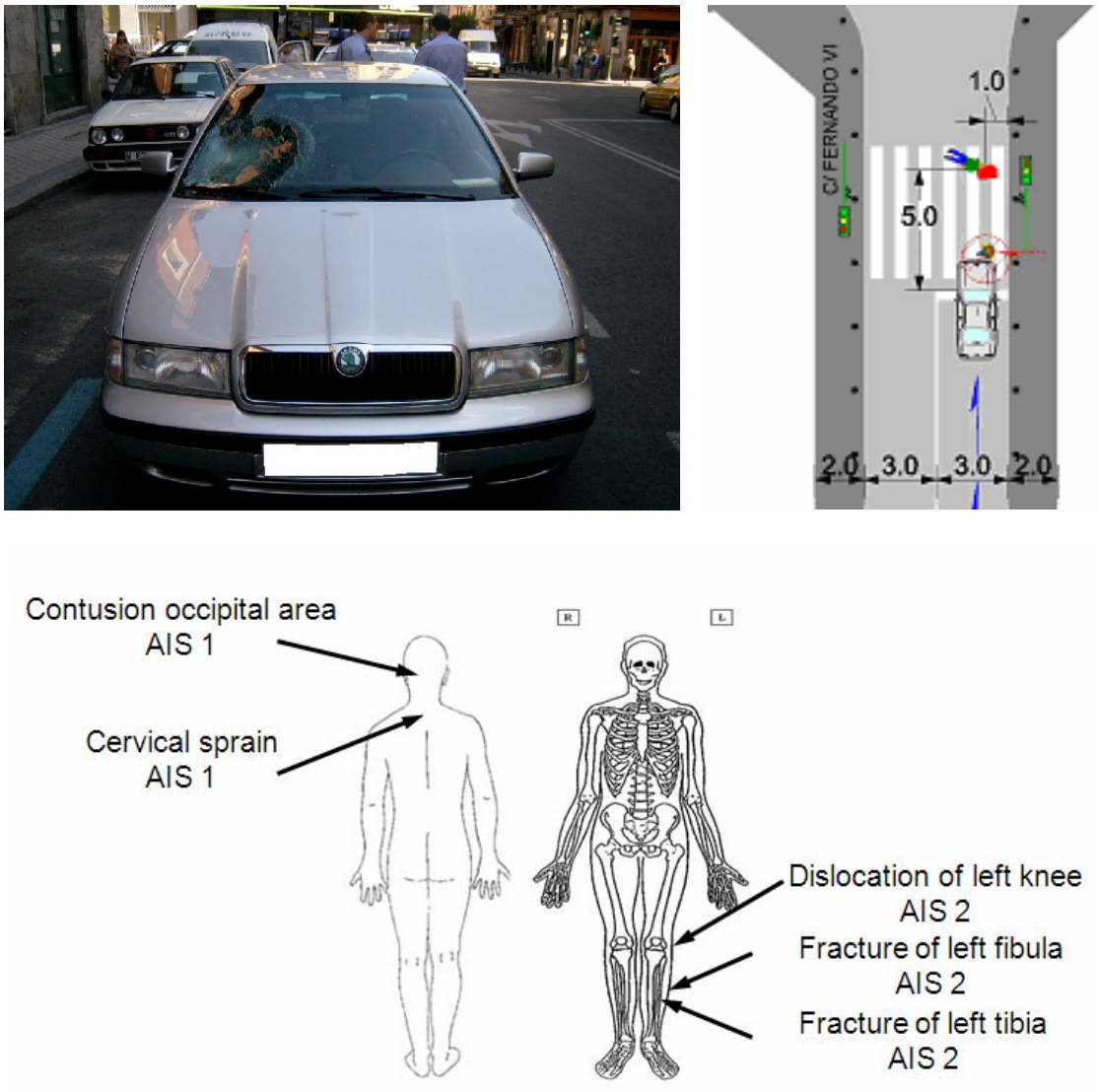

Figure 6-16: Case IP012 accident information (ABIDA, 2004).

A 65 years old female (1.58m, 52 kg) was trying to cross the street on the pedestrian crossing and was hit by the car. It is unclear in whose favour the traffic lights were at the moment of the accident. The car braked but could not avoid the pedestrian impact, being the car speed at the moment of impact estimated to be 28 km/h.

The pedestrian suffered several leg injuries (tibia and fibula fracture as well as knee dislocation) and a contusion in the occipital area of the head as well as a cervical sprain.

The car showed the evidence of the impact in the windscreen lower corner, (WAD=213cm, R51 cm) but no permanent deformation was registered in either the bumper or the bonnet of the vehicle.

Taking into account the real dimension of the pedestrian, the MADYMO5% have been used as the basis to scale the model and afterwards, being scaled to 65 years old.

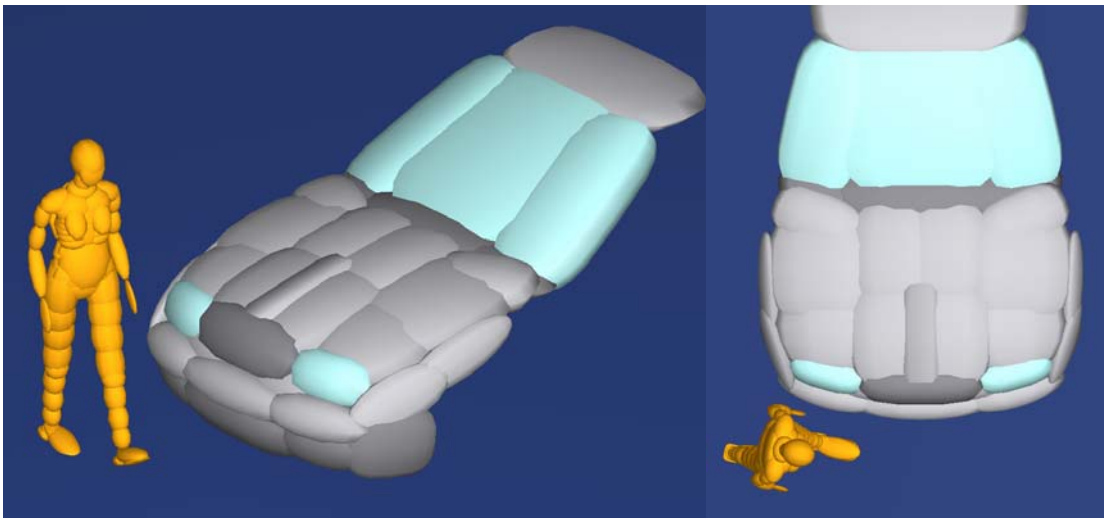

Figure 6-17: MADYMO accident reconstruction model IP012 (pedestrian+vehicle).

The most plausible reconstruction of this accident is presented in the next figure, with the pedestrian in walking position (0,6 m/s) and the left foot in front. With this initial posture and vehicle speed, the pedestrian reproduce the marks recorded in the scene and the injuries found are of similar relevance.

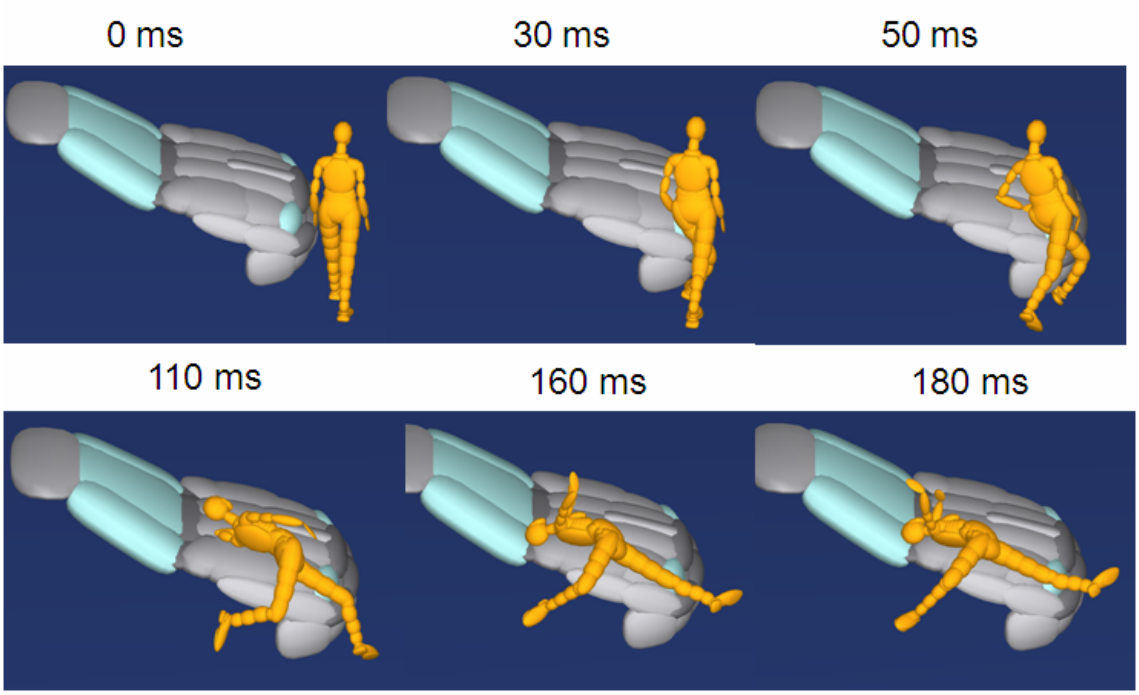

Figure 6-18: Sequence of special time points at accident case IP012.

At 30 ms the pedestrian left lower leg is struck by the bumper. It can be seen that is the only part being impacted and at 50 ms, the tibia fracture joint has reached its threshold suggesting a tibia fracture and starting a pedestrian rotation away from the vehicle.

Although the vehicle on the scene only showed permanent damages on the windscreen, it is obvious that the pedestrian also impacted in the bumper and the simulation highlights that this occurred with the right corner of the bumper.

Since the impact occurs in the outer third of the vehicle and on the leg in front, the pedestrian is forced to rotate backwards, impacting first with her left arm in the bonnet at 110 ms, and afterwards with the occipital part of the head on the lower corner of the windscreen at 160-180 ms.

This impact on the windscreen leaves a wide deformation on the real life vehicle as it occurs far enough of the A pillar, and similarly it is shown in the simulation. The impact point recorded on the scene and the one found in the simulation are separated 3 cm, which gives a good feedback on the quality of the simulation.

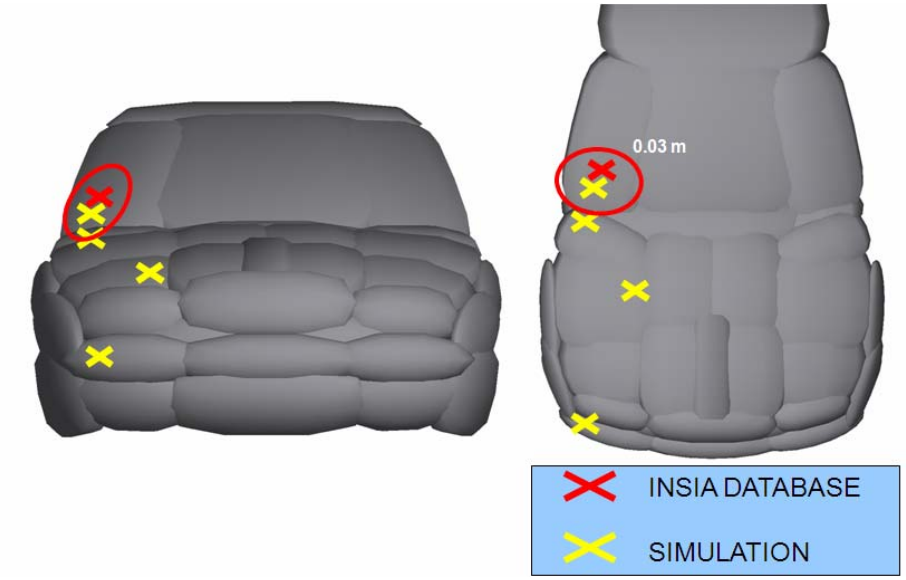

Figure 6-19: Impact positions from the real case and the simulation IP012.

Injury	Timing	Kinematics	Observations
Fracture of left tibia and fibula	30-50 ms	The left leg, which goes in front, is impacted by the corner of the bumper of the car	The maximum shear force in the lower leg is exceeded and the fracture joint is unlocked at 50 ms indicating that the lower leg is fractured

Dislocation of knee	30-50 ms	The knee is forced to bend in the bumper impact	No injury output available on the knee
Cervical sprain	150-160 ms	The head is impacting the windscreen with the occipital part	No injury output available
Occipital contusion	150-160 ms	The head is impacting the windscreen with the occipital part first	The head acceleration reach a maximum of 78 g at that point with a HIC value of 191 ((22% risk of MAIS 1, Prasad-Mertz 1997)

Table 6-8: Injury information on the simulation.

The injuries sustained by the pedestrian are matched to the kinematics and summarized in the table along with the observations from the outputs from MADYMO.

The output values are given in order to roughly indicate the severity of the impact, and just limited to the primary impact of the pedestrian with the vehicle and not any later landing on the ground.

6.2 Parametric analysis.

A simple parametric study has been performed by just including or not age dependent fracture limits on the pedestrian legs in each simulation in order to quantify its real effect in each case.

In these terms, the four scenarios have been analysed with and without adapted-to-age fracture limits in the legs, to assess its relevance. Once plausible kinematics was found for each scenario, aged-fracture limits were set back to its original values and the model was run again.

The outputs of these two cases in each reconstruction have been compared in terms in both leg fracture and posterior head kinematics parameters.

As it is shown in the table, the inclusion or not of adequate fracture limits in the pedestrian legs can lead to significant differences in the head later kinematics, impact locations and timing, although this relevance has not been found to be the same in the four scenarios.

In this respect, it can be seen that there are three different behaviours:

- In cases where there is not leg fracture found either with or without aged fracture limits, the scaling on age has no effect.

- In cases where leg fracture is found with and without aged fracture limits, the scaling on age has only a latter kinematic effect caused by the delay of the fracture in the legs.
- In cases where leg fracture is found only with aged fracture limits, the scaling on age has a great significance not only in the latter kinematics but also in the injury predictions of the model.

Case	Fracture limits	Leg fracture?	Head contact resultant velocity	Head contact timing
IP002	Aged 55	Neither occurred not predicted	8.39	203 ms
	Not aged	Neither occurred not predicted	8.39	203 ms
IP003	Aged 21	Occurred and predicted	6.57	175 ms
	Not aged	Occurred and predicted	6.23	173 ms
IP006	Aged 19	Occurred and predicted	6.15	144 ms
	Not aged	Occurred and predicted	6.12	140 ms
IP012	Aged 65	Occurred and predicted	4.32	180 ms
	Not aged	Occurred but not predicted	3.97	195 ms

Table 6-9: Differences in kinematics due to aged fracture limits.

As bone fracture limits do decrease with age, scaling in age is therefore more relevant when the accident scenarios involve elder pedestrian, while is less relevant in scenarios involving younger adults, with higher bone resistance that the typical adult values considered in the standard MADYMO human models.

This can be seen in the figure, where the IP012 case behaviour is plotted, highlighting not only the delay of the head contact, but also the change in the head acceleration values. Although the first effect is directly attributed to the lack of aged fracture limits, the second one is the consequence of a reduction in the head impact velocity. However, as the acceleration reached is also dependent on the stiffness of the structure the head is forced to impact that it is not the same in both cases, it can result in a higher or a lower acceleration peak although the head impact velocity has been decreased.

In any case, there are two overlapped effects that could be looked separately. On one hand, the influence in the latter head kinematics, which is especially critical in

reconstruction environments and, on the other hand, the prediction itself of the leg injuries, which has a wide relevance from a testing perspective point of view.

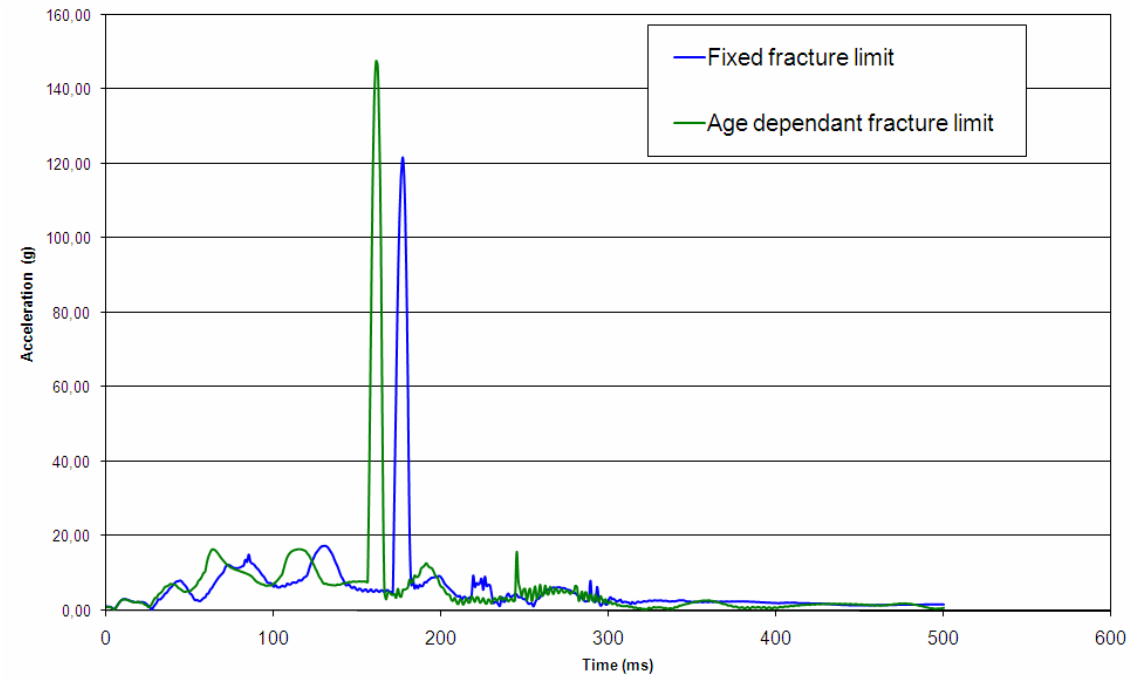

Figure 6-20: Effect of aged fracture limits on the legs to the later head kinematics. (IP012)

Regarding the first effect, as the pedestrian test procedures approach separately head and legs, this effect cannot be taken into account directly unless a more direct inclusion of the simulations would be considered in the future, however, this relationship highlights the importance to consider the existence of this coupling when proposing any improvements in the impact conditions of any of them.

Regarding the second effect, the scaling tools developed have shown that bone tolerance decreases with age (taken 65 years old as reference) around 20%-30%.To properly take this effect into account in the reconstructions, it has been demonstrated that fracture limits should be aged accordingly especially when dealing with elder pedestrian.

From a legislation perspective, if elder pedestrian are within the target population to cover, a similar downscale effect to the one herein reported should be undertaken for the testing devices or the thresholds values of the tests.

Considering how the current threshold has been set for the legform procedure, starting from 150g in the tibia acceleration and 5 kN and 300 Nm in the femur from EEVC WG17 proposal, being afterwards relaxed to in Directive 2003/102 to 200g in the tibia to be finally set in 170g in Regulation 2009/78 with some areas even reaching to 250g and keeping the femur assessment just with monitoring purpose, it seems rather unfeasible any measure aiming to reduce the thresholds directly a 20-30%.

To have a ground basis for a feasible proposal for such downscale, a new leg injury risk tolerance curve for elder pedestrians should be developed and widely accepted.

Due to the magnitude of this development, it is not undertaken within this thesis but instead, it can be a very interesting future research topic to continue working on pedestrian safety within this direction.

SECTION II: CONCLUSIONS

Section II has deepen into the fact that elder pedestrian have been shown to be a critical population in pedestrian accident trying to quantify the relevance of such age effect but also to assess the feasibility of including it as a variable in the pedestrian protection test procedures.

The nature of this analysis, including age as a parameter, has stepped forward the current state of the art in accident reconstructions and has requested the development of advanced mathematical models to accurately reproduce these real world scenarios, namely two, a scalable pedestrian in size and age to cover all ranges of adult population involved in pedestrian accidents and a number of vehicle mathematical models with detailed geometry and stiffness.

This thesis has approached these needs developing two different tools to construct these models:

- An aging tool, AgedMAT, that allows quantifying the age effect in the different human body materials and has set the basis to include age as a factor in the widely validated MADYMO pedestrian multibody model.
- A cost-effective methodology to construct ad hoc vehicle mathematical models.

Although these tools have been developed as a mean to reach a more ambitious target, their potential on their own for many other applications has promoted them to be one of the main tangible results of this thesis.

The first one has capitalized the knowledge already available in the MADYMO multibody pedestrian model to add its missing capability of being scaled in age. Taken into account the formulation of the model, this age scaling is focused on the legs, updating with age the fracture joints along the upper and lower leg. However, in order to give a wider coverage, an extensive literature review has analysed an broad range of human body tissues and the dependence with age of many of their material parameters, not only focused on these long bones.

Although many tissues have been analysed, only in a few of them, basically lower limbs bones (as needed) and some other ligaments and tendons, statistically relevant dependencies have been obtained. These dependencies have been checked not only at global level but also at coefficient level to ensure its validity and these have been integrated in the AgedMAT tool. A user friendly interface has been constructed for the tool to allow output a complete set of parameters at material level at given ages. As these outputs are given at material level, they could be transferred to any human model, either FE or multibody with a proper transformation taken into account the material models used. In the current case of the MADYMO model, an extra function considering geometry has been needed to transform the dependency at material level to the one at bone fracture level. This transformation is presented annexed to the AgedMAT and not integrated to leave room for a possible use of AgedMAT outputs directly with FE human models.

In the second case, the methodology in its essence is not new, but this thesis has made it to be cost-effective, as it has integrated the previously developed stiffness mapping tool with a parametric definition of the multibody frame of the vehicles to allow a quick integration with the vehicle detailed geometry.

This three-stepped methodology shows the following advantages to the user:

- The multibody frame, constructed parametrically, allows a simple adaptation to all vehicles, just by modifying a finite set of geometrical and inertial parameters.
- The stiffness mapping tool can define in each vehicle up to 60 areas with different stiffness just by knowing its EuroNCAP pedestrian test results or, depending of the objective of the model, using standard vehicle segment ratings.
- The geometry of the vehicle, obtained from whatever source and defined with the details needed in each case, is directly and easily fix to the multibody frame. In reconstruction cases, as the ones presented in this Section, the geometry is represented with multibody technologies as it is interacting with a multibody pedestrian model, but in Section III with the models interacting with a FE model, the geometry can be represented with facet surfaces.

With these two tools, four pedestrian accidents real world cases have been simulated in this Section II. Considering the sets of data available to reconstruct the accidents (vehicle

contact point, pedestrian injuries and throw distance), very plausible pedestrian kinematics have been obtained with the simulations, matching accurately the impact points recorded on the scene and predicting pedestrian injuries within the scope of the MADYMO human models.

Three objectives have been followed with these simulations:

- Analyse age as a factor influencing pedestrian kinematics.
    - The simulations have demonstrated that the scaling in size of the MADYMO model is necessary when reconstructing pedestrian accidents, but also that the scaling in age is vital not only to predict better leg injuries but also and mainly to lead to more realistic kinematics of the pedestrian, therefore including the age as another important parameter influencing the outputs of the simulations.
    - The parametric study developed highlights that as bone fracture limits do decrease with age, scaling in age is more relevant when the accident scenarios involve elder pedestrian, while is less relevant in scenarios involving younger adults, with higher bone resistance that the typical adult values considered in the standard MADYMO human models.
    - The most feasible alternative to include this age effect in the current test procedures would necessary imply to reduce the injury threshold proposed in a 20-30% to account for the bone resistance reduction of elder pedestrian, but this would need the development of a widely accepted leg injury risk curve specifically for elder pedestrian and this has been kept without the scope of this thesis.
- Identify trends in the occurrence of leg injuries.
    - In most cases the leg will usually be in extended position, being impacted at the vehicle speed with the most upfront part of the vehicle, typically in the bumper area. The simulations highlighted that this impact point of the car not only depends on the car geometry but also on the pedestrian size and being above or below the knee level determines the potential type of injury generated, being the vehicle stiffness in this area responsible of the severity of such injuries, along with the inherent age-dependent stiffness of the legs.
    - However, due to the nature of the lower limbs, the knee couples the femur and the lower leg at some extend transferring load from one part to the other, being therefore a key player influencing the injury outcome in pedestrian scenarios.
    - Unfortunately MADYMO models do not implement a detailed

representation of the knee ligaments and neither an injury threshold to estimate knee injuries potential, therefore more detailed models would be needed to analyze this coupling in detailed.

- Highlight the significance of the non fatal head injuries.
    - In the case of head injuries, although not age scaling is intrinsically considered it has been shown that by introducing age effect on the legs it does have an influence in the head latter kinematics, which can be of relevance in three of the four reconstructions in which head injuries are reported.
    - The reported AIS for head injuries in those cases suggest not critical injuries and the MADYMO outputs, in terms of injury criteria, have also predicted this low severity. However, the measurements used to predict these injuries are not adequate enough for that purpose, not only because they are only based on linear accelerations, on the inherent edge of reliability for MADYMO multibody models, but also because of the simplicity of the MADYMO head model.
    - To consolidate these trends, a deeper analysis should be performed using more detailed models with more robust head injury assessment capabilities.

SECTION III: FE ANALYSES IMPROVING PEDESTRIAN SAFETY ASSESSMENT

III

As concluded in the previous section regarding real world scenarios, multibody (MB) models have shown its relevance to define the overall behaviour of the pedestrians in these scenarios but lack injury assessment detailed capabilities to derive conclusions on head and leg injuries. This chapter will overcome these limitations working with FE human models instead of MB models.

In the case of the head injuries, the MADYMO model limitation of simplicity is tackled using detailed FE human models of the head. With the objective to just give broad suggestions for the pedestrian test procedure in this thesis, two reduced collaborations with Louis Pasteur University (ULP) and TNO have been undertaken in the framework of the APROSYS project (FP6-TIP3-CT-2004-506503), that analyse in detail the head impact according to a wide set of injury criteria. These collaborations have been performed separately but reported together in the first half of this Section III (Chapter 7), along with a brief description of the main features of the two head FE human model used.

In the case of the leg injuries, considering that the four accident reconstructions have involved variable pedestrian height and age (demonstrated to be very relevant to analyse real world scenarios) and the MADYMO model lacked details in the knee ligaments, a different analysis is needed at this point and it is approached by using a pedestrian FE human body model (THUMS) and impact him with a representative set of vehicles from the European fleet and compare its outputs to those seen with the Directive legform impactor. This study has highlighted the need to consider in the legform test procedure the influence of the upper part of the body for correctly assessing leg injuries and has proposed some feasible improvements of the impactor in that direction.

The whole study, as well as a comprehensive description of the FE model used is done in the second half of this Section III (Chapter 8).

7 FE ANALYSES OF PEDESTRIAN HEAD INJURIES

Although the analysis of pedestrian head injuries in detail is not one of the main objectives of this thesis, a brief chapter is included due to the collaboration performed in this respect with both ULP (University Louis Pasteur-Strasbourg) and TNO (The Netherlands).

Although these two collaborations have been done separately, both have taken as starting point the results of the MB real world accident reconstruction presented in the previous section, and both have had similar ultimate objectives. The result of these two collaborations is summarized in Baumgartner (2007) and Mordaka (2007).

7.1 Description of the FE head human models.

7.1.1 Comparison of head FE models used.

The ULP FE head model was developed by the University Louis Pasteur, from Strasbourg (Willinger, 2003). The ULP FEM of the head is three dimensional with a continuous mesh. It contains 14660 elements containing brick and shell elements and it weights 4.8 kg. This FEM includes the main anatomical components of the head: the falx of the brain and the tentorium of the cerebellum, the brain/skull interface, the brain and the cerebellum, the skull, the face and the skin.

The model was refined by Baumgartner (2001) modelling the lateral ventricles by introducing into the FEM a fluid solid coupling behaviour with an arbitrary Eulerian Lagrangian formulation and the cerebral spinal fluid (CSF) flow through the subarachnoidal space. The subarachnoïd space between the brain and the skull was represented by one layer of elastic brick elements to simulate the cerebrospinal fluid

(CSF).The Young's modulus of the subarachnoid space for this model was determined by using modal analysis, based on the fact that a brain-skull decoupling occurs at the first natural frequency of the human head at around 100-150 Hz. A large deformation formulation was used in order to have realistic strain estimation in this layer of brick elements, being validated against in-vivo vibration analysis.

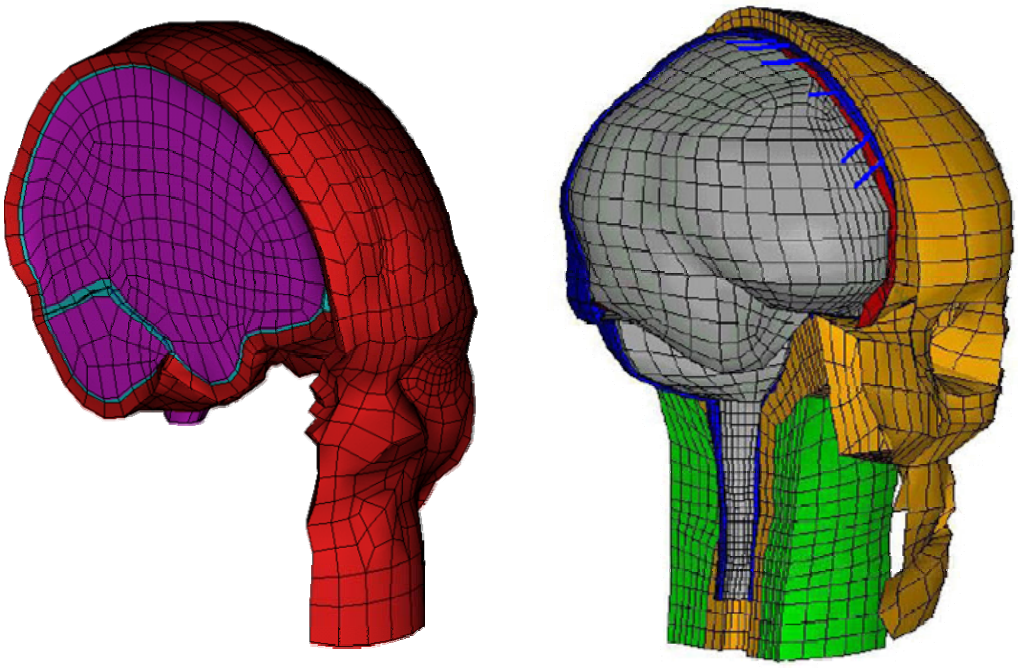

Figure 7-1: ULP (left) and KTH (right) head FE models

The ULP FEM is validated against experimental data from Nahum (1977) and Trosseille (1992) in terms of brain accelerations and pressures and against experimental data from Yogonandan (1994) regarding skull bones fractures.

The ULP FEM of the head is especially validated in case of long duration high dampened impacts that last more than 15 ms and that usually reveal an important rotational acceleration.

The KTH head FEM model was developed at the Royal Institute of Technology in Stockholm (Kleiven, 2002). It contains a total of 18400 nodes and it weights 4.2 kg.

The head model includes the scalp, the skull, the brain, the meninges, the cerebrospinal fluid (CSF) and eleven pairs of the largest para-sagittal bridging veins. A simplified neck, including an extension of the brain stem into the spinal cord, the dura and pia mater, and the vertebrae was also modelled. The CSF in this model was modelled with eight node brick elements as fluid elements.

To avoid large computational costs an average element thickness of about 1.0 mm was used for the model. For all the sliding interfaces a coefficient of friction of 0.2 was used. A

distributed parameter algorithm was adapted for the contact towards the brain tissue. This is a sliding contact algorithm that allows large relative motion and carries load in tension normal to the contact surface.

The CSF between the falx and the brain and between the tentorium and cerebrum/cerebellum was also included using the same type of fluid-structure contact algorithm. For these interfaces a constant CSF thickness of 1.5 mm was used for all models.

The KTH FEM has been validated against several relative motion experiments (Kleiven and Hardy 2002b), intra-cerebral acceleration experiments (Kleiven, 2006a), skull fracture experiments (Kleiven 2006b), and intra-cranial pressure experiments (Kleiven and von Holst, 2002). The post-mortem human subject (PMHS) experimental data used cover four impact directions (frontal, occipital, lateral and axial), short and long durational impacts (2-150 ms), high and low severity (sub-concussive to lethal), and both penetrating and non-penetrating injuries.

The main characteristics for both models, in terms of material model used and key mechanical values are summarized in the next table.

FEM part	Properties	Stockholm Model	ULP Model
Brain	Material model	Mooney-Rivlin (hyperelastic law)	Ogden's Model (hyperelastic law)
	v	0.4999994-0.4999997	0.499999
	ρ [kg/m^3]	1040	1040
Skull cortical bone	Material model	Sandwich structure with linear elastic law integrating failure	Composite structure with elastic laws
	E(MPa)	15000	15000
	ρ [kg/m^3]	1800	2000
	v	0.21	0.22
	σ_t [MPa]	90	Not considered
	σ_c [MPa]	145	Not considered

Skull trabecular bone	Material model	Sandwich structure with linear elastic law integrating failure	Composite structure with Elastic laws
	E(MPa)	4500	1000
	ρ [kg/m^3]	1500	1300
	v	0	0.24
	UTS [MPa]	35	Not considered
	UCS [MPa]	35	Not considered

E = Young's modulus, v = Poisson's ratio, UTS= Ultimate tensile stress, UCS= Ultimate compression stress. ρ = Density

Table 7-1: Summary of characteristics of both head FE models.

7.1.2 Human head injury mechanisms and tolerance limits.

Baumgartner (2007) performed a comprehensive summary of head injury types and their injury mechanisms, which is shown in the next paragraphs.

Five types of injuries are identified in the head, and possible injury mechanisms are associated. A brief reference to each of them is followed by the table analysing how each FEM model predicts with each injury type.

Head injury type	Possible injury mechanisms
Skull fracture (SF)	Bone loading
Extradural Haematoma (EDH)	Bone loading
Subdural Haematoma (SDH)	Brain-skull relative motion
Focal brain Contusion (CONT)	Local brain loading
Diffuse brain axonal or haemorrhagic injury (DAI)	Local brain loading

Table 7-2: Summary of head injury types and their injury mechanisms

7.1.2.1 Skull fracture (SF).

The fracture of the skull is an important phenomenon, with often dramatic consequences on brain loading that typically occurs in pedestrian head impact or in lateral car occupant head impact and sometimes, in helmeted motorcyclists.

A number of experimental results from cadaver head impact producing fracture are reported in the literature. Generally a force level of about 5 to 10 kN is needed to fracture the skull, depending on the impact area, the impactor surface shape and speed. Typically skull fracture is assumed to be linked to bone loading in terms of bone stresses or strains, so ideal rupture criteria should be based on stress and strain, or also strain energy within the skull structure.

However, in general terms in pedestrian head testing environments, the sole injury criterion used is HIC (head injury criteria), which is a combination of lineal accelerations of the head. Although typically, high values of HIC are associated to skull fractures, HIC alone can clearly not be a reasonable fracture criterion with an acceptable accuracy.

In ULP model, skull fracture is due to cranial bone loading (stress or strain) and predicted thanks to the implemented Tsai Wu criterion, which is based on maximal tension and compression stress sustained in shell elements. In Willinger (2003), a 50 % risk of fracture is encountered if strain energy or applied force, are respectively 2.2 J and 5.5 kN.

In KTH model, skull fracture is computed with bone loading (stress), being limited to 90 MPa for the compact bone (Robbins, 1969, McElhaney et al., 1970) and 30 MPa for the spongeous bone (Robbins, 1969, Melvin et al., 1970) through the use of simple elastic ideally plastic constitutive models.

7.1.2.2 Extradural haematoma (EDH).

EDH occurs due to rupture of blood vessels located between the dura matter and the the skull. These veins are strongly tied to the skull itself. Local skull deformation (sometimes accompanied with inner table rupture) consecutive to a hard impact conduces typically to EDH.

In the ULP model, EDH is supposed to be related to bone deformation mechanism. Therefore tolerance limits for EDH are very close to skull fracture (SF) criterion.

In the case of KTH model, no assessment is done on this type of injury due to its close relationship with skull fracture.

7.1.2.3 Subdural haematoma (SDH.)

SDH is a type of hematoma, a form of traumatic brain injury in which blood gathers within the outermost meningeal layer, between the dura mater, which adheres to the skull, and the arachnoid mater. Usually resulting from tears in veins that cross the subdural space, typically attributed to the brain/skull relative motion, subdural hemorrhages may cause an increase in intracranial pressure (ICP), which can cause compression of and damage to delicate brain tissue.

As the ULP head model approaches globally the CSF layer and no veins are modelled, the model computes the strain energy in the subarachnoidal space and uses a criterion

(based o real head impact simulation) to discriminate injury occurrence. A 50% injury risk of SDH injury exists if this energy is above 5.5 Joules.

In the case of the KTH model, the maximal principal strain was chosen as a predictor of this type of injury since it has shown to correlate well for mechanical injuries to the blood-brain barrier (Shreiber et al., 1997). It is suggested that maximal principal strain above 30-60% will lead to vascular rupture, according to Lövenhielm (1974) and Monson (2003).

7.1.2.4 Diffuse axonal injury (DAI).

Diffuse injuries are rarely visible and sometimes concern not only the axon but also small vessels conducing to diffuse petechia haemorrhages. Petechias can be spread out through the brain or be more localised in the brain stem exactly as axonal injuries.

Unlike brain trauma that occurs due to direct impact and deformation of the brain, DAI is the result of traumatic shearing forces that occur when the head is rapidly accelerated or decelerated, usually resulted from rotational forces or severe deceleration.

The major cause of damage in DAI is the disruption of axons, the neural processes that allow one neuron to communicate with another. Acceleration causes shearing injury, which refers to damage inflicted as tissue slides over other tissue. When the brain is accelerated parts of differing densities and distances from the axis of rotation slide over one another stretching axons that traverse junctions between areas of different density, especially at junctions between white and grey matter.

DAI can occur in every degree of severity from (very) mild or moderate to (very) severe and it is referred as concussion in the milder cases of diffuse axonal injury.

Concussion, mild brain injury, mild traumatic brain injury (MTBI), mild head injury (MHI), and minor head trauma may be used interchangeably, depending on the field. The term "concussion" is still commonly used in sports medicine, while 'MTBI' is a technical term used more commonly nowadays in general medical contexts.

While DAI typically causes unconsciousness and persistent vegetative state after head trauma, leading in 90% of the cases of severe DAI to a non reversible coma, concussion typically lead to just a transient loss of brain function.

Thibault reported isolated axon stretching and demonstrates that extension of about 15% can damage the axon irreversibly (1990), and suggested a maximal principal strain of around 10% to cause reversible injury to the axons (1993) which could be used as an approximate threshold for concussion.

Analytical and FE models have been used to demonstrate that DAI risk increases with head rotation acceleration which in turn introduces brain shearing. If the effect of axon elongation is known, the effect of shearing of an axon band has not been tested but could

also lead to axon dysfunction. In mechanics, a gel material (and brain is gel like) is characterized by its behaviour under shearing at both, behaviour and failure level.

From the literature point of view, it is well known that rotational acceleration leads to shearing inside the brain. Correlation between rotational acceleration and impulse duration with depth of shearing stresses distribution and DAI has often been described in the literature.

At the other hand, the importance of local geometry accidents are also often mentioned as local axonal and hemorrhagic injuries (such as brain stem, falx and tentorium) and all these entire phenomena induce shearing stress and strain.

At ULP a first approach to predict DAI was proposed by Kang (1997) simulating a real world accident with the head FE model. Results showed poor correlation between neurological injury and pressure (negative or positive) and good correlation with shearing stresses or strains. A limit brain Von Mises stress of 16 kPa was proposed at this time.

More recently, Willinger (2003) confirmed brain Von Mises shearing stress as a well correlated parameter for neurological injury. Proposed limits in terms of brain Von Mises stress for a 50% risk of moderate neurological injuries is 18 kPa and 38kPa for severe neurological injuries.

In the case of the KTH, the maximal principal strain has been selected to predict this injury as it has been found good correlation to neurological injuries suggesting that maximal principal strain around 10% would lead to brain concussion (Thibault, 1993) while when it is higher than 18-21% would leads to DAI (Morrison et.al, 2003).

7.1.2.5 Brain contusion (CONT).

Brain contusion, is a bruise of the brain tissue caused by multiple microhemorrhages, small blood vessel leaks into brain tissue. Contusions occur primarily in the cortical tissue in areas of the brain located near sharp ridges on the inside of the skull appearing as in coup or contre-coup injuries. In coup injuries, the brain is injured directly under the area of impact, while in contrecoup injuries it is injured on the side opposite the impact.

The brain may be contused when it collides with bony protuberances on the inside surface of the skull, located on the inside of the skull under the frontal and temporal lobes and on the roof of the ocular orbit. Thus, the tips of the frontal and temporal lobes located near the bony ridges in the skull are areas where contusions frequently occur and are most severe. Contusions, which are frequently associated with edema, are especially likely to cause increases in intracranial pressure (ICP) and concomitant crushing of delicate brain tissue.

At ULP contusion prediction is based on computed pressure at the coup and contrecoup area, therefore the detailed geometry of the model is of high importance to accurately predict it. Injury may occur in area where pressure is over 250 kPa or under -100 kPa.

In the KTH model, the strain level in the cortex is used as predictor of contusion based on Shreiber et al. (1997) who derived a threshold of 19% in principal strain in the cortex for a 50% risk of cerebral contusions.

Head injury type	ULP head model	KTH head model
Skull fracture (SF)	Global strain energy skull>2.2 J (50% risk SF)	Cortical Bone maximum stress>90 MPa Trabecular bone maximum stress>30 MPa
Extradural Haematoma (EDH)	--	--
Subdural Haematoma (SDH)	Global strain energy CSF >5.5 J (50% risk SDH)	Maximal principal strain 30-60%
Brain Contusion (CONT)	Brain pressure >250 kPa or brain pressure<-100 kPa	Maximal principal strain in cortex >19% (50% risk of CONT)
Diffuse axonal injury (DAI)	Brain Von Mises shearing stress>18 kPa (Moderate DAI) Brain Von Mises shearing stress>38 kPa (Severe DAI)	Maximal principal strain 10% (Concussion) Maximal principal strain 18-21% (DAI)

Table 7-3: Summary of injury threshold used in each model to predict head injuries.

7.2 Simulation matrix of real world scenarios with FE human head models.

Due to the FE head human model availability in terms of size and age (typically representing a 50% adult male), only the two scenarios involving pedestrians close to the male 50% adult (IP002 and IP006) have been analysed in detail using the two FE human head models.

The multibody models have defined the position and orientation, as well as the lineal and angular velocity of the head, in the very moment previously to the head impact and transferred to ULP and TNO for their individual simulations, as summarized in the Table 7-5.

Real world data	IP002	IP006
Injury description in the real world scenarios	Closed head injury with superficial scalp injury. Stuporous without loss of consciousness.	Slight closed craneum encephalic trauma, Haematoma in scalp in occipital area
Skull fracture	No	No
SDH	No	No
DAI	Yes, moderate	No
Contusion	No	No
Concussion	Yes	Yes

Table 7-4: Summary of head injuries for IP002 and IP006 scenarios.

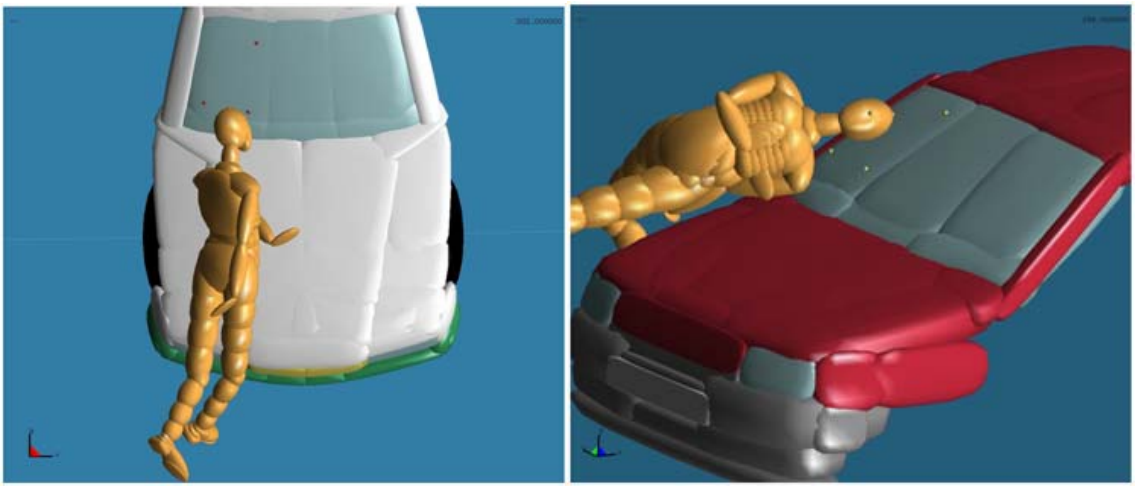

Figure 7-2: Selected cases boundary conditions set for the FE models.

Case	Components of head linear velocity (m/s)			Components of head angular velocity (rad/s)		
	Vx	Vy	Vz	Ωx	Ωy	Ωz
IP002	-6.2	2.36	-5.15	-24.4	6.04	14.5
IP006	-1.47	-0.57	-5.94	4.38	22.1	-2.37

Table 7-5: Summary of boundary conditions for IP002 and IP006 scenarios.

With these boundary conditions, the FE human body head models are initiated in their contact with the windscreen and their outputs were compared with the injury sustained in the real cases.

The simulations and analysis with each individual model have been performed individually by ULP and TNO, each one with one different FE human head model; however, a combined analysis of these two separate joint collaborations is performed in this thesis to identify more robustly the critical parameters leading to head injuries in pedestrian accidents.

The windscreen model in the ULP case was based on 1200 mm x 800 mm rectangular surface regularly meshed by using three layered composite shell elements. Both external laminated glass layers which have a thickness of 2.2 mm are linked together through an internal poly vinyl butyl membrane which has a thickness of 1 mm.

The mechanical behaviour adopted for both external laminated glass layers of the windscreen is an elastic plastic brittle law that allows rupture while the linking plastic membrane's mechanical behaviour is assumed to be linear elastic. Both mechanical behaviours are based on the experimental data determined by Haward (1975).

In the case of TNO, the car windshield was modelled using the TNO glass model consisting of three layers of glass-polymer with interlayer-glass. The polymer is modelled using a linear visco-elastic material model while the glass layers are modelled using a continuum damage model.

This model is based on an orthotropic crack model including direction-dependent failure stresses sampled from the failure distribution, which is Weibull-distributed and obtained from experiments on flat glass plates.

The windshield model was validated with the experiments of adult head form impacts against a car windshield, which were performed within APROSYS (2006). The computational results were compared to the experiments in terms of the glass crack distribution and head form acceleration and kinematics.

7.2.1 Pedestrian Case IP002

As it can be seen in the table, a concussion with moderate DAI are the only injuries reported and are adequately predicted in the ULP model simulations.

On the other hand, the KTH FE model simulations did predict the concussion as well as the moderate DAI, but they also predicted brain contusion, although it was not reported in the real world injuries.

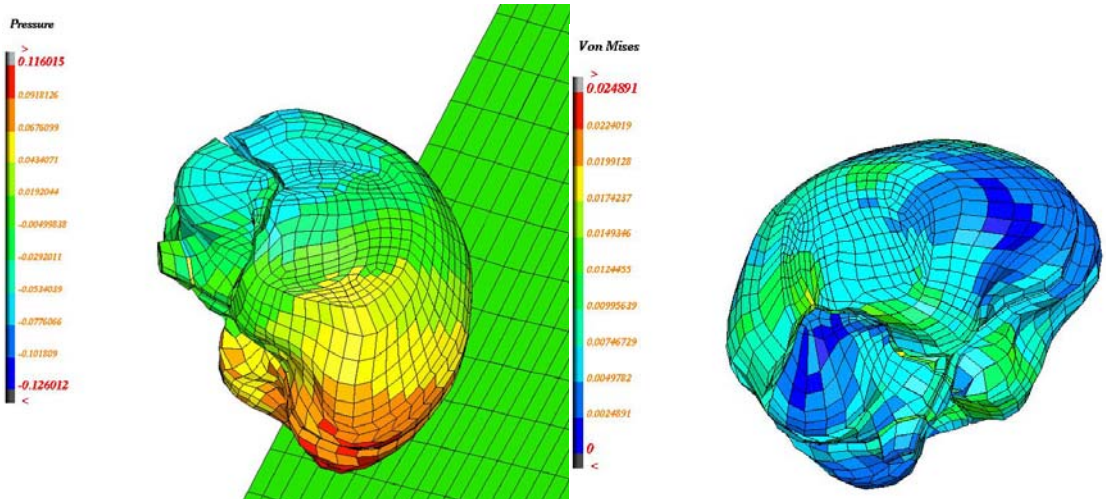

Figure 7-3: Pressure and Von Misses stress from ULP head model, (Baumgartner, 2007).

Calculated mechanical parameter	Max. Value	Predicted injury
Brain pressure [kPa]	100	No Contusion
Brain Von Mises stress [kPa]	18	Concussion-Moderate DAI
Brain/skull interface global strain energy [mJ]	225	NO SDH
Skull global strain energy [mJ]	1258	NO Skull fracture

Table 7-6: Summary of injury predictions of ULP head FEM in IP002.

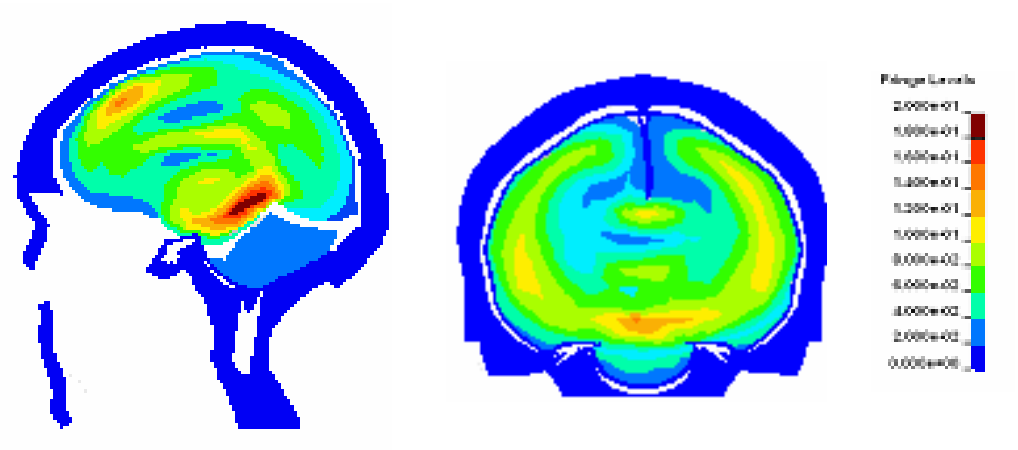

Figure 7-4: Strain distribution from KTH head model, (Mordaka, 2007).

Calculated mechanical parameter	Max. Value	Predicted injury
Maximal principal strain in brain	22.9	Concussion-Moderate DAI
		NO SDH
		Contusion
Max.Von Mises stress in outer/inner compact bone	5.9/2.0	No Skull fracture

Table 7-7: Summary of injury predictions of KTH head FEM in IP002.

7.2.2 Pedestrian Case IP006

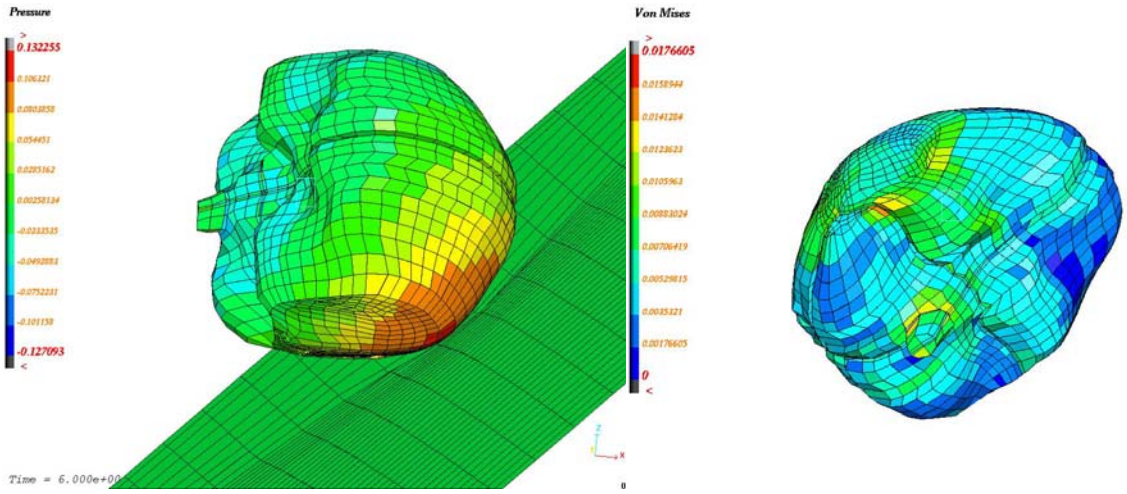

Figure 7-5: Pressure and Von Misses stress from ULP head model, (Baumgartner, 2007).

Calculated mechanical parameter	Max.value	Predicted injury
Brain pressure [kPa]	110	No Contusion
Brain Von Mises stress [kPa]	15	Concussion-No DAI
Brain/skull interface global strain energy [mJ]	1270	NO SDH
Skull global strain energy [mJ]	530	NO Skull fracture

Table 7-8: Summary of injury predictions of ULP head FE model in IP006.

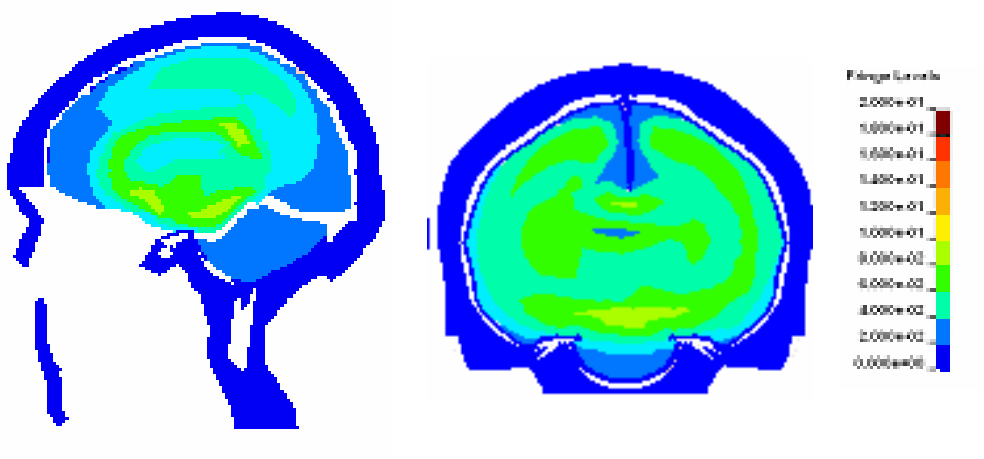

Figure 7-6: Strain distribution from KTH head model, (Mordaka, 2007).

Calculated mechanical parameter	Max. value	Predicted injury
Maximal principal strain in brain (%)	10.2	Concussion-No DAI
		NO SDH
		No Contusion
Max.Von Mises stress in outer/inner compact bone (MPa)	29.8/12.1	No Skull fracture

Table 7-9: Summary of injury predictions of KTH head FE model in IP006.

In this case, the concussion reported in the real world was predicted with the ULP FE model simulations as well as by the KTH FE model as the only injury of the head.

It can be seen in both cases high agreement of both models to reproduce the head injuries reported in the real world accidents, even though these were not too severe, and only mild head injuries were found.

In fact, in both cases, the brain concussion that occurred has been only predicted using the FE models of the local tissue behaviour and as such it is not possible to be predicted directly with head injury criteria considered globally.

Looking to the HIC obtained in the MB models of these two simulations, IP002 reached a HIC of 1105.6 and IP006 722.6 which based on Prasad-Mertz (1997) suggest a 62-25% respectively of MAIS 3 head injuries.

From these values the only conclusion to withdraw is that IP002 impact seems to be more severe that IP006, but no further qualitative assessment can be obtained. In fact, as HIC

original function was the prediction of head lineal fractures, the previous conclusion should be just delimited to “more severe in terms of lineal head fractures” and not extended to any other type of injury, which are typically caused by other different injury mechanisms.

From the process of reconstructing the scenarios serving as basis for this FE study, it has been found the dependency of the pedestrian head impact conditions with the initial pedestrian position in the moment of impact, showing great changes in the impact conditions due to small changes in this starting impact position.

Moreover, it has been shown in the simulations, but also found in literature that in pedestrian scenarios, head rotational acceleration is always presented due to the inherent lateral impact associated to pedestrian accidents. For such evidence, it would be necessary to consider further head injury criteria in the pedestrian headform testing protocols to complement HIC with the assessment of injury risk of suffering internal brain injuries linked to rotational acceleration.

Unfortunately, the implications of this approach will call for a complete reformulation of the headform test procedure and therefore it is out of the scope of this thesis, although a lot of effort has been devoted on such direction by ULP and TNO and other partners within the APROSYS project (FP6-TIP3-CT-2004-506503).

8 FE ANALYSES OF PEDESTRIAN LEG INJURIES

Taken into account the characteristics of pedestrian impacts found previously in the MB simulations, this chapter approaches leg injuries occurrence in pedestrian scenarios under pre-set boundary conditions to ease the understanding of the critical parameters leading to leg injuries.

For that, a full human FE body model (THUMS) is impacted by a set of representative vehicles of the European fleet at pedestrian Directive 2003/102 impact conditions. This simulation matrix analyses the behaviour of a real pedestrian when impacted by different types of vehicle and defines the desired critical parameters (kinematics and injury predictions) to be reproduced in the pedestrian legform procedure for all vehicles.

A second simulation matrix with these vehicles impacted with the pedestrian legform is also performed to identify at which extend these expectations are fulfilled in the current Directive as currently this pedestrian legform procedure uses some vehicle profile characteristics to delimitate the range of applicability of the test.

It is the intention of this chapter to understand further the basis of these limitations and propose improvements in order to eliminate them, meeting the real world requirements found with the full FE human body model and presenting a technical feasible solution from a test procedure perspective.

8.1 Description of the THUMS FE 50% male pedestrian model.

The THUMS (Total HUman Model for Safety) pedestrian model is a computational model to simulate motions and stress or strain distributions of the human whole body for impacts,

using the finite element method developed by Toyota (Maeno 2001). The THUMS reproduces anatomical geometry data and biomechanical properties of the human body, such as the stiffness of the bone and the flexibility of the skin, of a 50 percentile American male in a walking posture with approximately 60,000 nodes and 80,000 elements.

It includes the whole skeletal structure of the human body, both the trabecular part of the bones and the cortical one, as well as some main cartilages and ligaments of the body.

The bones are meshed with two layers. The cortical bone is meshed using shell elements and the trabecular using solid elements. The ligaments are meshed with shell elements which thicknesses have been adjusted depending on the ligament.

The skin and muscles that cover the bone are modelled with solid elements as well as the heart, lungs and the abdominal internal organs, which are simulated as a continuum body of solid elements.

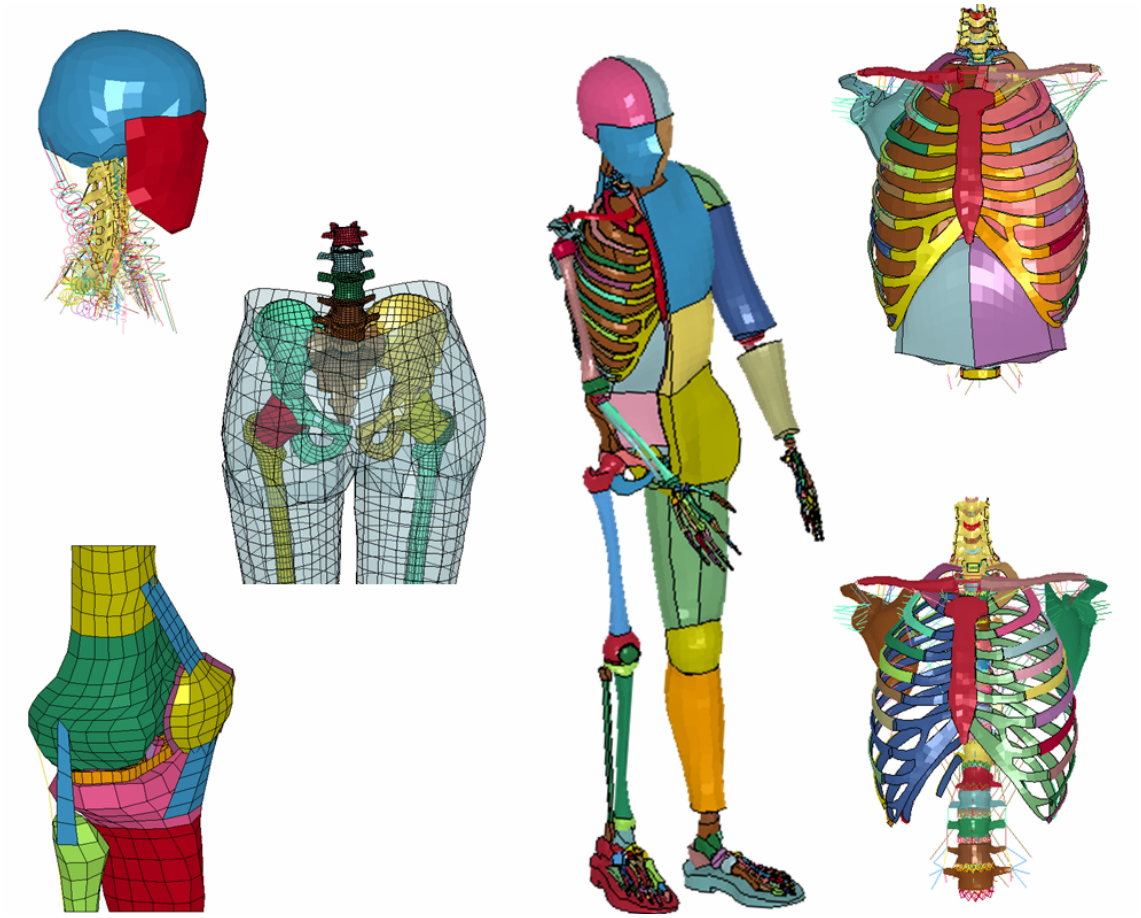

Figure 8-1: Overview of the THUMS model.

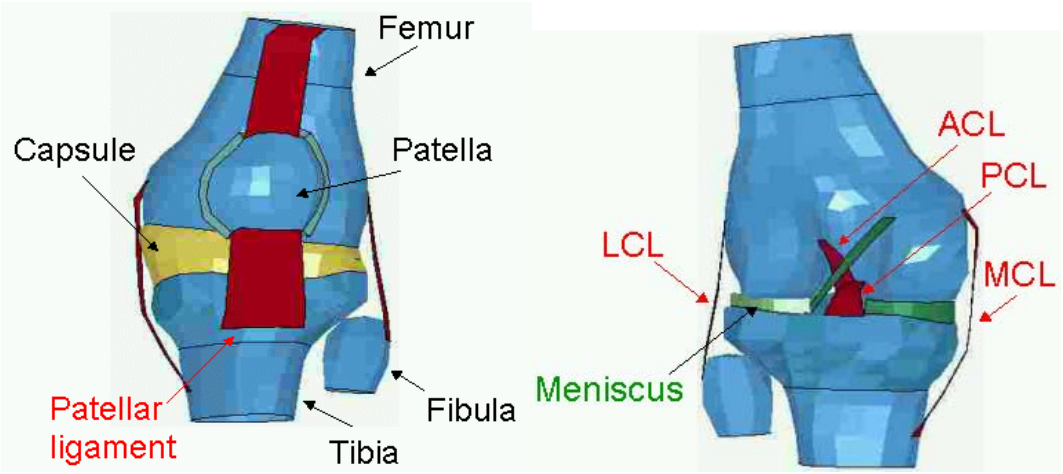

Figure 8-2: Knee of the THUMS FE model. Left) Bones and capsule Right) Menisci and ligaments (LCL: Lateral Collateral Ligament, MCL: Medial Collateral Ligament, ACL: Anterior Cruciate Ligament, PCL: Posterior Cruciate Ligament)

In the joints, the most relevant ligaments and tendons that connects the bones or the muscles are modelled with shell or beam elements while sliding interfaces are defined on the contacting surfaces of these joints to represent the joint motion.

The lower limbs of THUMS model include the cortical and spongy parts of the femur, tibia and their condyles, fibula and patella (cortical and cancellous) as well as the meniscus, the knee and ankle ligaments and the Achilles tendon. The knee joint consists of the femur and tibia articular surfaces, the menisci, the joint capsule, and the ligaments. Generally, material properties have been defined referring to Yamada (1970) and Abe (1996) as shown in the table.

Part	Density (kg/m^3)	Young modulus (MPa)	Material model
Cortical bone	2000	17000-23000	Elastic-plastic with strain rate dependency
Trabecular bone	860-1000	40-300	Elastic-plastic material
Ligament	1100	300-1000	Strain rate dependent material
Flesh	860	9	Visco-elastic material
Skin	1000-1600	22	Elastic-plastic with strain rate dependency

Table 8-1: Material properties for THUMS legs.

The model is implemented with failure criteria for the bones and the ligaments, (Nagasaka, 2003) to evaluate bone fracture and ligament rupture. In the cortical bones, the failure criterion is based on plastic strain of 3% and total elongation of 3% and for knee ligaments is based on 2% of plastic strain and total elongation of 15%.

A more thorough description of the whole model is presented in the next headings, analyzing more in detail the different levels of detail and modeling strategies followed in the different parts of the body within the model.

8.1.1 Head and neck.

The THUMS model has a simplified representation of the head anatomy. It divides the head in three main parts:

- A solid viscoelastic outer part, representing the head scalp and the face muscles, covered with a shell skin.
- An inner solid part that represents the brain. This inner part is not further divided into the actual different anatomical parts of the brain but it is represented as a rigid continuum.
- An intermediate rigid structure representing the bony structures of the skull and the face. This layer has three levels in the skull, where solid diploes lay between the inner and the outer shell layer of the skull cortical bones, but only one shell layer in the face, representing the cortical facial bones. The real skull cap is formed by different fused bones but the model does not distinguish between them but it only takes into account the foramen magnum, at the base of the skull, through which the spinal cord passes providing continuity for the central nervous system.

The human head connects, through the occipital bone, to the vertebral column at the atlas (C1) and the axis (C2), near the foramen magnum. This joint is represented in detail in the THUMS model and includes two set of ligaments as elastic shells.

- A set of ligaments which link the atlas to the occipital bone (articular capsules, anterior and posterior-atlanto occipital membrane and lateral atlanto-occipital ligaments) which allows the skull to move up and down.
- A set of ligaments that couple the axis to the occipital bone (tectoria membrane, alar ligaments and apical odontoid ligament) which allows the upper neck to twist left and right.

Moreover, THUMS also models the muscles from the posterior triangle of the neck that controls the head motion. The sternocleidomastoideus, the scalenus (posterior, medius and anterior), the longus capitis, the rectus capitis and the longus colli (vertical and inferior oblique) are represented in the model as spring-damper elements to control the head motion in rotation, extension, flexion and bending.

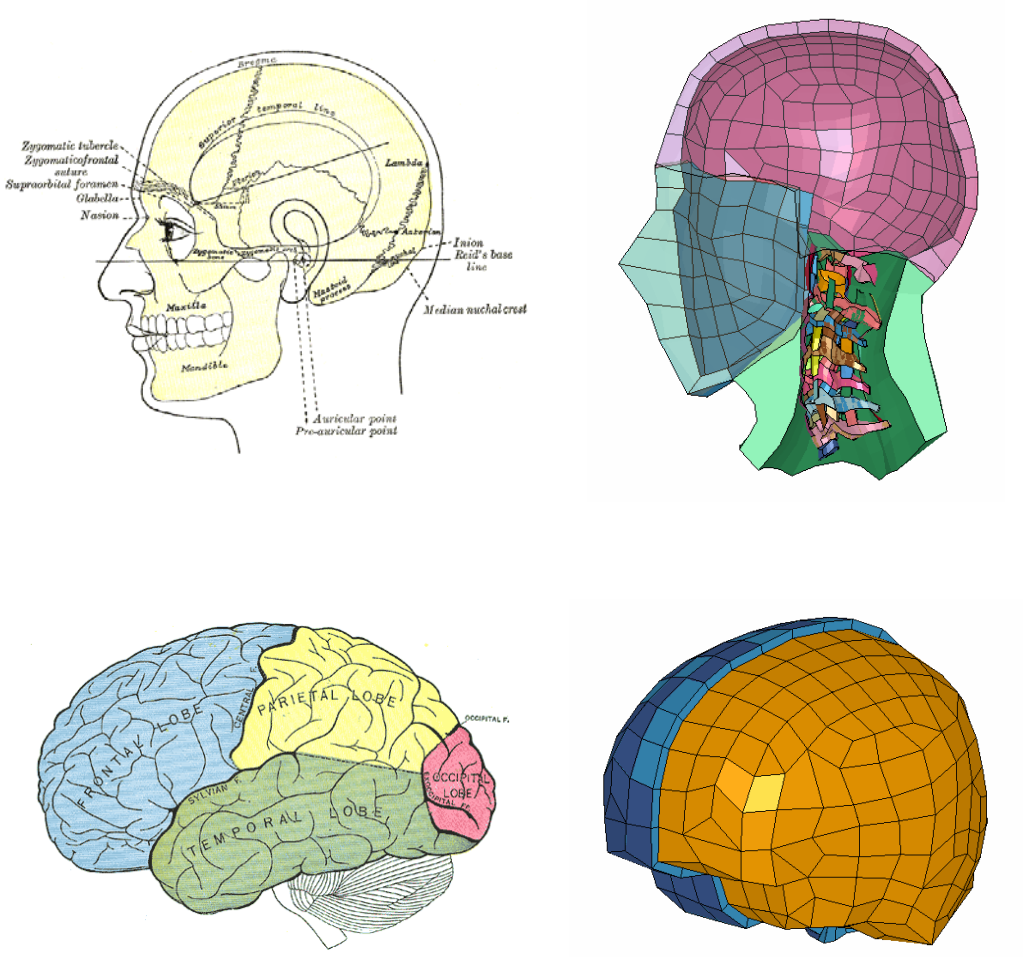

Figure 8-3: Head details in the THUMS model in comparison with the human body (left images from Gray's Anatomy, 1918).

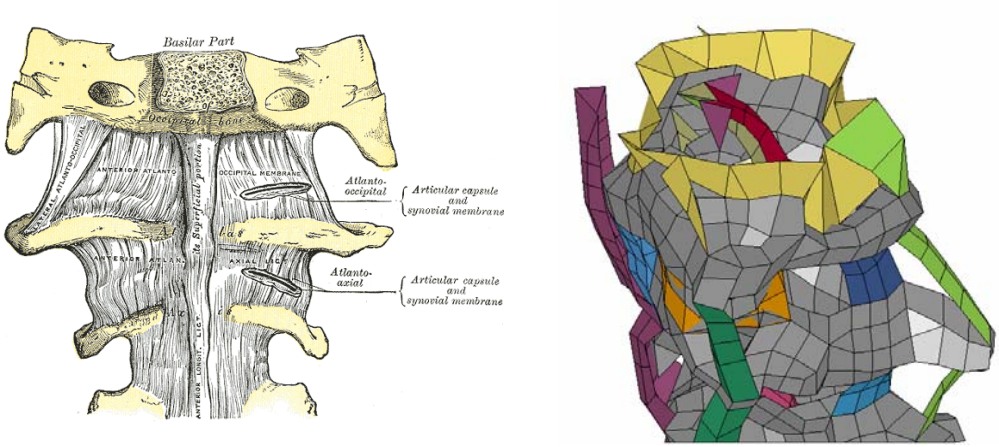

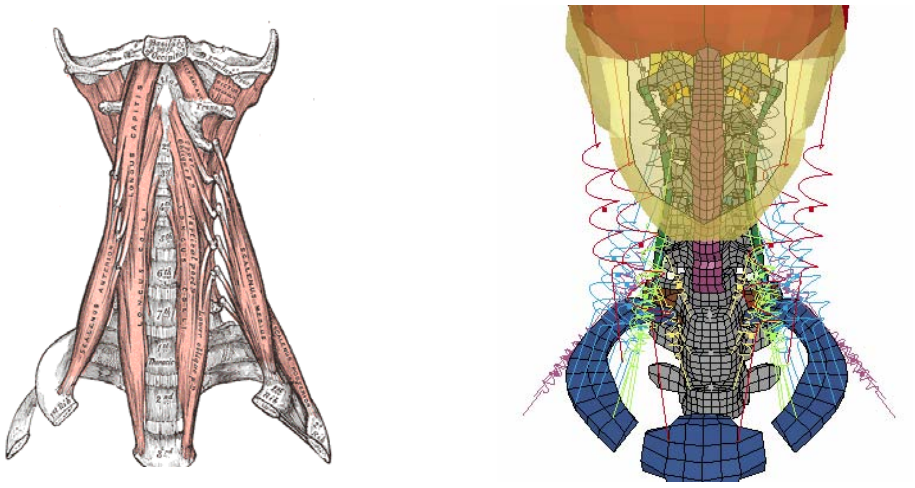

Figure 8-4: Head and neck details in the THUMS model in comparison with the human body (left images from Gray's Anatomy, 1918).

8.1.2 Spine.

The THUMS model has a detailed representation of the human spine. Therefore, as the human one, its spine consists of discrete bony elements (vertebrae), meshed with rigid solid elements, joined by passive ligamentous restraints, modelled as elastic shell, and kept separated by intervertebral discs and articulating joints, which are included in solid elastic elements covered with an elastic shell. A functional spinal unit (FSU) is comprised of a superior vertebra intervertebral disc and an-inferior vertebra osteoligamentous unit and it is the minimum unit to be analysed independently.

The spine is broadly divided into 5 regions: the cervical spine, the thoracic spine, the lumbar spine, the sacrum, and the coccyx.

- The cervical spine (C-spine) consists of 7 vertebrae (C1-C7) and the base of the skull.
- The thoracic spine (T-spine) consists of 12 vertebrae (T1-T12) and is where the ribs are attached.
- The lumbar spine (L-spine) consists of 5 vertebrae (L1-L5)
- The sacrum and coccyx consists of 5 fused vertebrae each (for the coccyx, 4 or 5).

The upper two vertebrae are the atlas (C1) and axis (C2). The atlas is a ring with no vertebral body whose bilateral superior facets articulate with the occipital condyles and whose inferior facets articulate with the axis. The axis looks more like the other cervical vertebrae but has a prominent spire of bone thrusting cranially from its vertebral body called the odontoid process. This process serves to keep the head attached to the rest of the body, together with the ligaments summarized in the previous heading.

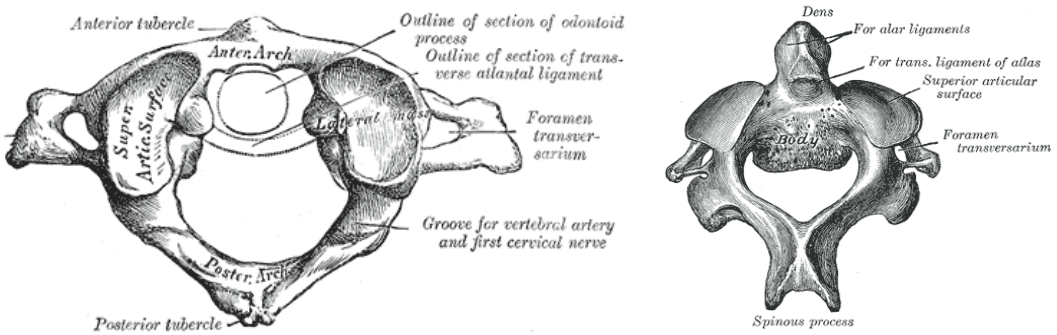

Figure 8-5: Atlas and axis vertebrae.

Excluding these two first vertebrae, each FSU in THUMS is connected by 10 ligaments, which serve to protect neural structures by restricting the motion of each FSU and absorbing energy during high speed and potentially injurious motions.

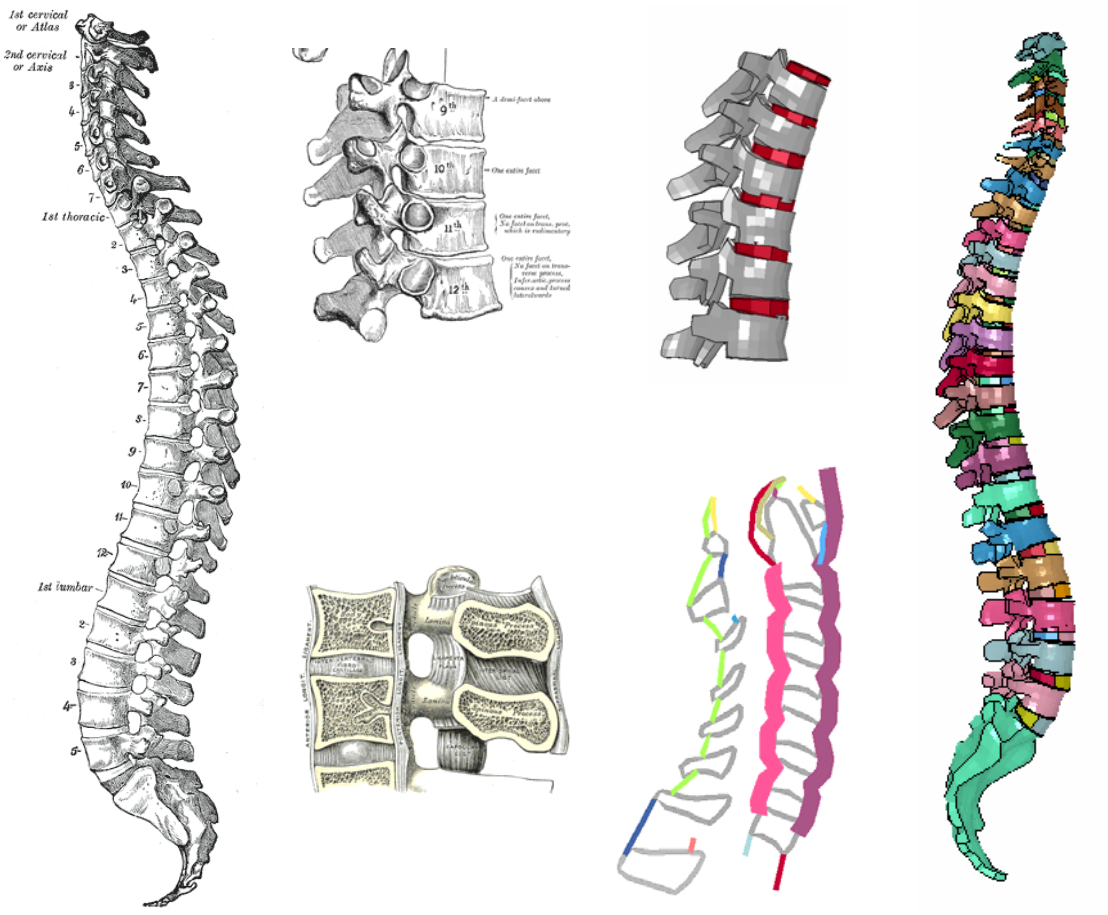

Figure 8-6: Spine details in the THUMS model in comparison with the human body (left images from Gray's Anatomy, 1918).

The THUMS model includes the following ligaments in each FSU:

- The anterior longitudinal ligament (ALL) that originates at the base of the skull and extends the entire length of the spine into the sacral region along the anterior aspect of the spine. Fibers of the ALL firmly attach to each vertebra, as well as to the intervertebral disc.
- The posterior longitudinal ligament (PLL) also extends the length of the spine along the posterior aspect of each vertebral body and anterior to the spinal cord.
- The ligament flavum (LF) originates bilaterally on the antero-inferior aspect of the lamina of the superior vertebral body and inserts on the postero-superior aspect of the lamina of the inferior vertebra.
- The inter transverse ligaments (ITL) and inter spinous ligaments (ISL) join transverse and spinous processes, respectfully, of adjacent vertebrae.
- The ligament nuchae (LN) is a fibrous membrane, which, in the neck, represents the supra spinal ligaments of the lower vertebrae. It extends from the external occipital protuberance to the spinous process of the seventh cervical vertebra.
- The supra spinous ligament (SSL) originates in the seventh vertebra and extends the length of the spine posterior to the ISL, while attaching firmly to the tip of each spinous process.
- The capsular ligaments (CL) that surround each facet joint.

8.1.3 Thorax and abdomen.

The THUMS model has a detailed description of the muscular and bony parts of the rib cage but has a very simplified representation of the inner soft tissues and the outer muscles and skin that covers the torso.

Three main parts can be distinguished in the THUMS thoracic area:

- A solid viscoelastic outer part, representing the torso, back and abdomen muscles, covered with a shell skin.
- An inner solid part that represents the viscera. This inner part is not further divided into the actual different organs but it is represented as a viscoelastic solid part, for the thoracic area and a crushable foam solid part for the abdominal area.
- An intermediate part representing the rib cage with very detailed definition. The rib cage is an osseo-cartilaginous cage, containing and protecting the principal organs of respiration and circulation. Its posterior surface is formed by the twelve thoracic vertebrae and the posterior parts of the ribs. The anterior surface, formed by the sternum and costal cartilages, is flattened or slightly convex and the lateral surfaces are convex; they are formed by the ribs, separated from each other by the

intercostal spaces, eleven in number, which are occupied by the intercostal muscles and membranes.

There are twelve ribs in each side. The first seven (true or vertebro-sternal ribs) are connected behind with the vertebral column, and in front, through the intervention of the costal cartilages, with the sternum. The remaining five are false ribs; of these, the first three have their cartilages attached to the cartilage of the rib above (vertebro-chondral) and the last two (floating or vertebral ribs) are free at their anterior extremities.

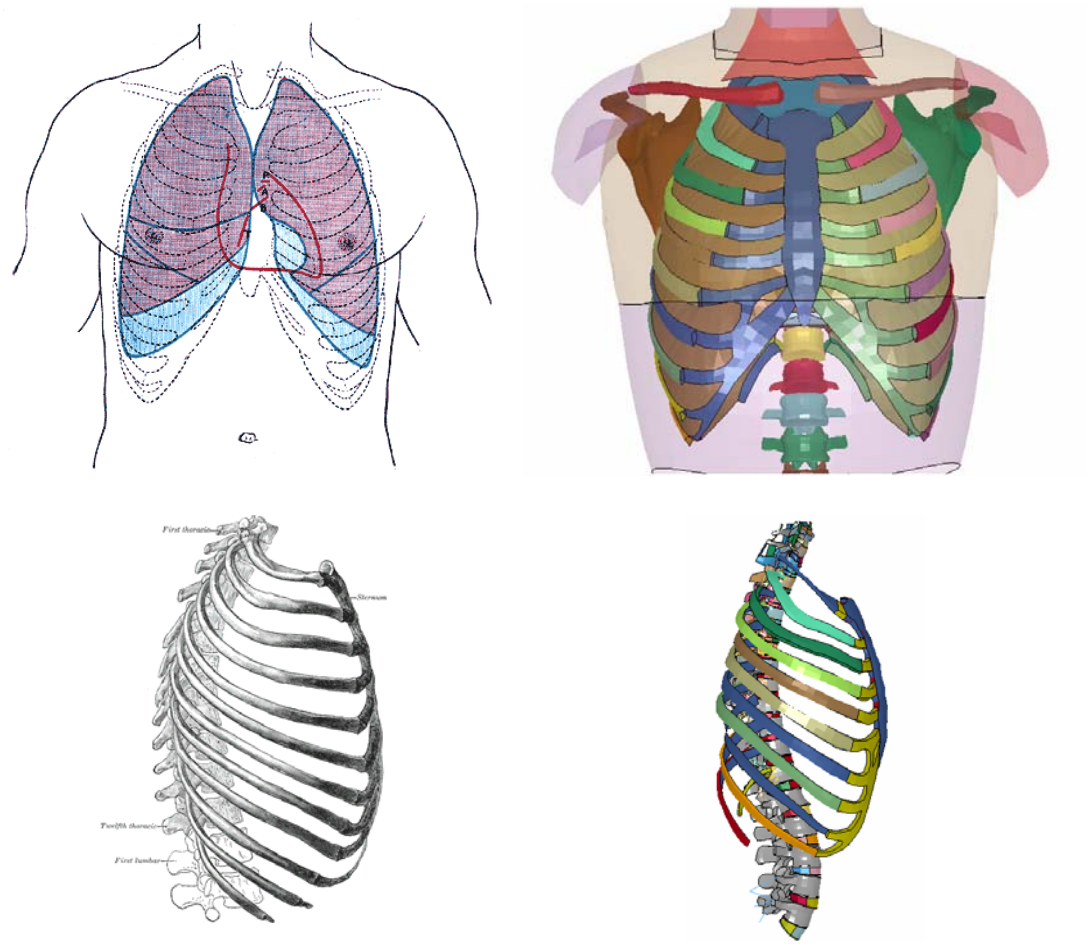

Figure 8-7: Thorax details from the THUMS model in comparison with the human body (left images from Gray's Anatomy, 1918).

The THUMS model characterizes each rib and the sternum with solid elastic plastic elements, representing the spongy part of the bones, and a shell covered of elastic plastic elements with strain rate dependency, to represent the cortical part of the bone. The ribs cartilages are also modelled as solid elastic plastic elements and the intercostal muscles as elastic shell elements.

8.1.4 Shoulder complex.

The THUMS model has a very detailed description of the shoulder girdle, formed by the scapulae and clavicles, joint together in the acromio-clavicular joint. Both bones are modelled in the THUMS model as solid elastic plastic in its spongy part and as shell elastic plastic with strain rate dependency in its cortical part.

The shoulder girdle is imperfect in front and behind, since in the front part the clavicle articulates in the sternoclavicular joint and in the rear, the shoulder girdle is connected to the trunk only by two groups of muscles.

The THUMS model considers these special features and includes a precise definition of these two joints and these two muscles groups.

Regarding the sternoclavicular joint, that connect medially the clavicle with the sternum, the model includes three set of ligaments as seatbelt elements.

- The Sternoclavicular Ligament (SCL) The sternoclavicular ligament is a broad band of fibers, covering the anterior and posterior surface of the articulation; it is attached above to the upper part of the sternal end of the clavicle, and, passing obliquely downward and medialward, is attached below to the sternum.
- The Interclavicular Ligament (ICL) This ligament is a flattened band that passes in a curved direction from the upper part of the sternal end of one clavicle to that of the other, and is also attached to the upper margin of the sternum.
- The Costoclavicular Ligament (CCL). This ligament is short, flat, strong, and rhomboid in form. Attached below to the upper and medial part of the cartilage of the first rib, it ascends obliquely backward and lateralward, and is fixed above to the under surface of the clavicle.

With respect the acromioclavicular joint, that connects the scapula and the clavicle, the THUMS model represent the articular capsule ligaments, as seatbelt elements, and the other five sets of ligaments as beam elements:

- The Superior Acromioclavicular Ligament (ACL) This ligament is a quadrilateral band, covering the superior part of the articulation, and extending between the upper part of the acromial end of the clavicle and the adjoining part of the upper surface of the acromion.
- The Inferior Acromioclavicular Ligament. (AACL) This ligament is somewhat thinner than the preceding; it covers the under part of the articulation, and is attached to the adjoining surfaces of the two bones.
- The Coracoclavicular Ligament This ligament serves to connect the clavicle with the coracoid process of the scapula. It does not properly belong to this articulation, but is usually described with it, since it forms a most efficient means of retaining

the clavicle in contact with the acromion. It consists of two fasciculi, called the trapezoid and conoid ligaments. The Trapezoid Ligament (TZL) is broad, thin, and quadrilateral: it is placed obliquely between the coracoid process and the clavicle. The Conoid Ligament (COL) is a dense band of fibers, conical in form, with its base directed upward.

- The Coracoacromial Ligament (CAL) This ligament is a strong triangular band, extending between the coracoid process and the acromion.

Regarding the muscles groups that complete the shoulder girdle back, the THUMS model represent all the muscles that connect the scapulae to the spine (trapezius, rhomboideus major and minor, latissimus dorsi and levator scapulae) and the serratus anterior and the subclavious, that connect them with the thoracic walls.

The pectoralis major and minor, which are the other two muscles that are involved in joining the shoulder to the thoracic anterior wall are not included since they are already considered in the outer part of the thorax as part of the chest muscles.

All these muscles are represented in THUMS as seatbelt elements but for the levator scapulae, which is defined as spring-damper element.

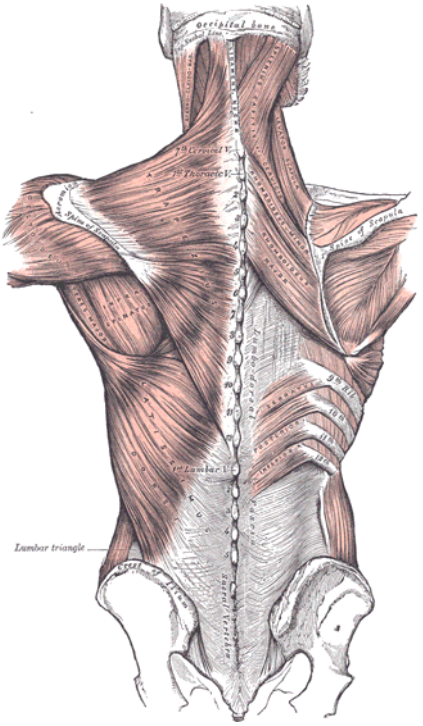

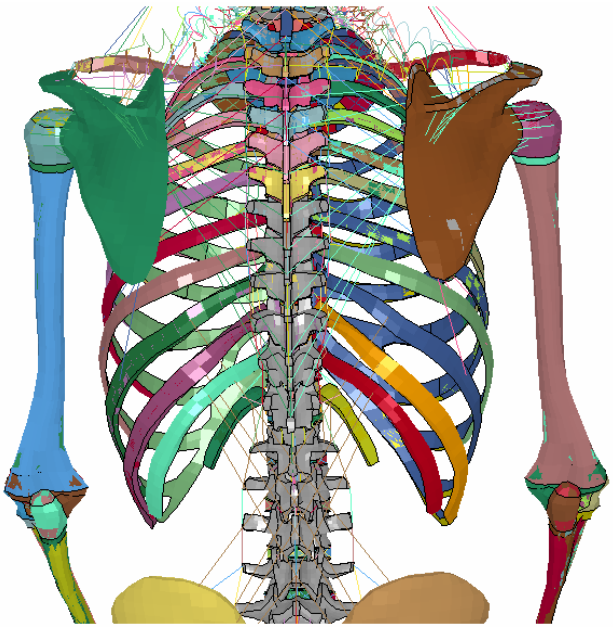

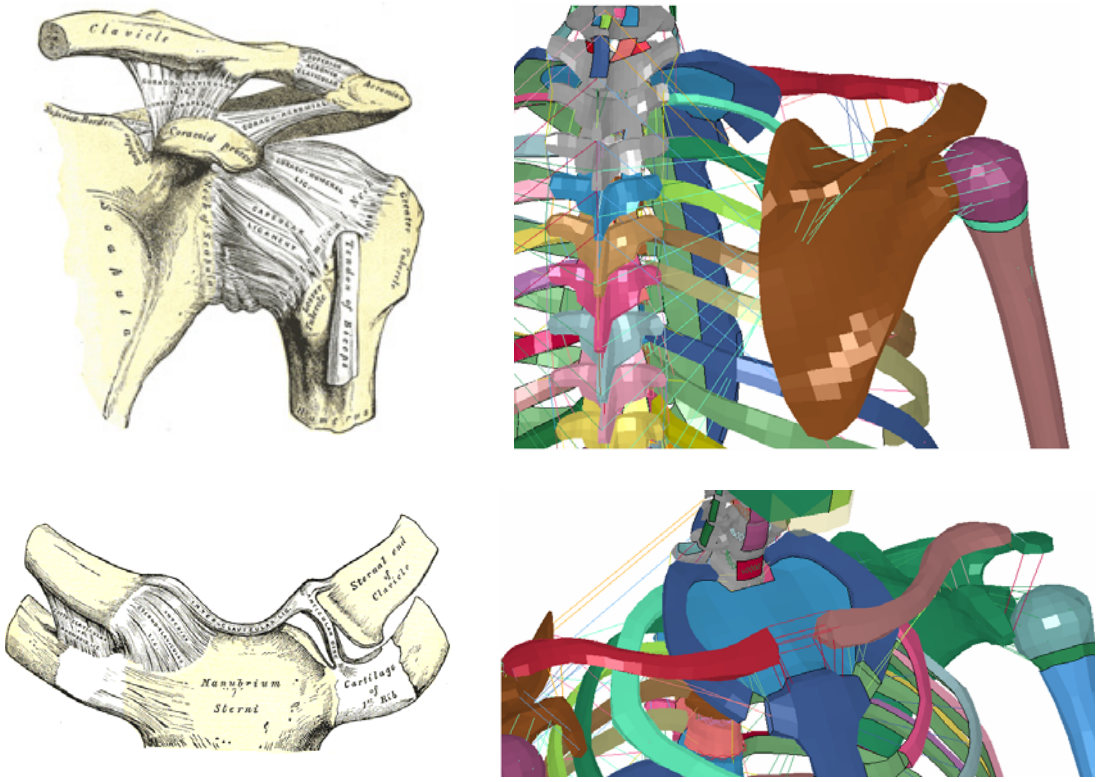

Figure 8-8: Shoulder details from the THUMS model in comparison with the human body (left images from Gray's Anatomy, 1918).

8.1.5 Arms and hands.

The arm consists of two parts: the upper arm and the lower arm. The upper arm articulates to the body in the shoulder and with the lower arm in the elbow, and the lower arm joints with the hand, in the wrist.

THUMS model defines accurately the skeletal part of them but the outer flesh part is simplified into a viscoelastic solid flesh.

There are three long bones in the arm (humerus in the upper arm and radius and ulna in the lower arm) with a similar structure. They consist of two extremities, of cancellous tissue, covered with a thin, compact layer and a body shaft, a compact tissue cylinder, thicker at the centre than toward the extremities, that contains a large medullar canal which extends along its whole length.

THUMS model represents this structure dividing each of the three bones into two extremities (proximal and distal) and a central shaft, with the spongy parts represented as solid elastic plastic elements and the cortical parts modelled as shell elements of elastic plastic material with strain rate dependency.

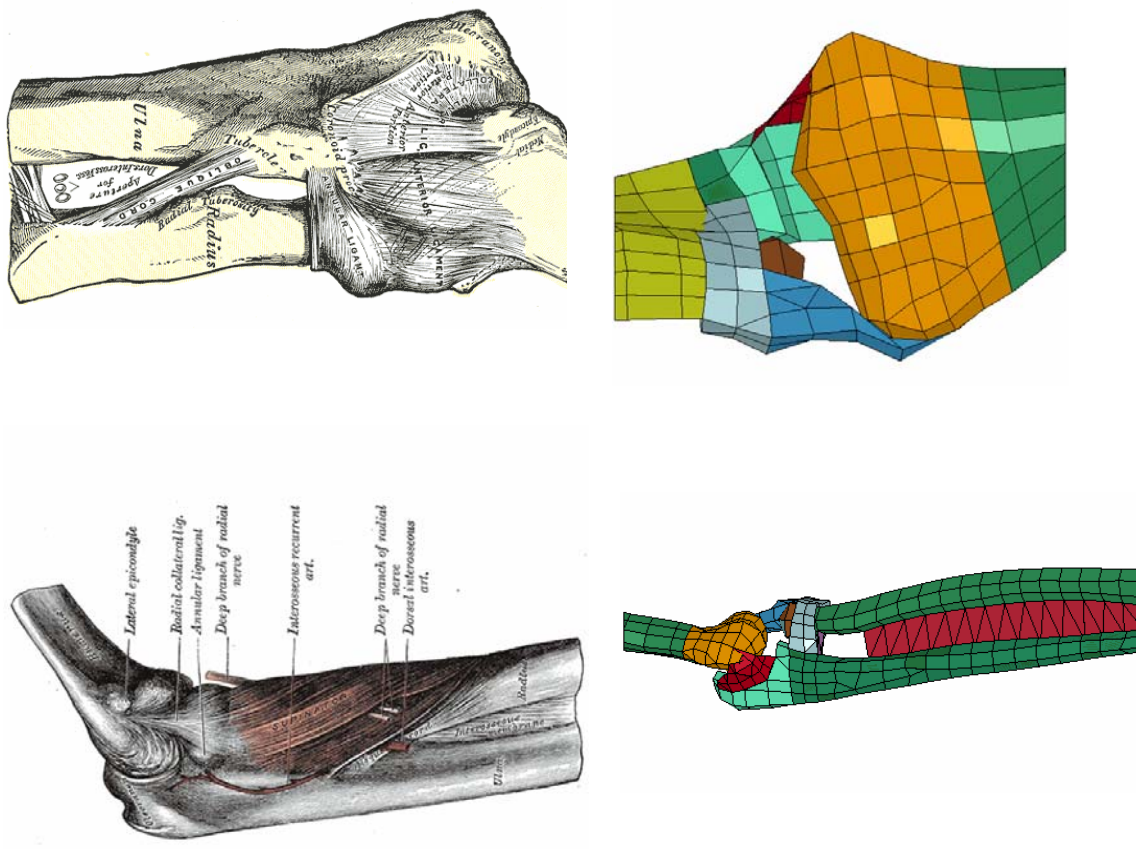

Figure 8-9: Elbow details from the THUMS model in comparison with the human body (left images from Gray's Anatomy, 1918).

There are two main joints in the arm: the elbow and the wrist.

The elbow-joint is a hinge-joint that articulates the upper and the lower arm. The humerus is received into the semilunar notch of the ulna, and the capitulum of the humerus articulates the head of the radius. The articular surfaces are connected together by a capsule, which is thickened medially and laterally, and, to a less extent, in front and behind. These thickened portions are four ligaments (the anterior, the posterior, the ulnar collateral and the radial collateral), however, THUMS model only considers the two collateral ligaments, as elastic shells, as they are responsible of maintaining the stability of the joint.

The wrist-joint is a condyloid articulation. The parts forming it are the lower end of the radius and under surface of the articular disk forming a transversely elliptical concave surface, the receiving cavity; and the navicular, lunate, and triangular bones that form a smooth convex surface, the condyle, which is received into the concavity. The joint is surrounded by a capsule, strengthened by four ligaments (the volar radiocarpal, the ulnar collateral, the dorsal radiocarpal and the radial collateral). THUMS model simplifies the

joint and the four ligaments are modelled together with elastic shell elements as a global radiocarpal ligament.

Moreover, the radius and the ulna are joint by ligaments through all their length.

- In the elbow area, the annular ligament, a strong band of fibres, represented in THUMS as an elastic shell mesh, encircles the head of the radius, and retains it in contact with the radial notch of the ulna. From the inferior border of this ligament, the quadrate ligaments extend to the neck of the radius. THUMS model also include this ligament as elastic shell element mesh.
- Along the shaft of both bones the interosseous membrane keeps them together. This broad and thin plane of fibrous tissue descending obliquely downward and medialward is included in THUMS as elastic shell element.

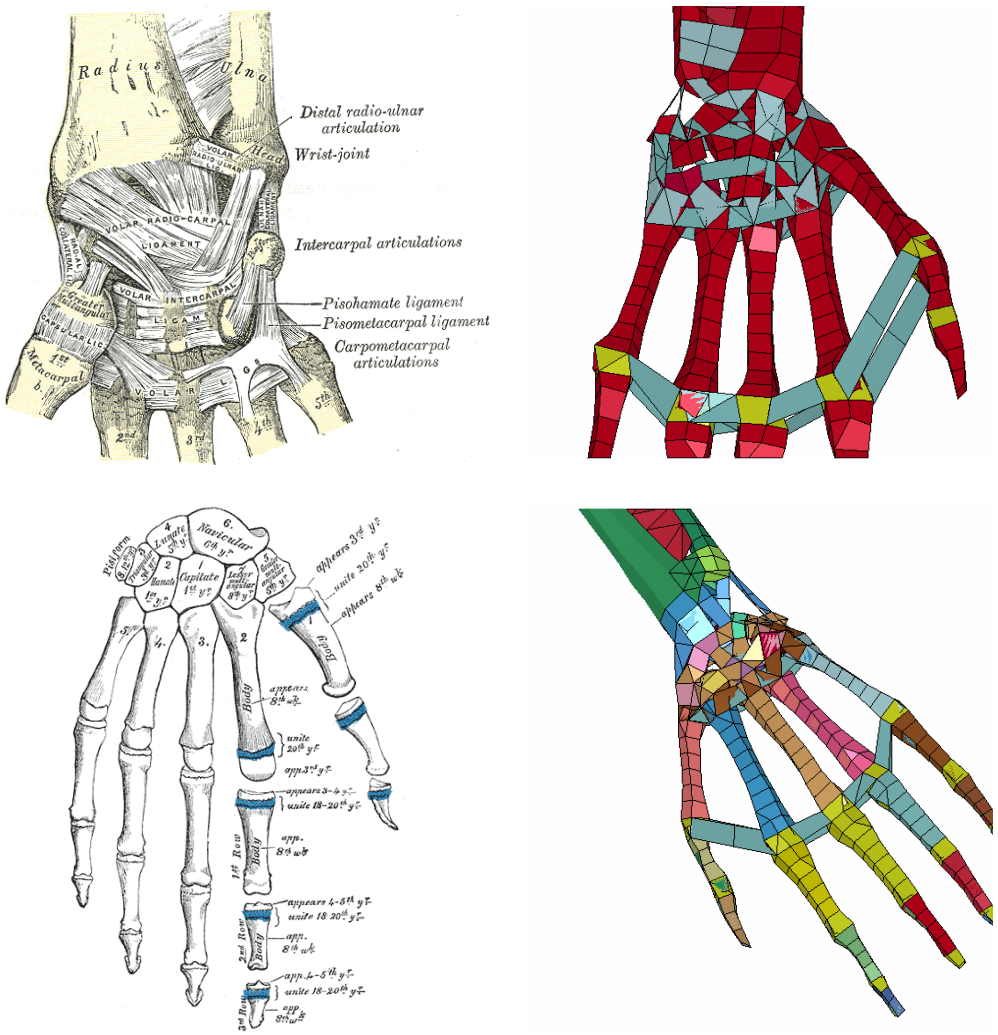

Figure 8-10: Wrist and hand details from the THUMS model in comparison with the human body (left images from Gray's Anatomy, 1918).

In the wrist area, the head of the ulna and the ulnar notch on the lower end of the radius are connected by the volar and dorsal radioulnar ligaments. These narrow bands of fibers are represented in THUMS as a whole, with shell elastic elements.

The hand is a complex bony structure including 27 small bones divided into three areas:

- Carpus or wrist bones (eight in number, arranged in two rows, those of the proximal row, from the radial to the ulnar side, are named the navicular, lunate, triangular, and pisiform; those of the distal row, in the same order, are named the greater multangular, lesser multangular, capitate, and hamate).
- Metacarpus or palm bones (five cylindrical bones which are numbered from the lateral side called ossa metacarpalia I-V).
- Phalanges or digit bones (three for each finger, and two for the thumb).

THUMS models all these bones with solid elastic plastic element meshes covered by a thin shell element layer of elastic plastic material with strain rate dependency.

The ligaments between the different sets of bones are also modelled in THUMS. It groups them into four parts meshed as elastic shell elements:

- Intercarpal ligaments.
- Carpo-metacarpal ligaments.
- Intermetacarpal ligaments.
- Phalangeal ligaments.

8.1.6 Pelvis complex.

The THUMS model has also a detailed description of the pelvis skeletal structure, as well as its joints with the spine (which supports) and the lower limbs (in which it rests).

The pelvis is composed of four bones: the two hip bones, the sacrum and the coccyx. The coccyx and the sacrum are formed by fused vertebrae and close the pelvis in its rear part while the hip bones form the sides and anterior wall of the pelvic cavity and they consists of three parts: the ilium, the ischium, and the pubis.

The union of the three parts takes place in and around a large cup-shaped articular cavity, the acetabulum, where the femoral head articulates to form the hip joint.

The THUMS model represents the hip bones as a whole with the spongy part as solid elastic plastic elements and its cortical part as shell elements of elastic plastic material with strain rate dependency, while it model the sacrum and the coccyx as rigid in its cortical and its spongy parts.

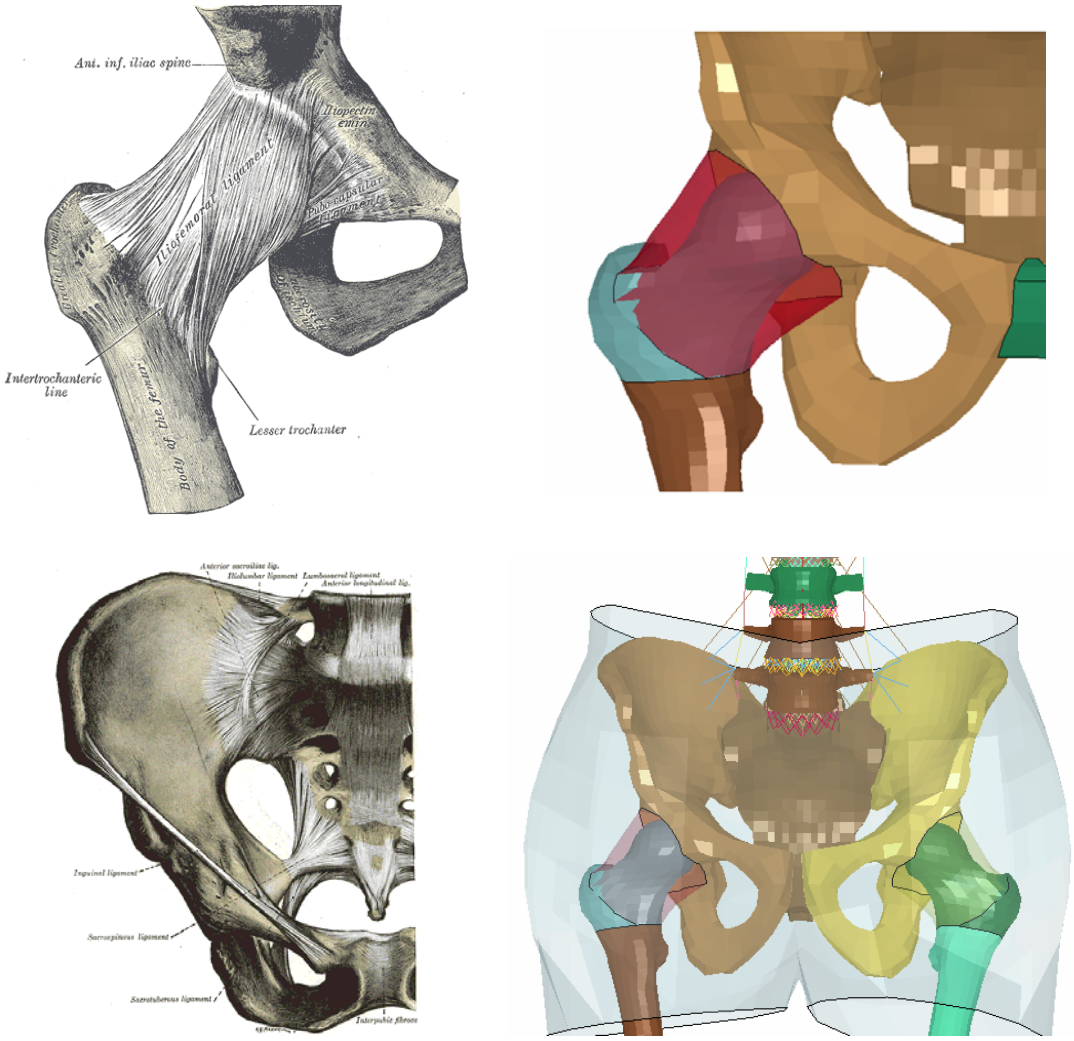

Figure 8-11: Pelvis details from the THUMS model in comparison with the human body (left images from Gray's Anatomy, 1918).

The connection of the pelvis and the spine is done at two levels.

- Connecting the fifth lumbar vertebra with the sacrum and the hip bones. The ligaments that connect the fifth lumbar vertebra to the sacrum are similar to those which join the movable segments of the vertebral column with each other, with the addition at each side, of the ilio-lumbar ligament. This ligament is attached in the spine to the lower and front part of the transverse process of the fifth lumbar vertebra and it connects, by two main bands to the pelvis, one to the base of the sacrum, blending with the anterior sacroiliac ligament; and the other one to the crest of the ilium. The THUMS model represents this ligament as an elastic beam.
- The second connection of the pelvis and the spine is done through the sacroiliac joint formed between the sacrum and the ilium. The articular surface of each bone

is covered with a thin plate of cartilage, thicker on the sacrum than on the ilium. These cartilaginous plates are in close contact with each other, and to a certain extent are united together by irregular patches of softer fibro-cartilage, and at their upper and posterior part by fine inter-osseous fibers. This articulation is not considered in detailed in THUMS model, and the linkage of the sacrum and the hip bone is modelled rigidly.

The hip joint is the linkage of the pelvis to the lower limbs. This joint is a ball-and-socket joint, formed by the reception of the head of the femur into the cup-shaped cavity of the acetabulum. The articular cartilage on the head of the femur, thicker at the center than at the circumference, covers the entire surface with the exception of the fovea capitis femoris, to which the ligamentum teres is attached.

The articular capsule is strong and dense. It is attached to the margin of the acetabulum. It surrounds the neck of the femur, being attached, in front, to the intertrochanteric line; above, to the base of the neck; behind, to the neck and below, to the lower part of the neck, close to the lesser trochanter. The different fibers from the articular capsule are reinforced by accessory ligaments, of which the most important is the ilio-femoral ligament.

THUMS model simplifies this joint and only an outer pelvis ligament part is modelled as elastic plastic material with strain rate dependency to represent all the ligaments that joint the acetabulum with the head of the femur.

8.1.7 Legs.

The leg consists of two parts: the upper leg and the lower leg. The upper leg articulates to the pelvis in the hip and with the lower leg in the knee, and the lower leg joints the foot in the ankle.

THUMS model defines accurately the skeletal part of them but the outer flesh and muscle part is simplified into a viscoelastic solid flesh.

There are three long bones in the leg (femur in the upper leg and tibia and fibula in the lower leg) with a structure similar to the long bones of the arms.

THUMS model represents this structure dividing each of the three bones into two extremities (proximal and distal) and a central shaft, with the spongy parts represented as solid elastic plastic elements and the cortical parts modelled as shell elements of elastic plastic material with strain rate dependency and failure.

There are two main joints in the leg: the knee and the ankle.

The knee joint consists of three articulations in one: two condyloid joints, one between each condyle of the femur and the corresponding meniscus and condyle of the tibia (medial and lateral); and a third between the patella and the femur.

This view of three-in-one knee joint is further supported by the existence in the middle of the joint of the two cruciate ligaments, which must be regarded as the collateral ligaments of the medial and lateral condyloid joints.

The eight ligaments that form these three joints are included in the THUMS model as shell meshes with elastic plastic material with strain rate dependency and failure properties.

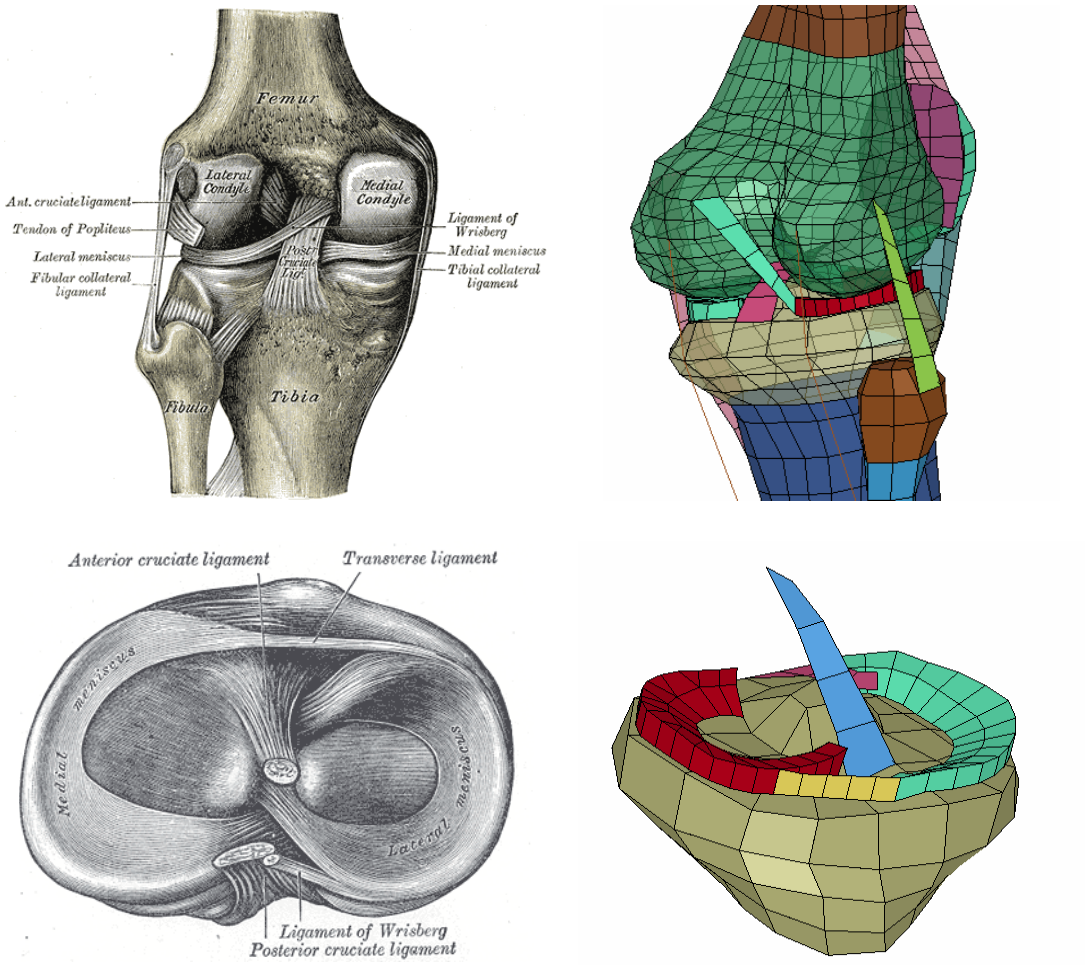

Figure 8-12: Knee details from the THUMS model in comparison with the human body (left images from Gray's Anatomy, 1918).

- The ligamentum patellae is the central portion of the common tendon of the Quadriceps femoris, which is continued from the patella to the tuberosity of the tibia. It is a strong, flat, ligamentous band, about 8 cm. in length.
- The tibial collateral is a broad, flat, membranous band, situated nearer to the back than to the front of the joint. It is attached, above, to the medial condyle of the femur and below, to the medial condyle and medial surface of the body of the tibia.

- The fibular collateral is a strong, rounded, fibrous cord, attached, above, to the back part of the lateral condyle of the femur and below, to the lateral side of the head of the fibula. The greater part of its lateral surface is covered by the tendon of the Biceps femoris.
- The cruciate ligaments are of considerable strength, situated in the middle of the joint, nearer to its posterior than to its anterior surface. They are called cruciate because they cross each other somewhat like the lines of the letter X; and have received the names anterior and posterior, from the position of their attachments to the tibia.
- The menisci are two crescentic lamellæ, which serve to deepen the surfaces of the head of the tibia for articulation with the condyles of the femur. The peripheral border of each meniscus is thick, convex, and attached to the inside of the capsule of the joint; the opposite border is thin, concave, and free. The upper surfaces of the menisci are concave, and in contact with the condyles of the femur; their lower surfaces are flat, and rest upon the head of the tibia; both surfaces are smooth, and invested by synovial membrane. Each meniscus covers approximately the peripheral two-thirds of the corresponding articular surface of the tibia.
- The transverse ligament connects the anterior convex margin of the lateral meniscus to the anterior end of the medial meniscus; its thickness varies considerably in different subjects, and it is sometimes absent.

The ankle-joint is a hinge-joint formed between the lower end of the tibia and its malleolus, the malleolus of the fibula, and the transverse ligament, which together form the reception of the upper convex surface of the talus and its medial and lateral facets. The bones are connected by the following ligaments.

- The Deltoid Ligament: The deltoid ligament is a strong, flat, triangular band, attached to the apex and anterior and posterior borders of the medial malleolus.
- The Anterior Talofibular Ligament. The anterior talofibular ligament, the shortest of them, passes from the anterior margin of the fibular malleolus, forward and medially, to the talus, in front of its lateral articular facet.
- The Posterior Talofibular Ligament: The posterior talofibular ligament, the strongest and most deeply seated, runs almost horizontally from the depression at the medial and back part of the fibular malleolus to a prominent tubercle on the posterior surface of the talus
- The Calcaneofibular Ligament: The calcaneofibular ligament is the longest of them. It is a narrow, rounded cord, running from the apex of the fibular malleolus downward and slightly backward to a tubercle on the lateral surface of the calcaneus.

The four ligaments are modelled independently with shell elements in THUMS, although the anterior and posterior talofibular and the calcaneofibular ligaments were formerly described as the three parts of the external lateral ligament of the ankle-joint.

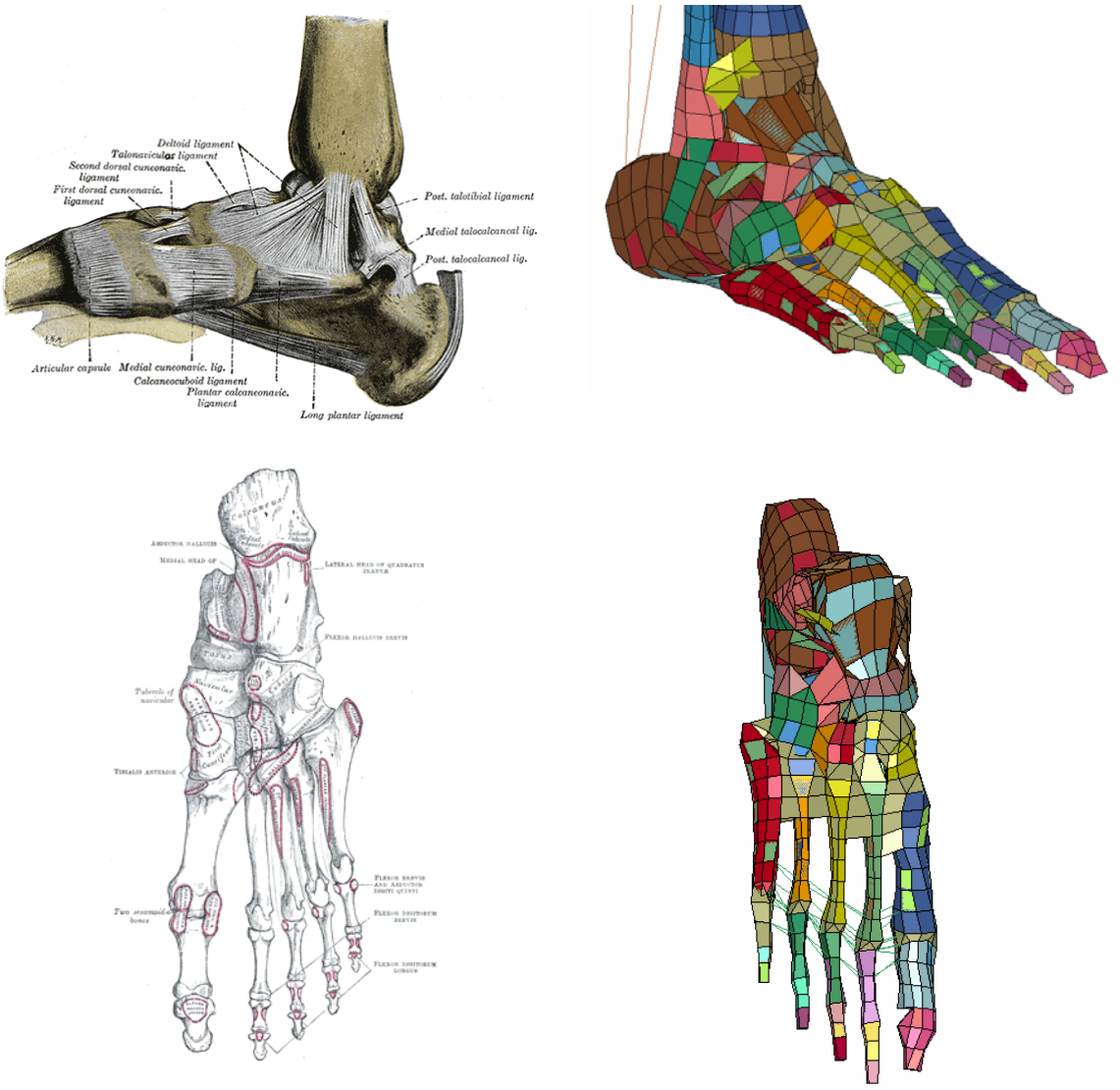

Figure 8-13: Ankle and foot details from the THUMS model in comparison with the human body (left images from Gray's Anatomy, 1918).

The skeleton of the foot is divided in three parts:

- The tarsus, composed of seven bones, (the calcaneus, talus, cuboid, navicular, and the first, second, and third cuneiforms) being the calcaneus the largest of them. It is situated at the lower and back part of the foot, serving to transmit the weight of the body to the ground, and forming a strong lever for the muscles of the calf.

- The metatarsus, consisting of five bones which are numbered from the medial side (ossa metatarsalia I.-V). Each can be divided into a body and two extremities. The body is prismoid in form, tapers gradually from the tarsal to the phalangeal extremity, and is curved longitudinally, so as to be concave below, slightly convex above. The base or posterior extremity articulates proximally with the tarsal bones, and by its sides with the contiguous metatarsal bones.

The phalanges, that correspond, in number (14) and general arrangement, with those of the hand; there are two in the great toe, and three in each of the other toes. They differ from them, however, in their size, the bodies being much reduced in length, and, especially in the first row, laterally compressed.

THUMS models all these bones with solid elastic plastic element meshes covered by a thin shell element layer of elastic plastic material with strain rate dependency.

The foot articulations between the different sets of bones are also modelled in THUMS wit shell elements and elastic properties. It can be distinguished two groups in the foot:

- The tarsus articulations (talo-calcaneal, talo-calcaneo-navicular, calcaneus-navicular, calcaneo-cuboid, cuneo-navicular, cuboid-navicular , intercuneiform and cuneocuboid). All the tarsus articulations are simplified in THUMS to two talo-calcaneous ligaments to link the talus with the calcaneous, the long plantar ligament and the calcaneous-navicular ligament to attach the calcaneous and the navicular, two cuboid-navicular ligaments to represent the cuboid-navicular articulation and two groups of talus ligaments to represent the rest of the intertarsal articulations.
- The rest of the foot articulations (tarso-metatarsal, intermetatarsal, metatarso-phalangeal and phalanges articulations) are simplified in THUMS to a unique part of ligaments (foot ligaments).

8.2 Description of the legform impactor FE model.

The FE legform model used in this analysis consists of two foam covered rigid segments, representing the femur (upper leg) and the tibia (lower leg). The 'femur' is defined as all components or parts of components above the level of the centre of the knee, the point about which the knee effectively bends, and the 'tibia' is defined as all components or part of components below the level of the centre of the knee.

The total mass of the impactor is 13.4kg, (femur 8.6kg and tibia 4.8kg). The center of the knee is located 494 mm from the ground level, rather similar to the one from THUMS FE model, being the centre of gravity of the femur 217 mm above this level and the one from the tibia 233 mm below.

These segments are joined by a deformable knee joint, modelled by a translational-revolute joint (CTR). The bending stiffness of the knee is modelled by a combination of two cardan restraints to allow bending in the knee in two directions. The shearing of the knee is restrained by a linear stiffness and linear viscous damping. The outer foam is modelled with finite elements as a FOAM material with strain rate dependency behaviour with the Johnson-Cook model.

The impactor is fitted with a uni-axial accelerometer in the non-impacted side of the tibia, 66 mm below the knee joint centre, and it is also instrumented to measure the bending angle and the shearing displacement between femur and tibia. Moreover, the mathematical model is also able to output the acceleration at the CoG of both the tibia and the femur.

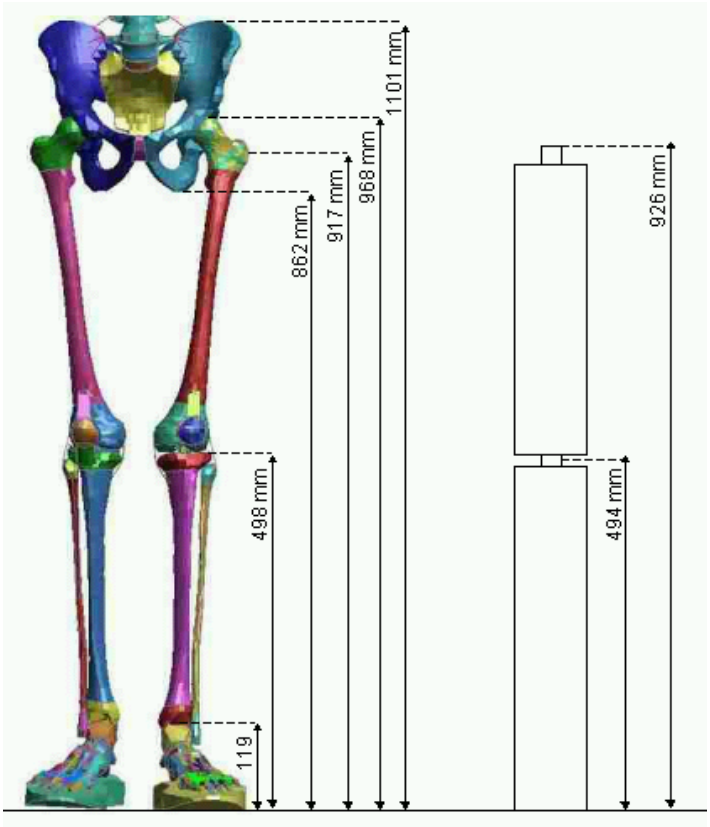

Figure 8-14: Comparison THUMS 50%ile legs and pedestrian legform impactor.

8.3 Description of the vehicle models.

A number of vehicles models have been constructed for these simulation matrixes following the methodology already presented in this thesis. As in this case no specific make and model were needed but representative vehicles within their sector, an average real vehicle has been selected from the geometry corridor built in each sector in APROSYS (2005).

Typically, the European fleet is divided into four vehicle categories that show relevant differences from a pedestrian study point of view:

- Super mini cars (SMC), with very short bonnets,
- Family cars (FC),
- Multipurpose vehicle (MPV), in general with bonnet angle higher than family cars
- SUVs, typically with higher bumpers and larger bonnet that the rest of vehicles.

To clearly set the rules in this sense, the pedestrian test procedures define a number of geometrical parameters in the front end of the part to determine the impact points and also, the limits of the different test configuration. These parameters are the following and also can be used to determine average values in each of the vehicle segments:

- 'The Upper Bumper Reference Line' identifies the upper limit to significant points of pedestrian contact with the bumper. It is defined as the geometric trace of the upper most points of contact between a straight edge 700 mm long and the bumper, when the straight edge, held parallel to the vertical longitudinal plane of the car and inclined rearwards by 20°, is traversed across the front of the car, while maintaining contact with the ground and with the surface of the bumper. Where necessary the straight edge shall be shortened to avoid any contact with structures above the bumper.
- 'The Lower Bumper Reference Line' identifies the lower limit to significant points of pedestrian contact with the bumper. It is defined as the geometric trace of the lower most points of contact between a straight edge 700 mm long and the bumper, when the straight edge, held parallel to the vertical longitudinal plane of the car and inclined forwards by 25°, is traversed across the front of the car, while maintaining contact with the ground and with the surface of the bumper.
- 'Upper Bumper Height' is the vertical distance between the ground and the upper bumper reference line, with the vehicle positioned in its normal ride attitude.
- 'Lower Bumper Height' is the vertical distance between the ground and the lower bumper reference line, with the vehicle positioned in its normal ride attitude.
- 'Bonnet Leading Edge Height' for any section of a car is the vertical distance between the ground and the bonnet leading edge reference line with the vehicle positioned in its normal ride attitude.
- 'Bumper Lead' for any section of a car is the horizontal distance between the upper bumper reference line, and the bonnet leading edge.

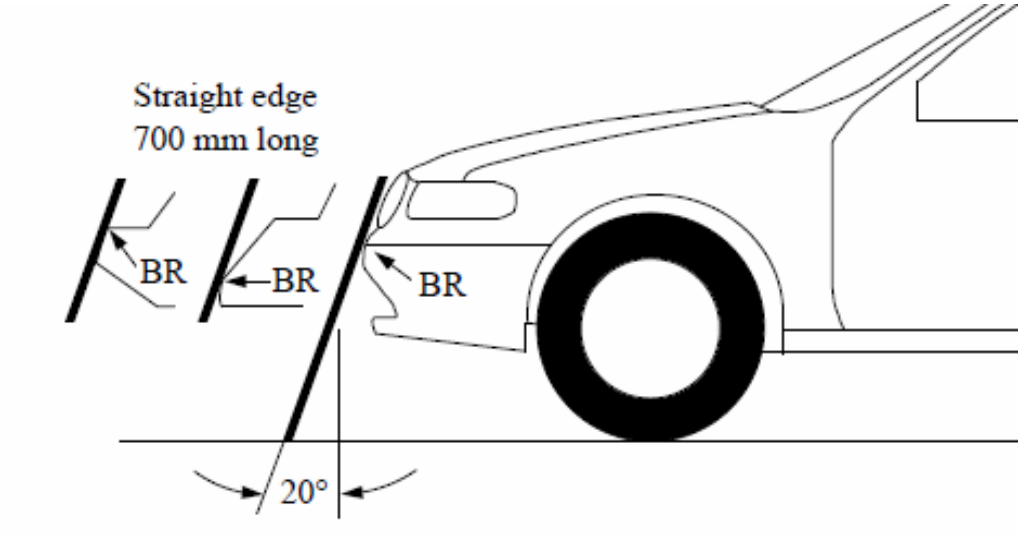
Straight edge
700 mm long
BR
BR
BR
20°

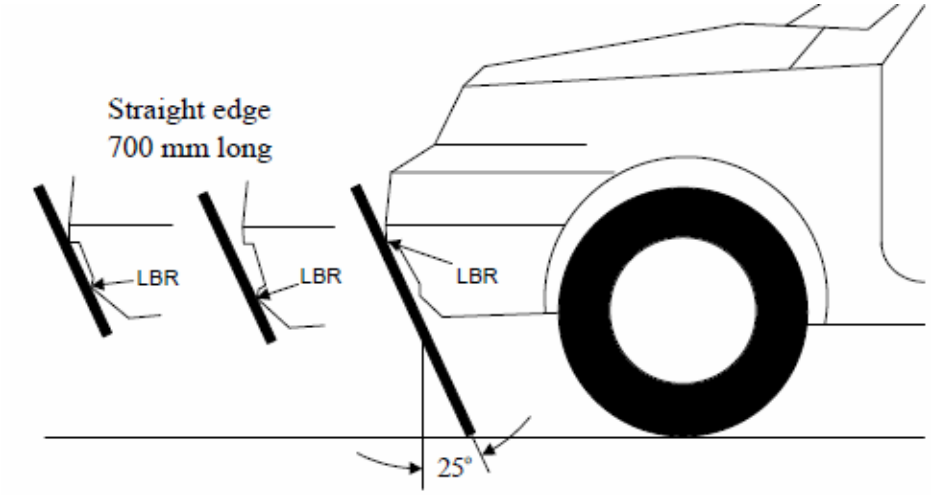
Straight edge
700 mm long
LBR
LBR
LBR
25°

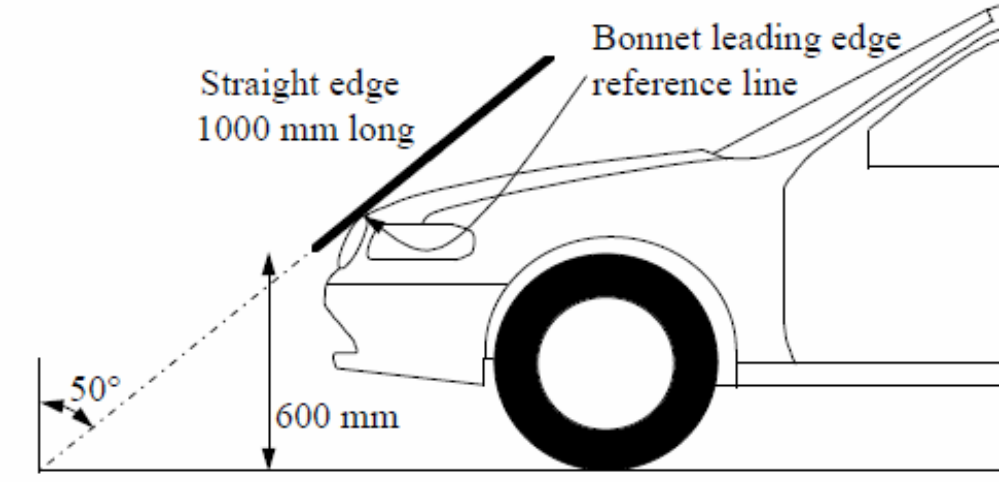
Bonnet leading edge
reference line
Straight edge
1000 mm long
50°
600 mm

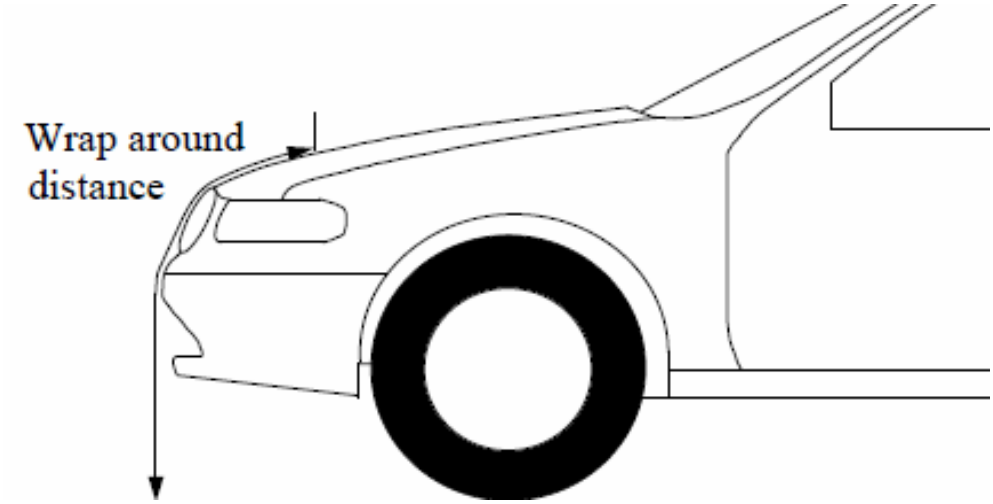

Figure 8-15: Determination of pedestrian test references: upper bumper reference line, lower bumper reference line, bonnet leading edge reference line and wrap around distance in the front end of a car.

- 'Bonnet Leading Edge Reference Line' is defined as the geometric trace of the points of contact between a straight edge 1000 mm long and the front surface of the bonnet, when the straight edge, held parallel to the vertical longitudinal plane of the car and inclined rearwards by 50° and with the lower end 600 mm above the ground, is traversed across and in contact with the bonnet leading edge. For vehicles having the bonnet top surface inclined at 50°, so that the straight edge makes a continuous contact or multiple contacts rather than a point contact, determine the reference line with the straight edge inclined rearwards at an angle of 40°. For vehicles of such shape that the bottom end of the straight edge makes first contact then that contact is taken to be the bonnet leading edge reference line, at that lateral position. For vehicles of such shape that the top end of the straight edge makes first contact then the geometric trace of 1000 mm wrap around distance, will be used as bonnet leading edge reference line at that lateral position.
- '1000 mm Wrap Around Distance' is the geometric trace described on the top of the bonnet by one end of a 1000 mm long flexible tape, when it is held in a vertical fore and aft plane of the car and traversed across the front of the bonnet and bumper. The tape is held taut throughout the operation with one end held in contact with the ground, vertically below the front face of the bumper and the other end held in contact with the bonnet top. The vehicle is positioned in the normal ride attitude.
- Similar procedures shall be followed, using alternative tapes of appropriate lengths to describe 1500 and 2100 mm wrap around distances.

According to APROSYS (2005), corridors were obtained from each of the vehicle segments as shown in the Figure 8-16.

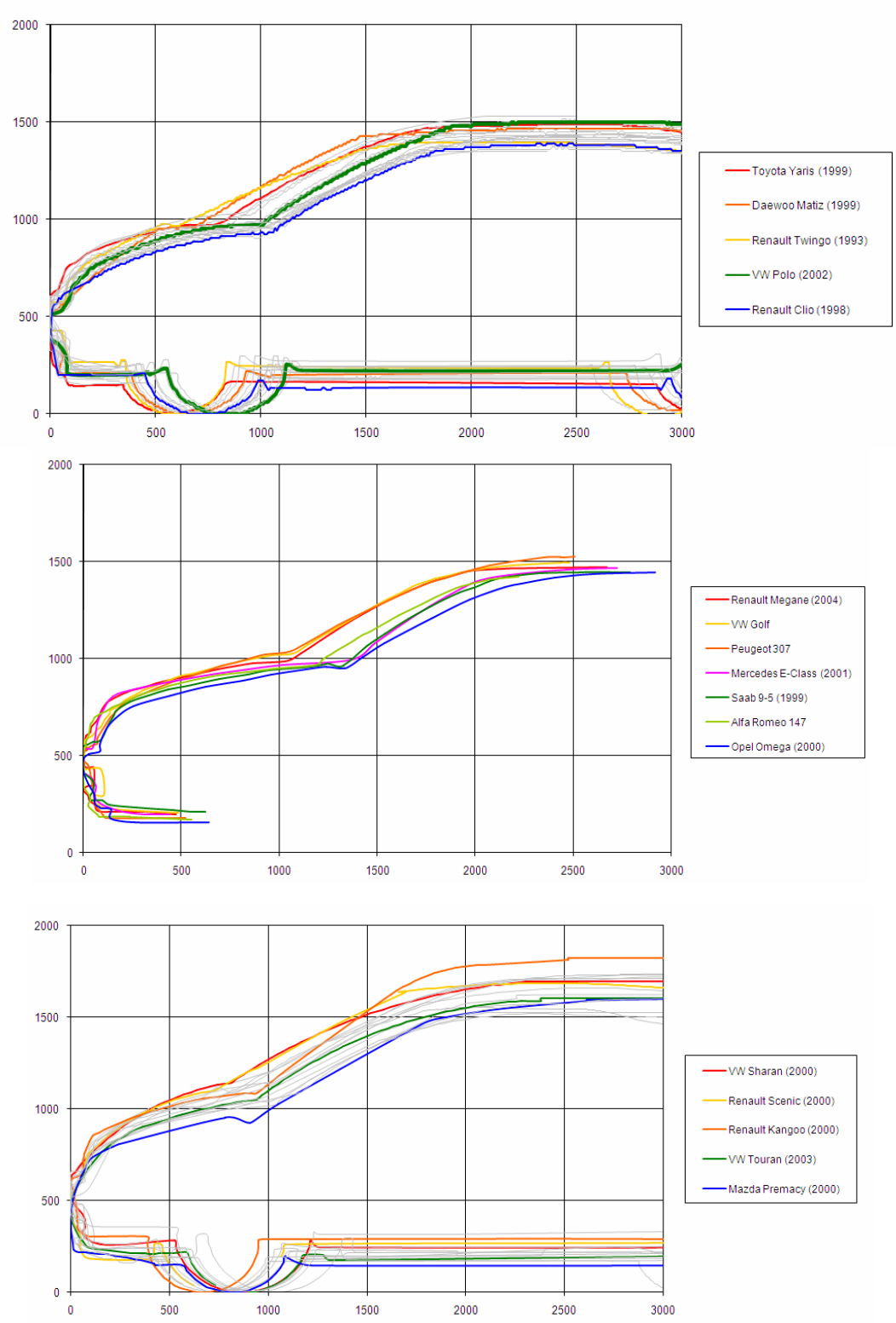

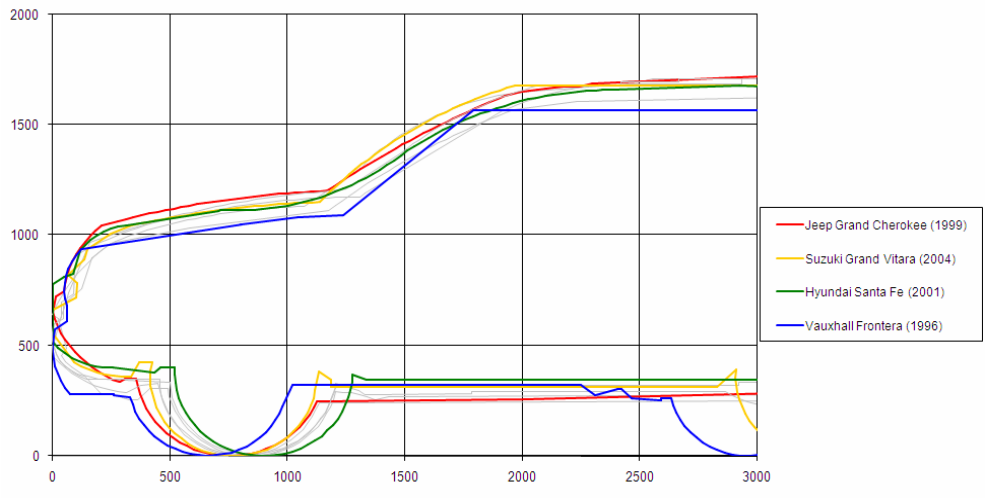

Figure 8-16: Average real vehicles from the vehicle segment corridors derived from APROSYS (2005).

It can be observed that the four vehicle segment corridors show significant difference from a pedestrian analysis point of view. While in the bumper area, there are clear overlapping in the corridors, bonnet length and angle and windscreen starting WAD and angle lead to clear corridors for the four segments.

However, as in this case, the focus is put on leg injuries and for that, the critical parameters are those from the bumper area, the SMC can be put together with the FC reducing the different segments to three:

- Family car (FC): Grouping SMC and FC.
- Multipurpose Vehicle: MPV.
- Crossover vehicle (SUV).

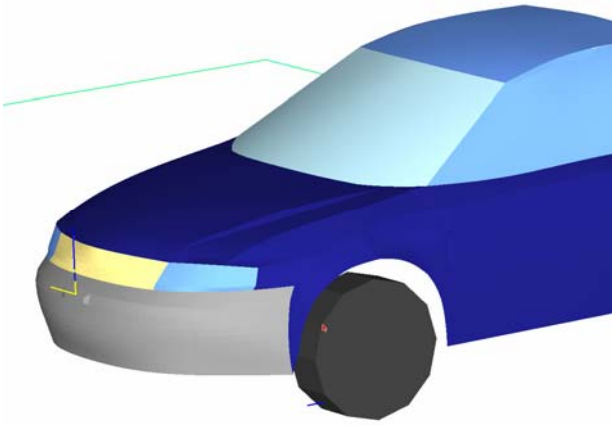

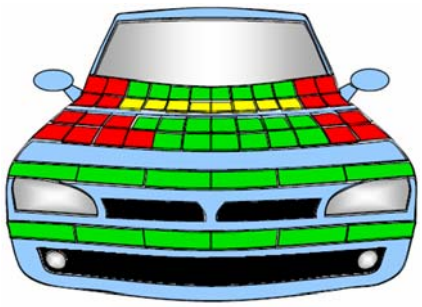

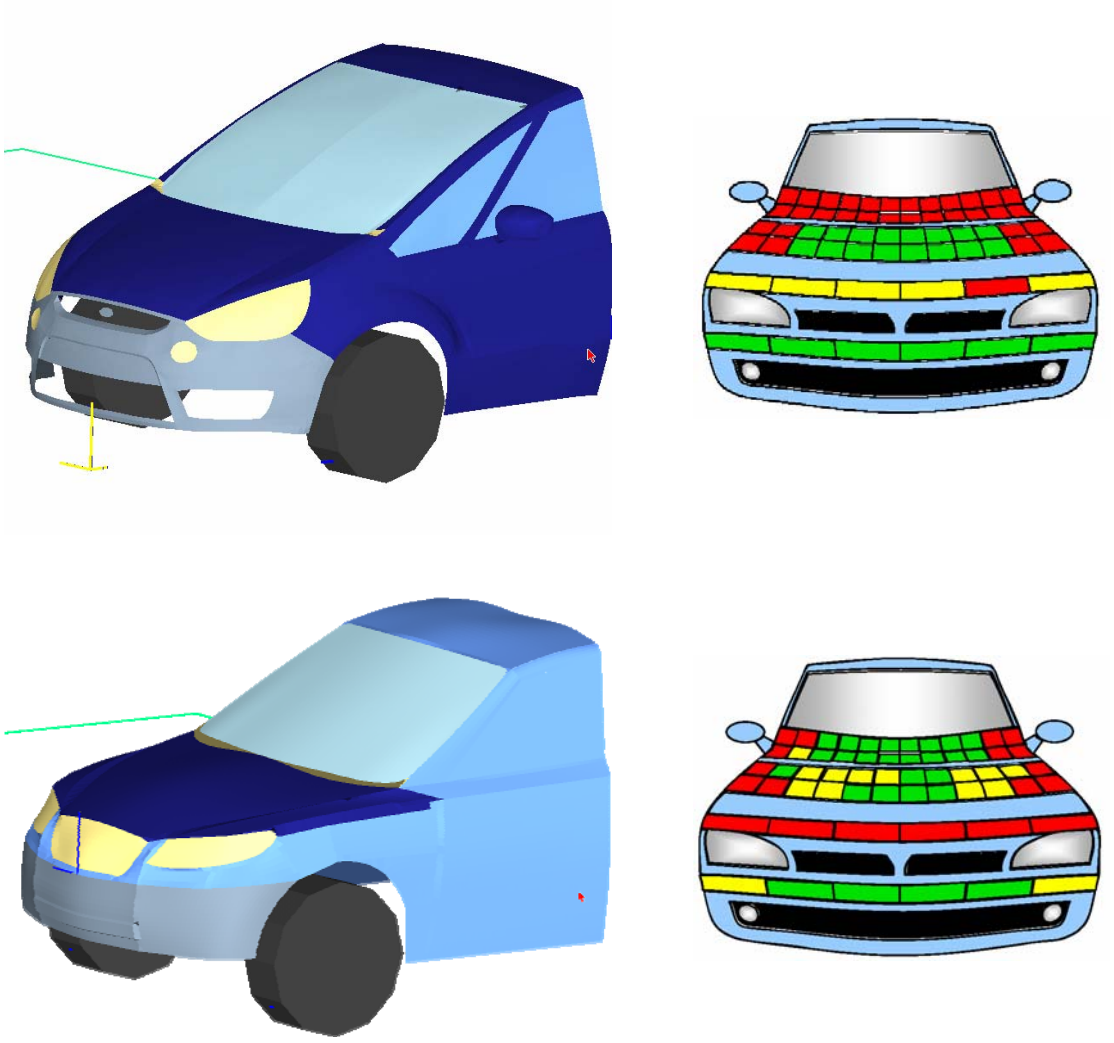

Figure 8-17: Selected vehicles and stiffness in each segment.

For each of the three segments a real vehicle has been selected (Audi A3, Ford S-Max, Hyundai Santa Fe) and their mathematical model developed with facet surfaces.

In terms of stiffness, the best rated maps of the segment have been used since they take already into account the current status of pedestrian safety solutions and any derived recommendation would be a step forward to improve cars already pedestrian friendly (Martinez, 2003).

In this case, all the impact areas of the bumper of the vehicles are fitted with “green” stiffness in the FC and the MPV while only some yellow stiffness is used for the corners of the SUV.

Regarding the bonnet leading edge area, also typically involved in the impact with the upper leg of the pedestrian, in the FC it is implemented with green stiffness, in the MPV is mainly fitted with yellow stiffness while in the SUV case the red stiffness is used.

8.4 Simulation matrix 1: THUMS vs. different vehicle segments.

As commented previously, this chapter aims to gain insight into the real world scenario basis for the pedestrian legform test procedure, highlighting the current limitation and providing evidences to propose improvements to this procedure.

For that, a first simulation matrix has been undertaken with a standing THUMS 50%ile FE human body being impacted with different vehicles at speed of 40 km/h. The kinematics of THUMS, with respect the three vehicle segments, is presented in the next figures for the relevant time window for the simulation.

	0 ms	15 ms	25 ms	40 ms
FC	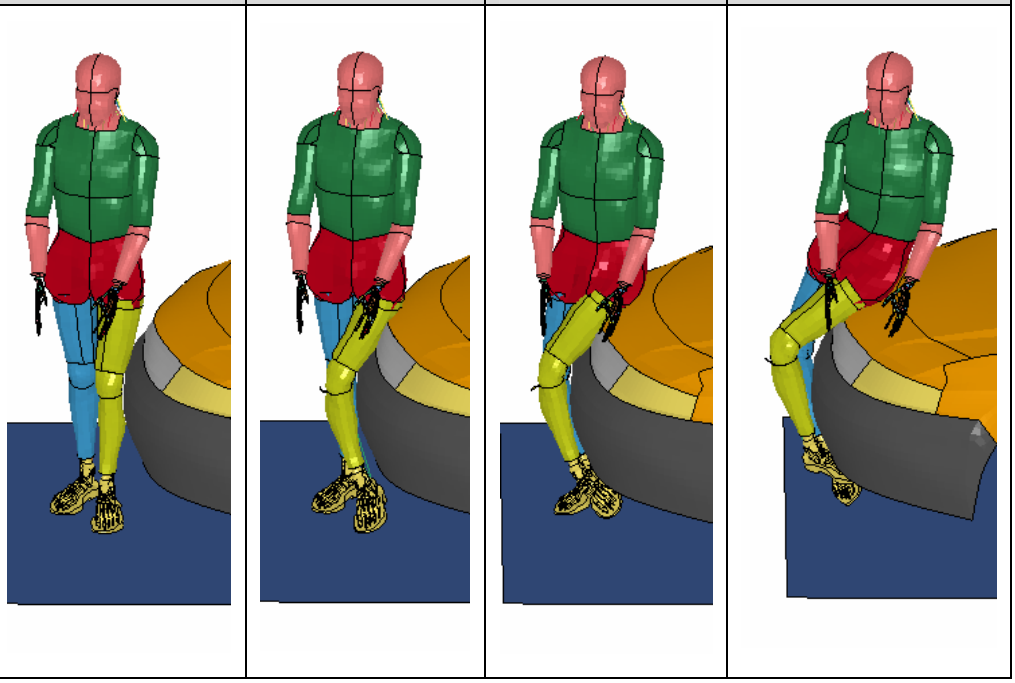			

Table 8-2: THUMS kinematics within the FC vehicle segment.

It is observed for the FC case that THUMS tibia supports a significant bending load during the whole kinematics as the impact with the vehicle occurs in the upper part of the tibia. This impact, together with the latter lower support at the low level, makes the tibia to bend between its epiphyses but without reaching to tibia fracture.

Regarding the upper body part, as the vehicle front is rounded, little support is given to the femur and therefore a high rotation of the whole body occurs towards the car bonnet.

In the case of the MPV, the impact occurs directly in the knee region and thus creating a load share between the tibia and the femur, making them to rotate similarly in the first instants of the impact.

	0 ms	15 ms	25 ms	40 ms
MPV	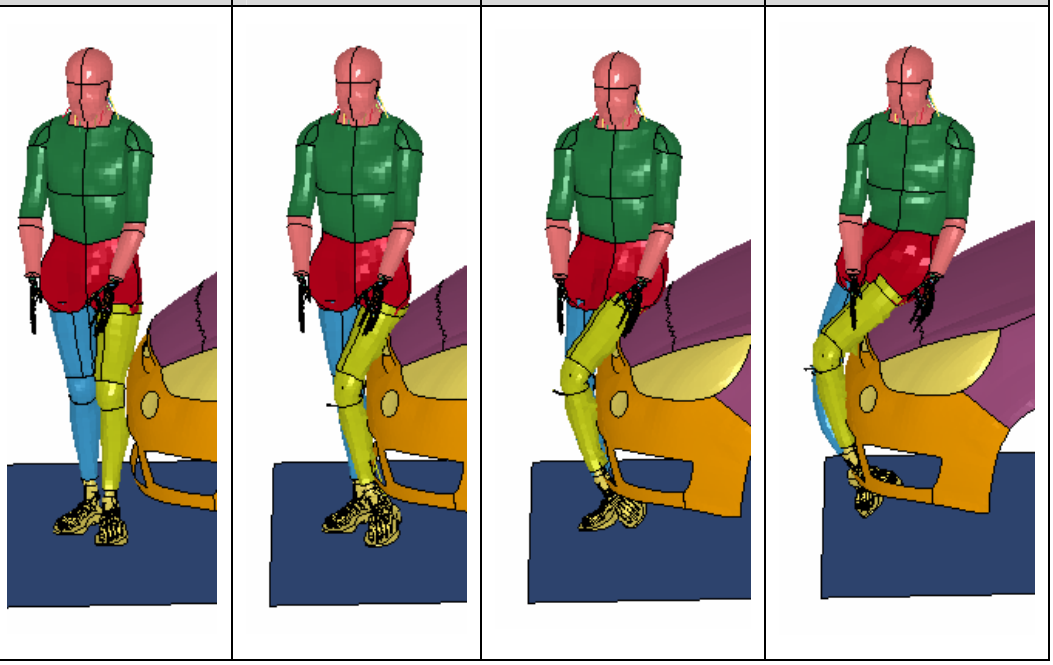			

Table 8-3: THUMS kinematics within the MPV vehicle segment.

	0 ms	15 ms	25 ms	40 ms
SUV	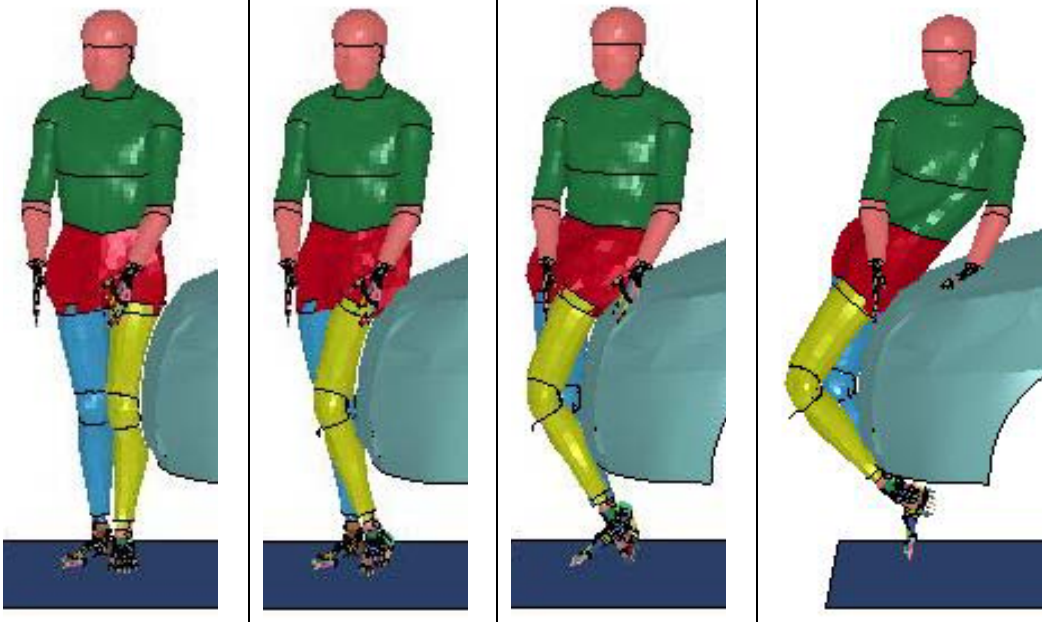			

Table 8-4: THUMS kinematics within the SUV vehicle segment.

As a result of this first impact, the THUMS model is pushed upwards from the knee, making the femur and the pelvis area to move towards the bonnet leading area of the vehicle. In a later stage, the tibia is impacted with the lower part of the bumper, being forced to bend as a whole section because the knee and the femur are already supported onto the bonnet and bumper leading edge of the vehicle and the lower part of the bumper offers support to the lower part of the tibia.

In the case of the SUV, the impact is clearly biased to the femur area, with very little support to the tibia. In this case, this lack of support for the tibia implies a high rotation as a rigid body when it is pulled by the knee, which is also significantly involved in the direct impact. As the vehicle front pulls upwards from the femur, the whole body is lifted from the ground early in the impact, delaying the femur and pelvis rotation towards the vehicle bonnet.

A node tracking analysis has been performed in all simulations, registering the position of a total 18 nodes along the leg with respect to the knee. This tracking analysis is plotted together in the next figure to analyze the kinematical differences across the three scenarios specifically for the impacted lower limb. It can be seen that, as previously commented, great difference occurs in terms of the tibia movement within the impact. While in FC and MPV cases, the tibia bending angle is significantly lower than the femur bending angle, in case of the SUV they are of similar magnitude.

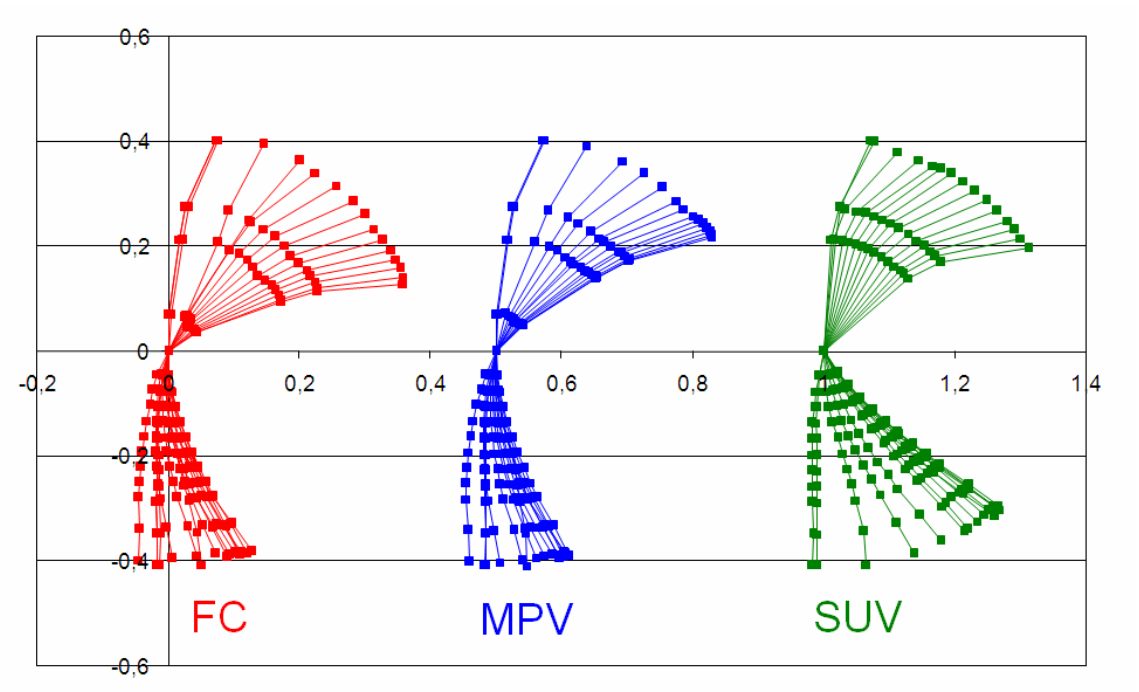

Figure 8-18: Kinematic difference of THUMS leg vs different vehicle segments

It is also observed that the bending of the femur also show important differences linked to timing. While in FC and MPV the femur bending is very high and starts to occur once the

first impact has occurred, in the case of the SUVs, this bending does not follow this first impact but it is delayed by a previous upwards movement of the whole supported femur.

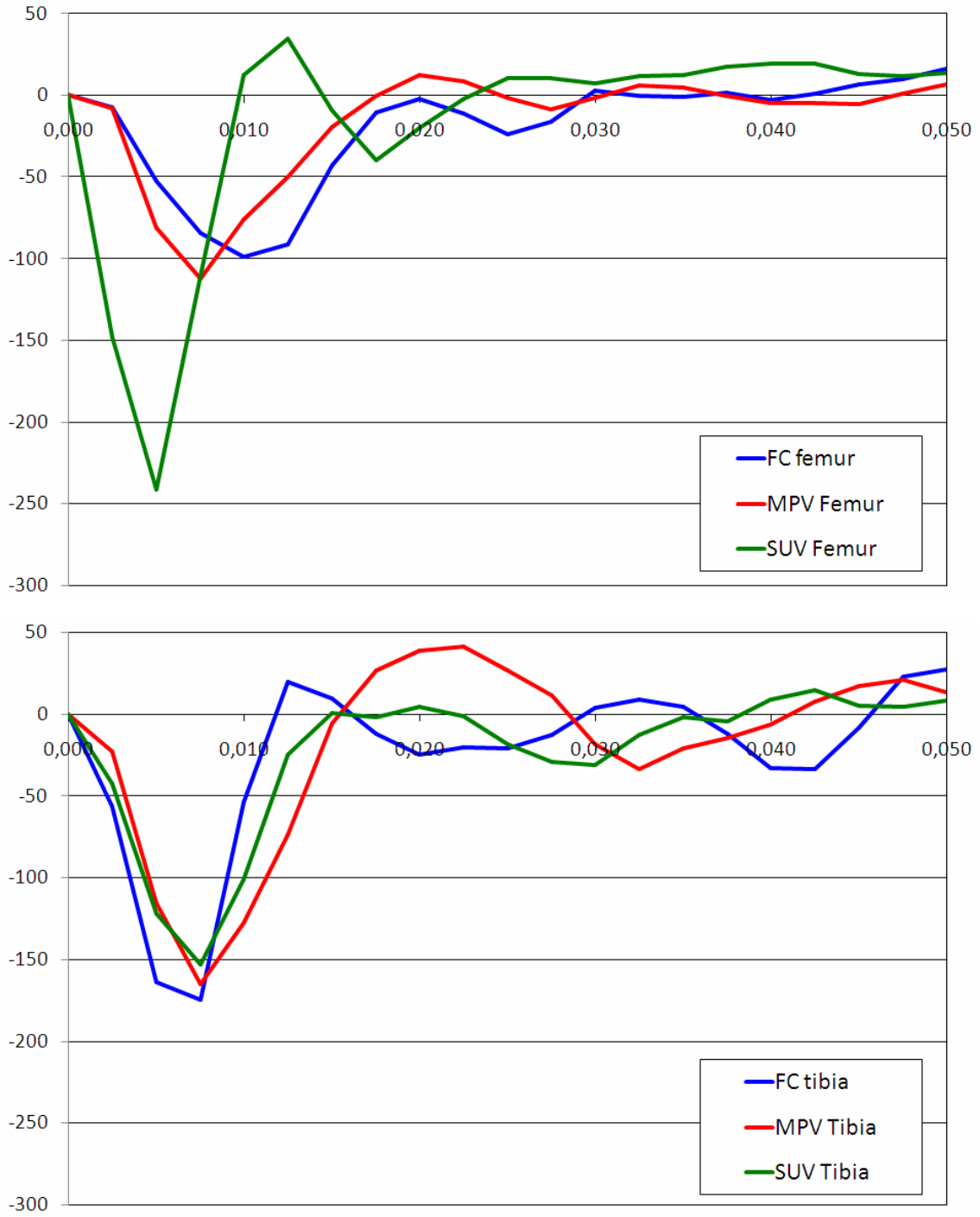

Figure 8-19: Femur and tibia accelerations (g) in the THUMS model in the different scenarios.

This difference is also highlighted looking to the tibia and femur acceleration of the simulations. While in the case of FC and MPV the femur maximum acceleration is close to 60%-70% of the tibia acceleration, in the case of the SUV this is reversed and the femur maximum acceleration is 1,5 times that from the tibia, changing the logic of the whole body kinematics.

Looking in fact in detail to the time history of the kinematics, not only in the case of the SUV the femur acceleration is doubling the FC and MPV cases, but also its maximum is reached before that from the tibia, while in FC and MPV occurs reversely. This change of order also indicates that the whole body kinematics shows significant differences.

	FC	MPV	SUV
Femur max acceleration	99 g	113 g	234 g
Tibia max acceleration	174 g	165 g	150 g
Ratio femur-tibia	0.56	0.68	1.56

Table 8-5: Ratio max femur acceleration and max tibia acceleration.

8.4.1 Analysis on the injury prediction.

Since THUMS model is equipped with injury prediction capabilities within the knee ligaments and the main bones of the lower legs, the occurrence of knee ligament ruptures and/or long bone fractures has been analyzed for all the scenarios, and it is reported in the next table and figures.

Injury	FC	MPV	SUV
Shaft bone fracture	No. Max. plastic strain 0.022 (interior part of the femur, 35ms)	No. Max. plastic strain 0.0207 (interior part of the tibia, 20 ms)	No. Max. plastic strain 0.0215 (interior part of femur, 25ms)
Ligament rupture	Yes. Medial Colateral, Anterior and Posterior Cruciate ligament rupture	Yes. Medial Colateral, and Anterior Cruciate ligament rupture	Yes. Medial Colateral ligament and, Anterior Cruciate ligament rupture

Table 8-6: Injury outputs of the THUMS model.

As it can be seen in the following figures, no shaft bone fracture is predicted in any of the models although in all of them plastic strain is found. On the other hand, multiple knee ligament ruptures are always found and in most cases it leads later to knee instability.

The evaluation of the stress distribution in THUMS legs for the FC shows that the load distribution starts in the knee region and extends for both femur and tibia bones. In this process, there are areas where the bones do reach plastic strains below the plastic strain limits up to similar maximum values, however, later in time, the femur reach higher plastic strain than the tibia.

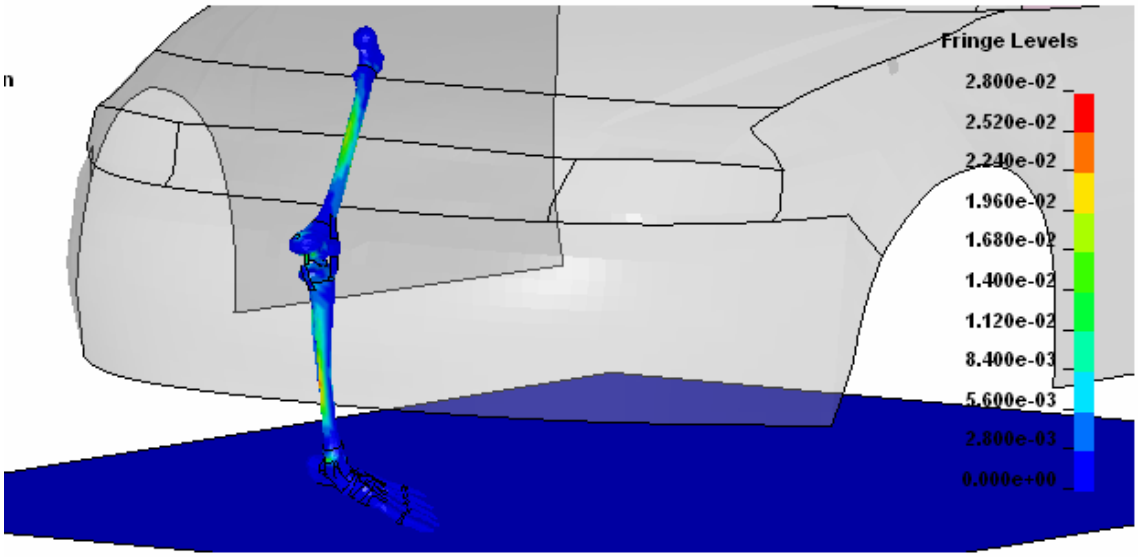

Figure 8-20: Plastic strain distribution in the THUMS legs in the FC case.

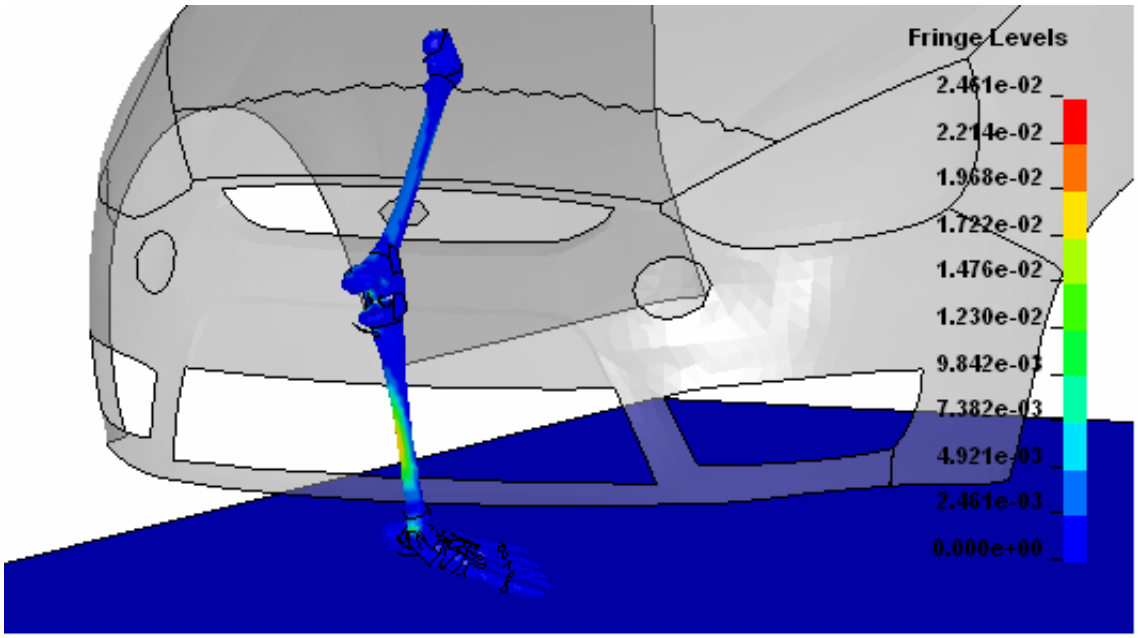

Figure 8-21: Plastic strain distribution in the THUMS legs in the MPV case.

In the case of the MPV, the initial impact distributes the load between the tibia and the femur, however in this case this distribution is biased towards the tibia where much more support is found, especially in its lower part, exceeding its yield stress but without reaching the plastic strain failure limits implemented in the model.

In the case of the SUV, in the initial impacts much of the energy is directly translated to the femur, reaching significantly higher values of stress and plastic strain than the tibia, which is just pulled by the remaining ligaments. In any case, high plastic strain is found in the femur but without reaching to the failure limits.

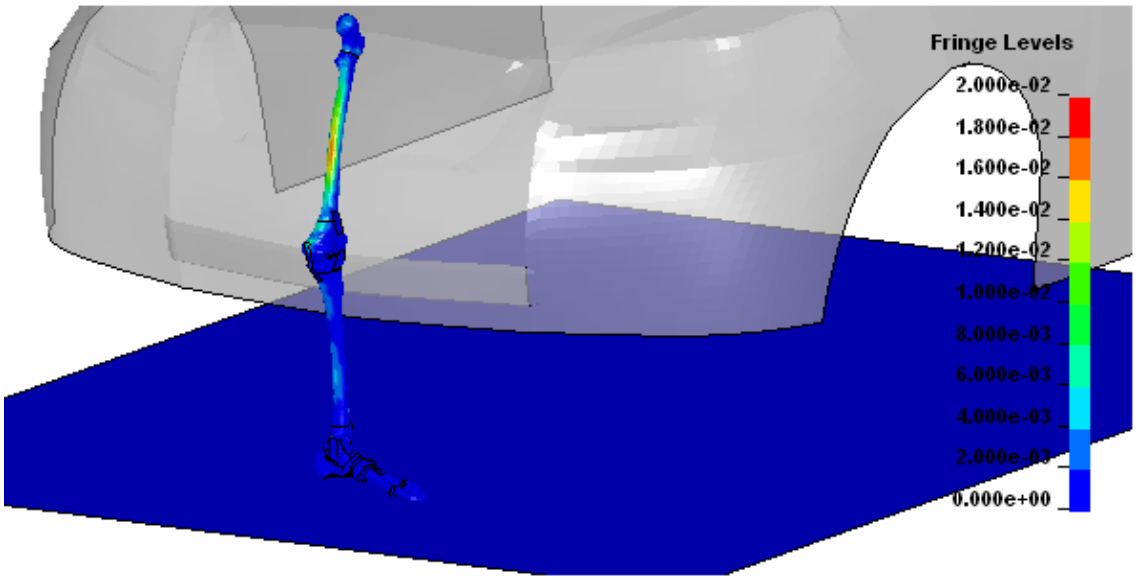

Figure 8-22: Plastic strain distribution in the THUMS legs in the SUV case.

In terms of ligaments, the same pattern is found in the three cases. First the MCL fails at the beginning of the impact and after that, the cruciate ligaments failed as they are not able to withstand the load needed to keep the tibia and femur condyles together without the MCL. This multiple failure leads to knee instability in all cases reaching high stresses in the tibia and femur condyles where the ligaments are inserted.

This multiple knee failure does also lead to very high values of knee bending in the impact.

8.5 Simulation matrix 2: Legform impactor vs. different vehicle segments.

In order to compare these real world pedestrian results with the outcome of the current pedestrian legform procedure a second matrix is undertaken using the same vehicle models. This time the EEVC legform impactor is impacting at 40 km/h and in free flight to the middle of the different vehicle front ends, reproducing the real setting of the pedestrian legform test configuration from Directive 102/2003 EC. The kinematics of the legform

impactor along the different vehicles is presented in the next figure for the relevant time window of the simulation.

	0 ms	15 ms	25ms	40ms
FC	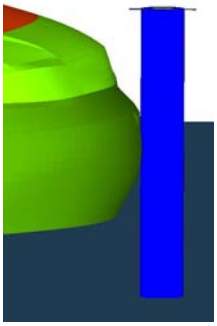	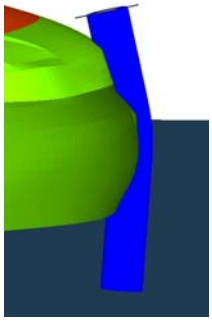	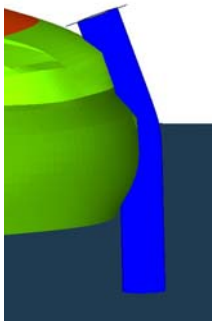	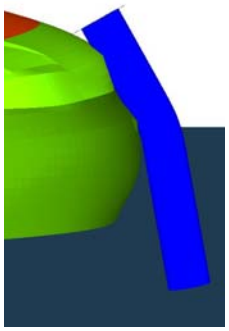
MPV				
SUV	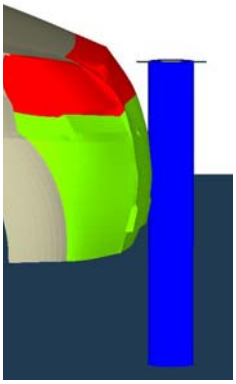	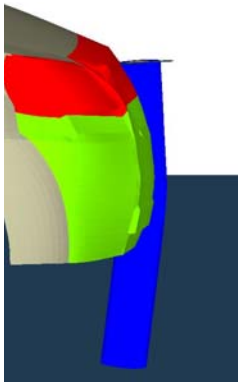	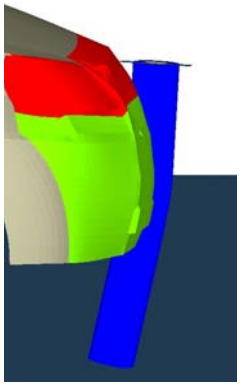	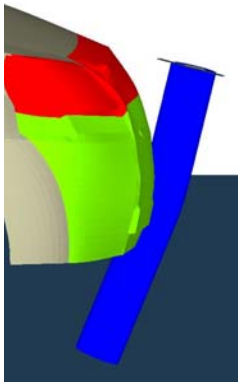

Table 8-7: Legform Impactor kinematics along the different vehicle segments.

It can be seen that the behaviour along the three vehicles is rather different. In the first case, the FC is impacting the legform below the knee level. It offers significant support to the tibia upper part while the femur bends slightly until it finds support on the grill. Following that phase, the whole impactor is forced to rotate towards the car bonnet already with a fixed knee angle.

In the case of the MPV, the impact is more centred in the knee region and both the femur and tibia bends similarly until they found support, in the lower part of the bonnet for the tibia and the grill for the femur. With this fixed knee angle, the whole impactor starts a rebound phase out of the relevant time window of the test.

Finally in the case of the SUV, the impact clearly takes place above the knee impacting the bumper on the femur region of the impactor. This impact leads to a rearward rotation of the impactor that, together with the lack of support of the lower part of the tibia makes the impactor to rebound from the vehicle with a significant reduced knee bending angle.

As in the previous case, the kinematics is being plotted in reference to the knee in the next figure. As the two section of the impactor are rigid only the nodes in the extremes as well as the knee are tracked. It can be observed in the figure the overall rotation of the impactor, towards the car in the FC and reversely in the SUV case while in the MPV such rotation is rather smaller.

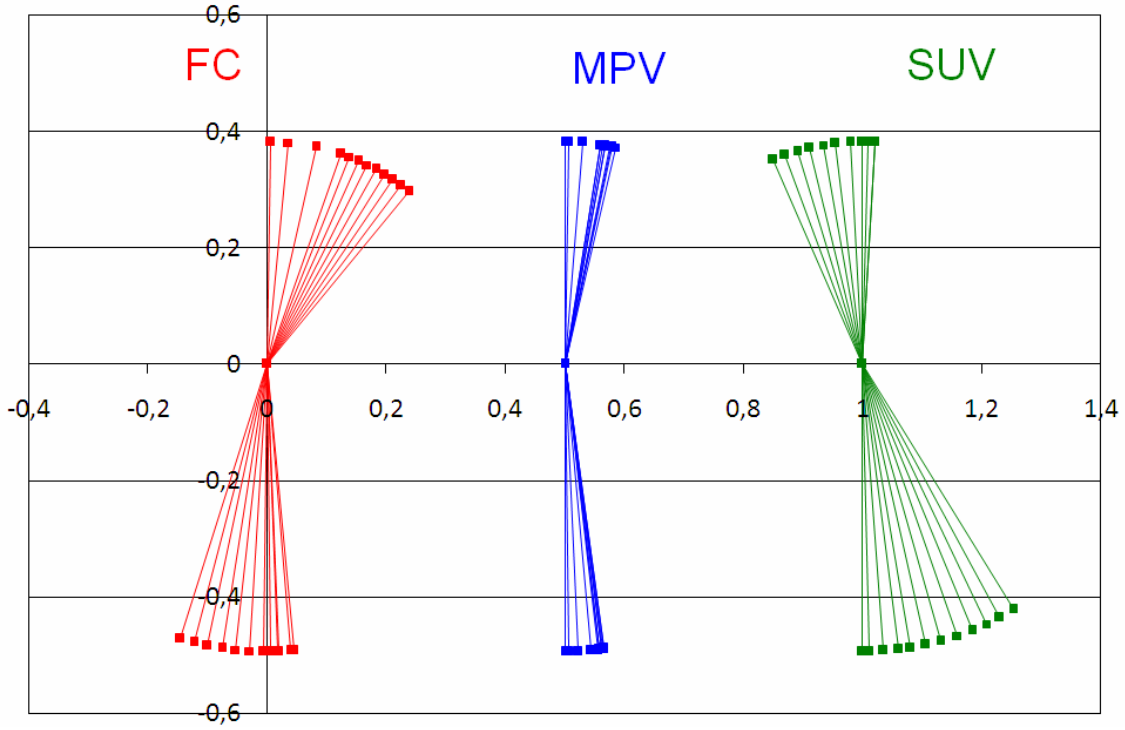

Figure 8-23: Kinematic difference of legform impactor vs different vehicle segments

It can be seen for the FC that both femur rotation and tibia rotation with respect to the knee increases during the impact, reaching a point where maximum bending is achieved. Once this point is achieved, the whole impactor rotates significantly towards the vehicle. As the tibia finds good support in the bumper the femur is the main contributor to the knee bending angle.

In the MPV case, as the impact is rather more centred both femur and tibia contributed similarly to the knee bending angle. In this case no whole rotation is observed but a kind of rebound from the vehicle front end.

Finally in the SUV case, basically the tibia is the only that contributes to the limited knee bending angle observed. The lack of support on the tibia together with the impact point in the femur induces a rearwards rotation of the whole impactor.

	FC	MPV	SUV
Femur max acceleration	77 g	97g	115g
Tibia max acceleration	99 g	100g	85g
Ratio femur-tibia	0.77	0,97	1.35

Table 8-8: Ratio max femur acceleration and max tibia acceleration.

These behaviours are also supported looking to the tibia and femur accelerations.

It can be seen that for the FC the tibia is more relevant in the impact, in the MPV cases, femur and tibia suffered similar accelerations while in the SUV case, the femur has higher acceleration and the rearwards rotation induced diminishes tibia expected acceleration. In the three cases, instability seems to take place in the rebound phase.

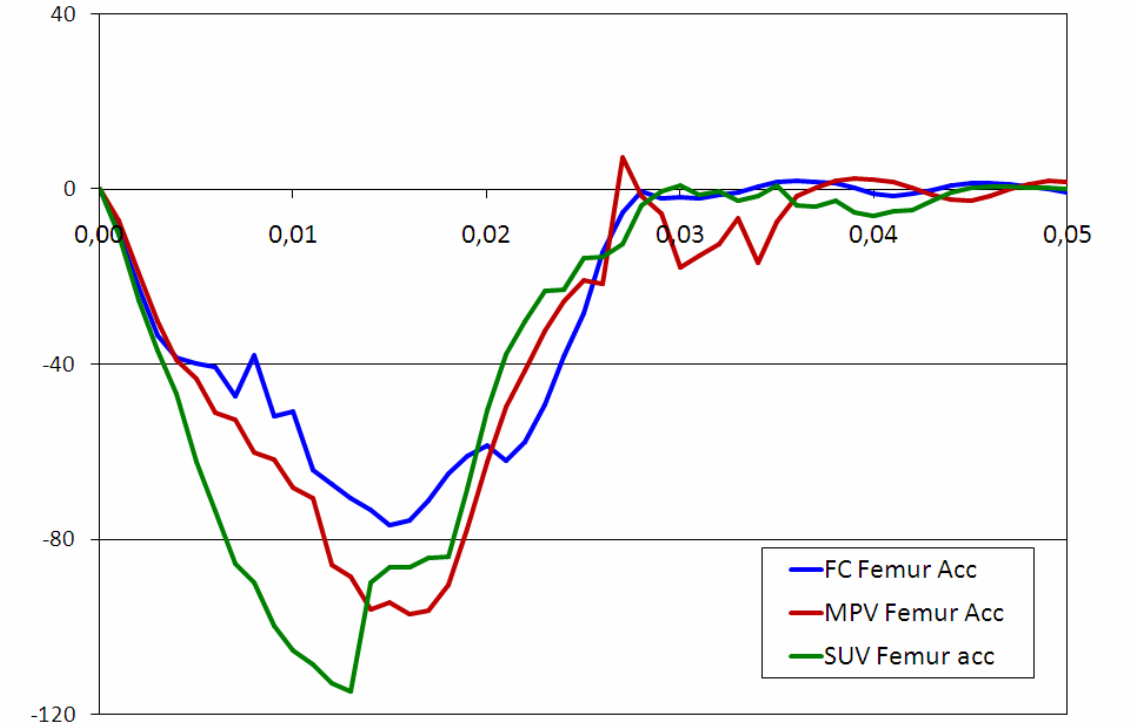

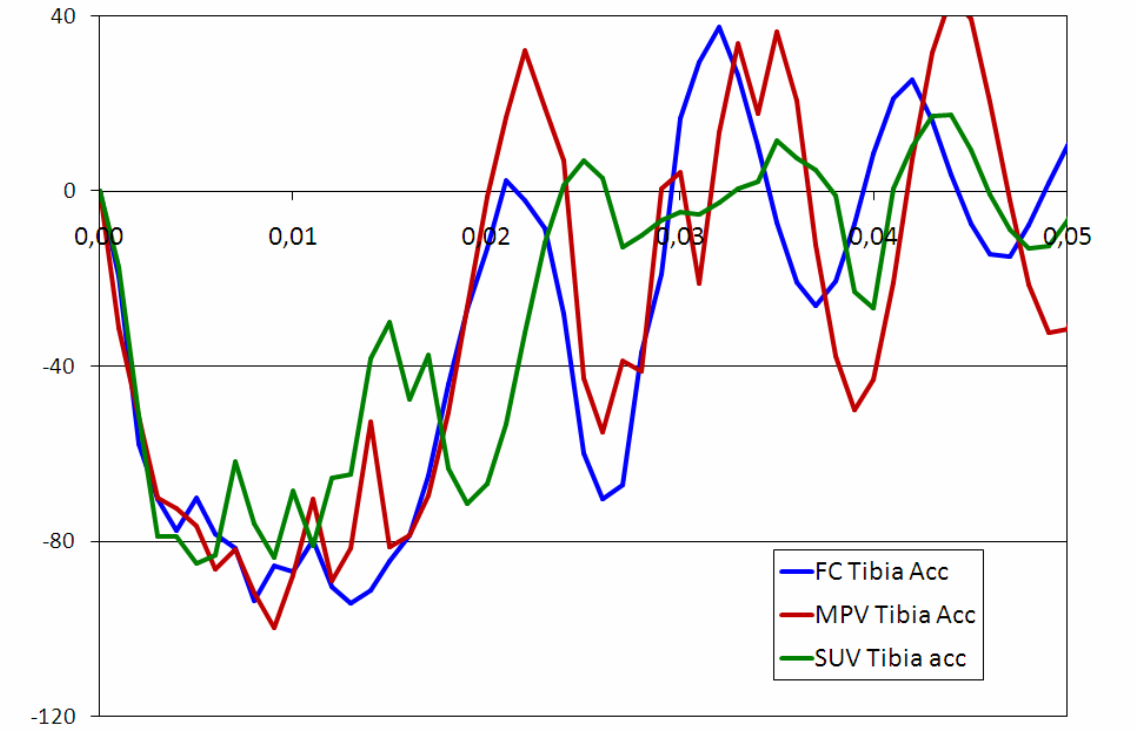

Figure 8-24: Femur and tibia accelerations (g) in the impactor in the different scenarios.

8.5.1 Analysis of the injury prediction.

The injury prediction capabilities of the legform impactor are based on three injury criteria, as defined by EEVC WG10, 1998 and EEVC WG17, 2002, namely, knee bending angle, knee shear displacement and tibia linear acceleration. Knee shear displacement and knee bending angle are linked to knee ligaments failure while tibia linear acceleration is linked to the prediction of bone fracture.

The acceptance levels for the knee bending angle were based on studies from Kajzer (1997) on cadavers concerning the shearing and bending effects in the knee joint at high speed (i.e. 40 km/h) lateral loading. When the preloaded cadaver knee was exposed to a bending deformation the two most common initial damage mechanisms occurred when the knee was bent laterally at an average angle of 15° for ligament avulsion failure or at an average angle of 16° for diaphysis/metaphysis failure. Using a similar test set-up and similar analysis techniques using the impactor (i.e. looking for initial damage values) they found a lateral bending angle of 15° in the legform bending test, which is identical to the average angle found in the cadaver tests. 15º as an acceptance level was the one proposed by EEVC. However, as this 15º was the bending angle were first damages were achieved but the angle increased still due the impact force, in the different pedestrian Directives this acceptance level was discussed and finally relaxed to 21º in Directive 2003/102/EC phase I and 19º in Directive 2009/78/EC phase II.

In the case of shearing, EEVC WG10 (1991) proposed an acceptance level of 6 mm for shear displacement, which was based on impact forces of 4 kN causing lateral shear displacements of 5-6 mm in cadavers. According to autopsies made after these tests it was found that rupture of the anterior cruciate ligament (ACL) is the typical injury associated with shearing mechanisms. When pulled it can be considered that about 25-30 mm of the ligament is lengthened and with an elongation at rupture of 20% (Yang, 1994), this corresponds to a limit of 5-6 mm for shearing displacement.

In later studies from Kajzer, (1997) it was found that when the preloaded knee joint of the cadavers was exposed to a shearing deformation at 40 km/h the two most common initial damage mechanisms occurred at an average peak shearing force of 2.4 kN for epiphysis failure or an average 2.9 kN for diaphysis/metaphysis failure. These shear forces were rather close to the 4 kN shear force taken as reference by EEVC WG10 to define the 6 mm acceptance level on the impactor shear displacement, so EEVC WG17 confirmed this 6 mm of shear displacement as acceptance level. This 6 mm have been maintained in the pedestrian Directives as acceptance level for shear displacement.

In the case of the tibia lateral acceleration two test series are the basis of the discussion for the acceptance levels.

Cesari (1998) performed a series of cadaver tests at average speed of 32 km/h. In 5 of the 11 cases tibia fractures were found, while 8 cadavers sustained AIS2 and/or AIS3 knee injuries. The maximum tibia acceleration for the cadavers sustaining a tibia fracture was 170g-270g (average 222g), while it was 185g-243g (average 202 g) for the cadavers sustaining no tibia injury

Bunketorp (1983) also performed a series of cadaver tests using both rigid bumpers resulting in tibia accelerations all above 200g and compliant bumpers resulting in tibia accelerations all below 120g. The 10 rigid bumper tests resulted in 7 lower leg fractures and the 10 compliant bumper tests in 2 lower leg fractures.

Rodmell (1998) derived injury risk functions from Bunkertorp (1983) using a cumulative normal distribution method using only fracture cases and compared it to the logistic regression method using all the data, both fracture and non-fracture. It is believed that the first method, analysing only the fracture case data, results more in a fracture distribution curve rather than in an injury risk curve, and therefore the second was preferred by the EEVC.

Based on that, EEVC WG17 recommended an injury risk level for tibia injury of 20%, resulting in approximately 160g according the cumulative normal risk injury risk function. As EEVC WG10 acceptance level was 150g for lateral tibia accelerations, assuming a good correlation between cadaver and impactor tests, it was decided to maintain this 150g as it already represented almost 20% of AIS2+ injury according to the previous injury risk curve.

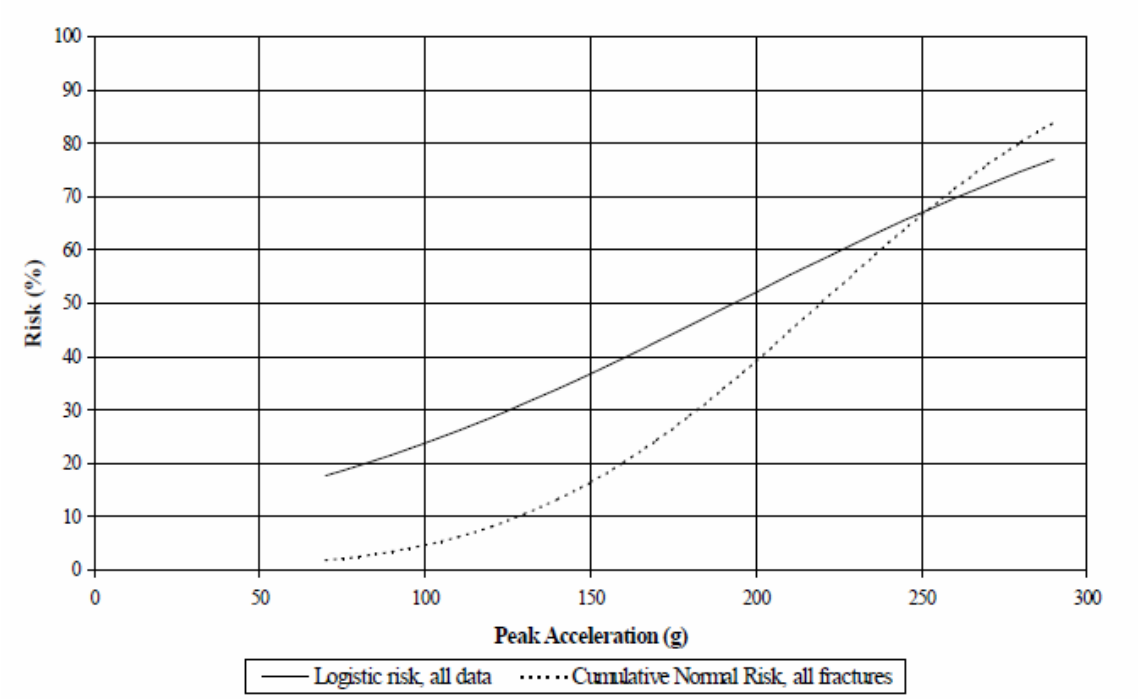

Figure 8-25: Comparison of AIS 2+ lower leg injury risk functions based on a logistic method and based on a cumulative normal method. EEVC WG17 (2002)

However, since this 150g seems to be too stringent, especially if compared with results from Cesari (1998) this acceptance level was discussed further when drafting the pedestrian Directive and finally relaxed to 200g in Directive 2003/102/EC phase I (approx. 50% risk of AIS 2+ lower leg injury) and 170g in Regulation 2009/78/EC phase II (approx. 25% risk of AIS2+ lower leg injury).

These three parameters have been measured in the three models and summarized in the next table.

Injury criteria	FC	MPV	SUV
Tibia acceleration	99 g	100g	85g
Knee bending	21º	20º	10º
Knee shear displacement	1.5 mm	1.45mm	1.30mm
Predicted injuries (EEVC WG17 (2002) criteria)	Knee ligament injury. No tibia fracture	Knee ligament injury. No tibia fracture	No knee injury. No tibia fracture

Table 8-9: Injury outputs of the impactor model.

It can be observed that the three tibia acceleration and the knee shear are rather below the acceptance levels while the knee bending angle is close or above the acceptance level depending on which it is considered.

As the vehicle models used had a compliant bumper scored green in EuroNCAP rating, tibia acceleration was already expected to be low since this measure is directly linked to bumper stiffness. However, knee parameters are not so stiffness dependent but geometry dependant and the tested models show lack of coordinated support in the tibia and femur part to limit knee bending.

According to EEVC original acceptance limits, which were the most stringent ones, in the FC and MPV cases the impactor would predict knee ligament injuries while in the SUV case would predict no injury at all.

If the legform behaviour is compared to the one shown with the full FE human models, there are a number of issues to be highlighted:

- The overall rotation of the impactor towards the vehicle observed in the whole FE human body is reproduced well for the FC and MPV but not by the SUV case.
- The bending effect on the tibia of the full FE human body is not reproduced by the rigid parts of the impactor in none of the cases due to obvious reasons, however, similar acceleration values are found for the tibia in all cases.
- The femur accelerations ratio found in full FE human body and the impactors are rather aligned in the FC and MPV cases, while for the SUV case, a reversed effect is observed.
- The knee bending angle found in the FE human models is in general larger than in the case of the impactors due to the knee instability where most ligament fails. Looking more in detail when these first disturbances appeared in the knee and linking it to the knee bending angle it is observed that these knee bending angle were 12º for FC, 10º for MPV and 11º for SUV.
- The contribution to knee bending from THUMS tibia and femur in the FC cases and the MVP cases are alike to those found with the impactor while in the case of the SUV the relative symmetry found with the FE human model is hardly reproduced by the impactor.
- As the impact point with the SUV and the impactor stands above the centre of gravity (CoG) of the whole impactor and it has no upper body mass, the compensating effect it has in this type of impact does not exist, leaving to a limitation of the usage of this impactor in these environments.
- In terms of injury risk assessment it can be observed that the injuries were well predicted with the legform in FC and MPV cases but not for the SUV case. In this

case, as the impactor is no longer representative of a real pedestrian, the Directive would suggest a direct femur impact with the upper legform impactor but no longer evaluating the possible existence of knee injuries that, as shown in the FE human model impacted by the SUV are likely to occur in these scenarios.

This set of conclusions would suggest that the impactor is fitting its testing purpose for the FC and the MPV cases, but not for the SUV case.

The key issue of that limitation is the lack of the upper body mass in the impactor, which is especially critical when the impact with the vehicle occurs close or above its overall centre of gravity (CoG).

In the full body pedestrian tests, as its overall CoG is in the pelvis area (In the THUMS FE human model at 1.014 m from the ground reference level), the impact with the vehicle is always occurring below its CoG, so the upper body mass creates a compensating effect during the impact. As the impactor lacks this effect, neither the kinematics nor the injury assessment is realistic in the impact with SUVs.

8.6 Recommendation of an improved legform test procedure.

Taking into consideration the essence of the problem: the impact occurs above the CoG of the impactor and this creates a not biofidelic response, the solution should focus on increasing such CoG to ensure that the impact would always occur below it, although it does not necessary mean that the impactor should have the same CoG than the human body.

For increasing the CoG of the impactor there are several options to be considered:

- Increasing the impact height in the test conditions. The test conditions as defined by EEVC and later translated to Directive 2003/102 defined that the impactor bottom should be at ground reference level at the moment of the impact, therefore if this height is increased it would have the same effect that increasing the whole CoG of the impactor.
- Adding mass in the upper part of the impactor. As the nature of the problem comes from a lack of upper body mass, an extra mass can be added in the upper part of the impactor and thus increase its overall CoG. The way this mass can be added is an extra issue since depending on the selected approach the design of the impactor can be maintained or radically changed.

Within the first approach, a number of reference (Matsui (2003), IHRA (2004), Konosu (2005)) have suggested that the design of the impactor itself was based on anthropometry measures without shoes, and typically pedestrian were wearing shoes when involved in the accidents. This issue is already been considered in the phase II of Directive 2003/102,

currently under Directive 2009/78, increasing the impact conditions to 25mm above the ground reference level.

Within the second, the nature of pedestrian test itself needs to be considered since the impactor needs to be propelled towards the vehicle at 40 km/h and if the mass is increased considerably this is not always technically feasible within the current state of the art of test apparatus. A mere mathematical approach to the problem done by Ratliff (2008) suggested an extra mass of 11 kg to be added in the upper end of the impactor, increasing its overall weight to 24.4 kg, which is on the limit of technical feasibility.

Moreover there are two ways of adding this mass on top:

- Re-adjusting the mass of the current femur of the impactor maintaining impactor overall height.
- Adding an extra section on top of the femur of the impactor and thus increasing the impactor overall height.

The selection of either of these options will have an effect in the behaviour of the impactor in the test environment, so, in this point a feasible optimization should be done, firstly analysing the minimum condition to guarantee that the impactor is always on acceptable working conditions for SUV cases, and secondly, analysing the technical limitations currently in place to ensure that the basics of this test are not altered significantly.

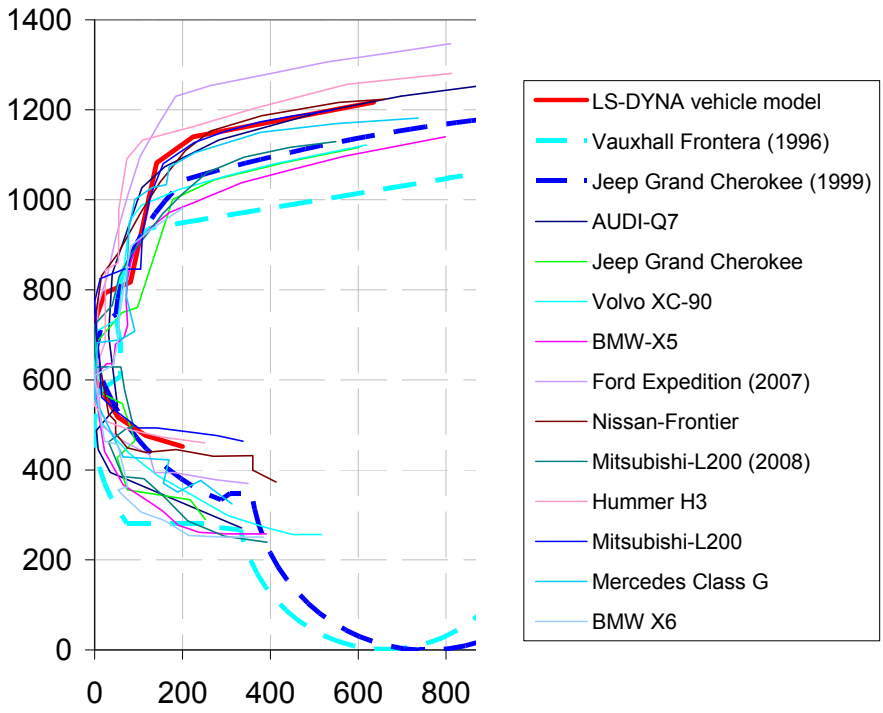

Figure 8-26: Extended SUV corridor bumper area measurements

To set this target conditions, the SUV corridor presented previously have been enlarged with other 13 models from the EU market to analyse its average bumper height and, therefore to set the minimum CoG increase needed in the impactor to cover properly most of them.

It can be concluded from the figure that typical European SUVs have an average LBR of 595mm and UBR of 780mm. Assuming that the impact with the impactor would occur in the medium part of this bumper, the target CoG of the impactor would be 680mm ± 25 to guarantee that the impactor would be impacted within or below its overall CoG in most cases.

Regarding feasibility limitations the first thing to consider is how the mass will be added to the impactor. If this is added to represent the upper body mass through a hip joint with the impactor, the whole legform will need a thorough re-design to accommodate this extra part accordingly and to ensure that in free flight conditions the impactor impacts the vehicle without a pre-rotation. This will also lead to a re-design in the test apparatus used to propel the leg and thus have an important associated cost to the test upgrade.

On the other hand, if the current legform design is maintained and the extra mass is added rigidly in its upper part, maintaining its overall dimensions and length, minor re-design will be needed in the impactor and the current testing equipments are still valid, given they are able to propelled an increased mass impactor.

Being this second option the most cost effective, it has been the selected choice. For that, a relationship is obtained between the CoG increase and the extra mass needed to achieve it in order to look for the minimum mass needed to be added. This relationship is plotted in the next figure together with indicative references of 50% and 100% increases in the overall impactor mass.

These two reference lines divide the figure in three clear areas where the cost, in terms of added mass, of increasing the CoG can be depicted. In the first area, it can be seen that with reduced added mass high CoG increases are obtained and this is less true once the overall CoG is intended to be higher than 650 mm.

Based on that, an considering the target set previously, it has been defined this 650mm as a feasible increased impactor CoG, which would mean to add in the upper part of the impactor a total of 5.3 kg. This mass would represent less than 50% of the current impactor mass and would increase the overall mass of the impactor to 18.7 kg which is still on the range of current test apparatus.

If this increase is combined with the one of increasing the impact conditions 25mm as suggested in the new Regulation, a total increase in the impactor CoG of 125mm would be achieved with minor changes in the impactor and thus with a low cost of implementation.

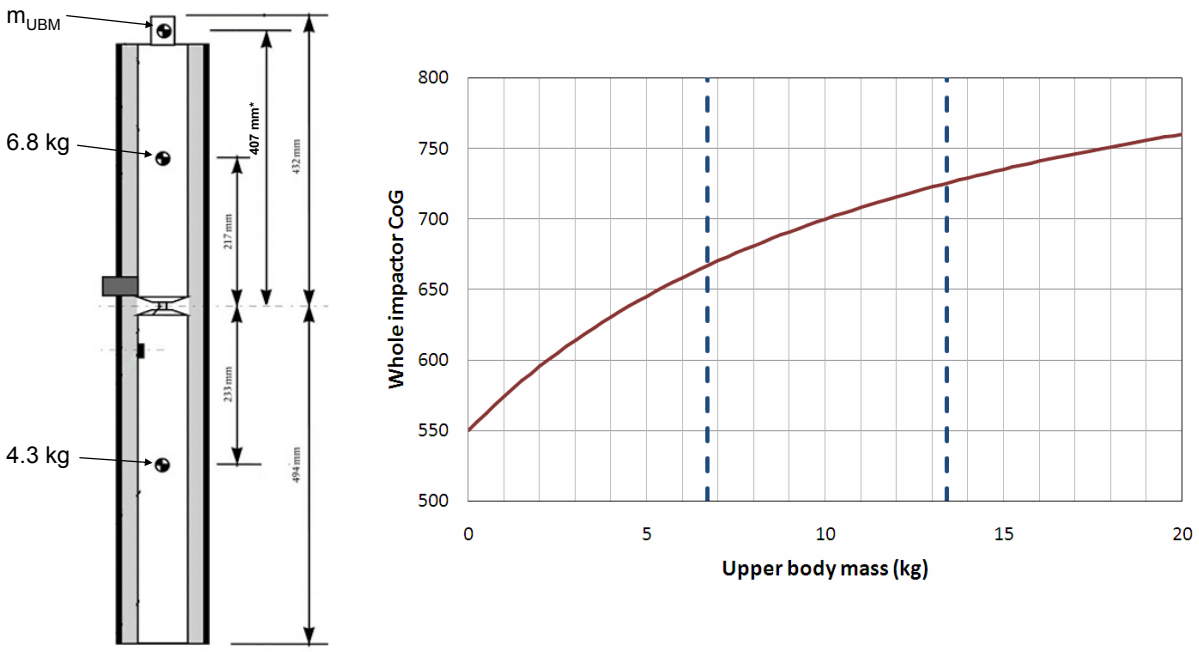

Figure 8-27: Relationship between the impactor CoG increase and the upper body mass to be added to the impactor.

To analyse how this upgraded test procedure would perform, the previous matrix has been replicated with these new conditions. Although the improvement of the impactor has been focus on the SUV segment, the FC and the MPV have been maintained in the matrix to ensure that the new impactor is still valid for those segments which were originally covered correctly by the impactor. The results of these simulations are presented in the next heading.

8.6.1 Analysis of the kinematics in the different scenarios.

The kinematics with the upgraded impactor is shown in the next figure and it is worth to compare it with the one from Table 8-7.

It can be seen that the FC is still impacting the legform below the knee level. The bumper supports the tibia upper part while the femur bends until it finds support on the grill. Due to the higher mass on the upper part of the femur, the femur bending creates a significant higher overall impactor rotation towards the car bonnet but without increasing the bending knee angle.

In the case of the MPV where the impact is now more centred in the upper part of the knee, both the femur and tibia bends similarly until they found support. However in this case, instead of the rebound phase seen in the original test a clear overall impactor rotation towards the vehicle is observed maintaining at this point the knee bending angle achieved so far.

	0 ms	15 ms	25 ms	40 ms
FC	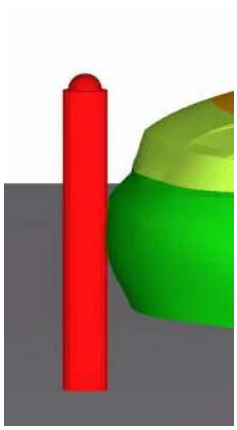	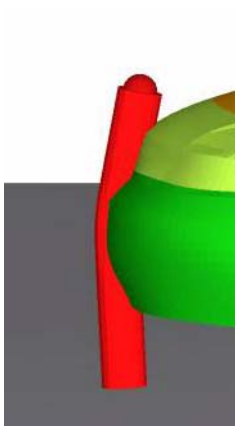	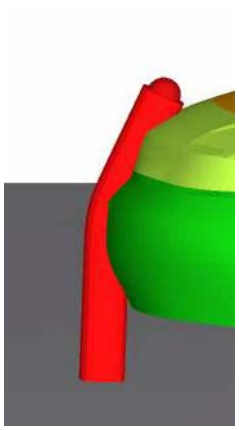	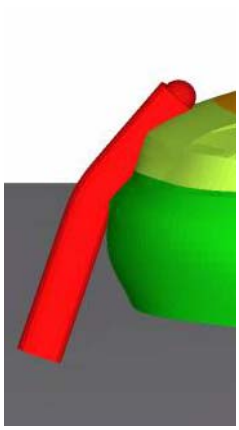
MPV	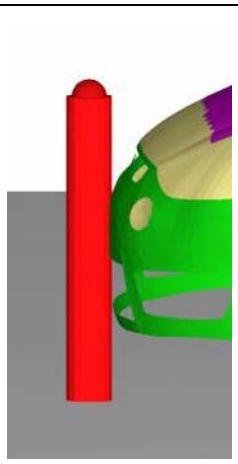	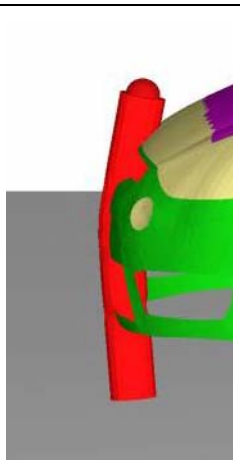	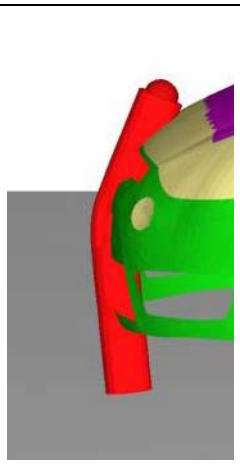	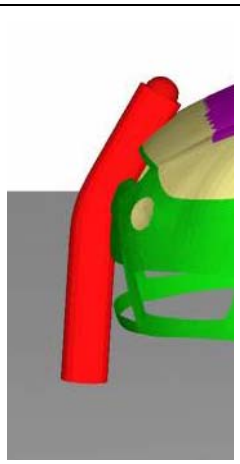
SUV	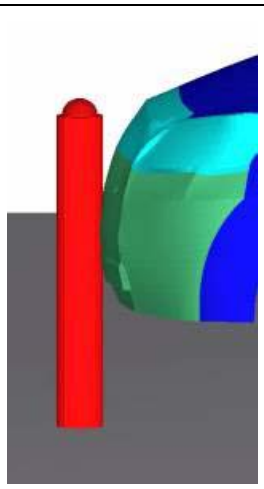	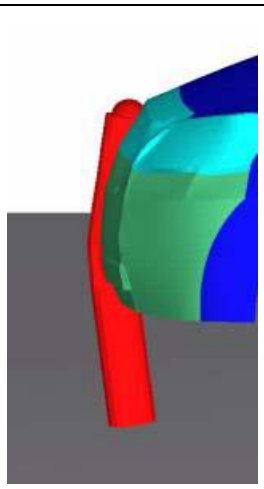	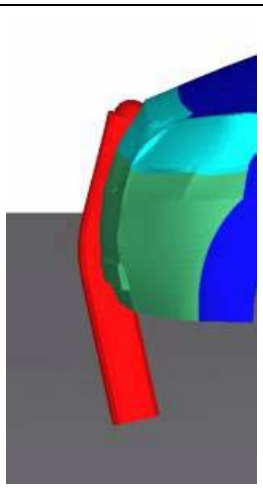	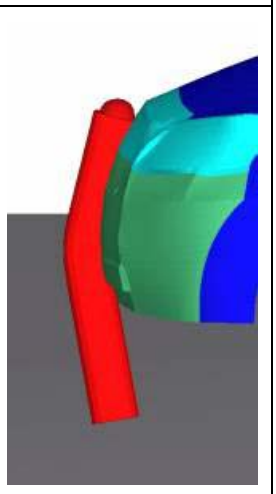

Table 8-10: Legform Impactor kinematics along the different vehicle segments.

Finally in the case of the SUV, the differences with respect the original test are very relevant. The impact clearly takes place in the femur and as such the tibia bends

significantly until it get support on the lower part of the bumper. As in this case the CoG of the impactor is above the impact point, the upper body mass compensates this lack of support of the tibia and creates an overall rotation of the whole impactor towards the vehicle. This change of behaviour of the impactor in the SUV case eliminates the non biofidelic rebound phase seen with in the original test and follows at some extend the one seen with THUMS model.

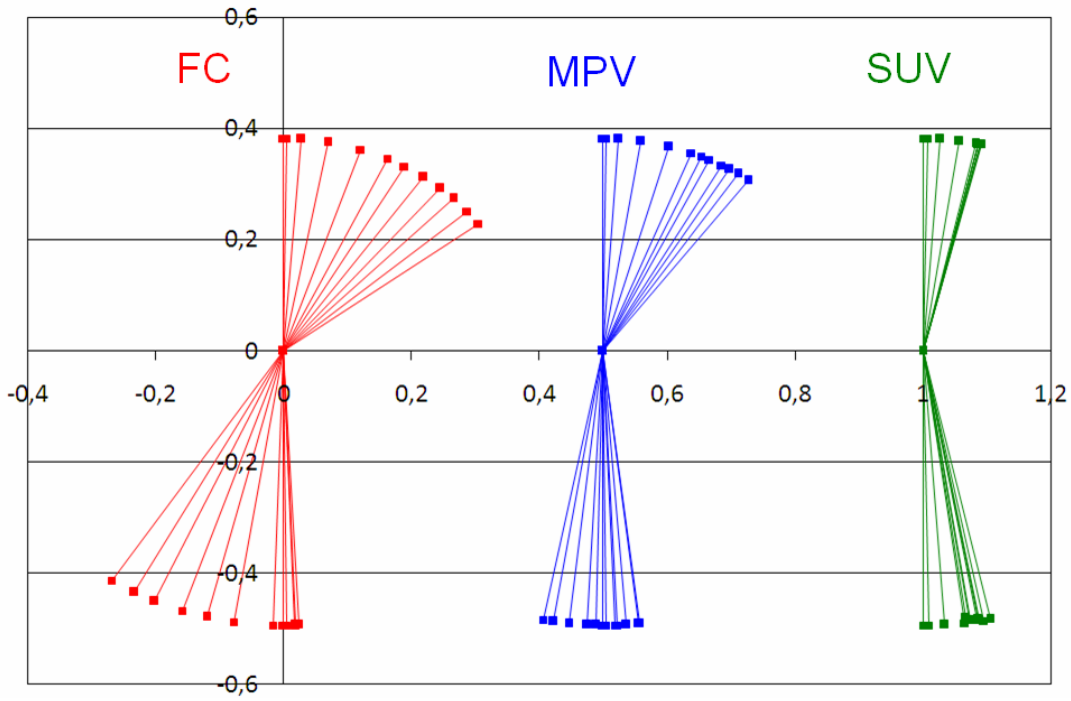

Figure 8-28: Kinematic difference of legform impactor vs different vehicle segments

As in the previous cases, the kinematics is being plotted in reference to the knee in the next figure. It can be observed an overall rotation of the impactor towards the vehicle in all cases, being less prominent as the impact point with the vehicle increases.

In all cases, it can be seen two clear phases in the test: a first one where knee bending increases and a second one, with fixed knee bending where the overall impactor rotates towards the vehicle. It can be seen for the FC that a similar bending angle to the one found with the original impactor is reached. As the tibia finds support and the femur was already the one contributing more to knee bending the only effect of the extra mass on the femur is limited to increase the overall impactor rotation towards the vehicle. In the MPV case, as the impact is rather more centred, the effect of the extra mass makes the femur to contribute more to the bending angle than before and therefore the knee bending angle increases significantly. Moreover, the rebound observed with the original impactor is no longer occurring and instead, some rotation towards the vehicle is observed although less prominent than in the previous case. Finally in the SUV case, the behaviour is radically improved. Instead of the rebound observed with the original impactor, it is observed that

not only the tibia contributes to the knee bending but also the extra mass of the femur forces it to bend leading to a knee bending relatively high. Moreover the rearward rotation of the impactor is avoided and instead a minor overall impactor rebound is observed.

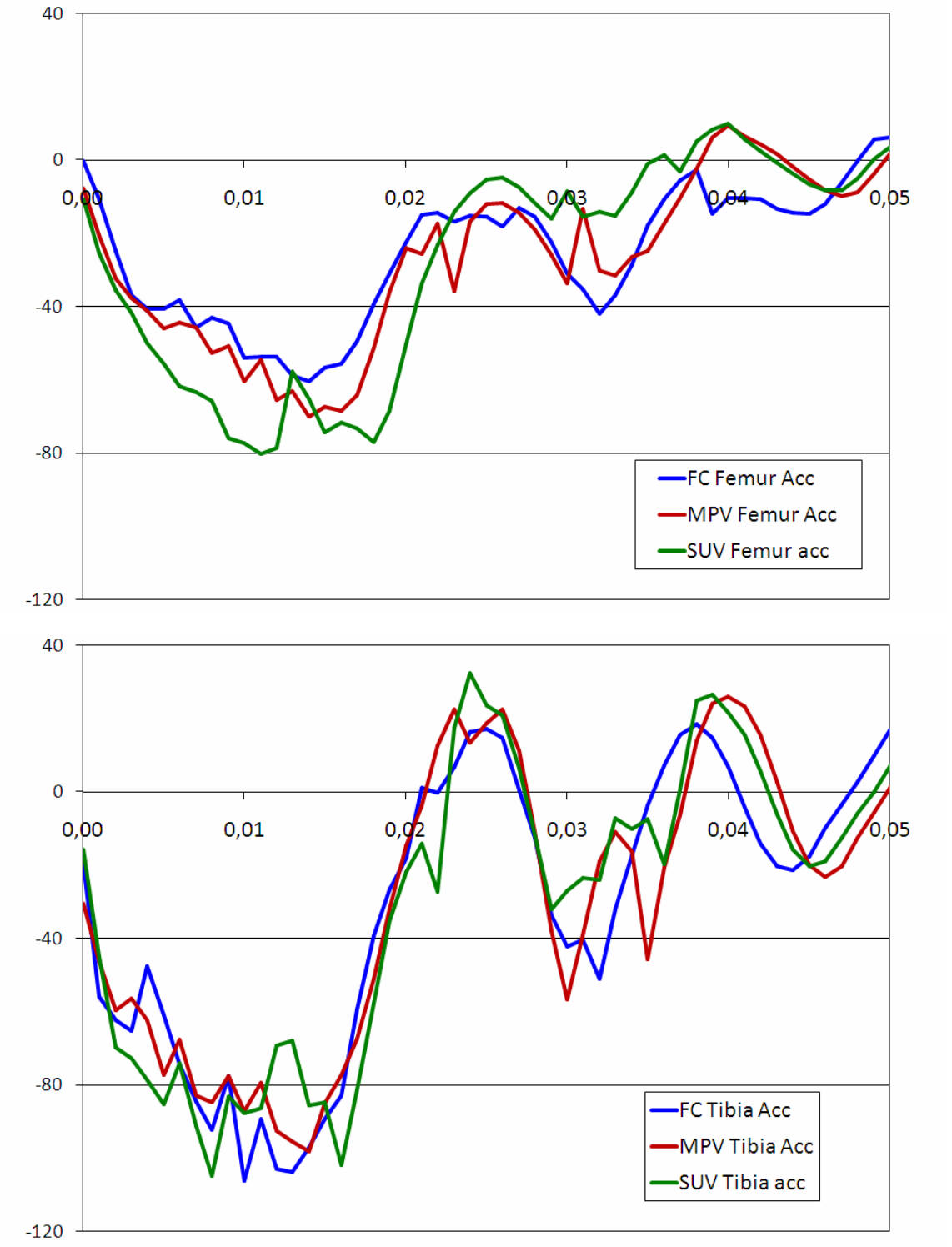

Figure 8-29: Femur and tibia accelerations (g) in the impactor in the different scenarios.

Looking in detail to the time history of the kinematics, it can be seen that for FC and MPV the maximum femur acceleration is reached after the maximum tibia acceleration while this is reverse in the SUV case, as already occurred in the THUMS simulations.

If compared the acceleration ratios (reported in next table) with the ones shown in THUMS it can be seen that they are closely the same for FC and MPV cases (60%-70%) but still rather different for the SUV case (150% in THUMS), although with the improved procedure has been achieved a 75% ratio with a relatively confident tibia acceleration measurement much better that one find with the original impactor.

	FC	MPV	SUV
Femur max acceleration	60 g	70 g	80 g
Tibia max acceleration	106 g	98 g	105 g
Ratio femur-tibia	0.56	0.71	0.76

Table 8-11: Ratio max femur acceleration and max tibia acceleration.

All this evidence would suggest that the improved impactor is still reproducing well the kinematics of the FC and MPV cases but now it shows also significant better results for the SUV segment.

8.6.2 Analysis of the injury prediction.

The three injury parameters from the impactor have also been computed in these cases and are summarized in the next table. It can be observed that the three tibia acceleration and the knee shear are rather below the acceptance levels while the knee bending angle is always above the acceptance levels. As the vehicle models have not been changed and nor its stiffness, tibia acceleration was already expected to be similar to the one found in previous cases and as such it occurs.

However, knee parameters are geometry dependant and the tested models show lack of coordinated support in the tibia and femur part to limit knee bending. In this context, the addition of the upper body mass combined with this uncoordinated support increases the femur contribution to knee bending, leading to higher knee bending in all cases.

For the FC, the increase is very moderate as the tibia is very well supported and the femur contribution to bending is limited. For the MPV, the femur and the tibia contribute similarly and the effect of increasing femur bending results in an important increase in the total knee bending angle. For the SUV, the upper body mass addition changes radically the kinematics leading to a realistic knee bending angle. This is composed of a significant contribution from the unsupported tibia and a limited contribution to the femur but

compared with the non realistic angle obtained in the original case, the overall increase is significant.

Injury criteria	FC	MPV	SUV
Tibia acceleration	106 g	98 g	105 g
Knee bending	23º	27º	26º
Knee shear displacement	2 mm	2 mm	3 mm

Table 8-12: Injury outputs of the impactor model.

These values would mean that in the three cases, FC, MPV and SUV the impactor would predict knee ligament injuries but any tibia fractures. These injuries are the same ones found with THUMS and therefore confirm that the improved impactor is also performing correctly in the injury assessment.

SECTION III: CONCLUSIONS

The Section III has presented two separate approaches using FE human models for head and leg injuries, different in nature but with the common objective of assessing their relevance for pedestrian scenarios and aiming to propose feasible modifications in the pedestrian directives to better assess these influences.

In the case of head injuries, separate collaborations with ULP and TNO analyse further two of the real world scenarios presented in Section II. These two separate studies reproduce with FE head models the impact window of the simulations when the head impacts with the vehicle and analyse a number of internal parameters in the head to predict the injuries.

The FE models have shown good correlation in predicting the injuries finding no skull fractures (as predicted by HIC) but matching also the neurologic injuries reported and occurring due to internal brain shear forces that were totally skipped by HIC criterion.

Although, it was found in literature (Kleiven, 2006a) that HIC predicted the strain level in the brain of a finite element (FE) model for purely translational impulses of short duration, the peak change in angular velocity showed the best correlation with the strain levels in an FE head model for purely rotational impulses.

This issue should lead to reconsider HIC as the only measure to assess the likelihood of any head injuries in pedestrian impacts, since HIC only treats the resultant translational acceleration and the duration of the impulse and no consideration is given to the direction of the impulse or rotational acceleration components.

It is found in studies by Ueno and Melvin (1995) and DiMasi et al. (1995) that the use of either translation or rotation alone may underestimate the severity of an injury, since, as reported in Zhang et al. (2004), both linear and angular accelerations are significant causes of brain injuries, as also corroborated in this study.

In the case of leg injuries, a more in-depth analysis has been undertaken involving two simulation matrixes with three mathematical vehicle models, representative of the family car, multipurpose vehicles and SUVs EU fleet segments.

- A set of full body pedestrian scenarios where the mathematical models of the vehicles are impacting a THUMS 50%ile FE model, an FE human model developed by Toyota that is implemented with failure criteria for the bones and the ligaments to allow the assessment of bone fracture and ligament rupture in pedestrian accidents.
- A set of pedestrian test Directive scenarios, where the same representative vehicles models have been impacted by the legform impactor FE model.

The first matrix has set the target behaviour to be reproduced in the test procedures for the different vehicles while the second has analysed how good these targets are fulfil with the current approach, both at injury prediction level and kinematic relevant issues. When compared, a number of differences have been highlighted but the most critical ones can be summarized as follows:

- In terms of kinematics, the overall rotation of the impactor towards the vehicle observed in the whole FE human body is reproduced well for the FC and MPV but not by the SUV case. Moreover, the contribution to knee bending from THUMS tibia and femur in the FC cases and the MVP cases are alike to those found with the impactor while in the case of the SUV the relative symmetry found with the FE human model is hardly reproduced by the impactor. As the impact point with the SUV and the impactor stands above the centre of gravity (CoG) of the whole impactor and it has no upper body mass, the compensating effect it has in this type of impact as shown in with THUMS, does not exist, leaving to a limitation of the usage of this impactor in these environments.
- Regarding the injury risk assessment, the injuries were well predicted with the legform in FC and MPV cases but not for the SUV case. In this case, as the impactor is no longer representative of a real pedestrian, the Directive would suggest a direct femur impact with the upper legform impactor but no longer evaluating the possible existence of knee injuries that, as shown in the FE human model impacted by the SUV are likely to occur in these scenarios, even without upper leg fracture.

This set of conclusions would suggest that the impactor is fitting its testing purpose for the FC and the MPV cases, but not for the SUV case being the key issue of that limitation the lack of the upper body mass in the impactor, which is especially critical when the impact with the vehicle occurs close or above its overall CoG.

The essence of this problem has been investigated further and an improved technically feasible legform impactor with an extra upper body mass is proposed. To define its requirements a three-stepped optimization is followed disregarding mere mathematical approaches.

1. Identify the minimum requirement where the impactor with the upper body mass is always on acceptable working conditions for all EU vehicles. For that a wide EU SUV geometrical corridor has been analysed and found that the average mid bumper height in this segment is 680mm ± 25. If the impactor CoG is set above this value, it can be guaranteed that the impactor would be impacted within or below its overall CoG in most cases.
2. Explore possibilities to add mass to the impactor in terms of minimizing its re-design efforts. The most cost effective option has resulted to be adding mass rigidly in the upper part of the impactor maintaining its overall dimensions and length.
3. Define the relationship between the impactor CoG increase and the extra mass needed. This relationship has shown that, at the beginning, with reduced added mass high CoG increases are obtained, however, this is less true once the overall CoG is intended to be higher than 650 mm.

Based on that, an considering the target set in step 1, it has been defined this 650mm as a feasible increased impactor CoG, which would mean to add in the upper part of the impactor a total of 5.3 kg. This mass would represent less than 50% of the current impactor mass and would increase the overall mass of the impactor to 18.7 kg which is still on the range of current test apparatus.

If this increase is combined with the one of increasing the impact conditions 25mm as suggested in the new Directive, a total increase in the impactor CoG of 125mm would be achieved with minor changes in the impactor and thus with a low cost of implementation.

In the final part of this Section III, the performance of this upgraded impactor is analysed by replicating the previous simulation matrix, not only with the SUV segment, the basics of this redesign, but also with the FC and the MPV to ensure that the new impactor is still valid for those segments which were covered correctly by the original impactor. The results of this matrix have shown that:

- In terms of kinematics, FC and MPV are still working similarly than with the original impactors while in the case of the SUV, as in this case the CoG of the impactor is

above the impact point, the upper body mass compensates this lack of support of the tibia and creates an overall rotation of the whole impactor towards the vehicle. This change of behaviour of the impactor in the SUV case eliminates the non biofidelic rebound phase seen with in the original test and follows at some extend the one seen with THUMS model.

- In terms of knee bending angle, it can be seen two clear phases in the test for all cases: a first one where knee bending increases and a second one, with fixed knee bending where the overall impactor rotates towards the vehicle. For the FC and MPV, a higher impactor rotation towards the vehicle is obtained than with the original impactors while in the SUV case, instead of the rebound seen with the original impactor, it is observed that not only the tibia contributes to the knee bending but also the extra mass of the femur force it to bend leading to a knee bending relatively high.
- In terms of tibia acceleration, as the vehicle models have not been changed and nor its stiffness, tibia acceleration was already expected to be similar to the one found in previous cases and as such it occurs, predicting no tibia fracture.
- In terms of knee injury parameters, in the three cases, FC, MPV and SUV, the impactor would predict knee ligament injuries being the case of SUV where more improvement is observed as the upper body mass addition changes radically the kinematics leading to a realistic high knee bending angle.
- This injury output is the same ones found with THUMS and therefore confirm that the improved impactor is performing correctly in predicting leg injuries in the three scenarios, enhancing the behaviour of the original impactor.

Having seen the good results of the UBM, the next step will be to transform this model into a real impactor and test in real environments. In this design process, it is recommended to replace the original hip end with a new one, able to easily accommodate the UBM ballast, maintaining the assembly reference planes of the hip end and take into account the paths of the instrumentation wires.

Due to the magnitude and needs of this process, this is kept out of the scope of the thesis but it is seen as an interesting development in the near future.

9 THESIS MAIN CONCLUSIONS AND OUTPUTS

Looking back to the origin of this thesis in 2003, it is clear that there were two milestones that clearly inspired its development. On one hand, the preparatory phases undertaken in INSIA-UPM to participate in the Integrated European project APROSYS (FP6-TIP3-CT-2004-506503) and on the other hand, the entry into force of Directive 2003/102 EC which defined a compulsory set of pedestrian tests for Europe.

The part of the APROSYS project dedicated to pedestrian, subproject 3, leaded by Crandfield Research Center (UK) aimed to define suitable improvements in the pedestrian test procedures in order to contribute to the debate on the second phase of such Directive, finally released in 2009 in terms of a Regulation. With this objective, a top group of manufactures, research centres and universities undertook together this ambitious subproject, and INSIA-UPM was selected to be one of them.

The opportunity of being involved and granted in this 4 years project with these entities has allowed not only access to first-hand information on pedestrian safety but also to open up collaborations with top researchers in pedestrian issues and at some extend, align our contribution to this project with the main topics addressed in this thesis. This close work with APROSYS has not only given strong arguments in how the thesis has approached pedestrian safety, but also it has taken enormous advantages of the synergies of both research works and its relevance in the research community, being in some cases INSIA-UPM contribution in APROSYS the basics of some of the part of this thesis (for instance, the stiffness mapping tool) and in some others, the conclusions derived in APROSYS the

motivations to bias the thesis exploration towards one way or another (i.e. the development of the aged pedestrian).

To fully exploit the key position of this project within the passive safety research community, the relevant publications of the results of this thesis have been framed in that context and in many cases, involved collaborations with other entities as Chalmers University (Sweden), Louis Pasteur University (France), TNO (the Netherlands) or Toyota Motor Europe (Belgium).

It is the objective of this final chapter to analyse individually all the relevant results of the thesis that contribute to the four thesis objectives, citing the relevant publication done at respect and linking them to other relevant results of the APROSYS projects and, when relevant, providing paths for future research.

The most relevant thesis results can be enumerated as follows:

- **A stiffness mapping tool.** It was presented in the Section I of the thesis and was developed as part of UPM-INSIA contribution to APROSYS project. The summary of this tool is done firstly in APROSYS Deliverable 312B and afterwards presented in the peer review ESV International Conference in 2007 with the following reference: Martinez L., Guerra L., Ferichola G., Garcia A., Yang J., (2007) Stiffness Corridors of the European vehicles for pedestrian simulations. Paper Number 07-0267-W. 20th Enhanced Safety of Vehicles Conference. As previously commented, this study is the first one of its kind developed at EU level and therefore is one of the most relevant results from this thesis as well as from APROSYS, being this article cited more than 20 times in many other studies latter studies within the research community.
- **An in-depth pedestrian accidentology study.** It was presented in the Section I of the thesis and was developed as part of INSIA-UPM contribution to APROSYS where it was integrated within the project with similar analysis performed in the UK, Germany and Sweden. After this overall integration a unique analysis was performed in order to derive trends valid across Europe and summarised in APROSYS D311 and afterwards presented in the peer review ESV International Conference in 2007 with the following reference: “Neal-Sturgess CE, Carter E., Hardy R., Cuerden R., Guerra L.J., Yang J. (2007) APROSYS European In-Depth Pedestrian Database. Paper number 07-0177-O 20th Enhanced Safety of Vehicles Conference.” Although this thesis only presents the Spanish part, the correlation found with other countries data has lead to obtain interesting results on empirical evidences of the elderly extra risk when they are involved in pedestrian accident scenarios as casualties.
- **An aging material software package AgedMAT.** It was presented in Section II and it was developed within this thesis when the APROSYS accidentology

analysis derived conclusions on the bias observed in elder pedestrian injury risk tolerance. It has been part of INSIA-UPM contribution to APROSYS SP5 on biomechanics, although the direct translation to the MADYMO aged pedestrian had been an extra, developed ad hoc to meet the needs of this thesis. This result has not been presented alone, although the AgedMAT software has been a deliverable itself of the project D512B, but together with its application to accident reconstruction of real world cases with the MADYMO aged pedestrian in the peer review international conference of IRCOBI 2007 with the following reference: Martinez L., Guerra L., Ferichola G., Garcia A., (2007) Pedestrian accident simulations methodology using detailed vehicle models and age-dependent leg fracture limits on the pedestrian. IRCOBI Conference 2007 or with FE human models in Martinez L., Guerra L., Ferichola G., Garcia A., (2008) "Desarrollo de una metodología para el análisis de atropello de peatones utilizando modelos de elementos finitos del cuerpo humano". XVII Congreso Nacional de Ingeniería Mecánica. In this case, age itself has not been considered within APROSYS SP3 but the thesis has highlighted the practical effect of its consideration or not, showing the relevance to have real injury risk functions decoupled between the adult population and the elderly populations. This offers wide possibilities of further research and reflexion, especially, when in many cases, the PMHS used to derive adult typical threshold values are on the age range of 70 or more.

- **A cost effective methodology to create vehicle mathematical models.** As this methodology, presented in Section II, was conceived very flexibly to offer wide possibilities to construct robust vehicle mathematical models, it has been used in a number of studies within the thesis and further and as such, it has been reported not only in the previous publication from IRCOBI 2007 but also in the next one from IRCOBI 2008 referenced as Martinez L., Compigne S., Guerra L., (2008) Influence of vehicle shape and stiffness on the pedestrian lower extremity injuries: Review of current pedestrian lower leg test procedure. IRCOBI Conference 2008. Moreover it has also been used in Martinez L., Guerra L., Ferichola G., Garcia A., (2008) "Desarrollo de una metodología para el análisis de atropello de peatones utilizando modelos de elementos finitos del cuerpo humano". XVII Congreso Nacional de Ingeniería Mecánica and also in Bovenkerk J., Lorenz B., Guerra L.J., Neal-Sturgess C.E.,(2007) Pedestrian Protection in Case of Windscreen Impact. Crash.Tech Conference 2007.
- **A set of real world scenario pedestrian simulations.** In order to test the usability of the tools developed, see the real influence of age in real world pedestrian accidents injury outcomes and kinematics, four real world pedestrian accidents have been mathematically modelled and simulated with scaled pedestrian according to the age and gender of the real pedestrian involved in the

accident. The results of some of these simulations were presented in Martinez L., Guerra L., Ferichola G., Garcia A., (2007) Pedestrian accident simulations methodology using detailed vehicle models and age-dependent leg fracture limits on the pedestrian. IRCOBI Conference 2007 and Martínez, L.; Guerra, L. J.; Ferichola, G.; García, A. (2007) "Estudio de atropello de peatones adultos y de la tercera edad mediante modelos matemáticos" VIII Congreso Iberoamericano de Ingeniería Mecánica.

- **An analysis of non fatal head injuries in pedestrian environment with FE human head models.** Although it has not been the core objective of the thesis and the studies herein included in Section III are just a drop in the ocean of the literature on pedestrian head impact, it has been considered convenient to dedicate some words to head injuries in this thesis as they are the top of death cause in pedestrian accidents. APROSYS SP3 did widely covered this part and therefore there were plenty of studies complementing the one here presented, that was published as two independent studies one from Baumgartner D., Marjoux D., Willinger R., Carter E., Neale-Sturgess CE., Hardy R., Guerra L., Martinez L., (2007) Pedestrian Safety Enhancement Using Numerical Methods. Paper No. 07-0426-O. 20th Enhanced Safety of Vehicles Conference, and the other one from Mordaka J., Kleiven S., van Schijndel-de Nooij M., de Lange R., Guerra L., Carter E., von Holst H., (2007) The importance of rotational kinematics in pedestrian head to windshield impacts, IRCOBI Conference 2008.
- **An in-depth study of leg injury occurrence in pedestrian environments.** This study presented in Section III was part of the contribution from INSIA-UPM to APROSYS SP3 on this topic, Within the project, this issue was approached together between INSIA-UPM and Toyota, the former focused on small and mini family car and MPVs and the latter focused in large family cars and SUVs. Lessons from this collaboration were used later to complement our study on FC and MPV with the SUV analysis performed and presented in this thesis. The summary of this study covering all geometries was presented first within APROSYS as Deliverable 332B and in the previously commented peer-reviewed IRCOBI 2008 article referenced as Martinez L., Compigne S., Guerra L., (2008) Influence of vehicle shape and stiffness on the pedestrian lower extremity injuries: Review of current pedestrian lower leg test procedure. IRCOBI Conference 2008. A more focus article on SUVs behaviour was also written later that will be published in the International Journal of Crashworthiness, referenced as Martinez L., García A., Guerra L., Alcalá E. Behaviour of high bumper vehicles in pedestrian scenarios with full FE human models.
- **A feasible proposal for an improved legform pedestrian test procedure with an upper body mass.** This proposal is presented in the last part of Section III and

it was the first part of the contribution from INSIA-UPM to the APROSYS SP3 on this topic. The conceptual design as well as the simulations included in this thesis was complemented later with a thorough re-design of the lower legform to allow the real implementation of the upper body mass and a further study focused on the SUV vehicle segment. This work has lead to the publication in the International Journal of Vehicle Crashworthiness a second article referenced as García A., Martínez L., Guerra L.J., Alcalá E.,. (2011*) Development of a pedestrian rigid legform impactor with upper body mass suitable to assess leg injuries in high bumper vehicles. Moreover, and presented in the final event of APROSYS project, held in Amsterdam in 2009, a prototype was build based on a real legform to demonstrate the feasible design proposed and presented as the Deliverable333b from the project.

9.1 Further developments.

Based on the results of this thesis, there are three research areas identified worth to be further investigated or developed, two of them closely linked to the age, in understanding its effect in the material properties of the human body and in its relationship to withstand injuries, and a third one, linked to the next steps to be addressed to propose a convincing and tested improved legform pedestrian test procedure with an upper body mass, as very promising preliminary results have been shown in this thesis.

- **Full characterization of human body tissue material properties and its variation with age.** This thesis has developed an aging material software package, AgedMAT, that has been found to be very useful to age some human material models, but with some limitations in many others. This limitation has been based on the lack of wide test series in a number of different human tissues or bones analysing their variation with age, especially in the case of data on child subjects, and the large variation found in “external factors” in the test series found in literature on areas such as subject preservation, specimen preparation or experimental set-up techniques that have shown to have a large effect on the measured material properties of human tissue. There is a clear need to define a best practice approach to minimise these effects at subject preservation level, working preferentially with unembalmed specimens than with embalmed specimens, at specimen preparation level, guaranteeing a proper alignment of the anisotropic material axis with the axis of the specimen to be tested and ensuring that the material does not dry out during preparation neither gets too hot during any cutting of the material eliminating any possible edge effect in the measurement of the properties and finally also, at experimental set-up level to ensure that the correct property of the material is being tested. For linear compression or tension tests, this means that the alignment of the heads must be accurate (aligned as well as possible), to reduce the potential effects of bending

modes in the specimen while in bending tests, it is important to closely control the effective size of the supports and loading head to minimise unintended or variable stress concentrations in the specimen. This area has therefore been identified as an important research field where more resources should be devoted to conduct further studies, both from a biomechanical point of view but also from a medical point of view in order to characterize all types of human tissues and their variances with age, considering which effect this has on their resistance to injury. The ultimate objective of developing further this research field would be to have enough quality data to build an AgedMAT-like software that could completely scale in age a full human body FE model, exploiting fully this way the possibilities of the mathematical modelling of pedestrian scenarios, currently available in multibody environments but not so far in FE environments.

- **Wide calibration of the injury severity classification used in crashworthiness scenarios specifically for elder population.** Along the thesis the current injury severity classification methods used in crashworthiness scenarios have been used, including the Abbreviated Injury Scale (AIS 90) used worldwide to classify the individual injuries sustained by traffic casualties according to their life-threatening risk, the MAIS code, that takes the maximum AIS of a casualty in any of its body parts, and the ISS (Injury Severity Score), that adds the three higher AIS injuries in a casualty as a method of numerically describing the overall injury severity of patients with injuries to more than one area of the body (Baker, 1974). However, the creation of those injury classifications as well as their calibration in accident scenarios was not done specifically considering the special features of elder population. It has been found in the thesis that the energy required to cause an injury reduces as a person ages, implying that elder casualties may be several times more likely to sustain a life threatening injury than younger ones, and that the pedestrian mortality is substantially higher among seniors than any other age group (also supported by wider epidemiology studies such as Knoblauch, 1995; Oxley, 1996 or NHTSA, 2001). These two conclusions would call for the need to fix adequately how these injury classification links with death risks considering in the process adjusted age-dependent risks functions. The consequences of this recalibration could be very significant, because if the current thresholds used to set injury criteria in pedestrian test environments is demonstrated not to be relevant for elderly vulnerable road users and needs to be decreased to consider this especially vulnerable and exposed target group, this will create a massive impact on the current approach to pedestrian safety and the way the current Pedestrian Legislation measures pedestrian protection assessment.
- **Further development of the pedestrian legform test considering the upper body mass.** This thesis has mathematically approached this issue demonstrating

that promising results are found in terms of both kinematics and injury output to ensure that with a single test all possible leg injuries can be measured considering how they couple between them. However, there are still a number of other issues to be further undertaken, developed and fine tuned. Firstly, while it has been predicted the knee injuries as well as the lack of tibia fractures in all cases, the lack of femur fractures has not been assessed appropriately. However, more research would be needed to first consolidate the current acceptance criteria for knee injuries and tibia acceleration when the overall mass of the impactor has increased, as it may need an update also in the knee ligament properties, and latter, to develop a proper wide-test-based femur injury risk function and its corresponding acceptance levels, based on femur acceleration. Secondly, as this study has shown just mathematical results, the next step will require building a physical prototype of the upper body mass ballast (already done in the APROSYS project) and test it with the lower legform impactor in real test environments with a wide set of vehicles to check its full functionality, robustness and repeatability fine tuning the needed modifications in the current impactor and defining those needs (if any) in the test apparatus that launch it towards the vehicle and in the impactor certification tests.

.

REFERENCES

ABIDA (2004). Base de datos de atropello de peatones en profundidad. Proyecto ABIDA (Estudio Accidentológico, BIomecánico y Dinámico de Atropello de peatones). Plan Nacional I+D 2000-2003. Referencia DPI 2001-2818.

Aparicio, F.; Martínez, L.; Páez, J.; Ferichola, G.; Guerra, L. J. (2005) Informe final proyecto ABIDA. Estudio Accidentológico, Biomecánico y Dinámico de Atropellos de Peatones. Plan Nacional de I+D. Ministerio de Ciencia y Tecnología de España DPI2001-2818.

APROSYS SP3 (2005) "Definition of vehicle and pedestrian/cyclist impact conditions" Deliverable 3.1.1. SP3 APROSYS project, VI PM TIP3-CT-2004-506503.

APROSYS SP3 (2005).The generalised geometry corridors, generic shapes and sizes of the vehicle fleet covering cars, MPVs and SUVs. Deliverable 3.1.2A SP3 APROSYS project. VI PM TIP3-CT-2004-506503.

APROSYS SP3 (2006) Impact response for complete components, Influence of geometry, interface conditions and impact energy. Deliverable 3.2.2. SP3 APROSYS project. VI PM TIP3-CT-2004-506503.

APROSYS SP5 (2006) "Age and gender material properties. Deliverable 5.1.2. SP5 APROSYS project. VI PM TIP3-CT-2004-506503.

APROSYS SP7 (2007) Generic car FE models for categories super mini cars, small family cars, large family cars, MPV and heavy vehicle. Deliverable 714A SP7 APROSYS project, VI PM TIP3-CT-2004-506503.

Arnoux P.J., Cavallero C., Chabrand P., Brunet C. (2002), Knee ligaments failure under dynamic loadings. International Journal of Crashworthiness, Vol 7 (3), pp. 255 – 268.

Baumgartner D., Marjoux D., Willinger R., Carter E.L., Neal-Sturgess C., Guerra L.J., Martinez L., Hermann K., Hardy R. (2007) Pedestrian safety enhancement using numerical methods. Paper Number 07-0426. ESV Conference 2007

Baker, S.P., et al., The injury severity score: a method for describing patients with multiple injuries and evaluating emergency care. Journal of Trauma, 1974. 14(3): p. p. 187-196

Baumgartner D., Willinger R., Diaw B.M., (2001) Finite element modelling of a protective helmet – parametric study and coupling with the human head, Proc. of the NAFEMS World Congress on the Evolution of Product Simulation, Come, Italie, vol. 2, pp. 727-738.

Baumgartner D., Marjoux D., Willinger R., Carter E., Neale-Sturgess CE., Hardy R., Guerra L., Martinez L., (2007) Pedestrian Safety Enhancement Using Numerical Methods. Paper No. 07-0426-O. 20th Enhanced Safety of Vehicles Conference

Bayraktar H.H., Morgan E.F., Niebur G.L., Morris G.E., Wong E.K., Keaveny T.M.(2004) Comparison of the elastic and yield properties of human femoral trabecular and cortical bone tissue. Journal of Biomechanics 37 (2004) 27–35

Beck TJ, Oreskovic TL, Stone KL, et al. (2001) Structural adaptation to changing skeletal load in the progression toward hip fragility: the study of osteoporotic fractures. J Bone Miner Res. 2001;16:1108–1119.

Behr M., Arnoux P.J., Serre T., Bidal S., Kang H.S., Thollon L.,Cavallero C., Kayvantash K., Brunet C.. “A Human Model for Road Safety: From Geometrical Acquisition to Model Validation with Radioss” Computer Methods in Biomechanics and Biomedical Engineering. Vol. 6, No. 4, August 2003, pp. 263–273.

Blanton P L and Biggs N L (1970). Ultimate tensile strength of fetal and adult human tendons. Journal of Biomechanics, 1970 (3) 181-189.

Bovenkerk, J., Lorenz, B., Zander, O., Guerra L.J., Neal-Sturgess C.E. (2007). Pedestrian Protection in Case of Windscreen Impact. Crash Tech Conferences 2007.

Bryon R. Gomberg, PhD2, Punam K. Saha, PhD, Felix W. Wehrli, PhD (2005). Method for Cortical Bone Structural Analysis From Magnetic Resonance Images. Acad Radiol 2005; 12:1320–1332

Bunketorp, O. et al.(1983) : Experimental Study of a Compliant Bumper System. SAE paper no. 831623, 1983.

Burstein A H, Reilly D T and Martens M (1976). Aging of Bone Tissue: Mechanical Properties. The Journal of Bone and Joint Surgery, 58 (A) 82-86.

Butler A.M., Walsh W.R. (2004) Mechanical response of ankle ligaments at low loads. Foot Ankle Int. 2004 Jan;25(1):8-12.

Butler D L, Kay M D and Stouffer D C (1986). Comparison of material properties in fascicle-bone units from human patellar tendon and knee ligaments. Journal of Biomechanics, 19 (6) 425-432.

Cesari, D. (1998). Pedestrian Protection - synthesis of experimental and simulation researches performed in France. INRETS, August 1998, EEVC WG17 document 92.

Coley G., Lange R. de, Oliveira P. de, Neal-Sturgess C., Happee R.. (2001) Pedestrian Human Body Validation Using Detailed Real-World Accidents. Proc. Int. IRCOBI Conf. Biomechanics of Impact.

Cook, T., (1976). An in plane method for determining the two dimensional stress-strain behavior of living human skin. In: Proceedings 29th ACEMB. Vol. 43.

Crandall J.R., Portier L., Petit P., Hall G.W., Bass C.R., Klopp G.S., Hurwitz S., Pilkey W.D., Trosseille X., Tarriere C., Lassau J.P. (1996) Biomechanical response and physical

properties of the leg, foot and ankle. Proc. 40th Stapp Car Crash Conference, SAE paper 962424.

Dalstra, M., Huiskes, R.(1995). Load transfer across the pelvic bone. Journal of Biomechanics 28, 715–724.

Di Masi, F., Eppinger, R.H., and Bandak, F.A. Computational analysis of head impact response under car crash loadings, Proc 39th Stapp Car Crash Conf, Society of Automotive Engineers, SAE Paper No. 952718, Society of Automotive Engineers, Warrendale, PA, 1995, 425-438.

Di Silvestro M.R., Wong M., Jurvelin J.S., Suh J-K.F.(2001) “Biphasic poroviscoelastic simulation of the unconfined compression of articular cartilage: I-simultaneous prediction of reaction force and lateral displacement”. J. Biomech. Eng. 2001:123:191-197.

Ding M., Dalstra M., Danielsen C.C., Kabel J., Hvid I., Linde F. (1997) Age variations in the properties of human tibial trabecular bone. Journal of Bone Joint Surgery Vol. 79-B, NO. 6, November 1997, pp 995-1002.

Elliot D.M., Setton L.A.(2001). Anisotropic and inhomogeneous tensile behaviour of the human annulus fibrosus: Experimental measurement and material model predictions. Journal of Biomechanical Engineering 123, 256-263.

Engin A.E. (1979a) Measurement of resistive torques in major human joints. Aerospace Medical Research Laboratory, Report AMRL-TR-79-4.

Engin A.E. (1979b) Passive resistance torques about long bone axes of major human joints. Aviation, Space and Environmental Medicine, 50(10): 1052-1057.

Eppinger R.H., Takhounts E.G. (2002) “On the development of survival criteria for rate sensitive materials”. Proceedings 44th Stapp Car Crash Conference Paper 2000-01-SC04.

European Commission (1991) Summary of the work of the consortium developing test methods to evaluate the protection afforded to pedestrians by cars (including test proposals). European Commission Study Contract No: ETD/89/7750/M1/28.

European Enhanced Vehicle-safety Committee EEVC (1982). Pedestrian injury accidents. 9th ESV Conference, Kyoto, November 1982.

European Enhanced Vehicle-safety Committee EEVC (1984). Cycle and light-powered two-wheeler accidents. 9th IRCOBI Conference, Delft, September 1984.

European Enhanced Vehicle-safety Committee EEVC (1985). Pedestrian injury protection by car design. 10th ESV Conference, Oxford, July 1985

European Enhanced Vehicle-safety Committee EEVC WG10 (1989). Study of test methods to evaluate pedestrian protection for cars. EEVC Working Group 10 report, 12th ESV Conference, Gothenburg, May 1989.

European Enhanced Vehicle-safety Committee WG10 (1991). Proposals for test methods to evaluate pedestrian protection for cars. EEVC Working Group 10 report. 13th ESV Conference, Paris, November 1991.

European Enhanced Vehicle-safety Committee EEVC WG10 (1994). Proposals for methods to evaluate pedestrian protection for passenger cars. WG10 report, November 1994.

European Enhanced Vehicle-safety Committee (1998a). Improved test methods to evaluate pedestrian protection afforded by passenger cars. WG17 report.

European Enhanced Vehicle-safety Committee EEVC WG17 (2002). ”Improved test methods to evaluate pedestrian protection for passenger cars. WG17 Report.

EuroNCAP 2001. “EuroNCAP pedestrian testing protocols” Version 3. April 2001.

EuroNCAP 2004. “EuroNCAP pedestrian testing protocols” Version 4.1 March 2004.

EU Directive 2003/102/EC relating to the protection of pedestrians and other vulnerable road users before and in the event of a collision with a motor vehicle and amending Council Directive 70/156/EEC

EU Regulation (EC) No 78/2009 on the type-approval of motor vehicles with regard to the protection of pedestrians and other vulnerable road users, amending Directive 2007/46/EC and repealing Directives 2003/102/EC and 2005/66/EC.

Frank C.B. (2004) Ligament structure, physiology and function. Journal of Musculoskeletal and Neuronal Interactions 2004; 4(2):199-201

Frankel V.H., Nordin M. (1980) Basic biomechanics of the skeletal system. Philidelphia, USA, Lea & Febiger.

Fung Y.C. (1993) Biomechanics: Mechanical Properties of Living Tissues, 2nd Edition. New York: Springer-Verlag; 1993.

Funk, J., Hall, G., Crandall, J.R., and Pilkey, W. (2000). Linear and quasi-linear viscoelastic characterization of ankle ligaments, Journal of Biomechanical Engineering 122, 15-22.

Funk J. R, Kerrigan, J. R., Crandall J.R., (2004) Dynamic bending tolerance and elastic plastic material properties of the human femur. 48th Annual proceedings Association for the Advancement of Automotive Medicine.

Gomberg BR, Saha PK, Song HK, Wehrli FW. Algorithm for measuring cortical bone thickness from high-resolution MR images [abstract]. In:Proc. ISMRM 8th Annual Meeting, Denver, CO; 2000; 2137.

Grahame, R., 1970. A method for measuring human skin elasticity in vivo with observations on the effects of age, sex and pregnancy. Clinical Science 39, 223–238.

Gray H. (1918): "Anatomy of the human body" 20th edition, thoroughly revised and re-edited by Warren H. Lewis. Philadelphia: Lea & Febiger, 1918. ISBN: 1-58734-102-6. On-line edition Published May 2000 by Bartleby.com.

Guo B., Liao D., Li X., Zeng Y., Yang Q. (2007) Age and gender related changes in biomechanical properties of healthy human costal cartilage. Clinical Biomechanics, Volume 22, Issue 3, Pages 292-297

Happee R., Wismans J. (1999) Pedestrian protection full-body simulations, dummy validation. Proc. VDA Technical Congress, Frankfurt.

Happee R., Ridella S., Nayef A., Morsink P., de Lange R., Bours R., van Hoof J. (2000) Mathematical human body models representing a mid size male and a small female for frontal, lateral and rearward impact loading. Proc. 25th IRCOBI Conference 2000.

Haug E., Beaugonin M., Montmayeur N., Marca C., Choi H.Y 2003. "Towards Legal Virtual Crash Tests For Vehicle Occupant Safety Design Using Human Models International Crashworthiness and Design Symposium 2003.

Haward R.N., (1975) Strength of plastics and glass, Cleaver Hume Press, New York.

Hendriks F.M, Brokken D., van Eemeren J., Oomens C.W.J., Aaijens F.P.T., Horsten J.B.A.M., "A numerical-experimental method to characterize the non-linear mechanical behaviour of human skin", Skin Res Technol, 9(-), 274-283, (2003).

Hewitt, J., Guilak, F., Glisson, R., Vail, T.P., 2001. Regional material properties of the human hip joint capsule ligaments. Journal of Orthopaedic Research 19, 359–364.

Horikoshi T, Endo N, Uchiyama T, Tanizawa T, Takahashi HE. (1999) Peripheral quantitative computed tomography of the femoral neck in 60 Japanese women. Calcif Tissue Int. 1999;65:447–453.

Hui J., Lewis J.L (2004) "Determination of Poisson's ratio of articular cartilage by indentation using different-sized indenters" Journal of biomechanical engineering 2004, vol. 126, no2, pp. 138-145

Hynd D. 2005. "EEVC WG9 Biofidelity corridor calculation method." EEVC WG12 document.

International Harmonized Research Activity Pedestrian Safety Working Group, (2004) IHRA/PS/295.

ISO-N455, “Road Vehicle – Anthropomorphic Side Impact Dummy – Lateral Response Requirements to Assess the Biofidelity of the Dummy “, ISO/TC22/SC12/WG5, Document N455, Revision 2,May 1996

Johnson G A, Tramaglini D M, Levine R E, Ohno K, Choi N-Y and Woo S L-Y (1994). Tensile and viscoelastic properties of human patellar tendon. Journal of Orthopaedic Research, 1994, Vol 12, 796-803.

Kajzer J., Cavallero C., Ghanouchi S., Bonnoit J., Ghorbel A. (1990) Response of the Knee Joint in Lateral Impact: Effect of Shearing Loads. Proc. 15th IRCOBI Conference Proceedings, pp. 293- 304.

Kajzer J., Cavallero C., Bonnoit J., Morjane A., Ghanouchi S. (1993) Response of the Knee Joint in Lateral Impact: Effect of Bending Moment. Proc. 18th IRCOBI Conference Proceedings, pp. 105- 116.

Kajzer J., Schroeder G., Ishikawa H., Matsui Y,Bosch U. (1997) Shearing and bending effects atthe knee at high speed lateral loading. Proc. 41stStapp Car Crash Conference, SAE paper No.973326.

Kamineni S., El-Attrache N.S., O'Driscoll S.W., Ahmad C.S., Hirohara H., Neale P.G., An K.N., Morrey B.F. (2004). Medial Collateral Ligament Strain with Partial Posteromedial Olecranon Resection The Journal of Bone and Joint Surgery (American). 2004;86:2424-2430

Kang H.S., Willinger R., Diaw B., Chinn B., (1997) Validation of a 3D anatomic human head model and replication of head impact in motorcycle accident by finite element modelling, Proc. of the 41st Stapp Car Crash Conf., pp. 329-338.

Kerrigan J R, Drinkwater D C, Kam C Y, Murphy D B, Ivarsson b J, Crandall J R and Patrie J. (2004):Tolerance of the human leg and thigh in dynamic latero-medial bending, International Journal of Crashworthiness, 9:6, 607-623.

Khosla S, Lufkin EG, Hodgson SF, Fitzpatrick LA, Melton LJ (1994) 3rd. Epidemiology and clinical features of osteoporosis in young individuals. Bone. 1994;15:551–555.

Kleerekoper M, Feldkamp L A and Goldstein S A (1986). The effect of aging on the skeleton – implications for changes in tolerance. P-186, Symposium on biomechanics and medical aspects of lower limb injuries, 29-30 October 1986, San Diego, California (SAE technical paper number 861926): Society of Automotive Engineers, Inc. (SAE), 400 Commonwealth Drive, Warrendale, PA 15096, USA.

Kleiven, S. Finite Element Modeling of the Human Head. Doctoral Thesis. Technical Report 2002-9, Department of Aeronautics, Royal Institute of Technology, Stockholm, Sweden, 2002.

Kleiven, S., Hardy, W.N. (2002) Correlation of an FE model of the Human Head with Experiments on localized Motion of the Brain – Consequences for Injury Prediction. 46th Stapp Car Crash Journal, 2002, 123-144.

Kleiven, S., and von Holst, H. (2002) Consequences of Head Size following Trauma to the Human Head. J. Biomechanics 35 (2), 2002, 153 – 160.

Kleiven, S. (2006a) Evaluation of head injury criteria using an FE model validated against experiments on localized brain motion, intra-cerebral acceleration, and intra-cranial pressure. International Journal of Crashworthiness, 11 (1), 65-79.

Kleiven, S. (2006b). Biomechanics as a forensic science tool - Reconstruction of a traumatic head injury using the finite element method. Scand J Forens Sci., 2, 73-78.

Knoblauch, R., et al., Older Pedestrian Characteristics for Use in Highway Design. US Department of Transportation. DOT FHWA-RD-93-177., 1995.

Koh S-W, Cavanaugh J M and Leach J P (2004). Mechanical properties of the shoulder ligaments under dynamic loading. Stapp car crash journal volume 48. SAE technical paper 2004-22-0006: Society of Automotive Engineers, Inc. (SAE), Warrendale, Pennsylvania, PA 15096, USA.

Konosu A., Issiki T., Tanahashi M. (2005) Development of a pedestrian lower extremity protection car using a biofidelic flexible pedestrian legform impactor. ESV Conference 2005. Paper Number 05-0106

Lawrence G., Hardy B. J., Carroll J.A., Donaldson W.M.S., Visvikis C., Peel D.A. 2004 “A study on the feasibility of measures relating to the protection of pedestrians and other vulnerable road users” Project FIF.2003937 Final Report.

Lemosse D., Le Rue O., Diop A., Skalli W., Marec P., Lavaste F. (1998) Characterization of the mechanical behaviour parameters of the costo-vertebral joint. European Spine Journal Vol 7, nº 1, p16-23. February 1998.

Lewis G., Shaw K. M. (1997). Tensile properties of human tendo Achillis: Effect of donor age and strain rate. Journal of Foot and Ankle Surgery, Nov-Dec, 36 (6) 435-445.

Li Z., Kim J.E., Davidson J.S., Etheridge B.S., Alonso J.E., Eberhardt A.W. (2007) Biomechanical response of the pubic symphysis in lateral pelvis impacts: A finite element study. Journal of Biomechanics 2007.

Lövenhielm, P. (1974). Strain tolerance of the Vv. Cerebri Sup. (bridging veins) calculated from head-on collision tests with cadavers. Z. Rechtsmedizin 75(2), 1974, 131-144.

Lu Y.M., Hutton W.C., Gharpuray V.M. (1998) The effect of fluid loss in the viscoelastic behaviour of the lumbar intervertebral disc in compression. Journal of Biomechanical Engineeering 120 (1), 48-54.

LS-DYNA (1998) Theory Manual May 1998. Copyright 1991-1998 by Livermore Software Technology Corporation, compiled by J.O. Hallquist.

LS-DYNA (2003) Keyword's User Manual Version 970. April 2003. Copyright 1992-2003 by Livermore Software Technology Corporation.

Ma D., Obergefell A., Rizer A. (1995) Development of human articulating joint model parameters for crash dynamics simulations. Proc. 39th Stapp Car Crash Conference, SAE 952726.

MADYMO 2003. "MADYMO Reference manual" V 6.1 TNO Automotive, April 2003.

Mak, A.F. "The apparent viscoelastic behavior of articular cartilage – the contributions from the intrinsic matrix viscoelasticity and interstitial fluid flows". J Biomech Eng 108 (1986) 123–130.

Maganaris, C.N. and Paul, J.P. (1999), "In vivo human tendon mechanical properties", Journal of Physiology, 521.1, pp. 307-313.

Martinez L., Ferichola G., García A., Guerra L.J. (2006) "Análisis estadístico de los accidentes de atropello de peatones a nivel nacional e internacional." Documento Técnico DT-1-001 Proyecto PROFIT 2005 CIT-370100-2005-22.

Martinez L., Guerra L., Ferichola G., Garcia A., Yang J., (2007) Stiffness Corridors of the European vehicles for pedestrian simulations. Paper Number 07-0267-W. 20th Enhanced Safety of Vehicles Conference.

Martínez, L., Guerra L.J., Ferichola G., García A., (2007) Pedestrian accident reconstructions methodology using detailed vehicle models and age-dependent leg fracture limits on the pedestrian. IRCOBI Conference 2007.

Martínez, L.; Guerra, L. J.; Ferichola, G.; García, A. (2007) "Estudio de atropello de peatones adultos y de la tercera edad mediante modelos matemáticos" VIII Congreso Iberoamericano de Ingeniería Mecánica.

Martinez L., Compigne S., Guerra L., (2008) Influence of vehicle shape and stiffness on the pedestrian lower extremity injuries: Review of current pedestrian lower leg test procedure. IRCOBI Conference 2008.

Martinez L., Guerra L., Ferichola G., Garcia A., (2008) "Desarrollo de una metodología para el análisis de atropello de peatones utilizando modelos de elementos finitos del cuerpo humano". XVII Congreso Nacional de Ingeniería Mecánica.

Martinez L., García A., Guerra L., Alcalá E. (2011) Behaviour of high bumper vehicles in pedestrian scenarios with full FE human models. International Journal of Crashworthiness (to be published in 2011-2012).

L. Martínez, L. J. Guerra, E. Alcalá, A. García. (2011*) Development of a pedestrian rigid legform impactor with upper body mass suitable to assess leg injuries in high bumper vehicles. International Journal of Crashworthiness (in peer review)

Matsui. Y. (2003), New injury reference values determined for TRL legform impactor from accident reconstruction test, International Journal of Crashworthiness 2003.

Matsui Y.; Ishikawa H., Sasaki A. (2006). Proposal of injury risk curves for evaluating pedestrian femur/pelvis injury risk using EEVC upper legform impactor based on accident reconstruction. International Journal of Crashworthiness, Vol. 11, Issue 2, pags. 97-104.

McElhaney J H (1966). Dynamic response of bone and muscle tissue. Journal of Applied Physiology, 1966 (21) 1231-1236.

McElhaney J.H., Fogle, J.H., Melvin, J.W., Haynes, R.R., Roberts, V.L., Alem, N.B.. (1970) Mechanical properties of cranial bone. J. Biomechanics, 3, 1970, 495 -511.

McElhaney J H, Roberts V L and Hilyard J F (1976). Handbook of human tolerance. Japan Automobile Research Institute, Inc. (JARI), Tokyo, Japan.

McInnis, D.; Cliff, W.; Ising, K.; (1997) “A comparison of moment of inertia estimation techniques for vehicle dynamics simulation.” SAE paper 970951 Society of Automotive Engineers, Warrendale, PA.

Meena D. Joshi, Jun-Kyo Suh, Takashi Marui, Savio L.-Y. Woo. (1995) Interspecies variation of compressive biomechanical properties of the meniscus. Journal of Biomedical Materials Research Vol 29, nº 7, pag 823-828.

Maeno, T., and Hasegawa, J.(2001). Development of a Finite Element Model of the Total Human Model for Safety (THUMS) and Application to Car-Pedestrian Impacts. 17th ESV Conference, 2001.

Matsui. Y., (2003) New injury reference values determined for TRL legform impactor from accident reconstruction test, international Journal of Crashworthiness 2003

Melvin J.W., McElhaney J.H., Roberts, V.L. Development of a Mechanical Model of the Human Head - Determination of Tissue Properties and Synthetic Substitute Materials. 14th Stapp Car Crash Conf, Society of Automotive Engineers, SAE Paper No. 700903, 1970.

Mizuno, K.; Kajzer, J.; (2000). Head Injuries in Vehicle-Pedestrian Impact. SAE paper 2000-01-0157, Society of Automotive Engineers, Warrendale, PA.

Mizuno, Y. (2003) Summary of IHRA Pedestrian Safety WG Activities - Proposed Test Methods to Evaluate Pedestrian Protection Afforded by Passenger Cars. 18th Conference ESV. Paper Number 580.

Monson. Axial mechanical properties of fresh human cerebral blood vessels. J Biomech Eng. 125(2), 2003, 288-94

Mordaka J., Kleiven S., van Schijndel-de Nooij M., de Lange R., Guerra L.J., Carter E.L, von Holst H. (2007). The importance of rotational kinematics in pedestrian head to windshield impacts. IRCOBI Conference 2007.

Morgan E F, Bayraktar H H and Keaveny T M (2003). Trabecular bone modulus-density relationships depend on anatomic site. Journal of Biomechanics, 36 (2003) 897-904.

Morrison III, B., Cater, H.L., Wang, C.C.B., Thomas, F.C., Hung, C.T., Ateshian, G.A. and Sundström, L.E.. A tissue level tolerance criterion for living brain developed in an in vitro model of traumatic mechanical loading. 47th Stapp Car Crash Journal, SAE Paper No. 2003-22-0006, 2003.

Mosekilde L, Mosekilde L, Danielsen CC. (1987) Biomechanical competence of vertebral trabecular bone in relation to ash density and age in normal individuals. Bone 1987;8:79-85.

Nahum A.M., Smith R., Ward C.C., (1977) Intracranial pressure dynamics during head impact, Proc. of the 21st Stapp Car Crash Conf., pp. 339-366.

Neal-Sturgess CE, Carter E., Hardy R., Cuerden R., Guerra L.J., Yang J. (2007) APROSYS European In-Depth Pedestrian Database. 2007 ESV Conference.

Neal-Sturgess, C.E. and A.M. Hassan, Calibration of AIS against fatality CCIS 1999-2005. 2006, Birmingham Automotive Safety Centre.

NHTSA webpage (1998). http://www- nrd.nhtsa.dot.gov. National Highway Traffic Safety Administration. Department of Transport. United States of America.

NHTSA (2001) Ageing and Transport: Mobility Needs and Safety Issues, O.S.E. Group, Editor. 2001, OECD: Paris, France.

Nowak, M.D., and Logan, S.E.: Strain Rate Dependent Permanent Deformation of Human Wrist Ligaments. Biomedical Sciences Instrumentation. 1988, 24:61-65.

Noyes F R and Grood E S (1976). The strength of the anterior cruciate ligament in humans and rhesus monkeys. Age-related and species-related changes. The journal of bone and joint surgery, 58 (A) 1074-1082.

Nyquist H.B., Cheng R., El-Bohy A.A.R., King A.I. (1985) Tibia bending: strength and response. Proc 29th Stapp Car Crash Conference. SAE Paper No.851728.

Odland, G., (1991). Structure of the skin. In: Goldsmith, L.A. (editor) Physiology, Biochemistry, and molecular biology of the skin. Oxford University Press, Oxford.

Oxley, J.A., et al. (1996) Differences in traffic judgments between young and old adult pedestrians. in Proc. 40th AAAM. 1996

Oxlund, H., Manschot, J., Viidik, A., (1988). The role of elastin in the mechanical properties of skin. Journal of Biomechanics 21 (3), 213–218.

Pistoia W, van Rietbergen B, Ruegsegger P. (2003) Mechanical consequences of different scenarios for simulated bone atrophy and recovery in the distal radius. Bone. 2003;33:937–945

Piziali R.L., Rastegar J.C. (1997) Measurement of the nonlinear, coupled stiffnerss characteristics of the human knee. Journal of Biomechanics, 10: 45-51.

Prasad P., Mertz, H. J., et al. (1997). Injury risk curves for children and adults in frontal and rear collisions. 41st Stapp Car Crash Conference, Lake Buena Vista, FL, USA, SAE, Warrendale, PA, USA.

Ratliff A.R., Designing a surrogate upper body mass for a projectile Pedestrian legform.Thesis The Ohio State University (2008)

Rauch F, Klein K, Allolio B, Schonau E. Age at menarche and cortical bone geometry in premenopausal women. Bone 1999; 25:69–73.

Rohlmann A, Zilch H, Bergmann G, Kolbel R. (1980). Material properties of femoral cancellous bone in axial loading. Part I: time independent properties. Arch. Orthop. Trauma Surg. 97:95–102

Robbins, D.H., Wood, J.L.. Determination of mechanical properties of the bones of the skull. Exp. Mech., 9(5), 1969, 236-240.

Roberts, A., “Test Procedures for Defining Biofidelity Targets for Lateral Impact Test Dummies”, Report of EEVC WG09, Proceedings of the 13th International Conference on the Enhanced Safety of Vehicles (ESV), Paris, France, 1991

Rodmell C., Lawrence G.J.L. (1998a) Further pedestrian accident reconstructions with the upper legform impactor. EEVC WG17 document 113. revision 1.

Rodmell, C. and G.J.L. Lawrence: (1998b) Comparison between dose-response and cumulative methods of injury risk analysis and implications on the JARI injury risk analysis. TRL, November 1998, EEVC WG17 document 111.

Saraf H., Ramesh K.T., Lennon A.M., Merkle A.C., Roberts J.C. (2007) Mechanical properties of soft human tissues under dynamic loading. Journal of Biomechanics 40 (2007) 1960–1967.

Schneider, L.W., Robbins, D.H., Pflüg, M.A., Snyder, R.G. (1983) Development of anthropometrically based design specifications for an advanced adult anthropomorphic dummy family, Volume 1. Report No. UMTRI-83-53-1, Michigan.SAE paper 970088.

Shreiber, D.I., Bain, A.C. and Meaney D.F. (1997). In vivo thresholds for mechanical injury to the blood-brain barrier. SAE Paper No. 973335, in: 41st Stapp Car Crash Conf., Society of Automotive Engineers, 1997, 177-190.

Speyer H., Seidl A. (1997) RAMSIS - A New CAD Tool for Ergonomic Analysis of Vehicles Developed for the German Automotive Industry.

Stitzel J.D., Cormier J.M., Barretta J.T., Kennedy E.A., Smith E.P., Rath A.L., Duma S.M., Matsuoka F. (2003) Defining regional variation in the material properties of human rib cortical bone and its effect on fracture prediction. Stapp Car Crash Journal, Vol. 47 pp. 243-265.

Takahashi Y., Kikuchi Y., Konosu A., Ishikawa H.(2000) “Development and Validation of the Finite Element Model for the Human Lower Limb of Pedestrians” 44th Stapp Car Crash Conference Paper 2000-01-SC22.

Tamura A., Watanabe I., Miki K., (2005) Elderly human thoracic FE model development and validation. 19th ESV Conference, Paper number 05-0229.

Thibault L., Gennarelli T., Margulies S., (1990) The strain dependent pathophysiological consequences of inertial loading on central nervous system tissue, Proc. of the IRCOBI Conf., pp. 191-202,

Thibault, L.E. (1993). Brain injury from the macro to the micro level and back again: What have we learned to date? Proc. IRCOBI Conf., Eindhoven, The Netherlands, 1993, 3-25.

TNO (2004) MADYMO Human Models Manual. The Netherlands, TNO Automotive.

TNO (2005). MADYMO Theory Manual (2005) Version 6.2.2 June 2005. Copyright 2005 by TNO.

Trosseille X., Tarrière C., Lavaste F., Guillon F., Domont A., (1992).Development of a FEM of the human head according to a specific test protocol, SAE n° 922527.

Ueno, K., and Melvin, J.W. (1995) Finite element model study of head impact based on hybrid III head acceleration: The effects of rotational and translational acceleration. J. Biomechanical Engineering. 117(3), 319-328

Untaroiu C., Darvish K., Crandall J., Deng B., Wang J.T.(2005) Characterization of the lower limb soft tissues in pedestrian finite element models. 19th ESV Conference, Paper Number 05-0250.

van Dommelen J.A.W., Jolandan M.M, Ivarsson B.J, Millington S.A., Raut M., Kerrigan J.R., Crandall J.R,, Diduch D.R. (2005) Pedestrian injuries: viscoelastic properties of human knee ligaments at high loading rates. Traffic Injury Prevention, Vol 6, nº 3, September 2005. pp. 278-287.

Van Hoof J., de Lange R., Wismans J.S.H.M (2003) Improving Pedestrian Safety Using Numerical Human Models. Stapp Car Crash Journal, Vol. 47 (October 2003), pp. 401-436.

Vera, C.; Martinez, L.; (2003). “Apuntes Teoría de vehículos y componentes.” ETSII UPM Madrid.

Walker P.S., Hajek G.V. (1972) The load bearing area in the knee joint. Journal of Biomechanics 5: 581-589.

Wall J C, Hutton W C and Cyron B M (1974). The effects of age and strain rate on the mechanical properties of bone. Proceedings of the 1974 international IRCOBI conference on the biomechanics of human bodies, 11-12 June 1974, Göteborg, Sweden: IRCOBI Secretariat, ONSER, 9 Chemin St. Jean, Bron, F-69500, France.

Wan Abas, W., Barbanel, J., 1982. Uniaxial tension test of human skin in vivo. Journal of Biomedical Engineering 4.

Willinger R., D. Baumgartner, (2003)Human head tolerance limits to specific injury mechanisms, International Journal of Crashworthiness, vol. 8, n°6, pp. 605-617.

Woodhead HJ, Kemp AF, Blimkie CJR, et al. Measurement of midfemoral shaft geometry: repeatability and accuracy using magnetic resonance imaging and dual-energy X-ray absorptiometry. J Bone Miner Res 2001; 16:2251–2259.

Wren T A L, Yerby S A, Beaupré G S and Carter D R (2001). Influence of bone mineral density, age, and strain rate on the failure mode of human Achilles tendons. Clinical Biomechanics 16 (2001) 529-534.

Yamada H (1970). Strength of biological materials. Ed. Evans F G: The Williams and Wilkins Company, 428 East Preston Street, Baltimore, Maryland 21202, USA.

Yang, J.(1994) Impact Biomechanics of the Lower Extremity in Traffic Accidents - Development and Validation of a Mathematical Model. Chalmers University of Technology, Thesis, Gothenburg, March 1994.

Yang J., Kajzer J., Cavallero C., Bonnoit J. (1995) Computer Simulation of Shearing and Bending Response of the Knee Joint to a Lateral Impact. 39th Stapp Car Crash Conference, p.p. 251-264.

Yang J.K., Lovsund P. (1997) Development and validation of a human body mathematical model for simulation of car-pedestrian impacts. Proc. 22nd IRCOBI Conference.

Yang J.K., Lövsund, P., J., Cavallero C., Bonnoit J. (2000) A Human-Body 3D Mathematical Model for Simulation of Car-Pedestrian Impacts. International Journal of Crash Prevention and Injury Control, Vol. 2(2), p. 131-149.

Yang, J. K. (2002). Review of injury biomechanics in car-pedestrian collisions. Crash Safety Division. Goteborg, Sweden, Chalmers University of Technology.

Yao, J., Yang J., et al. (2005). Reconstruction of head to bonnet top impact in child pedestrian to passenger car crash. IRCOBI Conference 2005.

Yasuki T., (2006a) Mechanism analysis of pedestrian knee bending angle by SUV type vehicle using Human FE model. International Crashworthiness Conference ICRASH 2006.

Yasuki T., (2006b) Mechanism analysis of pedestrian knee bending angle by sedan type vehicle using Human FE model. International Crashworthiness Conference ICRASH 2006.

Yin L., Elliott D.M. (2005) A homogenization model of the annulus fibrosus. Journal of Biomechanics 38 (2005) 1674–1684

Yogonandan N, Pintar F.A., Sances A., Walsh P.R., Ewing C.L., Snyder T., Snyder R.G., (1994) Biomechanics of skull fracture, Proc. of the Head Injury Symposium, Washington DC, pp. 227-236.

Zander T., Rohlmann A., Bergmann G. (2004) Influence of ligament stiffness on the mechanical behaviour of a functional spinal unit. Journal of Biomechanics 37 (2004) 1107–1111

Zhang, L. Yang, K.H., King, A.I. A Proposed Injury Threshold for Mild Traumatic Brain Injury. Journal of Biomechanical Engineering, 126(1), 2004, 226-236

Zioupos, P. (2001) Ageing Human Bone: Factors Affecting Its Biomechanical Properties and the Role of Collagen. Journal of Biomaterials Applications Volume 15 January 2001.